IMPERIAL COLLEGE OF SCIENCE, TECHNOLOGY & MEDICINE

University of London

FORCED VIBRATION CHARACTERISTICS OF MISTUNED BLADED DISC ASSEMBLIES

by

Hoi YIU

A thesis submitted to the University of London for the degree of Doctor of Philosophy

Centre of Vibration Engineering, Dynamics Section
Department of Mechanical Engineering
Imperial College of Science, Technology and Medicine
Exhibition Road
London SW7 2BX

November 1995

To My Mother

Acknowledgements

I would like to express my deepest appreciation to Professor D. J. Ewins for his kind supervision and guidance, and for putting up with me. Two other members, Dr. M. Imregun and Mr. D. Robb, in the Dynamics Section, to whom I am also indebted for them from numerous advice and discussions.

I would also like to thank the Science and Engineering Research Council (SERC), now as the Engineering and Physical Science Research Council (EPSRC) and the Rolls-Royce plc for providing the funding for this study. All the members of the Centre of Vibration Engineering should be mentioned here for their help. I especially wish to thank Dr. A. Stochniol, Dr. K.Y. Sanliturk, Dr. R.M. Lin, Dr. A.S. Nobari and Dr. I. Bucher for their help in the past few years. Thanks are also due to Mr. R. Mostofi, Mr. J. G. Marshall, Ms M.L.M Duarta, Mr. C. Leontopoulos and Mr. N. Imamovic with whom I have worked together as colleagues.

ABSTRACT

The existence of small variations in blade dimensions around a disc, commonly known as mistuning, can cause significant variations in the dynamic response of different blades within the same assembly. The first studies of mistuning were made almost 30 years ago. Since then, there have been many conflicting results found from different studies. Therefore, the targets of this research concentrate on giving a better understanding to the apparently different results of mistuning studies so that some general rules can be implemented for practical use.

After some studies of the different models used for bladed disc vibration analysis, the lumped parameter model has been selected for stochastic simulation purposes. Two classes of blade mistuning, frequency and damping mistuning, are defined, and most of the current simulation work concentrated on the first of these. This type of stochastic simulation approach has been further used here to study some new influences from blade mistuning, particularly the re-arrangement of a specific set of blades around a rotor. The results show surprisingly strong dependence of blade responses on the blade arrangement. A prediction method has also been developed for the worst and the optimal arrangement and numerical results show some agreement with the theoretical prediction. Another factor, which causes the blade critical responses to vary, is the bladed disc coupling strength. This effect is also affected by the amount of mistuning among the blades.

Damping mistuning has received attention only recently. In the present study, a simplified model of mechanical damping is used to study the consequences of different levels of effective dampers on each blade. Numerical results from these studies show slight localised effects on responses with the presence of a damping mistuning pattern. Again, the effect of damping mistuning seems to be affected by the coupling effects from the disc flexibility.

Moreover, a statistical analysis often involves a large number of samples from simulations or experiments in order to find any trends in the scatter, and hence requires a huge amount of computing or experimental effort. Here, an analytical alternative to find the probabilistic density function has been presented as a cheaper tool to the quantitative method of simulations used before.

Finally, the experiments on a bladed disc provide some comparison studies between analytical and test results.

NOMENCLATURE

The list of notation is used in this thesis apart from some specially defined terms in the text.

A	cross section area of the blade
D	flexural rigidity of the disc $D = \frac{E_d h^3}{12(1 - \upsilon^2)}$
E_d, E_b	Young's modulus of disc and blade
$E(x)$	Expected value or mathematical expectation
G	shear modulus of elasticity $G = \frac{E_b}{2(1 - \upsilon^2)}$
I_{xx}, I_{xy}, I_{yy}	blade bending moment of inertia
I_p	blade polar moment of inertia
J	torsional rigidity constant
I_n, J_n	Bessel functions
N	total number of blades on disc
$O()$	occurrences of an event
$P(x)$	cumulative probability function (CPF)
R	outer radius of disc
T_d, T_b	kinetic energy of disc and blade
U_d, U_b	potential (strain) energy of disc and blade
f_n	frequency parameter for a cantilever beam
g_n	frequency parameter for a uniform disc
h	thickness of disc
i	integer indicates blade number
j	$\sqrt{-1}$
l	length of blade
n	engine-order-excitation
$p(x)$	probability density function (PDF)
q	principal coordinates
r	integer indicates mode
t	time
α, β	taper ratios
χ_n	bending mode functions of uniform disc

Φ_n	bending mode functions of uniform beams
ψ	interblade phase angle
ϑ_n	torsion mode functions of uniform beams
γ_n, κ_n	frequency parameter for blade and disc in bending modes
φ_n	frequency parameter for blade in torsion modes
λ_n	eigenvalues
ρ_d, ρ_b	density of disc and blade materials
υ	Poisson's ratio
ω, Ω	frequency, speed
ξ	viscous damping coefficients
η	hysteretic damping coefficients
r, ψ	polar coordinates
u, v, θ	deformations of the elastic axis
x, y, w	physical coordinates system
ξ, η, ζ	transformed computational coordinates system for a uniform beam
$[C]$	damping matrix
$[D]$	hysteretic damping matrix
$[H]$	receptance or dynamic flexibility matrix
$[I]$	unit matrix
$[J]$	Jacobian matrix for transformation
$[K]$	stiffness matrix
$[M]$	mass and inertia matrix
$\{f\}, \{F\}$	applied force vectors
$\{x\}, \{X\}$	displacement vectors

CONTENTS

Chapter 1	**Introduction**	1
1.0	About this chapter	
1.1	Nature of Problems in Turbomachinery Blade Vibration	2
	1.1.1 Introduction	2
	1.1.2 Disc Vibration	3
	1.1.3 Blade Vibration	4
	1.1.4 Bladed Disc Vibration	6
1.2	Effects of Mistuning of Bladed Disc Assemblies	7
	1.2.1 Introduction	7
	1.2.2 Literature Survey	8
1.3	Objectives of the New Research	17
	1.3.1 Introduction	17
	1.3.2 Questions on the Objectives for the Project	18
	1.3.3 Preview of the Thesis	18
Chapter 2	**Free Vibration Analysis of Bladed Discs**	20
2.0	About this chapter	
2.1	General Introduction	21
2.2	Continuous Models	22
	2.1.1 Closed-form Receptance Coupling Method	22
	2.1.2 Energy Methods (Modal Synthesis Techniques)	22
2.3	Discrete Models	27
	2.3.1 Transfer Matrix Method (Myklestad-Prohl-Thomson Method)	27
	2.3.2 Lumped Parameter Models	28
2.4	The Finite Element Method	32
2.5	Experimental Study - Hammer Test	33
2.6	Results and Discussions	35
	2.6.1 Blade Vibration	36
	2.6.2 Blade Taper Effects	37
	2.6.3 Blade Tip Responses	39
	2.6.4 Disc Vibration	41
	2.6.5 Bladed Disc Vibration	43
2.7	Concluding Remarks	47

Chapter 3 **Blade Resonance Response Studies on Mistuned Bladed Disc Assemblies: A Stochastic Approach** 50

3.0 About this chapter
3.1 Introduction 51
3.2 Mathematical Model 52
3.3 Model Parameters 56
3.4 Mistuned Bladed Disc 57
3.5 Statistics of Mistuned Forced Response Characteristics 58
3.6 Blade Arrangements 63
3.6.1 Maximum Response Investigation 63
3.6.2 Optimal arrangements 66
3.6.3 Correlation studies of Blade Arrangements 73
3.6.4 Reliability of Small Samples from Experiments 82
3.7 Concluding Remarks 83

Chapter 4 **Mistuning Effects on Coupled Bladed Disc Resonant Responses** 85

4.0 About this chapter
4.1 Introduction 86
4.2 Mode Localisation of Vibrating Periodic Structures 87
4.2.1 Coupled 2-DOF Oscillator 88
4.2.2 Forced Response Analysis of the 2-DOF Oscillator 91
4.3 Bladed Disc Coupling Influences 92
4.3.1 Bladed Disc Coupling Factor 92
4.3.2 Mass Ratio Effect 95
4.3.3 Frequency Ratio Effect 98
4.3.4 Blade and Disc Coupling Effect 100
4.4 Weak Coupling Effect 106
4.5 Influences of Amount of Mistuning 106
4.6 Mistuning Parameter Plot 112
4.7 Concluding Remarks 113

Chapter 5 **Effects of Damping Mistuning on the Vibrations of Bladed Discs** 115

5.0 About this chapter
5.1 Introduction 116

5.2 Theoretical Background 117
5.2.1 State-space Formulation 118
5.2.2 Tuned System 119
5.2.3 Complex Modes 120
5.2.4 Forced response of a Non-proportionally Damped Bladed Disc 124
5.3 Blade resonant responses of Damping Mistuned Assemblies 125
5.4 Complex Modes in Damping Mistuned Assemblies 134
5.5 Case Study: Rainbow Test 138
5.5.1 Identify System Parameters 139
5.5.2 Modeshape Studies 140
5.5.3 Maximum Responses Studies 141
5.6 Concluding Remarks 141

Chapter 6 **Probabilistic Analysis of Mistuned Bladed Rotors** 156

6.0 About this chapter
6.1 Introduction 157
6.2 Fundamentals of Probability Density Functions 159
6.2.1 Probability Density Function 159
6.2.2Multiple Random Variables 161
6.3 Statistical Inference Method 163
6.3.1 The Moment Method 163
6.3.2 Some Common Probability Density Functions 164
6.4 Transform Variable Technique (The Close-Form Approach) 166
6.4.1 Theory 166
6.4.2 The Transform Variable Technique (TVT) Examples 167
6.4.3 A Single-Degree-of-Freedom System Study 169
6.5 A Probabilistic Method for Mistuned Bladed Discs 171
6.5.1 The Random Perturbation Technique 172
6.5.2 The Combined Closed Form-Perturbation Technique 172
6.5.3 A Two-step Transformation method 172
6.6 Concluding Remarks 176

Chapter 7 **Experimental Measurements on Mistuned Bladed Disc Responses** 178

7.0 About this chapter
7.1 Introduction 179

7.2 Theory 180
7.2.1 Travelling Wave Simulation 180
7.2.2 Force control process 185
7.3 Single Shaker Test 187
7.3.1 Experimental Procedure 188
7.3.2 Measurement Results 189
7.4 The Dual-Shaker Test 192
7.4.1 Numerical Simulations 192
7.4.2 Experimental Set-Ups 193
7.4.3 Measurement Results 195
7.5 Concluding Remarks 201

Chapter 8 **Conclusions and Further Work** 203

8.1 Discussion 204
8.2 Practical Guides for Mistuned Bladed Discs 206
8.3 Recommendations for Further Work 208
8.4 Conclusions 208

References 210

Appendices 223

CHAPTER 1

INTRODUCTION

About this chapter

This chapter presents a survey relating to studies of the vibration of turbomachines with particular reference to the mistuning effects on bladed disc assemblies. In many engineering applications, the consequences of small variations in dimensions are often ignored in design and, in practice, it is not easy to produce two components exactly 'identical'. However, these slight variations may cause catastrophic vibration problems for a cyclically symmetric structure, such as a bladed disc. This phenomenon is known as the "mistuning" effect, and often occurs even when the manufacturing variations are within small specified production tolerances. The outcome can severely affect the life-time of the whole engine because mistuning can generate the possibility of one or more blades, named *rogue blades*, suffering excessive stresses.

The central objectives of this Chapter concentrate on the different conclusions obtained from different researchers. These shall provide a suitable starting point for the rest of the thesis.

1.1 NATURE OF PROBLEMS IN TURBOMACHINERY BLADE VIBRATION

1.1.1 Introduction

Vibration can have serious consequences for structures because it can induce defects such as fatigue failures of structural members, and malfunctioning of critical parts, and will often generate unwanted noise. Generally speaking, any high-speed moving components are prone to vibration which can lead to stresses building up within the members and, possibly, to breakage. Turbomachines, including steam turbines for power generation and gas turbines for aircraft and marine propulsion, are high-speed rotating machines and hence the dangers of suffering severe vibration troubles are intensified. Furthermore, current design features of modern gas turbines in particular demand characteristics of light weight and high power while maintaining high reliability. In such conditions, it is necessary to study the vibration of turbomachines in great detail, since most failures of turbomachines are the result of fatigue caused by vibration.

Owing to the rapid developments of technologies in recent decades, the power and the efficiency of turbomachines have been improved significantly and so the structural components have to be made to suit for the higher demands of power and longer life requirements. For the design of a jet engine, the axial rotor is a very complex machine. This part of the machine often experiences high speeds of rotation, high-pressure stresses and some parts will be under high temperature. The construction of the core of a turbomachine consists of many rotor wheels, which are divided into sections of compressor and turbine stages.

From the principles of turbomachinery, the working fluid, which is directed by stationary blades known as stators or guide vanes, impinges on the rotating blades. The vibrations of these rotating blades often raise two major problems for the designers. One factor is the high stress induced on the rotating parts caused by vibrations. This factor shortens the desired fatigue life of parts in service. Second, the designers have to ensure that the deflections from the vibration of the rotating rotors do not lead to contact with the stator blades while maintaining the aerodynamic performance of the engine. In the past, many studies of rotating wheel vibration have been reported in literature.

Specifically, studies of turbomachinery blade vibration can be divided into three parts, namely: disc vibration, blade vibration and bladed disc vibration.

1.1.2 Disc Vibration

As early as 1924, Campbell reported a comprehensive study of the vibration problems on steam turbine discs [14]. In his paper, large and thin steam turbine wheels were investigated. The failures that he was trying to explain were mainly vibration-induced fatigue defects and ruptures caused by localised high stresses around holes of steam turbine discs. Campbell pointed out that the vibration problems were more important since the deflections from vibrations were more difficult to predict. At that time, Campbell simply applied disc vibration theory for his study although the structure had blades on the disc. A disc may have three features in its vibration characteristics. First, the disc can vibrate with a mode shape formed by a wave-like lateral deflection around the circumference of the disc, as shown in Figure 1.1(a).

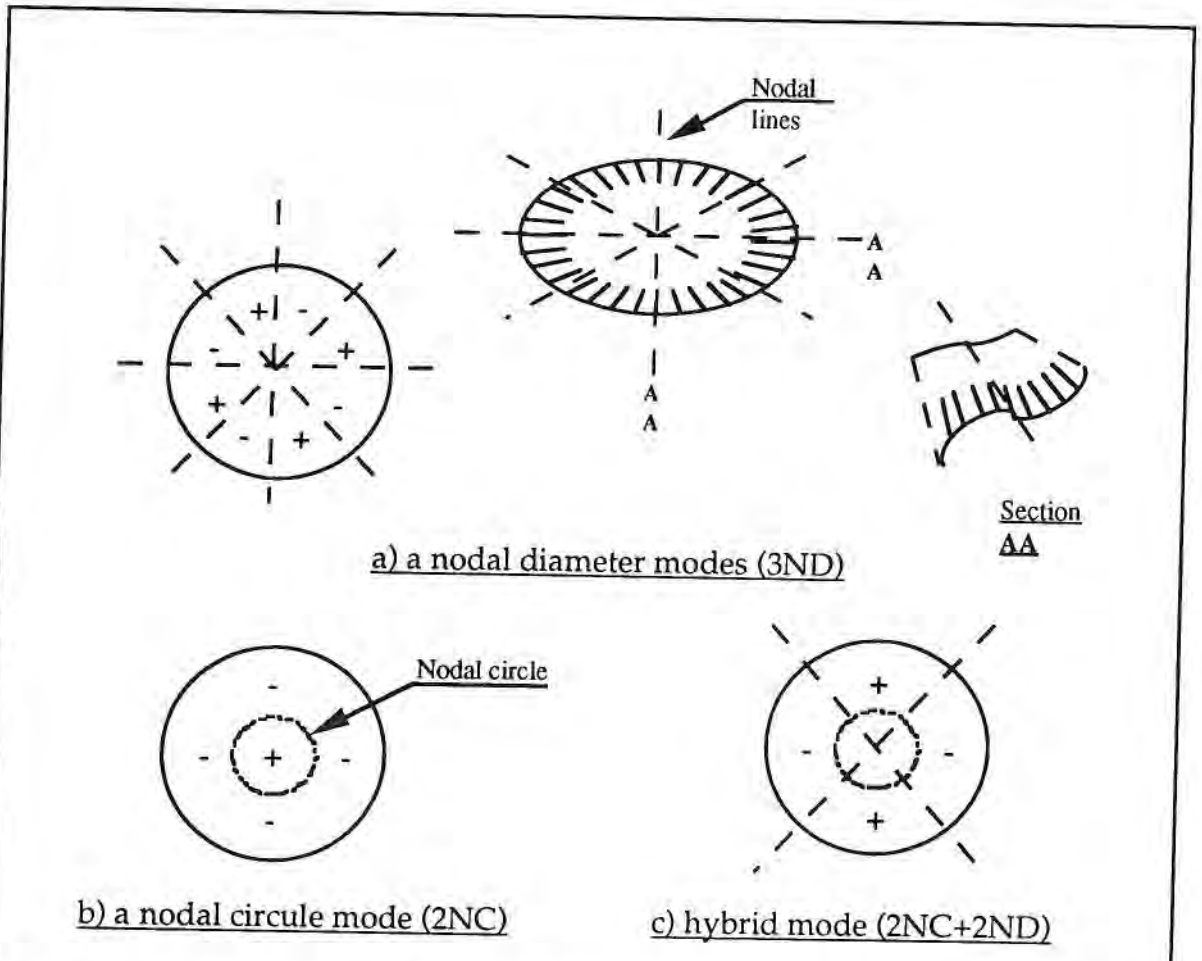

Figure 1.1 Examples of schematic diagrams showing some typical disc modes

This type of vibration is described as a "diametral mode" because there are a number of nodal diameter lines along which the amplitude of the wave is zero. In practice, this is the most common type of disc vibration as accounted by Campbell. Second, stationary nodes may also take the form of circular rings on the disc, which are known as "nodal circles". This family of vibration modes are known as the "axisymmetric modes" or the "circular modes", as shown in Figure 1b. Finally, hybrid modes, which are combinations of both circular and diametral nodes, were also surveyed by Campbell. Tobias and Arnold [142] further extended Campbell's work in 1957 to include imperfect rotating discs which behave more like real turbomachinery discs. Nevertheless, a rotor wheel is made of a set of blades mounted on a disc. The study of disc vibration alone is not sufficient since the vibration failure of a bladed disc assembly is most likely to be experienced in the blades.

1.1.3 **Blade Vibration**

Conventionally, a blade is often considered as a cantilever beam with its root as the fixed end and there have been numerous studies of beam dynamics in the past. Nevertheless, a multi-stage turbomachine compressor or turbine contains thousands of blades and many of them show different dynamic characteristics to each other. The failure of just one blade can lead to serious damage in other parts of the engine, and there are several examples of disasters caused by the failure of turbine blades due to excessive vibration in practice. Furthermore, the interaction between vibrating blades and the flow field can also induce aerodynamic instability. This leads to flutter which is a form of self-excited vibration. Research of blade flutter is still a major activity nowadays. Hence, it is equally important to study blade vibration as well as disc vibration.

The key factor for a blade to vibrate is the excitation which acts upon the blade by the working fluid. Trumpler and Owens in 1955 [145] suggested that the resonant peak amplitude of a vibrating blade, which also depended on the amount of damping at its root, would occur when a frequency of the exciting force or any of its multiples was close or equal to a natural frequency of that particular blade. So far, these studies could be either for steam or gas turbine blades. Armstrong and Steveson in 1960 [4] made more detailed studies of the different modes which could be found on blade vibrations for gas turbines, as shown in Figure 1.2, namely: flexural or flapwise modes, torsional modes, and

edgewise modes. They also commented on the various factors giving rise to blade vibration including the aerodynamic effects such as flutter and wakes. Armstrong reviewed some further developments on turbine blade vibration in 1967 [6] to bring the subject up-to-date by taking into account the use of snubbers, such as shrouds and lacing wires which transfer the forces generated as a result of deflected blades around the disc in order to minimise the vibration effects on the blades.

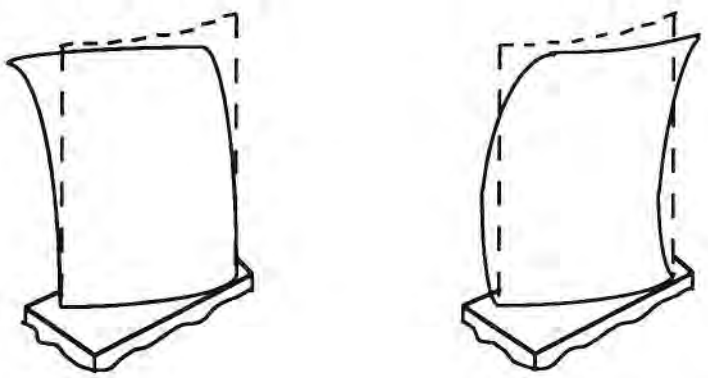

First mode Second mode

a) Flapwise or flexural modes of vibration

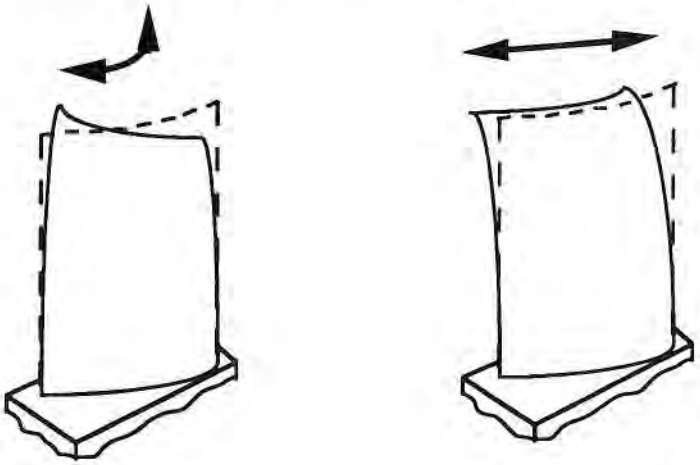

b) First torsional mode of vibration c) First edgewise mode of vibration

Figure 1.2 Common turbomachinery blade vibration modes (Armstrong and Steveson 1960 [4])

Later, surveys on blade vibrations have been reported by Leissa [87] in 1981, Rao [120] in 1977 and [121] in 1987, and Ewins and Henry [43] in 1988, amongst others.

1.1.4 Bladed Disc Vibration

Modern turbomachines are generally made of discs with separate blades mounted in the disc rim by fir-tree or pin-joint roots, and the blade vibration thus depends to some extent upon the flexibility of the roots. Since all the blades are mechanically coupled to the disc by a flexible root, the consequent interaction between the blades and the disc, especially that due to the disc flexibility effect, can significantly influence the dynamic behaviour of the blades. In reality, a bladed disc assembly tends to vibrate as a complete system rather than as individual cantilever blades or just a rotating disc. In addition, shrouds may also give rise to interactions between the blades. The study and analysis of the bladed disc assembly as a whole is necessary in order to bring the theoretical model close to the practical situation. The bladed disc is a set of blades, which may or may not be identical, attached to a common disc. Tuned bladed discs have been examined by many researchers. Johnson and Bishop [71] in 1955 used a simple spring-mass system to study the problem of multiple-modes at a single natural frequency. Armstrong et. al. [5] in 1966 showed that the natural frequencies of the tuned bladed discs can be evaluated by the receptance method. F.O. Carta [19] in 1967 discussed the effects of the aerodynamic instability of shrouded-bladed-disc assemblies. In 1975, Cottney and Ewins [22] reported on a receptance method for the analysis of a shrouded-bladed-disc. There are also numerous review papers of bladed disc assemblies, including mistuning effects, that have been published by Ewins [39] in 1980, Srinivasan [134] in 1984, Omprakash and Ramamurti [111] in 1988, and also Panwalker, Rajmani and Ramamurti [113] in 1990 etc.

Apart from the coupling effects on the bladed disc assembly (which influence the natural frequencies and mode shapes), there are various types of external excitation to be considered under engine running conditions. These affect the responses, such as stress and displacement, of the bladed disc. The most important excitation experienced by the blading is provided by the fluctuating forces applied when the blades pass though a steady but nonuniform fluid flow field caused by upstream obstacles such as stationary vanes, including stators or nozzles, and the struts which support the core of the engine. These fluctuating forces are normally considered in the form of cosine or sine variations in pressure with angular position of the disc, acting axially on the rotating blades. These particular excitations, which are associated with the rotation of the bladed disc, are at frequencies which are multiples of the engine rotating speed, and these are termed "engine-order excitations". However, the

design must avoid some points where there is an energy build-up inside the system to a major resonance. This can occur when the frequency of the exciting force equals the natural frequency of the vibrating bladed disc and the excitation profile has the same shape as the associated mode shape of the bladed disc. This happens when a particular engine-order excitation frequency is exactly coincident with a natural frequency of a similarly-ordered nodal diameter mode of the bladed disc. Most literature on bladed disc vibrations has studied the resonant responses of bladed assemblies. This is because the response of a blade on the disc is a prime factor to design engineers especially in case of mistuning.

1.2 EFFECTS OF MISTUNING OF BLADED DISC ASSEMBLIES

1.2.1 Introduction

"Mistuning" refers to the presence of small deviations of structural properties, such as mass or stiffness, between one blade and the others on a bladed disc assembly. Its effect can cause significant variations in the dynamic response of different blades within the same assembly during service. Such blade-to-blade nonuniformity can be the result of small differences caused by manufacturing tolerances, and the outcome can severely affect the life-time of the whole turbine assembly because such effects may generate the possibility that one or more blades (named "rogue blades") could suffer excessive stresses, while all other blades on the same stage are apparently stress-worthy. Furthermore, mistuning effects can be the result of normal wear in service, and therefore a study of its formation and behaviour is essential.

The causes of mistuning in bladed disc assemblies may be attributed to a number of factors, including:

(i) manufacturing tolerances on blade or disc dimensions;

(ii) friction damping at the blade roots or shrouds interfaces varying from blade to blade; or

(iii) aerodynamic effects on the blades not being uniformly distributed.

*Mis*tuning refers to the inherent variations in the properties of one or more blades because of manufacturing tolerances. *De*tuning is defined as some blades having their parameters deliberately selected or changed by a controlled amount [44]. Although mistuning has a severe detrimental influence on forced vibration response, it can sometimes be beneficial because some

mistuned blade patterns tend to raise the flutter boundary. Therefore, one may detune a bladed disc in a special pattern as a mean of exercising passive control of flutter. Furthermore, blade mistuning can also be classified as one blade mistuned, alternately mistuned or randomly mistuned, or other specified patterns.

1.2.2 Literature Survey

In many engineering applications, small imperfections away from the idealised model are usually ignored in design. However, Tobias and Arnold in 1957 [142] showed that imperfections in a spinning disc could have a markedly different dynamic response to that of the perfect or tuned disc considered by designers. In 1966, Whitehead [153] reported a theoretical analysis of the maximum response effects of mistuning on aerodynamically-induced vibrations of a bladed disc. The results showed that the responses of a mistuned bladed disc could be many times higher than in the tuned bladed system. Since then, many research workers have studied the problem and developed some useful results in the past twenty five years. The classifications of the work in the past include both structurally and aerodynamically-coupled and mistuned bladed discs. In Appendix I, a family tree shows the work published by different groups of people in the past 30 years. These groups might come from a particular research group in a university or a research institute, or from the research and development department of engine manufactures. Some of the most important contributions are reviewed below.

Whitehead

In 1966, Whitehead published the first study of the worst-blade case due to mistuning through a mathematical analysis of the torsional flutter of a cascade of blades. In his papers [157] he suggested that if there were N blades on a rotor, the worst blade in resonance would be subjected to a maximum stress increase up to a factor of $\frac{1}{2}\left(1+\sqrt{N}\right)$ times that of the "tuned" condition. He concluded that the effects of mechanical damping and mistuning of the blades were always favourable to control flutter. Ten years later in 1976 [158], he reported again that for mechanical coupling only the factor would reduce to $\frac{1}{2}\left(1+\sqrt{\frac{N}{2}}\right)$.

Wagner

Meanwhile, Wagner [148] independently used a mass-spring-damper model in 1967 to represent the turbine blades on a rotor, which were coupled through

flexible disc. The natural frequencies, mode shapes and forced response of this model were calculated and the results showed that the distribution gave large variations in peak blade stresses around the row. This result agreed in principle with Whitehead's theoretical predictions. Furthermore, it was found that the damping effects tended to average the response levels of the subsystems, and with the inclusion of a flexible disc, the vibrational energy input to the blade with low damping could be absorbed by other blades in the same row. This result greatly reduced the range of exciting frequencies in which peak blade stresses could occur and facilitates tuning blades to avoid resonance at the operating speeds.

Dye & Henry

Dye and Henry [28] attempted, in 1969, to illustrate Whitehead's predicted factor for the worst blade by making a numerical study based on a lumped-parameter mass-trolley-spring model. Although they could not find exactly the value predicted by Whitehead, they nevertheless observed that some blades displayed much higher amplitude than others. Different sets of mistune distributions, including single blade mistuning, alternate mistuning, random mistuning from a set of blades with a normal Gaussian blade cantilever natural frequency distribution, and sinusoidal distributed patterns were each analysed and tested. They showed that the Gaussian case and the case with only one blade mistuned gave much larger amplitudes than the other distributions. On their 43-bladed rotor model, a response increase factor of 2.82 was encountered when one blade was mistuned, and 2.44 for the asymmetric Gaussian case. Moreover, they showed that for some mistune distributions, which would be possible in practice, the stress level of some blades could be more than 35 percent greater than any other blades and these could be responsible for the so-called "rogue blade" failures.

Ewins et al.

Ewins reported a series of detailed studies of mistuning and detuning effects on bladed disc assemblies. The analytical model used was based on receptance methods that allowed the coupling of blades, disc, and shroud together. The first paper of the series were concerned with the calculation of the natural frequencies and of the modes which split as a result of detuning [31]. Bladed disc vibration modes were classified into families, each associated with one of the blade cantilever modes. Coincident resonances, which were defined as two distinct modes with different natural frequencies resonating at a common

critical speed, were credited with factors of blade detuning and accident of design [32]. The effects of random mistuning on the response under typical operating excitation conditions were then examined [33, 34] using 24-bladed and 30-bladed disc models for which both theoretical and experimental results were obtained and compared. The maximum stress for a randomly-mistuned bladed disc was found to be about twenty percent higher than that for the tuned case [35]. Finally, an experimental model [36] to study the aerodynamic excitation effects was also reported in 1976 and the results were compared with analytical results by Ewins and Rao [37]. Review papers by Ewins of bladed disc vibration with mistuning effects can also be found in 1980 [38, 39]. Ewins and Han in 1984 [40] examined selected blades in certain arrangements and found that for a particular set of mistuned blades, different arrangements produced different response levels, but that the blades which were the most mistuned suffered the worst response. The latter conclusion agreed with the comments made by Afolabi from 1986-88 [1-3], who studied the eigenvalue spectrum of a mistuned system to show that the maximum amplitudes are most likely to occur at the most mistuned blades. In the same year, Ewins and Imregun [41, 65] published two reports on the study of packeted bladed discs and aeroelastic vibration of mistuned bladed systems. In 1988 Singh and Ewins [128] established the basis of a probabilistic model of a bladed disc assembly. The latest work by Sanliturk [125] suggests a model to study a complicated bladed disc at a minimum cost.

Srinivasan et al.

Workers from United Technologies in the USA started a study of blade mistuning effects in 1975 by deriving an alternative model from other researchers at that time, as shown by El-Bayoumy and Srinivasan [30]. Analytical results of a mistuned 24-bladed disc were compared with those of Ewins [33] and good agreement was found. Comments were made that mistuning could cause higher stresses than suffered by the equivalent tuned system and the amount of overstress depended upon the frequency distributions and the deviation of blade frequencies from their mean value. Secondly, the blade experiencing the maximum stress level was not necessarily that of the most highly-mistuned blade and this point was different from the view of some other workers, for example, Afolabi in 1986-88. Finally, they also concluded that smooth mistuning distributions did not necessarily imply lower vibration stress levels [30].

The second part of their work was a continuation of the first part in order to extract more relevant guidance towards the practical design stage of gas turbines. Srinivasan and Frye [133] conducted tests on two different engine designs. In one case, a first-stage high-pressure turbine blade response was found to be due to strong 10th engine-order excitation, and for the other case the second-stage high-pressure turbine blade response was due to 5th engine order excitation. The results from the analysis showed that the former configuration, which was a 116-bladed disc, might have individual turbine blades responding at a level 1.95 times that of the perfectly tuned wheel, while the latter configuration, which was a 72-bladed disc, had a corresponding factor of 1.64. Sogliero and Srinivasan [132] in 1980 presented a third part of the study by analysing some randomly-mistuned blades which might lead to some individual blades displaying different frequencies to the rest of the blades around the rotor. A statistical approach was applied for the first time to estimate the service life of a specific bladed disc configuration.

In the same year, 1980, Srinivasan [134] also submitted a technical report to the NASA Lewis Research Centre as a preliminary study of fan blade torsional flutter by utilising first stage fan flutter data available from tests conducted at NASA. Mistuning was accounted for in the analysis so that individual blade inertia, frequency, and damping parameters could also be considered. The formulation which included both aerodynamic and mechanical coupling among the blades of the assembly was based on the model proposed by Whitehead [157]. This work was extended in 1984 by Srinivasan and Fabunmi [48] to include bending and torsional coupling of a cascade of cantilevered blades. This branch continued with the study of dual mode effects caused by mistuning to the flutter influence by Ford and Srinivasan in 1983 [46] and by Ford in 1987 [57]. This twin-mode analysis was capable of changing the flutter prediction for one particular mode from unstable to stable. Recently, Srinivasan and Tavares presented a flutter prediction formulation based on the feature of applying unsteady aerodynamic pressure directly rather than using the lift and moment coefficients as in the conventional method [136].

Kaza & Kielb et al.

This branch of studies undertaken by NASA concentrated on work using the mistuning between blades as a passive control to alleviate flutter problems in unshrouded, high-aspect-ratio turbofans. The results showed that mistuning had the potential to raise the flutter speed of a fan and it was believed that this

might eliminate the use of mid-span shrouds as these had an adverse effect on aerodynamic performance. Cascade blades in subsonic, transonic and supersonic flows were studied [76, 81]. Alternate mistuning and random mistuning effects were introduced and significant effects on flutter speed were found, depending on the cascade parameters, such as the excitations and the Mach number. They might have either a beneficial or an adverse effect on forced response. A simple aerofoil section, originally used for fixed wing flutter analysis, was adapted at the beginning. Later, a nonuniform blade model was developed [78]. Structural coupling was also included and it was found that this could affect both aerodynamic stability and the natural frequencies, [82]. Finally, disc flexibility was accounted for in the new model and the analytical results showed that it did not have much influence on flutter of either tuned or mistuned systems, but its effect might be significant on forced response, which was sensitive to small changes in system frequencies [79]. However, the conclusion was drawn that one percent of alternate mistuning could stabilise the cascade to a degree equivalent to adding 0.3 percent damping to the tuned system [83]. More recent studies by NASA on mistuning effects have been applied to the newly-developed propfan engines under subsonic flow condition [84, 97].

Another group from NASA, including Hoyniak and Fleeter, reported a series of studies of aerodynamic detuning effects mainly based on unstalled flutter stability [57-60] in 1984. "Alternate circumferential blade spacing", which means that the spacing of the adjacent rotor blades is nonuniform, can be used as an aerodynamic detuning of a cascade row. In addition, alternately varied spacing has been developed and can be used as a passive control of flutter. They further concluded that the greatest stability enhancement would result from a combination of aerodynamic and structural detuning. Finally, Topp and Fleeter [143] demonstrated the application of splitter blades used as both aerodynamic and structural detuning mechanisms.

Crawley et al.

The research of mistuned bladed discs at MIT was published first as the doctoral work of Fabunmi. His paper in 1980 stated that the phenomenon of "rogue blades" is not necessarily associated with the most mistuned blades, but rather with ones whose cantilever frequencies coincide with one of the tuned system natural frequencies [45].

Crawley's 1983 paper [24] showed how coupling of the blade motion can be caused by the in-plane inertia of the disc, and proposed that for a Finite Element analysis of a rotating bladed disc, the flexibility of the shaft and the rigid body motion of the disc should be taken into account. He demonstrated that such a structural model predicts the resonances of the experimental MIT rotor, even in the case of severe mistuning. Crawley and Hall, [25] 1985, and Crawley, [26] 1988, proposed a more systematic way of optimising the mistuning pattern by introducing a cost function, which is a measure of the difficulty of mistuning the rotor. Secondly, constraints which affect the stability margin of the rotor were also considered and then, finally, a numerical optimisation technique was applied to obtain the optimum rotor pattern from these two factors. Similar studies to theirs can also be found by Nissim, and Nissim and Haftka in 1985 [109, 110].

Dugundji and Bundas [27] (1984) used a standing wave method to study excitation effects on mistuned assemblies. They showed that the standing wave can be used as an alternative to the traditional travelling wave approach.

Bendiksen et al.

In 1984, Bendiksen [9] applied the perturbation method to study mistuning effects. This approach introduced a mistuning parameter which is a small factor to scale the assembly matrix so that small variations can be added to the perturbed mass or stiffness matrices. Bendiksen showed in his case studies that an alternately mistuned system is better than a randomly mistuned one for flutter control. However, he also concluded that a critical reduced frequency exists below which mistuning alone cannot stabilise the system. In 1986, Valero and Bendiksen further examined the effect of the blade-shroud interface by using the Finite Element method with mistuning effects [146]. They commented that the shroud interface angle has no influence on the mistuning effects, but mistuning gave evidence of lower frequency modes where the interblade coupling strength was relatively weak. Hence, they concluded that highly localised responses are most likely to occur in systems where mistuning is concentrated in relatively few elements.

Wei and Pierre [152,153] further used perturbation analysis in 1988 to investigate mistuned systems for both free and forced vibration. They

concluded that the mistuning effect is related to the internal coupling of the system. Weakly coupled assemblies are highly sensitive to small disorder, or mistuning, while strongly coupled systems respond in a similar way to the corresponding tuned system. This agreed with the results from Bendiksen et al. After these studies, friction damping has also been included in 1989 and much the same conclusion was drawn as before [154]. Moreover, their recent paper [155] showed the comparison of various statistical approaches to mistuned assemblies together with the use of a statistical perturbation analysis to mistuned assemblies. They concluded that the accuracy of the analytical statistics depended on the amount of mistuning and damping.

Muszynska & Jones

This branch of research concentrates mainly on the effects of the friction damping which exists in joints, or is deliberately introduced to the system at the blade platforms. In 1983, Muszynska and Jones described a bladed disc model which was based on a five-degree-of-freedom subsystem representing one section of the assembly [102–104]. This allowed factors such as the effects of blade mistuning, blade-to-disc and blade-to-blade nonlinear frictional damping, blade-to-blade stiffness coupling, and different types of excitation to be included. They divided the subject of mistuning into "classical" problems, due to the small variations of structural properties, and "non-classical" problems that contribute to the nonuniform interblade friction force, the excitation force, or the interblade excitation phase angle. They also defined a friction parameter which is the square root of the ratio of generalised friction force to the amplitude of the exciting force, and noted that "non-classical" mistuning may lead to significant variations of the response amplitudes and the related stresses as well [72,73].

MacBain et al.

Stange and MacBain set up an experimental project in 1983 to investigate a mistuned bladed disc that had two closely-spaced dual orthogonal modes [137]. Various combinations of steel or aluminium bolts, nuts and washers were added to a tuned disc to mistune it. The first few resonant modes of the bladed disc model were determined by using time-averaged holography. An analytical model of this case study was also completed by MacBain and Whaley in 1984 [92]. Conclusions were drawn that mistuning of the dual mode resulted in a maximum resonant response greater than, or equal to, that of the tuned system. The damping effect was directly related to mistuning. In the

same year, Jay, MacBain and Burns also reported both analytical and experimental work on blade responses due to vane interaction [70]. The test was done on an actual engine so that travelling wave excitations could be studied. They concluded that for a mistuned bladed disc, care must be taken as to where to place the strain gauges, since they showed that using a minimal number of gauges could lead to the unfortunate condition of locating a gauge on a nonresponsive blade.

Griffin et al.

A thorough study of the statistical aspects of mistuning was reported by Griffin and Hoosac in 1984 [50] and, for the first time, the resonant responses of a large number of bladed discs excited by different engine orders were calculated. Their results showed that maximum blade amplitudes occurred in blades whose blade-alone natural frequencies were nearly equal to a frequency at which the system would resonate if the blades were identical (that is, a tuned system frequency). For their 72-bladed system, an increase of stress factor of 2.18 was reported. Secondly, it was necessary to use engine data to infer the dynamic forces acting on the stage. Moreover, they found that the fatigue life of a mistuned disc is always shorter than that for the tuned disc. Finally, two schemes for reducing the consequences of mistuning were proposed; firstly, by sorting the blades by frequency into matched sets and secondly, by applying alternate mistuning.

The use of an aerodynamic code to compute the fluid coupling influence into the same model was continued by Basu and Griffin (1986), [8]. Conclusions were drawn to the effect that mistuning effects could be closely related to the engine order of excitation and the stiffness of the disc together with the number of blades. In 1988, Griffin [51] summarised the previous work done by this branch and commented that the analysis was useful to calibrate engine tests. It could be utilised to predict fleet durability so that potential vibration problems could be detected and corrected at an early design phase. More recently, Griffin has presented a report [52] on how to instrument the strain gauges for a blade from the stochastic analysis. In addition to a statistical analysis, Griffin and Sinha have reported studies on friction damper effects on mistuned bladed discs (1985) [49].

Analytical methods for a statistical approach to mistuning were presented by Sinha (1986) [130] who developed an approach based on the model used by Sinha and Griffin [129]. The analytical technique of statistics used by Sinha was a method used earlier by Huang [61, 62] to study the vibration of unsymmetrical structures. Sinha and Chen [131] used a higher-order algorithm, in 1989, to calculate the distribution of occurrences of the responses of a blade from a larger population. In the following year, they also included damping effects in the model [20]. However, this model was only applicable to bladed discs with closely-spaced blades.

Others

Other individuals working in the general area include: Ortolano, La Rosa and Welch (1981) [112] who studied a practical mistuned case of a low-pressure steam turbine wheel and discovered that by adopting a long arc shroud around the circumference the stress level caused by the first mode vibration due to mistuning could be significantly reduced. Irretier in 1982–83 [68, 69] published the results of a mistuning study by modified component mode synthesis. Gu and Gao (1987) [53] thought that a well-refined analytical method rather than a simplified model was essential for the study of mistuning in order to avoid all the conflicts arising from different researchers using different models. A component mode synthesis method was used. They commented that the maximum vibration amplitude could be varied if the degree of mistuning changed. Rzadkowski (1988, 1990, 1994) [122, 123, 1124] has examined the mistuning problem by using the Ritz method, analysing the disc by thick plate theory and the blade by beam theory. The distribution of the detuned blades around the disc could then be specified from the stress point of view. Wang and Yau (1990) [149] commented on the mistuning effects due to the interface damping between the shrouds. Vorobiev et al. applied Finite Element method to study mistuning effect of impellers, also in 1990 [147]. More recently, in 1991, Khader and Masoud [85], considered the mistuning effect to a bladed disc model supported by a flexible continuous shaft. They suggested that all the possible modes of the mistuned bladed disc were affected by the shaft motion, in contrast to the case of tuned systems, where only a limited number of modes were affected by the same motion. Other contributions in recent years include Kaneko, Mase Fujita and Nagashima who also present a new sensitivity method for mistuning studies [75].

1.3 OBJECTIVES OF THE NEW RESEARCH

1.3.1 Introduction

Nowadays, turbomachines are widely used in both civil and military applications. The above survey shows that many research projects on this particular aspect of turbomachinery have been undertaken in the past forty years. There are many studies of the structural dynamics of turbomachinery blades in order to increase the reliability and their performances. From these, the physical natures of tuned bladed assemblies are quite clear, but the consequences of mistuning are still not fully solved. After nearly thirty years since mistuning was first considered to have significant effect for bladed disc assemblies, the arguments of the published reports show that mistuning can be either an adverse or a beneficial effect to structural dynamics and aerodynamics respectively. Table 1.1 shows some typical findings of the blade resonance response levels increased as a result from blade mistuning.

Years	*Researcher(s)*	*No. of Blades N*	*Highest response/ Tuned Response*
1966	Whitehead	24 72	$\frac{1}{2}(1+\sqrt{\frac{N}{2}}) = \begin{cases} 2.23 \\ 3.50 \end{cases}$
1969	Dye and Henry	43	**2.44**
1969	Ewins	24	**1.21**
1975	El-Bayoumy and Srinivasan	24	**1.20**
1976	Srinivasan and Frye	116 72	**1.95** **1.64**
1984	Ewins and Han	33	**1.60**
1984	Griffin and Hoosac	72	**2.18**
1984	MacBain and Whaley		**1.20**
1988	Afolabi	30	**3.50**

Table 1.1

Although most of these values are numerical findings based on some mathematical model, these models can be made representative of some particular bladed disc configurations, and from these numerical figures, they

indicate that there are different points of view as to the extent of the effects of mistuning. Furthermore, there are arguments about which is the most critical blade on a mistuned rotor. The main objective of the project is to identify the factors which are causing or are affected by the mistuning in a bladed disc assembly. Accordingly, the following specific questions can be used as a summary of the objectives of this new research work.

1.3.2 Questions on the Objectives for the Project

The main outstanding questions concerning mistuning effects of bladed discs can be summarised as follows:

Q.1 *What is the effect of blade mistuning on forced vibration response?*
(i) What is the worst effect by a certain mistuned blade pattern?
(ii) What is the nature of "rogue blades"?

Q.2 *If blade mistuning causes significant changes than an otherwise tuned bladed disc, are there any factors which may directly affect the mistuning effects? Can these factors be used to avoid some blades being suffering from higher than tuned blade responses if mistuning problem happened in practice?*
(i) What is the disc coupling effect on blade mistuning?
(ii) What is the change of peak responses with different amount of mistuning levels?

Q.3 *How much worse will a mistuned bladed disc vibration response be than for a tuned system?*
How can this higher than tuned blade response level controlled in design?

Q.4 *Which blade will be mostly affected by mistuning?*
In practice, where should strain gauges be sited so as to get the most useful experimental results?

Q.5 *What is the optimum arrangement of a set of blades?*
(i) How much mistuning can be allowed for a fixed range of responses?
(ii) What should be the maximum stability? (For example: can the mistuning effects be used as a passive control towards flutter?)

In conclusion, the studies of mistuning effects are still required after 25 years. Since manufacturers would prefer to allow larger tolerances because of the high cost of machining, mistuning may well become even more significant in the field. Recently, these studies are turning to statistical approaches, which allow manufacturers to select a blade pattern from a large set of blades.

1.3.3 Preview of the Thesis

The contents of this thesis include investigations which seek some new understanding to mistuned bladed discs as well as presenting a closed-form probabilistic study for mistuned bladed discs. Finally, experimental techniques for the study of mistuned bladed discs are also examined and applied as a correlation to the numerical studies.

Chapter 2 shows some methods for numerical predictions of bladed disc characteristics with particular interest in introducing the energy method. This chapter also establishes the advantages and disadvantages of the different mathematical models which currently can be found in the literature, so that a suitable model can be selected for the studies in the rest of the chapters.

Chapter 3 reports a study of the mistuning effects of bladed disc systems by forced response vibrations. The simple lumped parameter model has been used so that stochastic simulation analysis can be applied for large number of bladed disc assemblies with mistuned blades on a particular rotor wheel. An investigation of arrangements of blades around a disc is also presented to show some optimal and critical conditions for a particular set of blades.

Numerical studies are also presented in chapter 4 using the direct simulation technique developed in chapter 3 to study the blade-disc coupling influence on the worst blade response under mistuning effects. Chapter 5 is an extension of the previous chapter showing the studies of the other class of mistuning, the damping mistuning effects.

Chapter 6 attempts to predict the mistuned blade response probability density (PDF) distribution via a probabilistic analysis. This study also tries to explain the profile of the response PDF as obtained from previous chapters in an analytical way.

Chapter 7 presents the experimental techniques used with mistuned bladed disc testpieces in an attempt to show correlation of the mathematical model and the experimentally measured results for a bladed disc assembly.

Finally, Chapter 8 concludes the work for the whole project and reviews the need for any further work in the subject.

CHAPTER 2

FREE VIBRATION ANALYSIS OF BLADED DISCS

About this chapter

This chapter describes a study of the different mathematical modelling techniques used in the past for solving bladed disc vibrations. There are many different mathematical techniques to model the dynamics of bladed disc assemblies. So far, two classes of model have been used to represent a bladed disc assembly for numerical analysis, namely: the continuous model and the discrete model. The difference between the two classes is that the mass of the structure is discretized and lumped for the latter case.

Furthermore, there are also different numerical methods developed in the past to model a bladed disc assembly based on either the continuous or the discrete model. This chapter describes some of the common methods used, including the closed-form receptance method, the energy method, the transfer matrix method and lumped parameter method. Finally, a tuned 30-bladed disc is used to test different mathematical methods to demonstrate the results from these methods so that one can compare the advantages and disadvantages for each of them. The comparisons of the methods base only on the free vibrations although all methods can be adapted for forced vibrations.

2.1 GENERAL INTRODUCTION

Since experimental work is usually expensive, the mathematical models have always been alternatives to rig tests for all the time. From the survey made in chapter 1 on the mistuned bladed disc vibrations, one can clearly observe that there are various mathematical methods with which to model the physical system of a bladed disc. Generally, mathematical models of bladed discs comprise two different classes, *discrete* and *continuous*. Each of these also consists of other different methods to implement the numerical procedures. In the past, some research workers concerned that the conflicting results in the studies of mistuned bladed discs might be due to some models used being over simplified [53]. Therefore, this chapter presents a study of some mathematical methods used to simulate bladed disc vibration.

Afolabi gave a general form to the equations of motion for a rotating bladed disc as follows, [3]:

$$[\mathbf{M}]\{\ddot{x}\} + ([\mathbf{C}] + \Omega[\mathbf{F}])\{\dot{x}\} + ([\mathbf{K}] + \Omega^2[\mathbf{E}] + j[\mathbf{D}])\{x\} + [\mathbf{A}(\omega,v)]\{x\} = \{f\} \qquad (2.1)$$

where,

[M], [C], [D], [K] are the mass, viscous and hysteretic damping, and stiffness matrix respectively,
[F] is the gyroscopic matrix,
[E] is the centrifugal stiffness matrix,
Ω is the engine running speed,
{f} is the external loading,
[A(ω,v)] is the aerodynamic coupling matrix,
ω is the excitation frequency and v is the fluid velocity.

By applying a harmonic transformation, equation (2.1) can be written as follows:

$$\{X\} = [\mathbf{H}]\{F\} \qquad (2.2)$$

where [H] is the dynamic flexibility or receptance matrix. However, the bladed disc structure is a very complicated system. The exact dynamic equations for practical bladed discs are not easy to obtain [5] because the structures are often too complicated to model. Some assumptions must be made to the numerical

model using the experience observed from rig tests. This may create limitations to a mathematical formulation. In the past, many of these mathematical models have been developed and tried by different researchers. The aim of this chapter is to compare the results using different methods to analyse a simple experimental 30-bladed disc.

2.2 CONTINUOUS MODELS

Theoretically, the analytical model applies to structures having continuously distributed mass and elasticity. Such structures possess an infinite number of degrees of freedom. The equations of motion of continuous systems can be derived either by force equilibrium (closed-form) or by the energy method.

2.2.1 Closed-form Receptance Coupling Method

This is one of the earliest numerical methods used for bladed disc vibration. A thorough description on the closed-form differential equations of beams and the receptance coupling method can be found from Bishop and Johnson [12]. Armstrong [5] was the first to apply this method to the vibrations of bladed discs. He used continuous beam theory (Bernoulli-Euler beam) to represent the turbine blades which were coupled to a disc through their receptances. Ewins, later [34], improved the model by adding a shroud around the bladed assemblies, and Cottney [21] further improved the coupling co-ordinates of a blade to 6-degrees-of-freedom and geometry nonuniformity could be modelled by using multi-stage beams with different dimensions. BLIPA is a commercial software based on this theory to calculate the natural frequencies of a perfectly tuned bladed disc [66]. This program has been used in this project to validate other numerical models and to demonstrate basic vibration characteristics of bladed discs.

2.2.2 Energy Methods (Modal Synthesis Techniques)

"Energy methods are based on the use of one or more of the energy principles of mechanics, e.g., conservation of energy, virtual work, Hamilton's principle, Lagrange's equations, etc.", [63]. Exact solution of the differential equations of elasticity and dynamics for complex structures presents a formidable analytical problem which can be solved in closed form only in simple geometrical cases. Furthermore, the rotation effects of bladed discs are also difficult to solve in an exact form. Energy equations are relatively easy to formulate and to solve. The rotation and centrifugal terms can also be added easily [16]. In the past, most

developments based on energy methods involved the Finite Element method, which is a general procedure to analyse engineering structures. However, there have been applications of energy methods in bladed disc vibrations [53, 77-79, 124]. The following formulation is the Rayleigh-Ritz method applying the modal functions of a Bernoulli-Euler beam and a circular disc as the displacement trial functions.

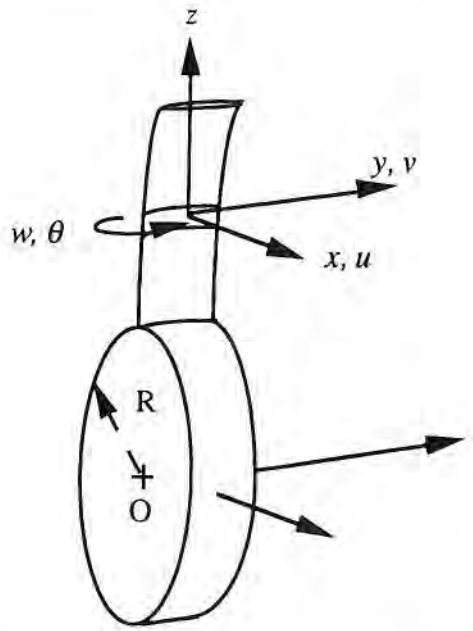

Figure 2.1 A bladed disc model

Figure 2.1 shows the coordinate system of the bladed disc, and the strain energy expression for the *i*th bending-bending-torsion coupled blade can be found as follows:

$$(U_b)_i = \frac{1}{2}\int_0^L \{ E_b I_{yy}\left(\frac{\partial^2 u}{\partial^2 z}\right)^2 + 2E_b I_{xy}\frac{\partial^2 u}{\partial^2 z}\frac{\partial^2 v}{\partial^2 z} + E_b I_{xx}\left(\frac{\partial^2 v}{\partial^2 z}\right)^2 + GJ\left(\frac{\partial \theta}{\partial z}\right)^2 \} dz \qquad (2.3)$$

The strain energy for the bending mode of the disc can also be expressed as follows:

$$(U_d) = \frac{D}{2}\int_0^{2\pi}\int_0^R \{\left(\frac{\partial^2 u2}{\partial^2 r} + \frac{1}{r}\frac{\partial u}{\partial r} + \frac{1}{r^2}\frac{\partial^2 u}{\partial^2 \psi}\right)^2 - 2(1-\upsilon)^2\frac{\partial^2 u}{\partial^2 r}\left(\frac{1}{r}\frac{\partial u}{\partial r} + \frac{1}{r^2}\frac{\partial^2 u}{\partial^2 \psi}\right)$$
$$+ 2(1-\upsilon)\left(\frac{\partial}{\partial r}\frac{1}{r}\frac{\partial u}{\partial \psi}\right)^2 \} r\, dr\, d\psi \qquad (2.4)$$

The kinetic energy of the ith blade can also be written as follows:

$$(T_b)_i = \frac{1}{2}\int_0^L \rho A\,[\dot{u}^2 + \dot{v}^2]\,dz + \frac{1}{2}\int_0^L \rho I_p\,\dot{\omega}^2\,dz \qquad (2.5)$$

The kinetic energy of the disc is as follows:

$$(T_d) = \frac{1}{2}\int_0^{2\pi}\int_0^R \rho h\,\dot{u}^2\,r\,dr\,d\psi \qquad (2.6)$$

Hence, the total energy of the system can be defined as follows:

$$U = (U_d) + \sum_{i=1}^{N}(U_b)_i \quad ; \quad T = (T_d) + \sum_{i=1}^{N}(T_b)_i \qquad (2.7)$$

where N is the total number of blades on the disc.

However, an exact solution of the energy equation is unobtainable and so an approximate solution provides the alternative way. The choice of trial functions decides the structural model. If, however, a spline function is used, the Finite Element model is formulated and, of course, discretization and refinements are required to improve the accuracy of the result. Here, the uniform mode function of bending and torsion of a beam and the bending mode function of a uniform flat disc are used as the trial functions. The bending mode shapes of a uniform cantilever beam can be written as follows:

$$\Phi_n = \cosh(\gamma_n z) - \cos(\gamma_n z) - Q_n[\sinh(\gamma_n z) - \sin(\gamma_n z)] \qquad (2.8)$$

where $Q_n = \dfrac{\cosh(\gamma_n l) + \cos(\gamma_n l)}{\sinh(\gamma_n l) - \sin(\gamma_n l)}$ and n are the mode numbers.

The constant $\gamma_n l$ can be deduced from the following condition:

$$\cosh(\gamma_n l)\cos(\gamma_n l) - 1 = 0 \qquad (2.9)$$

The torsional mode shape of a cantilever beam can be written as follows:

$$\vartheta_n = C\sin(\varphi_n z) \tag{2.10}$$

for $\varphi_n l = \frac{2n-1}{2}\pi$ and C is a constant

The radial-bending mode shape for a free-free flat disc can be found as follows, [95]:

$$\chi_n(r) = J_n(\kappa_n r) - c\, I_n(\kappa_n r) \tag{2.11}$$

where

$$c = \frac{(\kappa_n R)^2 J_n(\kappa_n R) + (1-\upsilon)[(n-n^2)J_n(\kappa_n R) - (\kappa_n R)J_{n+1}(\kappa_n R)]}{(\kappa_n R)^2 I_n(\kappa_n R) + (1-\upsilon)[(n-n^2)I_n(\kappa_n R) + (\kappa_n R)I_{n+1}(\kappa_n R)]}$$

and I_n, J_n are the Bessel functions and κ_n is a disc frequency parameter, which are the roots of the following equation:

$$\frac{(\kappa_n R)^2 aa + n^2(1-\upsilon)cc}{(\kappa_n R)^2 bb - n^2(1-\upsilon)dd} = 0 \tag{2.12}$$

with

$$aa = nJ_n(\kappa_n R) - (\kappa_n R)J_{n+1}(\kappa_n R)$$
$$bb = nI_n(\kappa_n R) + (\kappa_n R)I_{n+1}(\kappa_n R)$$
$$cc = (n-1)J_n(\kappa_n R) - (\kappa_n R)J_{n+1}(\kappa_n R)$$
$$dd = (n-1)I_n(\kappa_n R) + (\kappa_n R)I_{n+1}(\kappa_n R)$$

However, these displacement functions represent only the substructure displacements of the blading and the disc. The integrated displacement function involves the coupling between the blades and the disc. This requires some extra conditions to describe the junction boundary conditions between the blade roots and the disc rim. A detailed account of substructure coupling can be found from the report by Craig and Chang [23]. Hurty's method of fixed interface coupling technique is used here. This coupling effect, mathematically, must satisfy the compatibility and equilibrium conditions at all the junction coordinates between the blades and the disc as follows:

$$(u_{\text{blade root}})_i = (u_{\text{disc rim}})_i \tag{2.13a}$$
$$(F_{\text{blade root}})_i + (F_{\text{disc rim}})_i = 0 \tag{2.13b}$$

Therefore, the trial function of a blade must satisfy the boundary conditions as shown in Equations (2.13). This requires an extra boundary coordinate q_{cc}

which is equal to the disc rim deflection. For convenience, the bladed disc function at disc rim can be approximated using a single quadratic shape for axial deflection of the disc. For all possible nodal diametral modes, one can define the displacement for the bladed disc junction as follows:

$$u_d = \left(\frac{r}{R}\right)^2 \cos(n\phi)\, q_d \tag{2.14}$$

By considering the displacement and slope continuity at the junction, the function, which satisfies the boundary conditions, was used by Kaza and Kielb [79] as follows:

$$\chi_{cc} = (1 + 2\,z\frac{L}{R})u_d \tag{2.15}$$

The displacements are hence equated to a modal coordinate based Ritz function as follows:

$$u = \sum_{i=1}^{m_1} \Phi_i\, q_i \exp(j\phi) \tag{2.16a}$$

$$v = \sum_{i=1}^{m_2} \Phi_i\, q_i \exp(j\phi) + \chi_{cc} q_{cc} \tag{2.16b}$$

$$\theta = \sum_{i=1}^{m_3} \vartheta_i\, q_i \exp(j\phi) - \frac{\partial \chi_{cc}}{\partial \psi} q_{cc} \tag{2.16c}$$

where m_1, m_2 and m_3 are the numbers of modes required,

cc indicates the coupling boundary between the blades and the disc,

$\phi = \frac{2\pi i}{N}$, and

$j = \sqrt{-1}$

For a cyclically symmetric structure, there are normally $\left(\frac{N}{2} + 1\right)$ nodal patterns for an odd number of blades, N, and $\frac{N}{2}$ nodal patterns for an even number of

blades. Furthermore, there are $\left(\frac{N}{2}-1\right)$ of double modes if the number of blades is even and $\left(\frac{N-1}{2}\right)$ double modes if the number of blades is odd.

By substituting the displacement functions into the energy equations and then using the Lagrange equation, a set of equations of motion is formed as follows:

$$[\mathbf{M}]\{\ddot{q}\} + [\mathbf{K}]\{q\} = \{0\} \tag{2.17}$$

This method is a general Rayleigh-Ritz method (or simply 'the Ritz method' as referred to in many Eastern European references), and the solution of these equations can be obtained by solving the standard eigenvalue problem. Although, equation (2.15) shows the free vibrations of a bladed disc, the forced vibration response can also be formulated by the Rayleigh-Ritz method [53]. Normally, the blade tip displacement is more desirable and can be found by transforming the modal coordinates using the known mode shapes.

2.3 DISCRETE MODELS

Discrete models are based on the discretization of a complex structure into small sub-elements where each sub-element consists of lumped masses connected by some elastic elements. One numerical technique is the transfer matrix method or the Myklestad-Prohl-Thomson method [105, 106, 114, 141].

2.3.1 Transfer Matrix Method (Myklestad-Prohl-Thomson Method)

The original ideal for this method was due to Holzer for the prediction of torsional natural frequencies of shafts. Myklestad, in 1947, showed that the bending of a beam could also be discretised into lumped masses connected by massless elastic bars [105, 106]. Coincidentally, Prohl independently reported a similar method at about the same time [114]. However, this new technique involved quite a lot of tedious algebraic expressions, especially when the number of discretizations is large and at that time calculations were only performed by desk calculators. This problem was not solved until Thomson, in 1950 [141], showed that the properties of each section or station could be expressed in matrix form. Since then, the name 'transfer matrix' appeared in literature. Ehrich, in 1956, further modified the method to circular disc vibrations [29], and in 1975, El-Bayoumy and Srinivasan applied the disc transfer matrix coupled with single-degree-of-freedom oscillators as blades and

studied the effects of blade mistuning [30]. Huang in 1980 [61] presented a paper on shrouded bladed disc vibration by the transfer matrix method. However, this method was not a very popular tool for the analysis of bladed disc vibration, although it is rather effective in rotor dynamics studies. One reason is that very fine discretization is needed to obtain good accuracy and normally computation time is long. Nevertheless, the idea of discretization has been transferred and combined with other methods by some researchers. For example, Cottney discretized a blade into several beam elements and a disc into several annulus, and then coupled all the closed-form receptances of each substructure to formulate the system receptance properties [21].

2.2.2 Lumped Parameter Models

However, the most popular discrete model is probably the mass-spring-damper model. One of the early attempts to simulate mistuning cases on bladed disc assemblies was the model developed by Dye and Henry in 1969 [28]. In their model, each blade was represented by a lumped mass on top of a massless spring attached to a trolley. The frictionless trolleys linked through elastic springs represented sectors of the disc. This model was later modified further by Afolabi [1] to include the effects of shrouds around the blades by adding an extra mass and an extra spring to connect these masses.

The parameters of the model can be identified if the modal properties of each substructure are known. The blade can be represented by a cantilever beam and can be considered as a single-degree-of-freedom oscillator as shown in Figure 2.2.

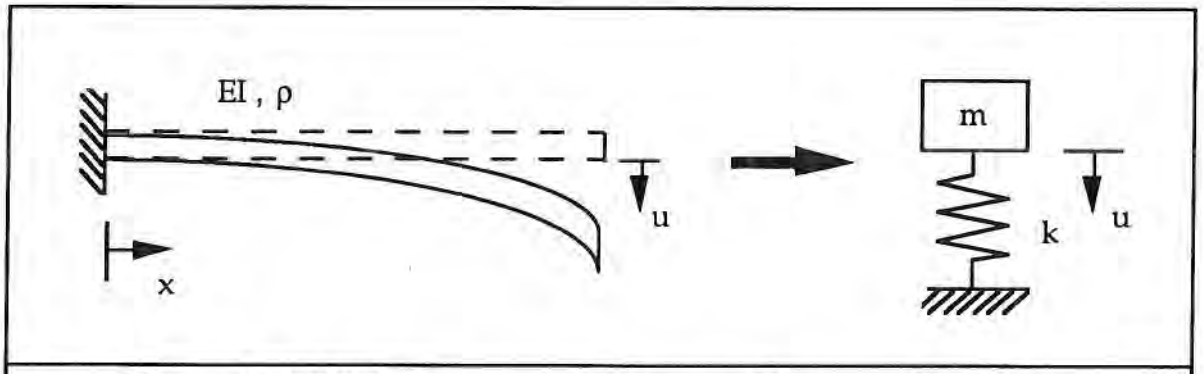

Figure 2.2 SDOF system representing a uniform cantilever beam

The bending equation of motion of a continuous cantilever beam can be written as follows:

$$\frac{\partial^2}{\partial^2 x}\left(EI\frac{\partial^2 u}{\partial^2 x}\right) = \rho A \frac{\partial^2 u}{\partial^2 t} \tag{2.18}$$

The exact solution for the natural frequencies of the cantilever beam from this partial differential equation are as follows:

$$\omega_n = f_n\sqrt{\frac{EI}{\rho A l^4}}\ ; \qquad f_n = 3.5156,\ 22.0336 \text{ etc.}$$

The natural frequency of the mass-spring system is then given as follows:

$$\omega^2 = \frac{k}{m} \tag{2.19}$$

By considering only one particular beam mode, and by analogy between the continuous beam and the mass-spring model, one can find the following relationship,

$$\omega^2 = \frac{k}{m} = f_n'\frac{3EI}{\rho A l^4} = f_n'\frac{3EI/l^3}{\rho A l} \tag{2.20}$$

From equation (2.20), it can be identified that $\frac{3EI}{l^3}$ is the blade tip static stiffness of a cantilever beam, and ρAl is the mass of the beam. The factor f_n' is equal to $\frac{f_n^2}{3}$ which depends on the mode of vibration and boundary conditions. For the first bending mode of uniform cantilever beam, f_1' is approximately equal to 4.12.

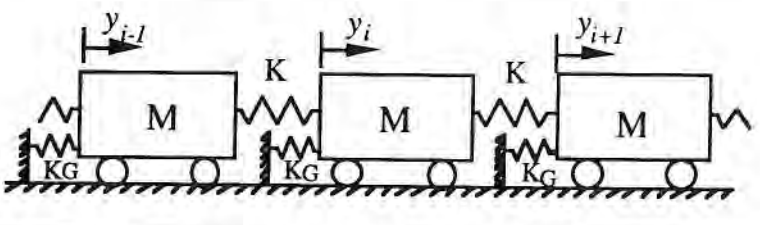

Figure 2.3 Mass-spring model for disc-alone assembly

The disc parameters can be identified in a similar way. The disc can be divided into N sectors [28]. Each portion will contain a blade as shown in Figure 2.3.

The equation of motion of the mass-spring system for the disc-alone vibration can be written as follows, [1]:

$$K_G + 2K\left(1 - \cos\left(\frac{2\pi r}{N}\right)\right) - \omega^2 M = 0 \qquad (2.21)$$

where r is an integer representing a particular number of nodal diameters. The stiffnesses of K_G and K are the static stiffnesses of a circular disc. The equation of the dynamic characteristic of a circular disc is then required to convert the static parameters to dynamic ones. The governing equation of a thin vibrating plate can be written as follows:

$$D\nabla^4 u + \rho_d h\ddot{u} = p_d(x,y,t) \qquad (2.22)$$

and the frequency parameter for free vibration has the form as follows:

$$g_n^2 = \frac{\rho h \omega_n^2}{D} \qquad (2.23)$$

or

$$\omega_n^2 = g_n^2 \frac{D}{\rho h} = g_n^2 \frac{K_e}{M} \qquad (2.24)$$

where g_n is the frequency parameter which depends upon the mode of vibration, the boundary conditions of the disc and the material property of the Poisson's ratio. For a free-free steel disc, g_n equals 2.32 for the 0 circle 2 diameter mode, 3.54 for the 0 circle 3 diameter mode, etc. see Prescott [117]. The stiffness K_e is the equivalent static stiffness of the disc and has the form as follows:

$$K_e = K_G + 2K\left(1 - \cos\left(\frac{2\pi r}{N}\right)\right) \qquad (2.25)$$

It should be noted that the stiffness K_G is only a small value that prevents the rigid body motion of the disc and hence, for simplicity, K_G can be neglected when evaluating K. This is true because the stiffness K_G does not affect the dynamic characteristics of the system. The static deflection for a circular disc may be found from Roark's formula [166] which is written as follows:

$$NK = \frac{P}{\delta} = \frac{16\pi D(3+\upsilon)}{R^2(1+\upsilon)} \tag{2.26}$$

The parameter M can be found by dividing ω_n by the corresponding g_n and then substituting into equation (15) as follows:

$$\left(\frac{\omega_n}{g_n}\right)^2 = \frac{K_e}{M} = \frac{K_G + 2K\left(1 - \cos\left(\frac{2\pi r}{N}\right)\right)}{M} \tag{2.27}$$

The coupled system parameters can then be found by using the blade-alone and the disc-alone parameters. Figure 2.4 shows the slightly modified model which has been used by Yiu for parametric studies [164].

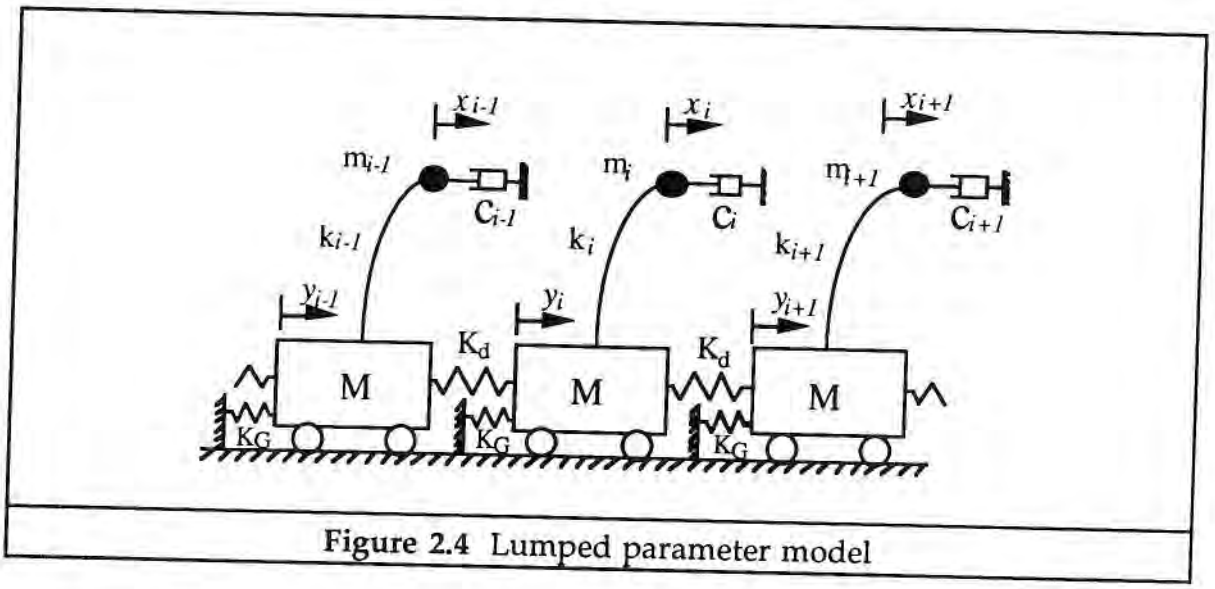

Figure 2.4 Lumped parameter model

The kinetic energy of the two subsystems is shown as follows:

$$T = (T_d) + (T_b)_j = \frac{1}{2}(m_j\dot{x}_j^2 + M_j\dot{y}_j^2) \tag{2.28}$$

The potential energy of the two subsystems is shown as follows:

$$U = (U_d) + (U_b)_j = \frac{1}{2}k(x_j - y_j)^2 + \frac{1}{2}K(2y_j - y_{j-1} - y_{j+1})^2 + \frac{1}{2}K_G y_j^2 \tag{2.29}$$

The damping dissipation energy D of the two subsystems is shown as follows:

$$D = \frac{1}{2}c_j\dot{x}_j^2 \tag{2.30}$$

The static forces at the connection point of the two subsystems must be balanced, i.e.

$$kx_j + K(2y_j - y_{j-1} - y_{j+1}) = P \tag{2.31}$$

Substitute into the Lagrange equation as follows:

$$\frac{\partial}{\partial t}\left(\frac{\partial T}{\partial \dot{q}}\right) - \frac{\partial T}{\partial q} + \frac{\partial D}{\partial \dot{q}} + \frac{\partial U}{\partial q} = Q + \Gamma\frac{\partial P}{\partial q} \tag{2.32}$$

where Γ is the Lagrange multiplier. From the constraints, the coupled system must satisfy the condition of equation 2.31. Hence, the coupled equations of motion for the lumped mass-spring system as shown in Figure 2.4 can be written in matrix form as follows:

$$[M]\{\ddot{x}\} + [C]\{\dot{x}\} + [K]\{x\} = \{f\} \tag{2.33}$$

The greatest benefit of a lumped parameter model is in performing a forced response analysis. Many numerical results by using the lumped mass model can be found in references [50, 125]. The dynamic behaviour of a bladed disc can be more generally represented by lumping more masses on each blade.

2.4 THE FINITE ELEMENT METHOD

The finite element model is a piecewise continuous model, which applies the energy theory as mentioned in section 2.1.2 but discretized over the geometrical domain [167]. An admissible spline function is used as the trial function which defines the physical co-ordinates as follows:

$$u = \sum_{k=1}^{node} S_i u_i; \qquad v = \sum_{k=1}^{node} S_i v_i; \qquad \theta = \sum_{k=1}^{node} S_i \theta_i \text{ etc.}$$

where S_i are the shape functions and node is the number of nodes per element. Each shape function is a set of polynomials used to interpolate the geometric shape which can be selected by the user as beam, plate, shell or brick elements etc. In this way, one approximates the solution by some lower order trial functions. The accuracy can be improved by refining the discretized elements.

However, the Finite Element method can model some complicated structures in great detail, such as modern turbine blades which are no longer simple twisted beams or plates, but solid elements.

The Finite Element method usually sets up a large matrix with many degrees-of-freedom to solve due to the domain discretization. As a result, the direct use of Finite Elements to mistuned bladed disc problems is not very common. Normally, component mode synthesis is used so that the whole structure is sub-divided into many substructures which can be easily analysed by Finite Element analysis. Characteristics of the whole bladed disc are then determined through component mode coupling of the substructures (see reference [69]). However, the finite element method has the advantage of being more adaptable to complicated geometrical structures.

2.5 EXPERIMENTAL TEST - Hammer Test

Experimental modal analysis (or Modal Testing) refers to the process of extracting modal parameters from test measurements, and hence of obtaining a modal model of the tested structure. The modal model is one which consists of two sets of properties: one containing the natural frequencies and damping factors of the modes included, and a second one which describes the shapes of the corresponding modes. In order to derive a modal model referred to a particular set of n coordinates, one needs to measure and analyse a set of n FRF (Frequency Response Function) curves, all sharing either the same 'reference' excitation point or response point. The minimum requirement is either one row or one column of the full FRF matrix $[\mathbf{H}(\omega)]$, [42]. In this test, a row of FRFs was obtained by fixing the accelerometer but changing the position of the force. A row vector of the matrix $[\mathbf{H}(\omega)]$ can be found as follows:

$$H_{ij}(\omega) = \sum_{r=1}^{N} \frac{{}_rA_{ij}}{\omega_r^2 - \omega^2 + i\eta_r\omega_r^2} \qquad (2.34)$$

ICATS® is a commercial modal analysis software package [64] which uses the measured FRFs to find the natural frequencies, the modal damping factors, and the modeshapes. The facilities, in the program MODENT, can use either line-fit or circle-fit on a FRF to find the natural frequencies and the modal damping factors mode by mode. The facilities, such as GLOBAL-M or GRF-M, can analyse multiple FRFs and to produce the modeshapes [64]. However, it is

useful to notice that the numerator of expression (2.34) is the modal constant (${}_rA_{ij}$) and the denominator is made up of the natural frequency (ω_r) and the damping factor (η_r). With the data from the FRF, one can calculate the value of the modal constant of each mode. The eigenvector can be used to construct the modal constant which is made up from the mode shape amplitudes of the structure at the points where the force and the response were measured. This is represented by the expression shown as follows:

$$ {}_rA_{ij} = ({}_r\phi_i).({}_r\phi_j) \tag{2.35}$$

The modeshapes can then be animated by using the post-processing software, MODESH, which reads the eigenvalues and eigenvectors file (.EIG) created by MODENT. In animated modeshapes, the nodal diameter (ND) pattern can be clearly identified.

One common way to find the free vibration modes of a structure is by hammer or impact testing. In this experiment, the analyser used was a B&K 2032 FFT Analyser. Figure 2.5 shows the set-up of the apparatus for the hammer test. A modal testing kit including a hammer, a B&K force gauge, and a B&K accelerometer was used. The frequency range covered during the tests was 0-400 Hz. This range was chosen so that all the first family of bladed disc modes of vibration could be found. The analyser was then set to apply an exponential window on the accelerometer time signals and the FRF data from the analyser was transferred to an ASCII file on a personal computer (PC) by using MODACQ though the link of the GPIB interface.

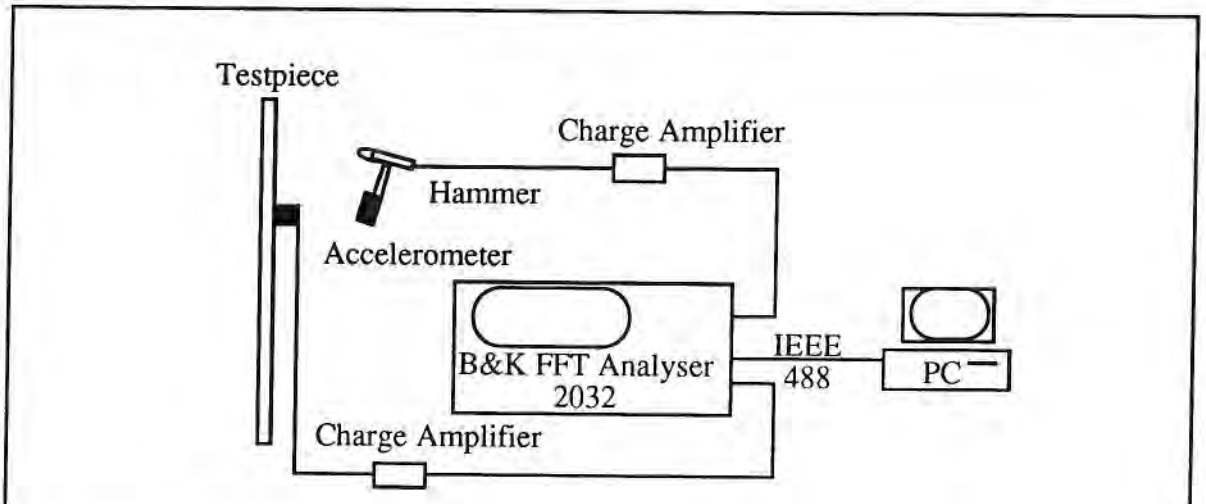

Figure 2.5 Experimental set-up for hammer test

The hammer test measured the frequency response functions (FRF) for all the blades by doing the measurement on each blade around the rotor while fixing the accelerometer at one position. Then, the analyses from the modal analysis program give the modal characteristics of the bladed disc. Table 2.1 shows the natural frequencies and modal damping factors found from the test on the 30 bladed disc.

Modes	Natural frequency (Hz)	Damping factor (%)
2 ND	103.30	1.87
3 ND	163.00	1.16
4 ND	194.57	0.96
5 ND	211.68	0.90
6 ND	221.94	0.84

Table 2.1 Some results from hammer test on the 30 bladed disc

2.6 RESULTS AND DISCUSSION

There are several computer programs used or developed in this study. BLIPA is a program based on the closed form receptance method developed by Armstrong and Ewins to analyse the vibrations of bladed discs. The program was originally written by Cottney [21] but updated by Imregun and others [66]. A new computer program has been coded in this project for the Rayleigh-Ritz method and results were obtained. Finally, a commercial Finite Element package is used. ANSYS® is a well-known commercial package of the Finite Element method used world-wide. This package also provides options such as the modal cyclical symmetric for solving problems such as a bladed disc [140].

Numerical studies from these programs are compared by using a 30 bladed disc with simple geometry. The blades are made with uniform rectangular cross sections and the disc is a uniform flat circular plate. The overall dimensions of the bladed disc are shown in Table 2.2. Numerical results are obtained by different numerical methods, as mentioned above, to find the free vibration characteristics of blade-alone, disc-alone and bladed discs.

Number of blades (N): 30

Blade dimensions
length (l) = 0.2 m width (w) = 0.0173 m thickness (t) = 0.0127 m

Disc dimensions
radius (R) = 0.2626 m thickness (t) = 0.0127 m

Young's modules for steel (E) = 207 GPa
specific density = 7.85
Poisson's ratio (υ) = 0.287

Table 2.2 Bladed disc dimensions and material properties

2.6.1 Blade Vibrations

Blade-alone vibration characteristics can be considered as those of a beam-type structure with its root cantilevered. The 30 bladed disc is made of uniform straight beams and a uniform flat disc. The blade dimensions and properties can be found from Table 2.2. Table 2.3 shows a comparison of the results using the different analyses for the bending modes of the cantilever beam.

The results from BLIPA can be regarded as solutions of exact form. Errors from computation can therefore be considered very small. The ANSYS® Finite Element model used ten 2-node beam elements, and each node has 6-degrees-of-freedom. The relative errors can be seen to vary from 0.2% in the first mode up to 1.26% for the third mode. However, the Rayleigh-Ritz method can be found with good comparisons to the exact values.

Modes	BLIPA (Hz)	ANSYS (Hz)	Rayleigh-Ritz (Hz)
1F	263.9	263.2	263.4
2F	1651.5	1641.7	1650.5
3F	4625.5	4563.9	4621.6
1E	358.8	358.2	358.8
2E	2248.4	2226.1	2248.4

Table 2.3 Comparison results from BLIPA, ANSYS and Rayleigh-Ritz method of a uniform beam

2.6.2 Beam Taper Effects

The geometry of a turbomachine blade is complex, often with effects of taper, twist and stagger. Apart from the Finite Element Method, which can model the geometry of the structure in great detail by discretization, an approximate technique is required for the remaining mathematical models. BLIPA divides each blade into several uniform sections. Each uniform section can have different dimensions such as cross section or length. This allows one to approximate a tapered beam by using a stepped beam. A comparison of BLIPA results with Finite Element and experimental ones can be found from Visser [156].

The Rayleigh-Ritz method can approximate these effects by the technique of geometrical mapping transformation. This technique applies a linear mapping transformation, such as the cross sectional properties of the beam, as shown as follows:

$$I = I_0(1 - \alpha z)(1 - \beta z)^3; \qquad A = A_0(1 - \alpha z)(1 - \beta z) \tag{2.36}$$

where α and β are the width and breadth parameters of the beam respectively. These properties are then transformed from the physical coordinates (x,y,z) to a computational domain (ξ,η,ζ) which consists only of a simple geometrical shape. This transformation theory is usually based on volumetric consistency for a continuum, such that an infinitesimal volume as shown in Figure 2.6 can be expressed as follows:

$$d(\text{volume}) = dxdydz = |\mathbf{J}|\, d\xi d\eta d\zeta \tag{2.37}$$

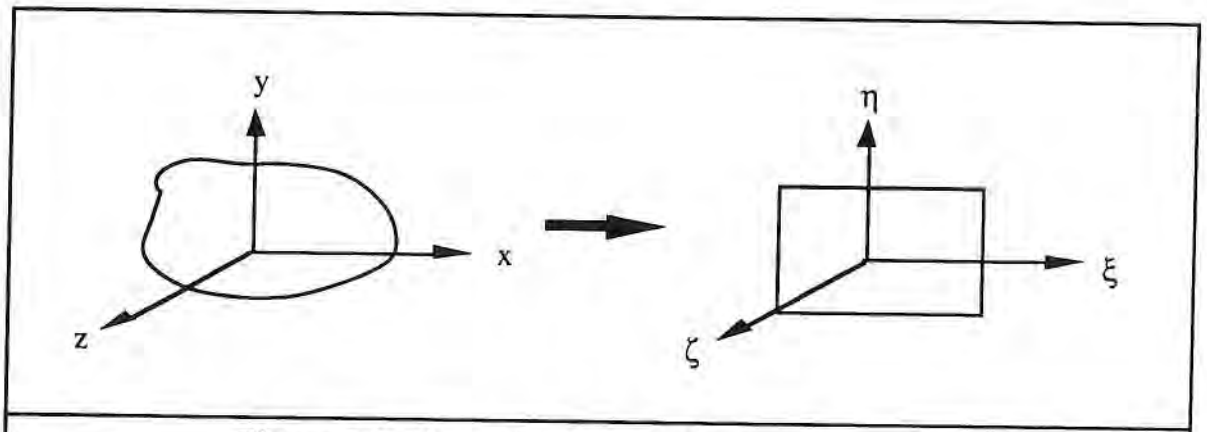

Figure 2.6 Geometrical mapping transformation

for which J is the Jacobian with the form as follows:

$$J = \begin{pmatrix} \frac{\partial x}{\partial \xi} & \frac{\partial x}{\partial \eta} & \frac{\partial x}{\partial \zeta} \\ \frac{\partial y}{\partial \xi} & \frac{\partial y}{\partial \eta} & \frac{\partial y}{\partial \zeta} \\ \frac{\partial z}{\partial \xi} & \frac{\partial z}{\partial \eta} & \frac{\partial z}{\partial \zeta} \end{pmatrix} \tag{2.38}$$

$\alpha = \beta$	Martin [94] (Rayleigh-Ritz with polynomials)	Rao [119] (Galerkin method with polynomials)	Rayleigh-Ritz (using uniform beam modes)
0.1	1.045	1.056	1.045
0.2	1.095	1.119	1.096
0.3	1.150	1.198	1.157
0.4	1.211	1.295	1.228
0.5	1.278	1.420	1.316
0.6	1.349	1.580	1.425
0.7	1.427	1.791	1.567
0.8	1.509	2.075	1.763
0.9	1.597	2.460	2.050
1.0	1.690	2.958	2.481

Table 2.4 Comparison of taper effect results for the fundamental mode

The results from the Rayleigh-Ritz method are compared with those of Martin [94] and Rao [119]. Martin applied a polynomial function as the assumed mode deflection for the Rayleigh-Ritz method, while Rao used the Galerkin method with a polynomial as the weight function. Table 2.4 shows the comparison of the ratios between the natural frequencies of tapered beams and the natural frequencies of a uniform beam (with $\alpha = \beta = 0$), which is defined as follows:

$$\omega_n = f_n \sqrt{\frac{EI_o}{\rho A_o l^2}} \qquad f_n = 3.5156,\ 22.0336 \text{ etc.}$$

Next, higher order modes (with $\alpha = 1$ and $\beta = 1$) are also compared and the results from the Rayleigh-Ritz method show good agreement with the exact values given by references [150] and [160].

mode of vibration	Martin (Rayleigh-Ritz with polynomials)	Exact value (Ward and Wrinch [150,160])	Rayleigh-Ritz (using uniform beam modes)
1	1.6900	2.4800	2.4807
2	0.7602	0.9599	0.9698
3	0.5516	0.6242	0.6659
4	0.5021	-	0.5771
5	0.4777	-	0.4195

Table 2.5 Comparison of higher modes of tapered beam

Again, from Table 2.5, the results obtained from the Rayleigh-Ritz method using uniform beam modes show good agreement with the exact values. Finally, it should be noted that the actual geometry of the turbomachine blades is far more complicated than that of tapered beams. More accurate results require the solution from a Finite Element analysis. However, tapered beams may be used for compressor blades and some of the turbines for parametric studies. The computational effort is much smaller for the Rayleigh-Ritz method using uniform beam modes than for a Finite Element analysis.

2.6.3 Blade Tip Responses

The tip receptance (or the frequency response function) of a uniform cantilever beam has the closed-form solution described by Bishop and Johnson as follows:

$$H_{ll} = \frac{\cos(\lambda l)\sinh(\lambda l) - \sin(\lambda l)\cosh(\lambda l)}{EI\lambda^3[\cos(\lambda l)\cosh(\lambda l) + 1]} \qquad (2.39)$$

where $$\lambda = [\frac{\omega^2 A\rho}{EI}]^{1/4}$$

The lumped mass model of the beam already has its characteristics at the blade tip. Therefore, the tip receptance of the beam model shown in Figure 2.2 has the form as follows:

$$H = \frac{1}{\sqrt{k - \omega^2 m}} \qquad (2.40)$$

However, the Rayleigh-Ritz method solves the equations of motion in the principal domain. In this case, a transformation of coordinates is required for finding the tip receptance on the blade. This transformation can be done on the equations of motion so that the eigenvectors correspond to the tip coordinates as follows:

$$[\Phi(l)]^T[M][\Phi(l)]\{\ddot{u}_t\} + [\Phi(l)]^T[K][\Phi(l)]\{u_t\} = \{0\} \tag{2.41}$$

where $[\Phi(l)]$ is the transformation matrix according to the tip coordinate.

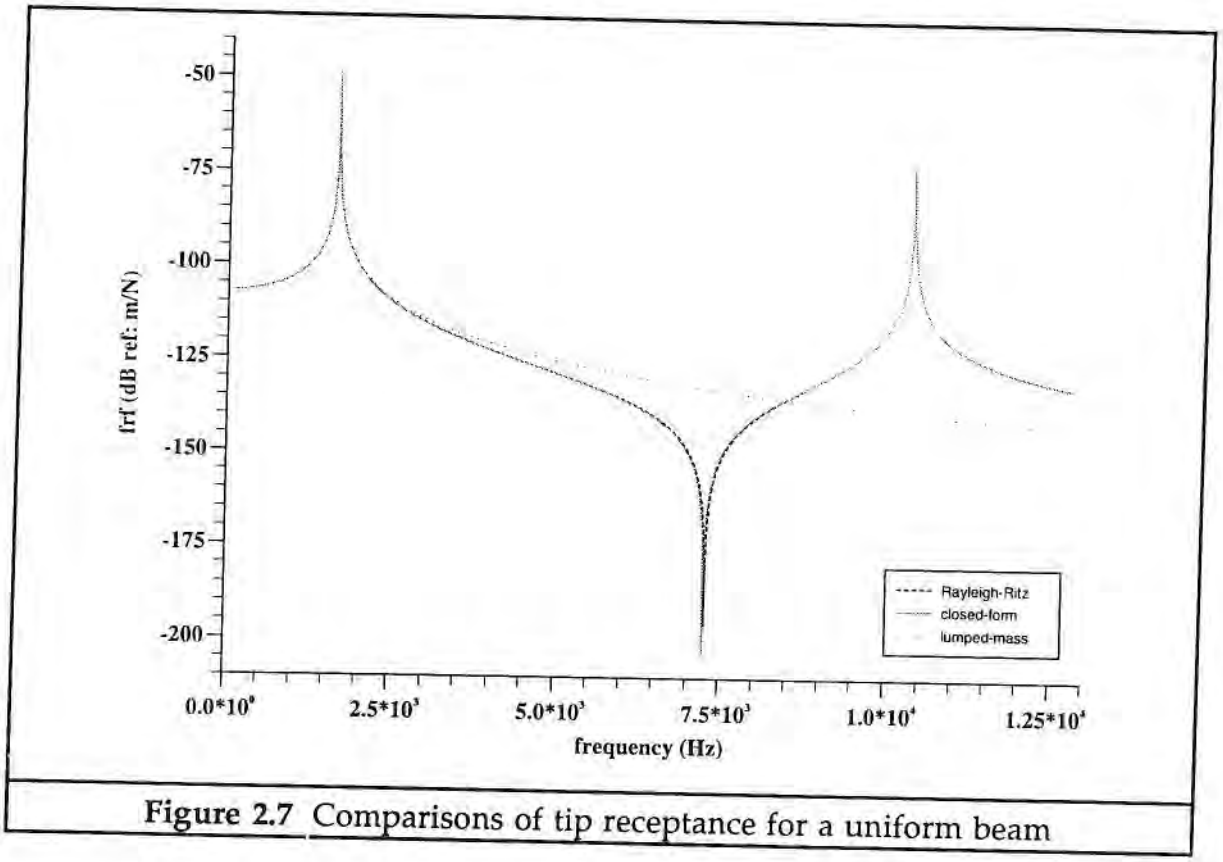

Figure 2.7 Comparisons of tip receptance for a uniform beam

Figure 2.7 shows the comparisons of different methods on the tip receptances of a uniform beam. Obviously, the SDOF lumped parameter model can only approximate one mode since it has only one degree of freedom. This study is very useful in the sense of showing the limitations from the lumped parameter model. However, the accuracy for a particular mode is good and if one is only interested in this mode, this model can be representative to the problem.

2.6.4 **Disc Vibrations**

Disc-alone vibrations have also been studied here. These studies include the exact solution from BLIPA, the Rayleigh-Ritz method and the Finite Element analysis.

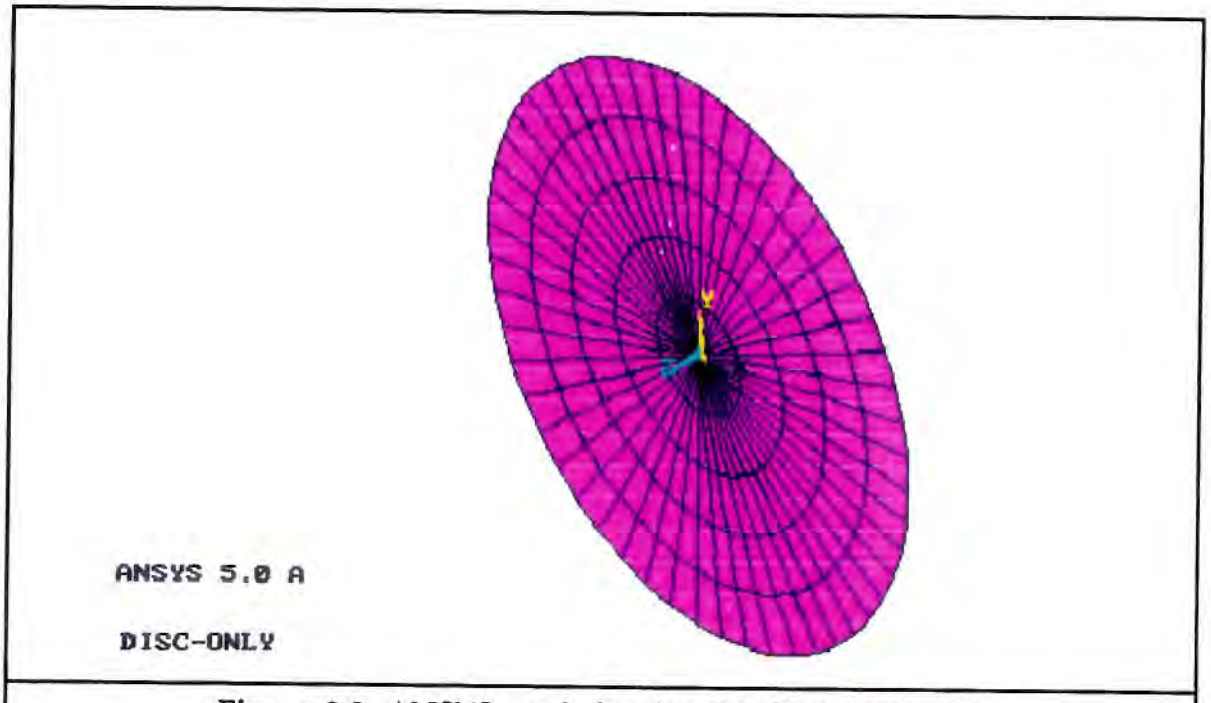

Figure 2.8 ANSYS mesh for the disc (8-node shells)

The Finite Element results were obtained from the general purpose program, ANSYS. The mesh shown in Figure 2.8 is the disc geometry using the 8-node shell element. The boundary condition of disc used for the analysis is a free-free and uniform flat circular plate with dimensions shown in Table 1. For the Rayleigh-Ritz method, the trial function used for the disc is the mode function for a free-free uniform circular disc as shown in equation (2.11).

Nodal diameter	BLIPA	Rayleigh-Ritz	ANSYS (shell)
2	246.727	253.718	242.9
3	572.149	587.508	558.8
4	1003.687	1035.514	971.5
5	1538.877	1596.196	1475.1
6	2175.864	2268.287	2063.5
7	2913.289	3050.841	2731.2

Table 2.6 Comparison of natural frequencies of the disc (Hz)

Table 2.6 shows some numerical values of the first family disc modes evaluated from using different methods. Figure 2.9 plots these modes by comparing both BLIPA, the Rayleigh-Ritz method and the ANSYS Finite Element method.

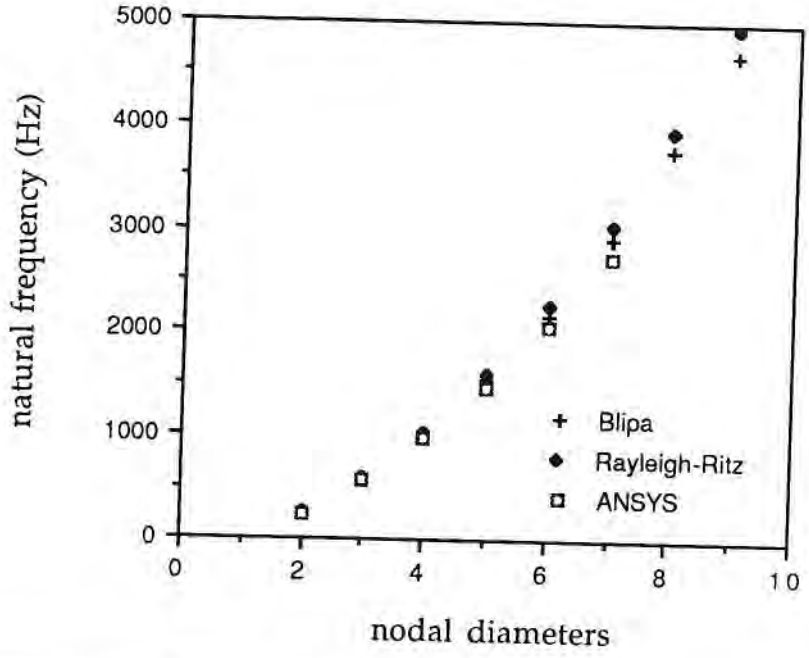

Figure 2.9 First family modes of the disc

Here, the Rayleigh-Ritz results show slightly higher natural frequencies, especially for higher nodal diameters, but this may be due to the floating-point calculations since all the frequency parameters of the disc have been performed inside the computer by using equation (2.12). Furthermore, there are good agreements between the theoretical method and the Finite Element analysis. The 8-node quadrilateral elements were used because they included the second-order deflection effect.

2.6.5 **Bladed Disc Vibration**

The vibration of the assembled bladed discs displays some different dynamic characteristics to those of the disc-alone vibrations or the blade-alone vibrations. The bladed disc modes or "the assembly modes" show some combined effects of the disc-alone and the cantilever blade-alone characteristics [34]. Both of the receptance coupling method and the Rayleigh-Ritz method were used here to show the vibration characteristics of the coupled system of the 30-bladed disc.

Another numerical comparison of the bladed disc is made using the Finite Element method. There are a few commercial packages that can be used and each package has its own advantages over others. Here, the general purpose package, ANSYS®, was used for solving the 30 bladed disc. Two different analyses using the Finite Element method have been examined. Originally, the geometrical mesh of the bladed disc structure for ANSYS consisted of 600 of the 8-node quadrilateral elements to represent the disc and 10 beam elements to represent each blade as shown in Figure 2.10. These beam elements and shell elements were previously used for the analysis of cantilever blade-alone vibrations and the disc-alone vibrations, respectively. The accuracy obtained from those analyses on the components was quite satisfactory.

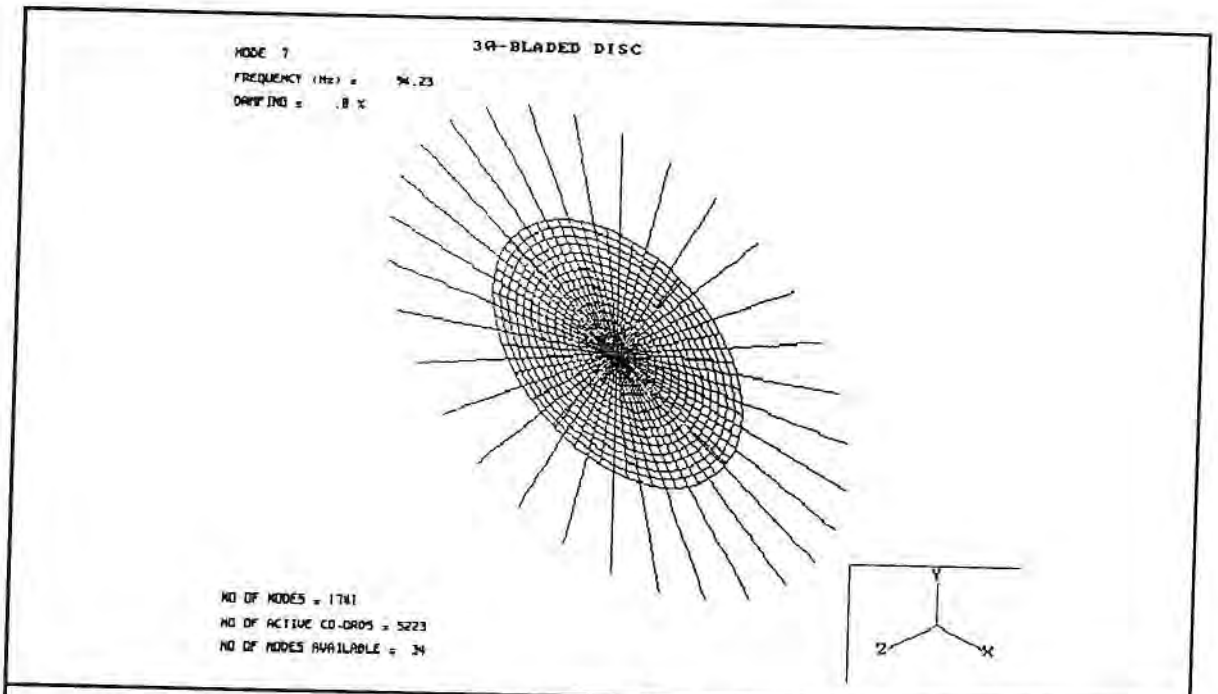

Figure 2.10 Full geometrical mesh of the 30 bladed disc for ANSYS

However, when the same elements were used for the coupled bladed disc, the accuracy of the results seemed to be affected by some factors. One factor of this may be due to the different types of elements used. Second, the shell elements used for modelling the disc may not be good for transverse shearing. This problem shows when they couple with beam elements, i.e. the blades, but can be solved by using meshes made of a single type of elements. In this case, two more different types of meshes were used, the 8-node shell elements and the

20-node brick elements. Both of these two meshes contain only one type of element to model the entire bladed disc.

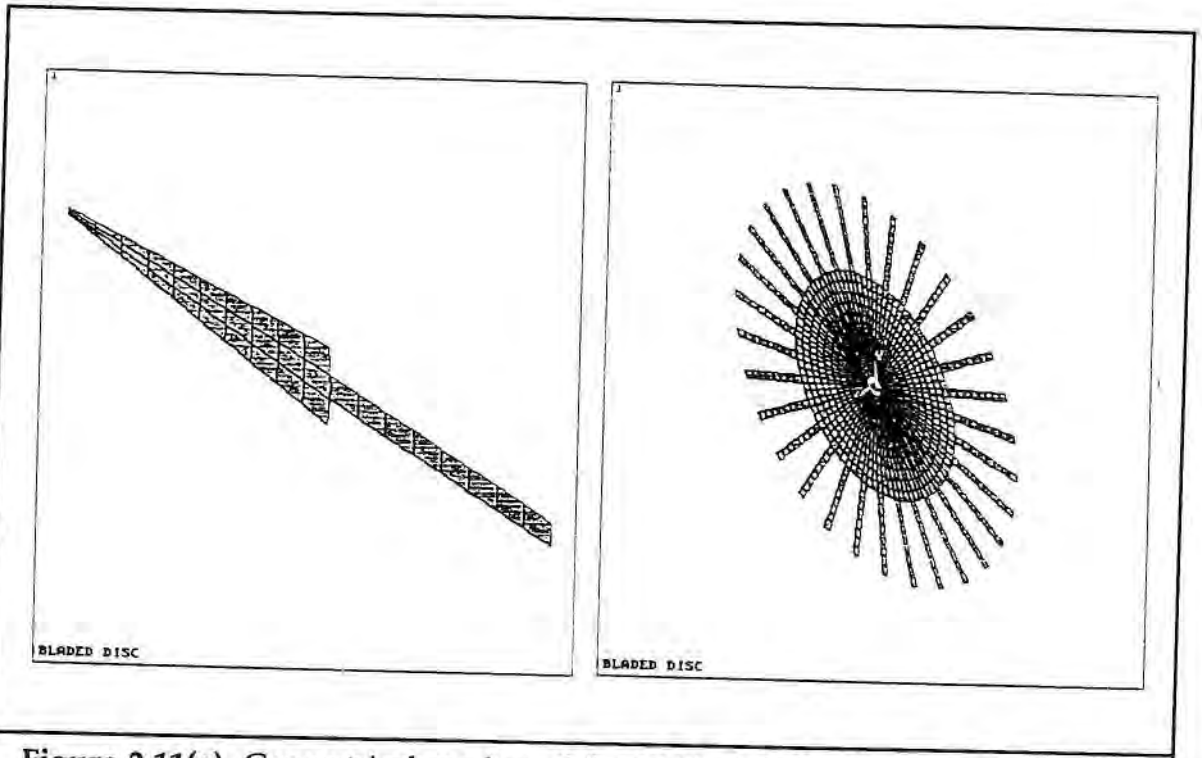

Figure 2.11(a) Geometrical meshes of the 30 bladed disc for cyclic symmetry analysis

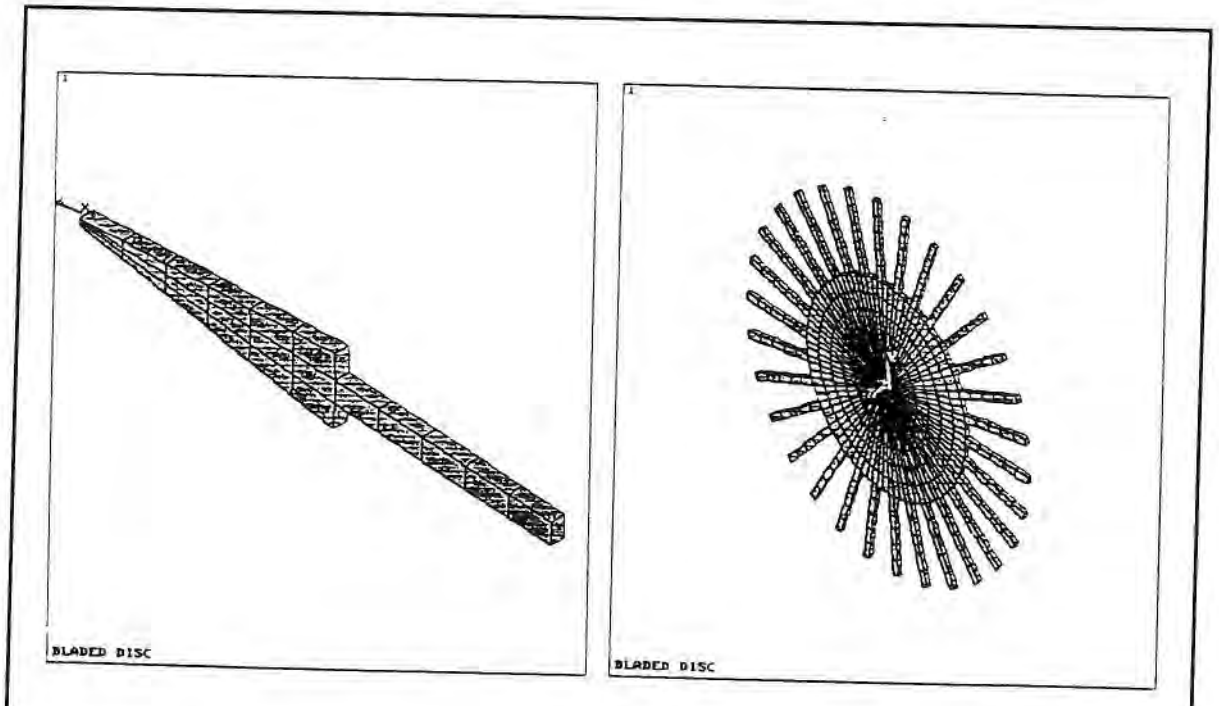

Figure 2.11(b) Geometrical meshes of the 30 bladed disc for cyclic symmetry analysis

Nevertheless, these two meshes substantially increased the number of DOFs so that these meshes required large memory spaces. An alternative way to solve this problem was to use the option of cyclic symmetry. By this approach, only one sector of the full geometry was created and solved. The program could then automatically assemble the rest of the similar sectors by rotating the sector displacement with the appropriate sector angle. The meshes of the sectors and the generated full geometries are shown in Figure 2.11. The shell-elements mesh is expecting to give more accurate results than the previous shell and beam model since all incompatibilities between the shell and the beam elements are eliminated. Moreover, the brick-elements mesh gives the best results because the brick elements contain the transverse shearing which the shell elements are in shortage. The results from all three meshes are shown in Figure 2.12.

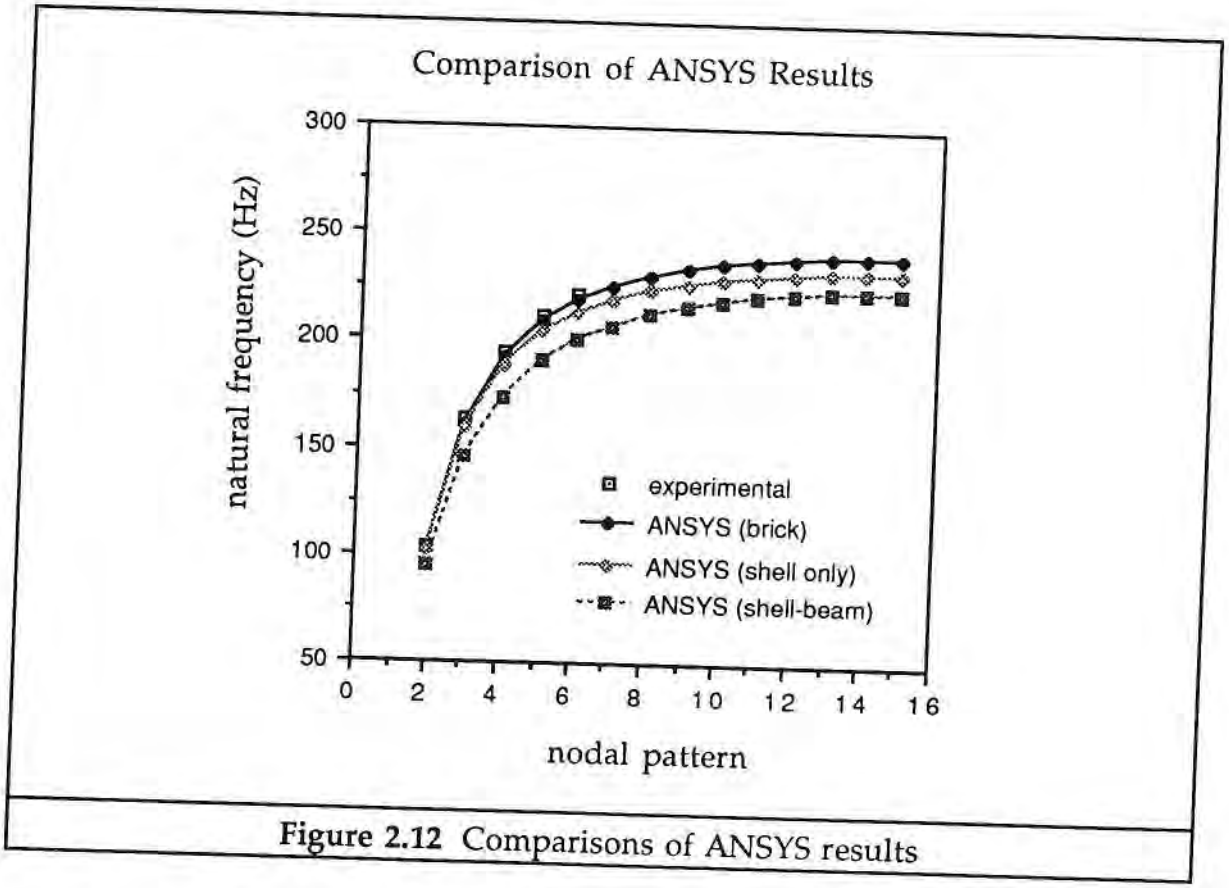

Figure 2.12 Comparisons of ANSYS results

Furthermore, the first ANSYS mesh consists of a total number of degrees-of-freedom of more than 17,000 for the full model of the bladed disc. The second and the third meshes apply the cyclic symmetry method and the 8-node shell sector consists about 943 degrees-of-freedom per sector while the 20-node brick element sector includes approximately 672 degrees-of-freedom per sector. To

conclude, the results from the 20-node brick element is the best in terms of accuracy for the bladed disc dynamic analysis. The CPU time required for each of the cyclically symmetrical solutions using the 20-node brick element is approximately 3 hours on a PC-486. From this study, the cyclical symmetric option gives good results as a full model only for tuned bladed discs. However, a full model of a bladed disc using 20-node brick elements will consume a lot of storage space and time. Therefore, it is not feasible to use such a model for the analysis of mistuned bladed disc.

The last model studied in this analysis is the lumped mass-spring model. The model parameters of the bladed disc can be identified by using the theory described in section 2.2.2. Table 2.7 shows the mass and stiffness values deduced for the 30 bladed disc.

blade mass	m = 0.0837 kg
blade stiffness	k = 229277.1 N/m
disc section mass	M = 0.1362 kg
coupled disc stiffness	K_d = 0.5956E6 N/m
	K_G = 45.5 N/m

Table 2.7 Lumped mass-spring model parameters

Finally, more results are presented here. These comparisons of results mainly include the receptance coupling method using BLIPA, the Rayleigh-Ritz method, the Finite Element (ANSYS) results, the lumped mass-spring model and some of the experimental results. The results of natural frequency against the nodal diameters from all the methods mentioned are shown below in Figure 2.13.

To sum up, the computational effort for the Finite Element analysis is usually huge compared with the other simpler methods. The model from ANSYS took about 200 minutes of CPU time to solve just the modal cyclically symmetrical structure. However, BLIPA and the Rayleigh-Ritz only took 5 minutes of CPU time to complete their calculations. Nevertheless, this structure is made of simple geometries and hence is not so economic to apply a Finite Element. In the real world, structures such as fan blades or turbine blades are geometrically very complicated and simpler methods cannot be applied. Finite Element analysis will be the sole solution to these problems. Nevertheless for mistuning bladed discs, the modal cyclically symmetrical

approach is also no longer valid and so a simpler model has to be sought. Therefore, the lumped mass-spring model was widely used in the past by many researchers for mistuning studies, especially for statistical studies where many different assemblies were analysed.

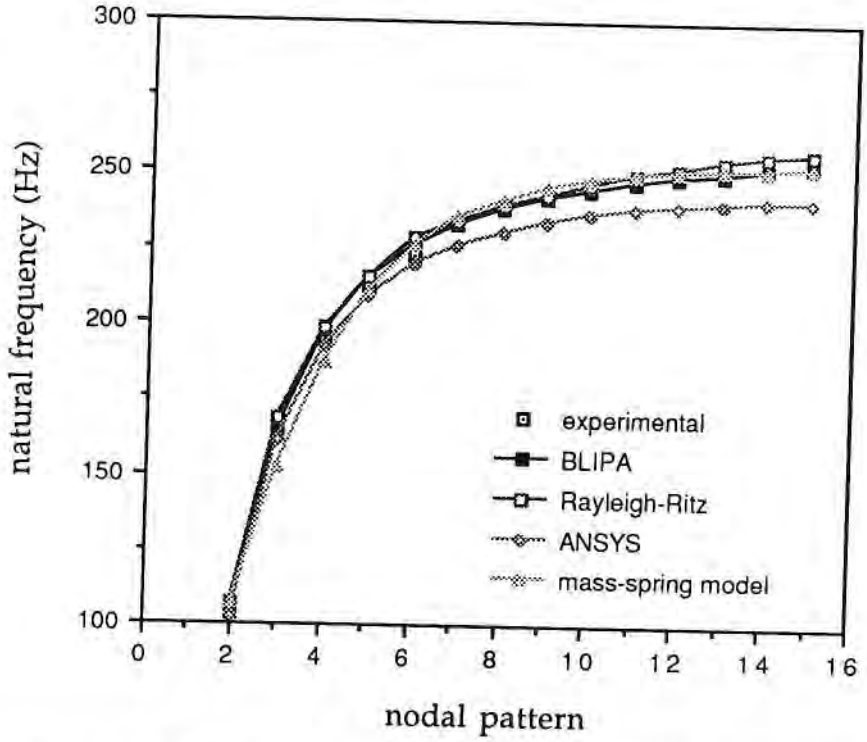

Figure 2.13 First family assembly modes of the 30 bladed disc

2.7 CONCLUDING REMARKS

This chapter has presented a study on several mathematical models for bladed disc vibration analysis. The accuracy and limitations of the models were assessed during the studies. Some comments are summarised about the models used in this chapter.

The closed-form receptance coupling method, the Rayleigh-Ritz method and the Finite Element method are all direct modelling of the actual structures. These include detailed physical dimensions and material properties of the structure. However, due to the complexity of the geometry of the actual bladed disc, the application of each method is limited by its approach to approximate the complex geometry of the structure. The Finite Element method clearly provides the best solution to model a complicated geometry, especially actual

blades with a variable cross section area. The closed-form receptance coupling method approximates a complex blade by using stepped beams, while the Rayleigh-Ritz method approximates geometrical variations by uniform tapers. Nevertheless, any complexity of the geometry in the model may cause errors to the solutions. Although these two methods have superior speed and memory requirement advantages over the Finite Element method, they are more suitable for extensive parametric studies especially for time-consuming jobs.

Some common finite elements were also shown here for the analysis of bladed discs. Different types of finite elements may affect the accuracy of the solutions. There are three different meshes used to show the comparisons of different results from different meshes. The beam-shell mesh models the blade with 2-node beam elements while the disc with 8-node shell elements. The shell mesh models the whole blade disc with 8-node shell elements and the brick mesh models the bladed disc with 20-node brick element. Two approaches of using the Finite Element method were also studied due to the memory and storage problems. First, the full model can be used to solve mistuned bladed discs but it requires large in-core memory and storage space. Second, the modal cyclically symmetrical model gives equally accurate results for tuned bladed disc vibration analysis and requires less memory than the full models. However, the analysis using the latter approach is only limited to tuned bladed discs since only one sector of the structure is solved for solutions. Furthermore, the numerical results show that the 20-node brick elements are better elements to analysis the bladed disc. Also, meshes of the same elements for the whole structure are better than using different elements for different parts of the structure. Generally, all elements used seem to be 'softer'. Stiffer elements, such as 9-node shell or triangular elements, may give higher natural frequencies for all the modes, but all these elements may suggest further increase of the NDOFs. Therefore, the work shown here did not make any attempt for these elements.

Although only stationary structures are considered here, the Rayleigh-Ritz method has the potential for the study of bladed discs with rotational effects, as shown in reference [79]. Since the energy formulation is in scalar form, different effects can simply be added together. In this analysis, the blade has been modelled by the beam function. It is also possible to model the blade by shell functions as shown in reference [88] so that the blade camber bending

effect can be included. This may give a better approximation for some turbine blades as their behaviour is more like plate vibrations. Furthermore, the eigenfunctions are directly formulated from the assumed orthogonal modes and hence this method is more efficient in computation since great accuracy can be achieved from only a few modes. Another possible feature for the Rayleigh-Ritz method is the inclusion of some friction damping effects between the blades and the disc.

Finally, the lumped mass-spring model is only a representative model. The model parameters are found only if the vibration characteristics of the actual bladed disc are known and often it is used in association with one of the other methods to study the forced vibration response of blades of a bladed disc. Therefore, it is normally used associated with another modelling method, such as the Finite Element model, or even experiment in order to obtain the exact model parameters. However, this model is extremely simple and fast to calculate the forced vibration response. As shown from the comparison, it can give good accuracy if the model parameters are properly identified. It is hence very popular to simulate large populations of bladed discs for statistical analysis using this method [50, 125], where one needs to study the physics of vibrations of a structure.

CHAPTER 3

BLADE RESONANT RESPONSE STUDIES ON MISTUNED BLADED DISC ASSEMBLIES: A STOCHASTIC APPROACH

About this chapter

In this chapter, two types of blade mistuning are defined. Frequency mistuning is due to either stiffness or inertia variations in the blades while damping mistuning is attributed to the differences on blade dampers. A study which presents a forced response analysis examines a mistuned 36-bladed disc by a simple lumped mass-spring-damper model. The deterministic blade responses of this model can be obtained by imposing a Lane's rule type of excitation [86]. If the mistuning parameter, such as blade frequency or blade damping, is a random variable of the bladed disc assembly, the blade responses on a disc may exist as many combinations of blade response levels depending on how the blades are arranged around the disc. In practice, bladed discs are drawn from large blade populations and the blade selection processes are usually random.

In another section, the blade responses are examined for some 40 different builds, each of which is a different arrangement of one set of particular blades around a rotor. The results show that the maximum peak response changes according to the blade arrangement, and the critical blade is not necessarily the same one for different arrangements. These results may help to explain the 'rogue blade' phenomenon which states that one particular blade suffers an unexpected high-level stress than other blades in the row. A condition to find such a critical arrangement is derived and can be used to avoid excessive blade vibration by controlling the blade selection processes.

3.1 INTRODUCTION

The main hazards for a bladed disc assembly under running conditions are the resonant response levels when the exciting frequencies pass though resonances of the structure during operation. These levels of increased amplitude are particularly serious if the blades of the assembly are mistuned. In this case, not only does the frequency splitting effect of the modes cover a wider excitation frequency range, but each blade amplitude is also different from when all blades are identical. From the early days that people observed mistuning effects, they found that the worst resonant blade amplitude may be many times larger than the response levels if the rotor were tuned. However, an interesting point in the past was that there were many results and conclusions which differed from each other, and these caused a series of arguments on the topic. A review in Chapter 1 showed some of the different opinions from different research workers. From such a detailed survey of the literature concerning vibration problems in mistuned bladed disc assemblies, some numerical studies have been made here to understand the unresolved problems in mistuned bladed discs.

Recently, Sanliturk [125] applied a direct simulation method to calculate the forced vibration response of a bladed system under a wide range of possible engine running conditions, and the results helped to reconcile some conflicting conclusions obtained by different researchers in the past. However, he could not clearly state the factors causing mistuned blade responses to vary from case to case. Because of this, it was essential to study further the resonant response behaviour of mistuned bladed systems. Also, in a recent review paper, Ewins summarised some comments on the mistuning studies of the past and drew up some guidelines for future study [44].

The main objective of this chapter is to present a forced response analysis which can provide us with a tool for parametric studies. Such an analysis will need to solve many mistuned bladed discs using a stochastic simulation. Second, a study of blade arrangement effects to a set of mistuned blades leads to the first discovery of some insight to the behaviour of rogue blades. These blades have the characteristics of response levels which are much higher than others in the row when the assembly is mistuned. Furthermore, the results demonstrate that the mean values of the arrangements are very close to each other while the worst blades from different arrangements are scattered.

Finally, it has also been found here that the blade arrangements have some correlation to the blade responses patterns. A condition stating the optimal or critical arrangement for a set of blades on a disc is also studied here.

3.2 MATHEMATICAL MODEL

Generally, the physical properties of a structure, such as the mass, flexibility and energy dissipation properties, are distributed continuously throughout the structure. In the previous chapter, various mathematical models have been discussed. For modelling a complex structure, the Finite Element method is a well-known adequate solution. However, the Finite Element method has the disadvantage that a large computational resource is required for forced response analysis. For the majority of large structures, it is expedient to substitute an idealized model which is better adapted to mathematical analysis and has approximately the same dynamic response as the real structure. Furthermore, the blade mistuning parameter is usually regarded as a random input to a deterministic model of a bladed disc system. Therefore, the behaviour of randomly mistuned bladed discs can only be analysed by a way of stochastic simulation. In this case, a large number of calculations of deterministic systems with randomly-varied properties are required to ensure convergence to the desired results. Hence, an alternative discrete model, consisting of few lumped masses and stiffness elements to represent the blades and the disc, is thought to be more suitable.

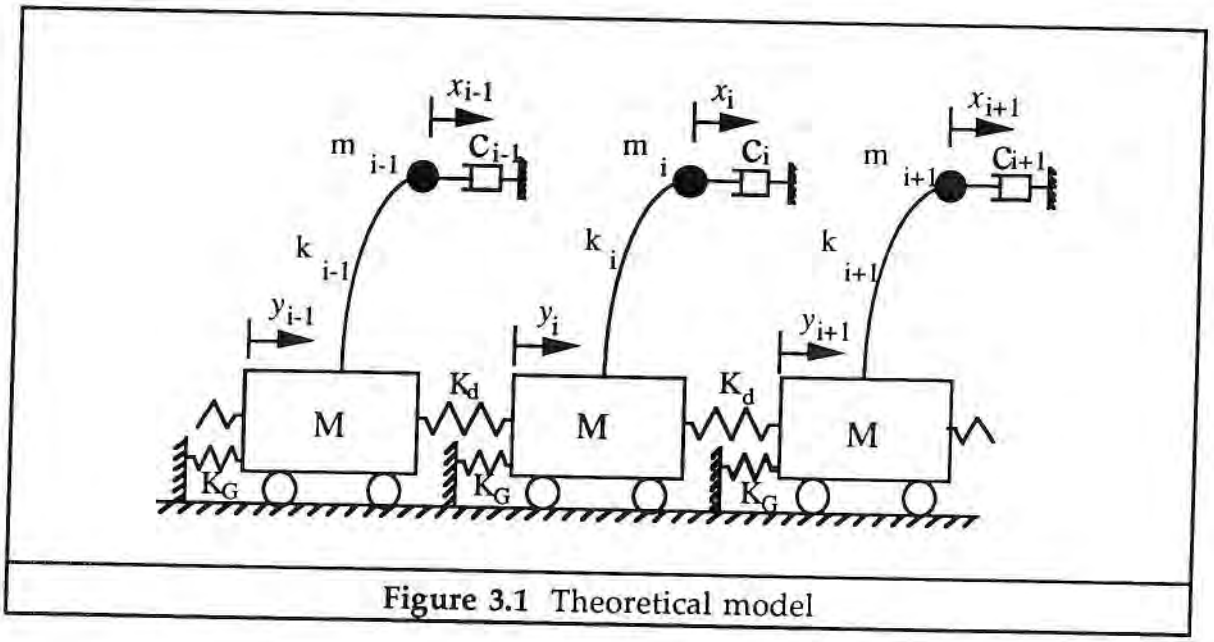

Figure 3.1 Theoretical model

One of the early attempts to simulate mistuning cases on bladed disc assemblies was using the model developed by Dye and Henry in 1969 [28]. In their model, each blade was represented by a lumped mass on top of a massless spring attached to a trolley. The frictionless trolleys were linked though elastic springs to represent the disc. Therefore, the complete bladed disc consists of N such substructures, where N represents the number of blades or sections on the bladed disc. This model, shown in Figure 3.1, has been used throughout this study, but damping has been considered more generally than in the original Dye and Henry model. Furthermore, this model can also represent a shrouded bladed disc as shown by Afolabi [1] who included the effects of shrouds around the blades by adding an extra mass and an extra spring to connect these masses. The equations of motion of the system can be written as sets of simultaneous equations as follows:

$$m_1\ddot{x}_1 + c_1\dot{x}_1 + k_1^* x_1 - k_1^* y_1 = f_1$$
$$M_1\ddot{y}_1 - k_1^* x_1 + (k_1^* + 2K_d + K_1 + K_G)\, y_1 - K_d\, y_N - K_d\, y_2 = 0$$

$$\vdots$$

$$m_i\ddot{x}_i + c_i\dot{x}_i + k_i^* x_i - k_i^* y_i = f_i$$

$$M_i\ddot{y}_i - k_i^* x_i + (k_i^* + 2K_d + K_i + K_G)\, y_i - K_d\, y_{i-1} - K_d\, y_{i+1} = 0$$

$$\vdots$$

$$m_N\ddot{x}_N + C_N\dot{x}_N + k_N^* x_N - k_N^* y_N = f_N$$
$$M_N\ddot{y}_N - k_N^* x_N + (k_N^* + 2K_d + K_N + K_G)\, y_N - K_d\, y_{N-1} - K_d\, y_1 = 0$$

where $k^* = k + jd = (1 + j\eta)k$, with η being the hysteretic damping ratio. This leads to a system matrix of the form shown as follows:

$$[\mathbf{M}]\{\ddot{x}\} + [\mathbf{C}]\{\dot{x}\} + ([\mathbf{K}] + j[\mathbf{D}])\{x\} = \{f\} \qquad (3.1)$$

By assuming a harmonic transform, the excitation forces and the displacements can be written as follows:

$$\{f\} = \{F\}e^{j\omega t}, \qquad \{x\} = \{X\}e^{j\omega t} \qquad (3.2)$$

Therefore, equation (3.1) can be transformed to the following equation.

$$\{X\}e^{j\omega t} = [Z(\omega)]^{-1}\{F\}e^{j\omega t} \tag{3.3}$$

where $[Z(\omega)]$ is the dynamic stiffness matrix

$$[Z(\omega)] = [K] - \omega^2[M] + j([D] + \omega[C])$$

The most commonly encountered source of excitation for turbomachinery rotor stages arises from the wake patterns caused by upstream obstacles such as stator vanes, struts, or guide vanes, when the fluid flows past thought them. The presence of such obstacles results in the fluid flow being distorted into a circumferentially wave-like pattern acting axially on the bladed disc, known as engine-order excitation, as shown in Figure 3.2.

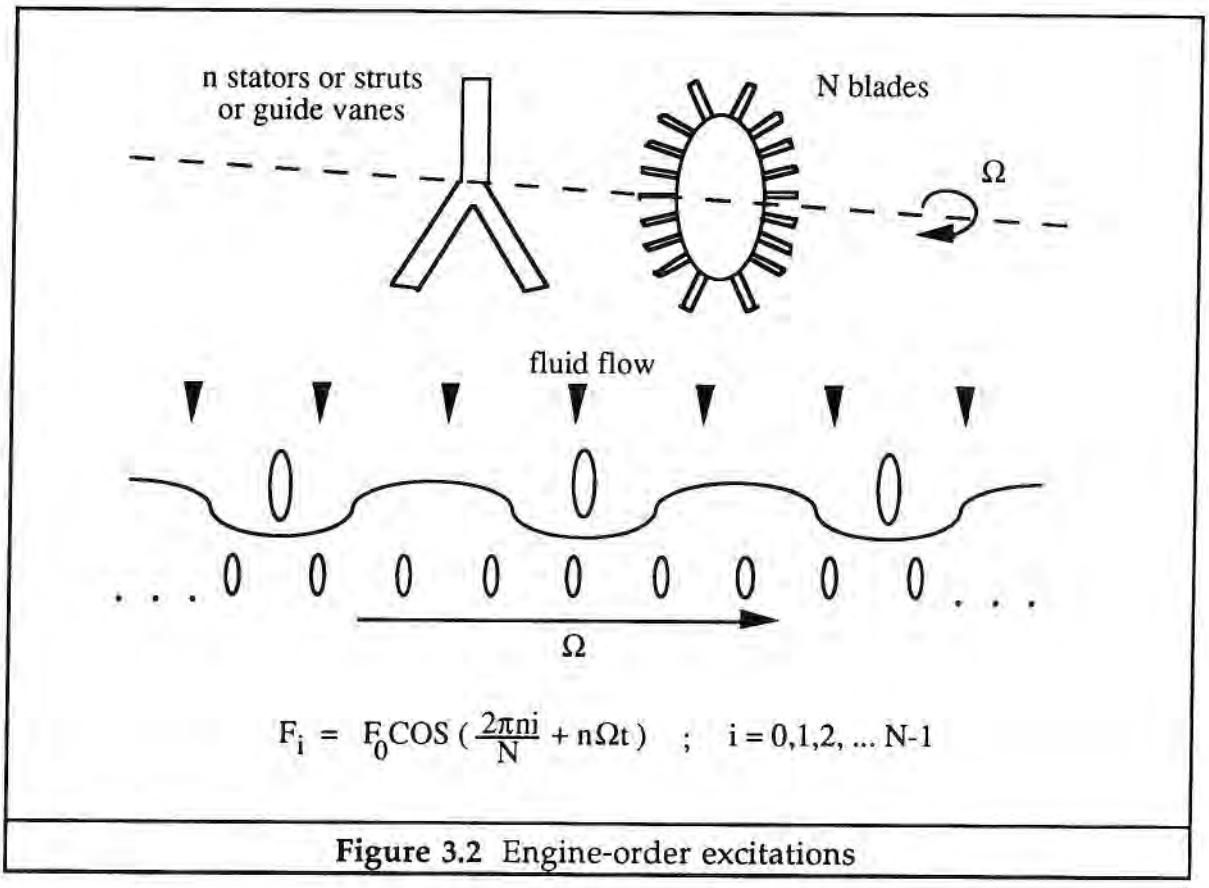

Figure 3.2 Engine-order excitations

If one applies a Fourier analysis to the distortion pattern, n integer numbers of obstacle will cause the nth Fourier component to be dominant. This component has the potential to excite a bladed disc resonance at speeds corresponding to the intersection of the excitation frequency and that particular Fourier component. Lane, in 1950, first pointed out that this type of

excitation has the characteristic of equal amplitude but varied by a constant phase [86]. Furthermore, the number of obstacles upstream attributes to the phase difference between blades. This number is termed as the engine-order (EO) of excitation and the excitation on the *i*th blade by an *n*th engine order (*n*EO) excitation force pattern can be written as follows:

$$F_i = A_i \exp[j(i-1)\psi], \qquad \psi = \frac{2\pi n}{N} \tag{3.4}$$

Where A_i is the amplitude of the force acting on the *i*th blade, ψ is also called the interblade phase angle, j is $\sqrt{-1}$, and N is the number of blades in the row. For simplicity, the amplitude of the force is taken to be unity.

The blade responses from the equation of motion (3.1) can be solved either by the modal summation method or by the direct method as indicated by equations (3.5) and (3.6) respectively.

$$\{X\} = \sum_{r=1}^{N} \frac{[\phi]\ [\phi]^T \{F\}}{\omega_r^2 - \omega^2 + i(2\omega_r \omega \xi_r + \eta_r \omega_r^2)} \tag{3.5}$$

$$\{X\} = [\mathbf{Z}(\omega)]^{-1} \{F\} \tag{3.6}$$

Where $[\phi]$ is the mass-normalised eigenvectors matrix, ξ_r is the viscous damping coefficient and η_r is the loss factor for the *r*th mode, and $\omega_r = \sqrt{\frac{k}{m}}$ is the natural frequency for undamped free vibration.

The modal summation method shown in equation (3.5) requires the eigensolutions of the vibration problem and if a complex eigensolver, such as complex QR algorithm in NAG library F02AKF, is applied, the eigenvectors will result in a slight error for the perfectly tuned bladed disc. This is due to the pairs of "identical" natural frequencies (eigenvalues) of an axisymmetric structure. If, however, a small perturbation is added to the system, so that the double paired eigenvalues are just slightly separated from each other, but the results still approximate to a tuned bladed disc, good responses can be obtained in this way. During the course of this research, several possible of perturbations to system have been tried. Generally, if equation (3.5) is undamped, a small perturbation to one of the elements of the stiffness matrix (a ratio between 0.01 to 0.0001) can solve the problem. Hence, the direct

method is very reliable in all cases but efficiency drops if the system is large. On the other hand, the efficiency for the modal method is good for large systems. A computer program has been written to solve the equation of motion (3.1) using both the modal method and the direct method. Figure 3.3 shows blade tip responses of tuned and mistuned 36 bladed disc under 6 EO excitation by both methods to solve equation (3.1).

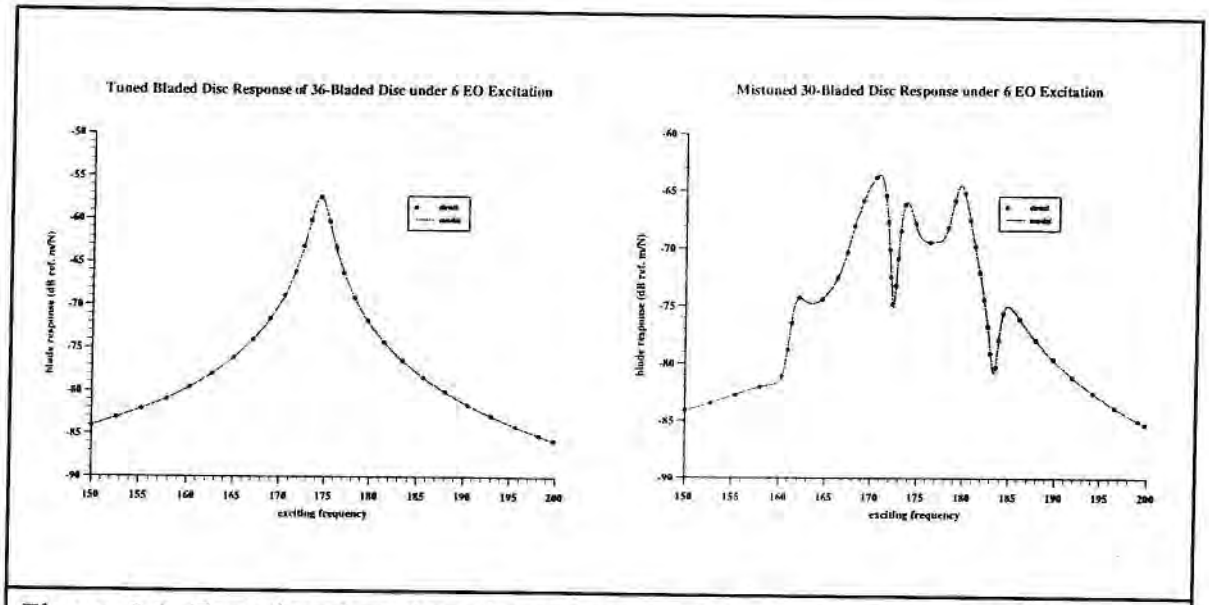

Figure 3.3 Tuned and mistuned response amplitude of a 36-bladed disc under 6 EO excitation (blade No. 1 only)

3.3 MODEL PARAMETERS

In Chapter 2, an analytical method of identifying model parameters for a lumped mass-spring model of a simple bladed disc was introduced. However, for a structure with a complex shape, either the modal testing technique or the finite element model to simulate the testing situation is required to identify the parameters for the model, for example, see Afolabi [1].

Tuned bladed disc data:		
$m = 0.05$ kg	$k = 65384.16$ N/m	
$M = 0.18$ kg	$K = 941532.0$ N/m	$K_G = 65.384$ N/m
$\eta = 0.2$ %	$\zeta = 1.0$ %	
Mistuned bladed disc:		
mean cantilever frequency = 182 Hz	standard deviation = 5.82 Hz	

Table 3.1 Structural Parameters

The model adopted for this numerical study is the 36-bladed disc model used by Sanliturk [125] for his study. The structural parameters for the tuned model are as shown in Table 3.1.

The new computer program was checked against the results obtained by Sanliturk for an undamped tuned system. In the case of a tuned system, the natural frequencies from the first family of the 36-bladed disc assembly are shown as Figure 3.4, and agree exactly with the results obtained by Sanliturk.

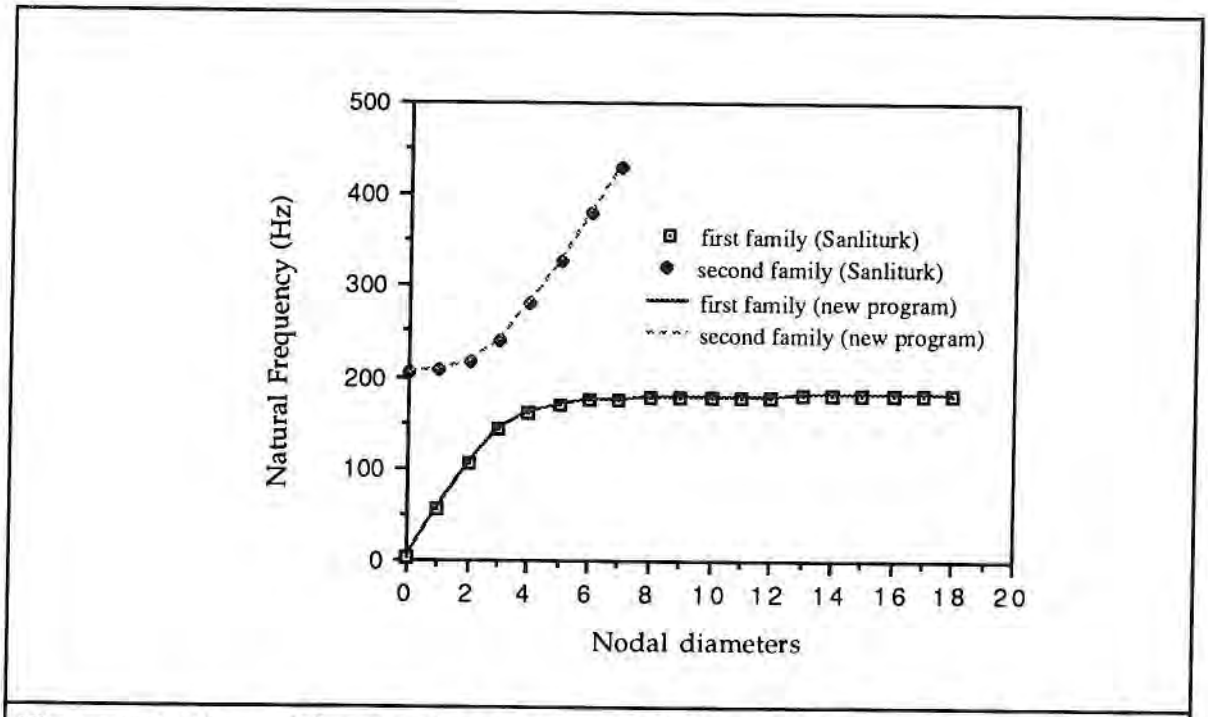

Figure 3.4 Natural frequencies versus nodal diameter for tuned 36-bladed disc

3.4 MISTUNED BLADED DISCS

Conventionally, blade mistuning means that there are small blade-to-blade variations in either mass or stiffness. However, in practice, it is not so easy to account for the actual source of the deviations. From measurements, the cantilever blade natural frequencies are different for all the blades manufactured. This is often considered as the *frequency mistuning*. Another type of mistuning is the *damping mistuning* which is mainly due to the friction rubbing at contact points and the aerodynamic drags from fluid. This class of mistuning is particularly important when there are under-platform dampers applied to the blades on a rotor. Chapter 5 will have more detailed discussions of this type of mistuning.

Moreover, there are also different patterns of mistuning which can be studied. The most common ones are: alternate mistuning, random mistuning, and single-blade mistuning. The patterns used thought out the rest of this thesis concentrate on the single-blade-mistune and the random mistune. The former one is not usually found in practice, because only one blade out of the whole assembly being different from the rest is an unlikely prospect. However, it can be found useful in laboratory or theoretical studies to gain some basic understanding of the mistuning behaviour of bladed disc dynamics. Random mistuning is much closer to the realistic situation. Turbomachine manufacturers usually produce a large number of blades for a particular bladed disc assembly. These blades are, of course, not identically to each other, but the deviations can be controlled by specifying dimensional tolerances. From experience, the distribution of the blade-alone natural frequency referring to the whole blade population is approximately Gaussian or normal.

However, some researchers (for example, see Wei and Pierre, 1988 [152, 153]) considered that the distribution of blades on one specific bladed disc is also Gaussian. Strictly speaking, this is not necessarily the case and the chance that a particular bladed disc has a normal distribution of blade properties is extremely small. Furthermore, another feature of randomly mistuned systems is the mistuning parameter used to the blades. Some researchers defined the stiffness or the blade length to be the mistuning parameter. Nevertheless, it was quite well defined by Dye and Henry that "*the natural frequencies of a set of blades are likely to conform to a Gaussian distribution with the extreme ends of the range cut off in some cases. The amount of 'cutoff' will vary depending on manufacturing and operating requirements applicable to the particular stage*". The work in this thesis will follow the definition proposed by them so that the study will confine to a realistic situation. The mistuning to the blades on a rotor is added as perturbations onto a tuned or mean blade cantilever natural frequency.

3.5 STATISTICS OF MISTUNED SYSTEM FORCED RESPONSE CHARACTERISTICS

Statistics provides a quantitative method to measure the frequency of repetition for some variables or discrete events. The mathematical model of these bases on the observations of raw data collected. Normally, large amounts of data are required to obtain certain reliable results. Furthermore, stochastic

simulation is a branch of experimental mathematics, resting on a theoretical basis which consists of simulating different possible deterministic models and mimicking the behaviour of a complicated statistical event. In 1984, Griffin et al. simulated a large blade population in order to correlate the distribution of peak responses [50] and later Sanliturk used the same approach to simulate the forced responses under all possible engine orders for a 36-bladed disc.

One area of the present study is to examine the factors which influence the profile (or envelope) of the statistical plot, which is the plot of peak responses from a large number of case simulations. However, discrepancies of results form other researchers detected at an early stage of that study led to the discovery of some additional factors which influence the shape and the profile of a statistical response plot. It was found that the blade selection procedure used to choose blades from a large population to form the set on a bladed disc assembly affects the system's response levels. Different selections may result in the response plot having a different shape. Griffin et al. specified a blade selection criterion that satisfied the limits of percentage of the frequency scatter and a limit of the moment weight, which is a measure of the criterion of dynamic balance. Sanliturk selected a blade as if its cantilever natural frequency was within the two cutoff extremes applied to an otherwise normal distribution. The limits of the distribution can be judged by the standard deviations of the blade population. However, the present study uses a 'culling' process as defined by Griffin [50].

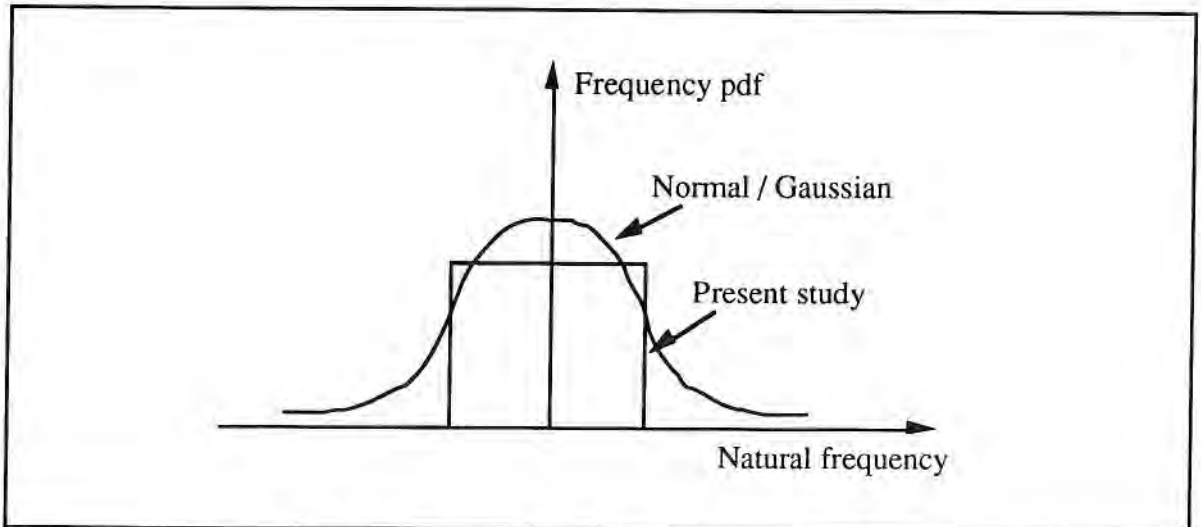

Figure 3.5 PDF of different methods for blade selections

This is a very simple way to select a blade from a uniform population by rejecting any blade if its cantilever natural frequency is outside certain

specified limits, as shown in Figure 3.5. Nevertheless, all blade selection procedures employ a random number generator, see Appendix III. Usually, the blades produced from a large quantity are bound to follow a normal distribution on the cantilever blade natural frequencies. Numerically, the Box and Muller algorithm can generate random numbers with a Gaussian distribution [118]. These random numbers will have the mean equal to zero and the standard deviation equals to unity. Therefore, shifting and normalisation are required to put the generated distribution to the suitable blade distribution. From this point, there may be different ways to select the blades to be assembled. The first way applies the same procedure as by Sanliturk, where the standard deviation of the blade population is limited to a design value, see Figure 3.6. There are a total of 25,200 samples and the standard deviation of the blade cantilever natural frequencies is 5.6 Hz for this example.

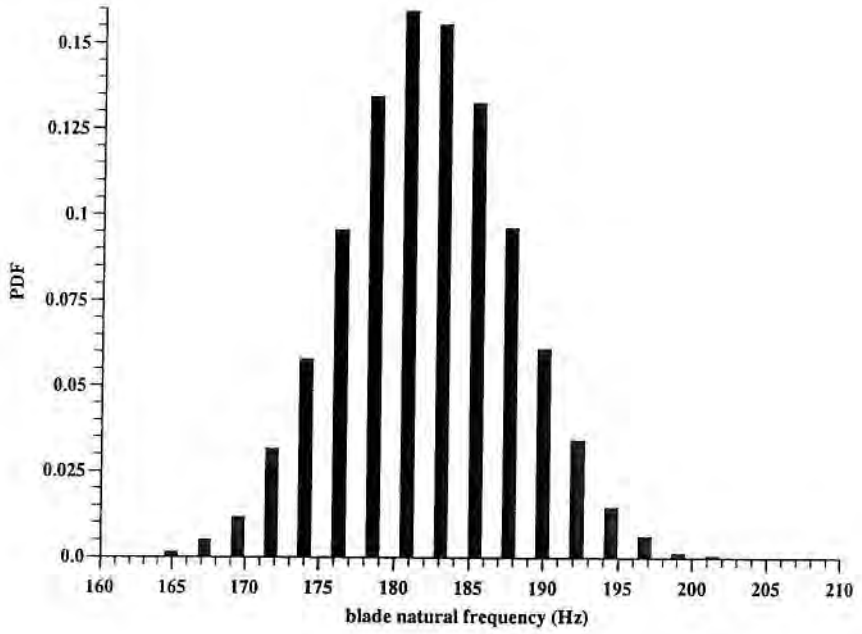

Figure 3.6 Normal distribution of blade cantilever natural frequency with standard deviation about 5.6 Hz

A 36-bladed disc is used to find the forced blade responses under a 6 engine-order of excitation. Seven hundred 36-bladed discs have been selected as samples and the blades, whose distribution has already been shown in Figure 3.6, are assembled arbitrarily around the discs. Since there are about 25200 data,

3.1 INTRODUCTION

The main hazards for a bladed disc assembly under running conditions are the resonant response levels when the exciting frequencies pass though resonances of the structure during operation. These levels of increased amplitude are particularly serious if the blades of the assembly are mistuned. In this case, not only does the frequency splitting effect of the modes cover a wider excitation frequency range, but each blade amplitude is also different from when all blades are identical. From the early days that people observed mistuning effects, they found that the worst resonant blade amplitude may be many times larger than the response levels if the rotor were tuned. However, an interesting point in the past was that there were many results and conclusions which differed from each other, and these caused a series of arguments on the topic. A review in Chapter 1 showed some of the different opinions from different research workers. From such a detailed survey of the literature concerning vibration problems in mistuned bladed disc assemblies, some numerical studies have been made here to understand the unresolved problems in mistuned bladed discs.

Recently, Sanliturk [125] applied a direct simulation method to calculate the forced vibration response of a bladed system under a wide range of possible engine running conditions, and the results helped to reconcile some conflicting conclusions obtained by different researchers in the past. However, he could not clearly state the factors causing mistuned blade responses to vary from case to case. Because of this, it was essential to study further the resonant response behaviour of mistuned bladed systems. Also, in a recent review paper, Ewins summarised some comments on the mistuning studies of the past and drew up some guidelines for future study [44].

The main objective of this chapter is to present a forced response analysis which can provide us with a tool for parametric studies. Such an analysis will need to solve many mistuned bladed discs using a stochastic simulation. Second, a study of blade arrangement effects to a set of mistuned blades leads to the first discovery of some insight to the behaviour of rogue blades. These blades have the characteristics of response levels which are much higher than others in the row when the assembly is mistuned. Furthermore, the results demonstrate that the mean values of the arrangements are very close to each other while the worst blades from different arrangements are scattered.

Finally, it has also been found here that the blade arrangements have some correlation to the blade responses patterns. A condition stating the optimal or critical arrangement for a set of blades on a disc is also studied here.

3.2 MATHEMATICAL MODEL

Generally, the physical properties of a structure, such as the mass, flexibility and energy dissipation properties, are distributed continuously throughout the structure. In the previous chapter, various mathematical models have been discussed. For modelling a complex structure, the Finite Element method is a well-known adequate solution. However, the Finite Element method has the disadvantage that a large computational resource is required for forced response analysis. For the majority of large structures, it is expedient to substitute an idealized model which is better adapted to mathematical analysis and has approximately the same dynamic response as the real structure. Furthermore, the blade mistuning parameter is usually regarded as a random input to a deterministic model of a bladed disc system. Therefore, the behaviour of randomly mistuned bladed discs can only be analysed by a way of stochastic simulation. In this case, a large number of calculations of deterministic systems with randomly-varied properties are required to ensure convergence to the desired results. Hence, an alternative discrete model, consisting of few lumped masses and stiffness elements to represent the blades and the disc, is thought to be more suitable.

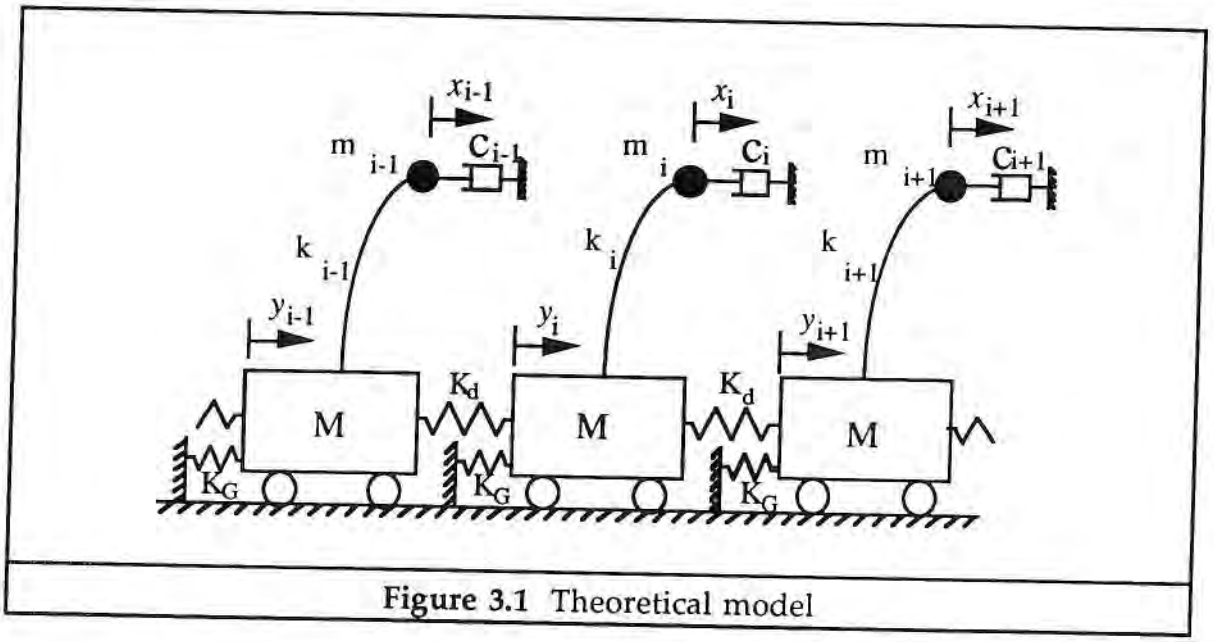

Figure 3.1 Theoretical model

One of the early attempts to simulate mistuning cases on bladed disc assemblies was using the model developed by Dye and Henry in 1969 [28]. In their model, each blade was represented by a lumped mass on top of a massless spring attached to a trolley. The frictionless trolleys were linked though elastic springs to represent the disc. Therefore, the complete bladed disc consists of N such substructures, where N represents the number of blades or sections on the bladed disc. This model, shown in Figure 3.1, has been used throughout this study, but damping has been considered more generally than in the original Dye and Henry model. Furthermore, this model can also represent a shrouded bladed disc as shown by Afolabi [1] who included the effects of shrouds around the blades by adding an extra mass and an extra spring to connect these masses. The equations of motion of the system can be written as sets of simultaneous equations as follows:

$$m_1\ddot{x}_1 + c_1\dot{x}_1 + k_1^* x_1 - k_1^* y_1 = f_1$$
$$M_1\ddot{y}_1 - k_1^* x_1 + (k_1^* + 2K_d + K_1 + K_G)\, y_1 - K_d\, y_N - K_d\, y_2 = 0$$

$$\vdots$$

$$m_i\ddot{x}_i + c_i\dot{x}_i + k_i^* x_i - k_i^* y_i = f_i$$

$$M_i\ddot{y}_i - k_i^* x_i + (k_i^* + 2K_d + K_i + K_G)\, y_i - K_d\, y_{i-1} - K_d\, y_{i+1} = 0$$

$$\vdots$$

$$m_N\ddot{x}_N + C_N\dot{x}_N + k_N^* x_N - k_N^* y_N = f_N$$
$$M_N\ddot{y}_N - k_N^* x_N + (k_N^* + 2K_d + K_N + K_G)\, y_N - K_d\, y_{N-1} - K_d\, y_1 = 0$$

where $k^* = k + jd = (1 + j\eta)k$, with η being the hysteretic damping ratio. This leads to a system matrix of the form shown as follows:

$$[\mathbf{M}]\{\ddot{x}\} + [\mathbf{C}]\{\dot{x}\} + ([\mathbf{K}] + j[\mathbf{D}])\{x\} = \{f\} \qquad (3.1)$$

By assuming a harmonic transform, the excitation forces and the displacements can be written as follows:

$$\{f\} = \{F\}e^{j\omega t}, \qquad \{x\} = \{X\}e^{j\omega t} \qquad (3.2)$$

Therefore, equation (3.1) can be transformed to the following equation.

$$\{X\}e^{j\omega t} = [Z(\omega)]^{-1}\{F\}e^{j\omega t} \tag{3.3}$$

where $[Z(\omega)]$ is the dynamic stiffness matrix

$$[Z(\omega)] = [K] - \omega^2[M] + j([D] + \omega[C])$$

The most commonly encountered source of excitation for turbomachinery rotor stages arises from the wake patterns caused by upstream obstacles such as stator vanes, struts, or guide vanes, when the fluid flows past thought them. The presence of such obstacles results in the fluid flow being distorted into a circumferentially wave-like pattern acting axially on the bladed disc, known as engine-order excitation, as shown in Figure 3.2.

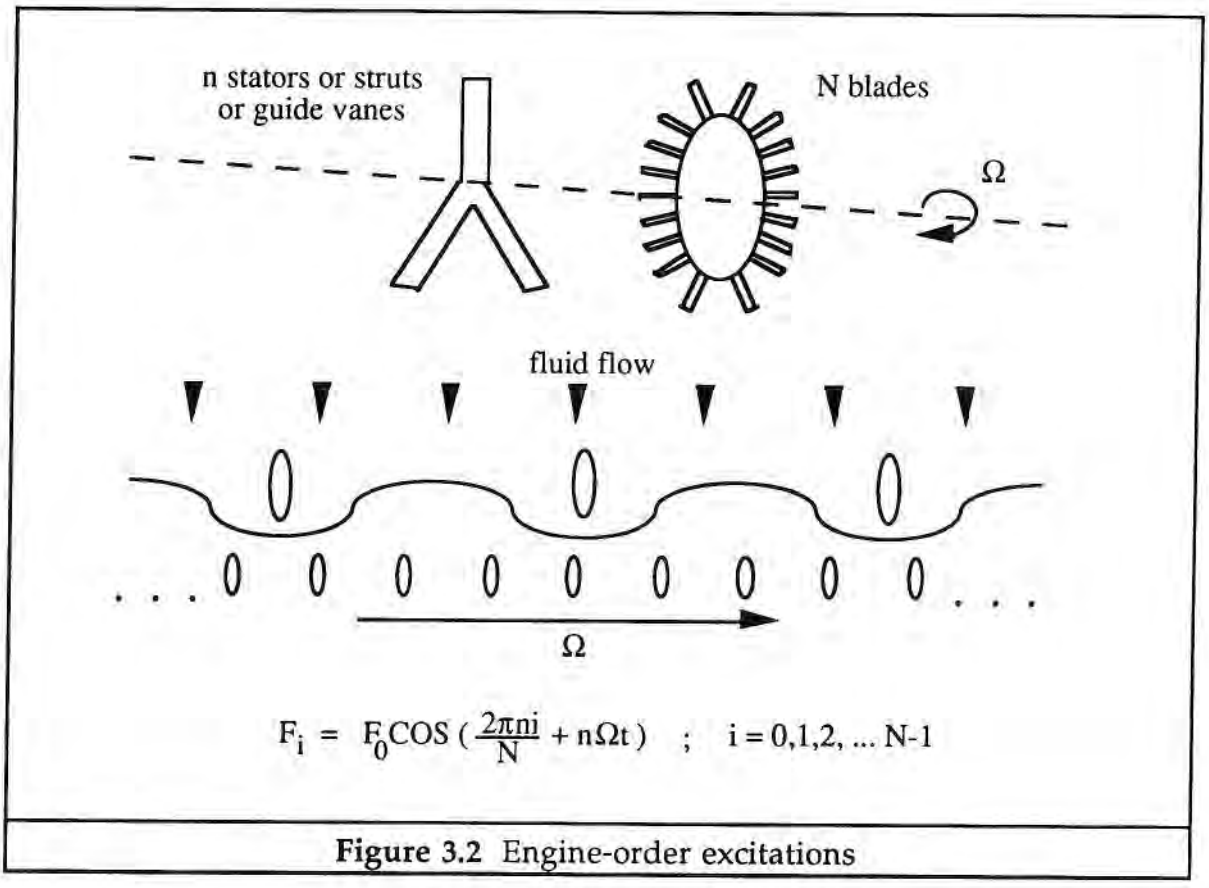

Figure 3.2 Engine-order excitations

If one applies a Fourier analysis to the distortion pattern, n integer numbers of obstacle will cause the nth Fourier component to be dominant. This component has the potential to excite a bladed disc resonance at speeds corresponding to the intersection of the excitation frequency and that particular Fourier component. Lane, in 1950, first pointed out that this type of

excitation has the characteristic of equal amplitude but varied by a constant phase [86]. Furthermore, the number of obstacles upstream attributes to the phase difference between blades. This number is termed as the engine-order (EO) of excitation and the excitation on the *i*th blade by an *n*th engine order (*n*EO) excitation force pattern can be written as follows:

$$F_i = A_i \exp[j(i-1)\psi], \qquad \psi = \frac{2\pi n}{N} \tag{3.4}$$

Where A_i is the amplitude of the force acting on the *i*th blade, ψ is also called the interblade phase angle, j is $\sqrt{-1}$, and N is the number of blades in the row. For simplicity, the amplitude of the force is taken to be unity.

The blade responses from the equation of motion (3.1) can be solved either by the modal summation method or by the direct method as indicated by equations (3.5) and (3.6) respectively.

$$\{X\} = \sum_{r=1}^{N} \frac{[\phi]\ [\phi]^T \{F\}}{\omega_r^2 - \omega^2 + i(2\omega_r \omega \xi_r + \eta_r \omega_r^2)} \tag{3.5}$$

$$\{X\} = [\mathbf{Z}(\omega)]^{-1} \{F\} \tag{3.6}$$

Where $[\phi]$ is the mass-normalised eigenvectors matrix, ξ_r is the viscous damping coefficient and η_r is the loss factor for the *r*th mode, and $\omega_r = \sqrt{\frac{k}{m}}$ is the natural frequency for undamped free vibration.

The modal summation method shown in equation (3.5) requires the eigensolutions of the vibration problem and if a complex eigensolver, such as complex QR algorithm in NAG library F02AKF, is applied, the eigenvectors will result in a slight error for the perfectly tuned bladed disc. This is due to the pairs of "identical" natural frequencies (eigenvalues) of an axisymmetric structure. If, however, a small perturbation is added to the system, so that the double paired eigenvalues are just slightly separated from each other, but the results still approximate to a tuned bladed disc, good responses can be obtained in this way. During the course of this research, several possible of perturbations to system have been tried. Generally, if equation (3.5) is undamped, a small perturbation to one of the elements of the stiffness matrix (a ratio between 0.01 to 0.0001) can solve the problem. Hence, the direct

method is very reliable in all cases but efficiency drops if the system is large. On the other hand, the efficiency for the modal method is good for large systems. A computer program has been written to solve the equation of motion (3.1) using both the modal method and the direct method. Figure 3.3 shows blade tip responses of tuned and mistuned 36 bladed disc under 6 EO excitation by both methods to solve equation (3.1).

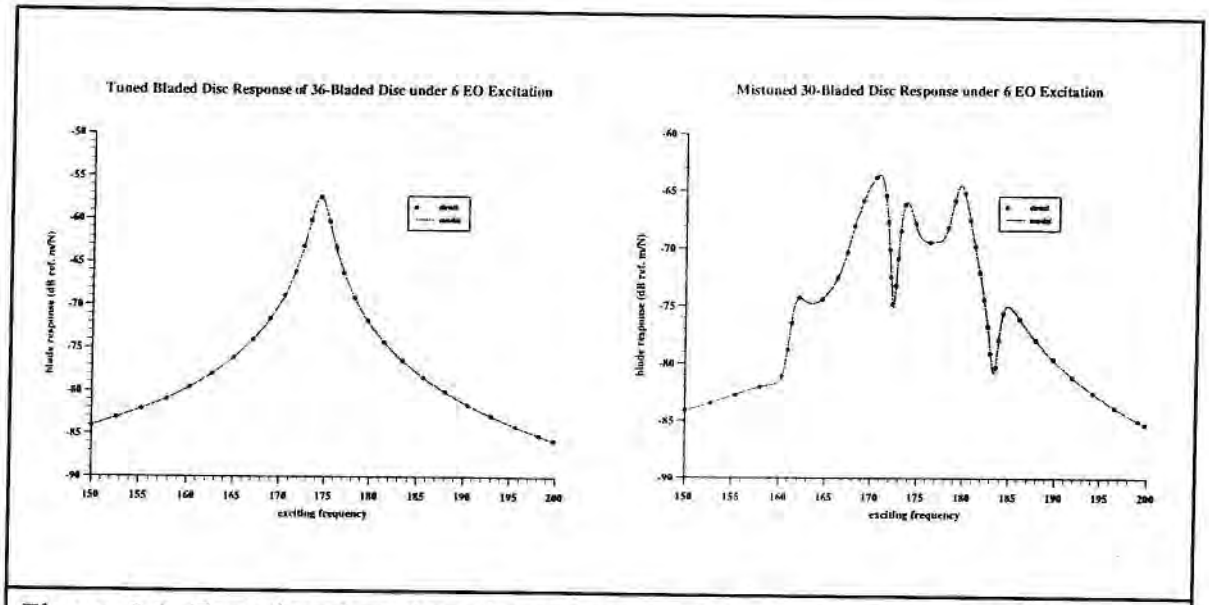

Figure 3.3 Tuned and mistuned response amplitude of a 36-bladed disc under 6 EO excitation (blade No. 1 only)

3.3 MODEL PARAMETERS

In Chapter 2, an analytical method of identifying model parameters for a lumped mass-spring model of a simple bladed disc was introduced. However, for a structure with a complex shape, either the modal testing technique or the finite element model to simulate the testing situation is required to identify the parameters for the model, for example, see Afolabi [1].

Tuned bladed disc data:		
$m = 0.05$ kg	$k = 65384.16$ N/m	
$M = 0.18$ kg	$K = 941532.0$ N/m	$K_G = 65.384$ N/m
$\eta = 0.2$ %	$\zeta = 1.0$ %	
Mistuned bladed disc:		
mean cantilever frequency = 182 Hz	standard deviation = 5.82 Hz	

Table 3.1 Structural Parameters

The model adopted for this numerical study is the 36-bladed disc model used by Sanliturk [125] for his study. The structural parameters for the tuned model are as shown in Table 3.1.

The new computer program was checked against the results obtained by Sanliturk for an undamped tuned system. In the case of a tuned system, the natural frequencies from the first family of the 36-bladed disc assembly are shown as Figure 3.4, and agree exactly with the results obtained by Sanliturk.

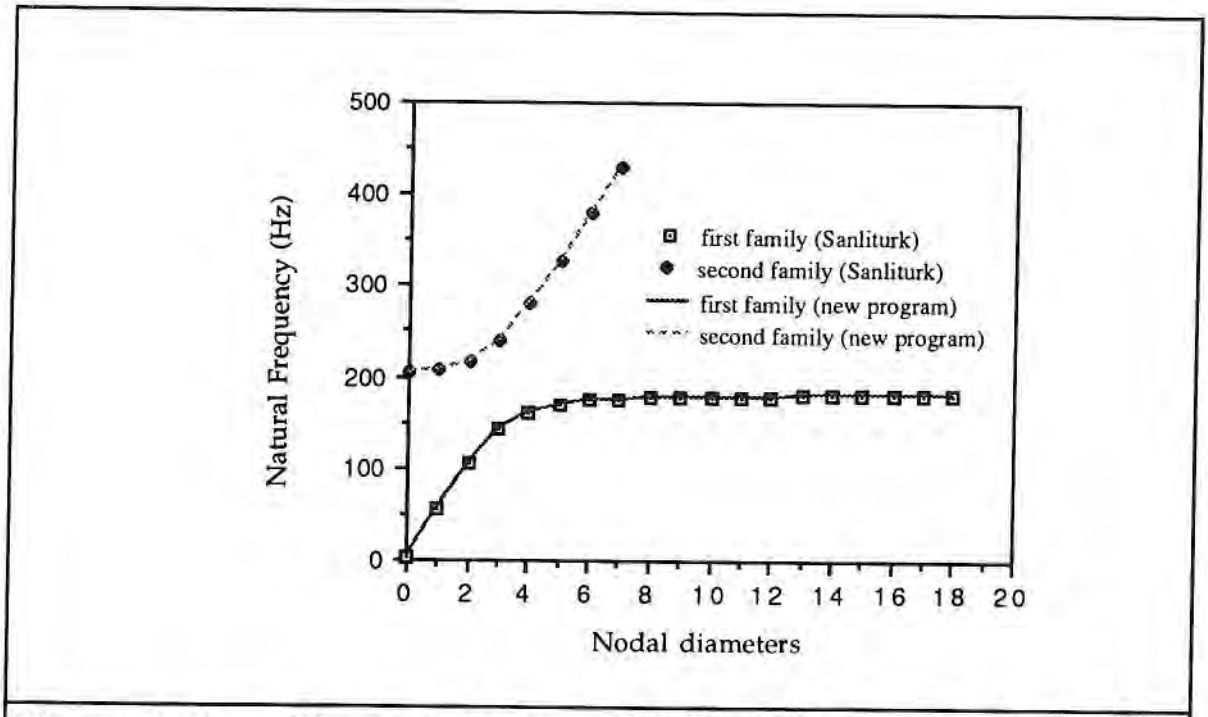

Figure 3.4 Natural frequencies versus nodal diameter for tuned 36-bladed disc

3.4 MISTUNED BLADED DISCS

Conventionally, blade mistuning means that there are small blade-to-blade variations in either mass or stiffness. However, in practice, it is not so easy to account for the actual source of the deviations. From measurements, the cantilever blade natural frequencies are different for all the blades manufactured. This is often considered as the *frequency mistuning*. Another type of mistuning is the *damping mistuning* which is mainly due to the friction rubbing at contact points and the aerodynamic drags from fluid. This class of mistuning is particularly important when there are under-platform dampers applied to the blades on a rotor. Chapter 5 will have more detailed discussions of this type of mistuning.

Moreover, there are also different patterns of mistuning which can be studied. The most common ones are: alternate mistuning, random mistuning, and single-blade mistuning. The patterns used thought out the rest of this thesis concentrate on the single-blade-mistune and the random mistune. The former one is not usually found in practice, because only one blade out of the whole assembly being different from the rest is an unlikely prospect. However, it can be found useful in laboratory or theoretical studies to gain some basic understanding of the mistuning behaviour of bladed disc dynamics. Random mistuning is much closer to the realistic situation. Turbomachine manufacturers usually produce a large number of blades for a particular bladed disc assembly. These blades are, of course, not identically to each other, but the deviations can be controlled by specifying dimensional tolerances. From experience, the distribution of the blade-alone natural frequency referring to the whole blade population is approximately Gaussian or normal.

However, some researchers (for example, see Wei and Pierre, 1988 [152, 153]) considered that the distribution of blades on one specific bladed disc is also Gaussian. Strictly speaking, this is not necessarily the case and the chance that a particular bladed disc has a normal distribution of blade properties is extremely small. Furthermore, another feature of randomly mistuned systems is the mistuning parameter used to the blades. Some researchers defined the stiffness or the blade length to be the mistuning parameter. Nevertheless, it was quite well defined by Dye and Henry that "*the natural frequencies of a set of blades are likely to conform to a Gaussian distribution with the extreme ends of the range cut off in some cases. The amount of 'cutoff' will vary depending on manufacturing and operating requirements applicable to the particular stage*". The work in this thesis will follow the definition proposed by them so that the study will confine to a realistic situation. The mistuning to the blades on a rotor is added as perturbations onto a tuned or mean blade cantilever natural frequency.

3.5 STATISTICS OF MISTUNED SYSTEM FORCED RESPONSE CHARACTERISTICS

Statistics provides a quantitative method to measure the frequency of repetition for some variables or discrete events. The mathematical model of these bases on the observations of raw data collected. Normally, large amounts of data are required to obtain certain reliable results. Furthermore, stochastic

simulation is a branch of experimental mathematics, resting on a theoretical basis which consists of simulating different possible deterministic models and mimicking the behaviour of a complicated statistical event. In 1984, Griffin et al. simulated a large blade population in order to correlate the distribution of peak responses [50] and later Sanliturk used the same approach to simulate the forced responses under all possible engine orders for a 36-bladed disc.

One area of the present study is to examine the factors which influence the profile (or envelope) of the statistical plot, which is the plot of peak responses from a large number of case simulations. However, discrepancies of results form other researchers detected at an early stage of that study led to the discovery of some additional factors which influence the shape and the profile of a statistical response plot. It was found that the blade selection procedure used to choose blades from a large population to form the set on a bladed disc assembly affects the system's response levels. Different selections may result in the response plot having a different shape. Griffin et al. specified a blade selection criterion that satisfied the limits of percentage of the frequency scatter and a limit of the moment weight, which is a measure of the criterion of dynamic balance. Sanliturk selected a blade as if its cantilever natural frequency was within the two cutoff extremes applied to an otherwise normal distribution. The limits of the distribution can be judged by the standard deviations of the blade population. However, the present study uses a 'culling' process as defined by Griffin [50].

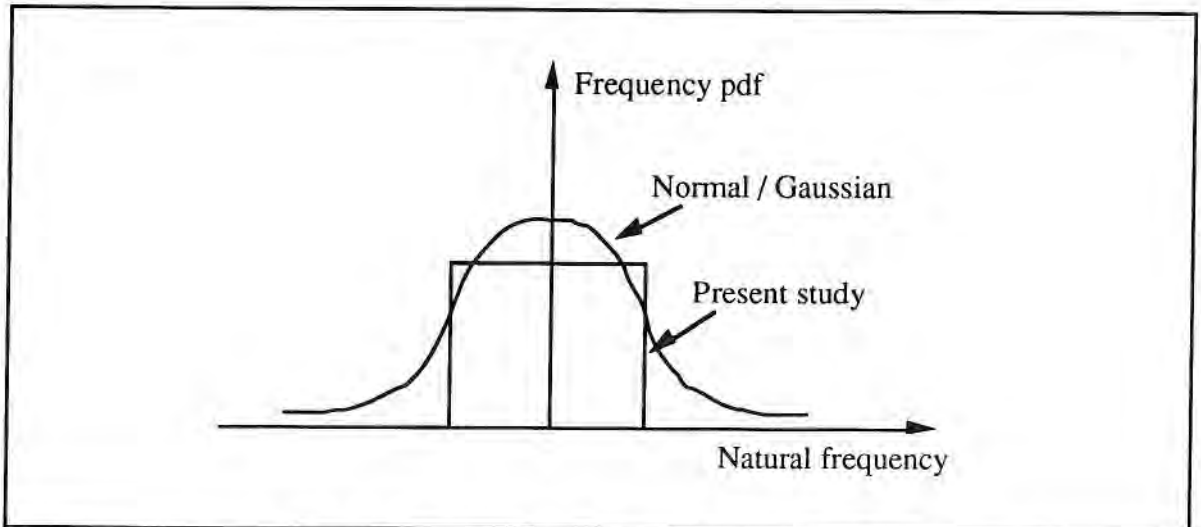

Figure 3.5 PDF of different methods for blade selections

This is a very simple way to select a blade from a uniform population by rejecting any blade if its cantilever natural frequency is outside certain

specified limits, as shown in Figure 3.5. Nevertheless, all blade selection procedures employ a random number generator, see Appendix III. Usually, the blades produced from a large quantity are bound to follow a normal distribution on the cantilever blade natural frequencies. Numerically, the Box and Muller algorithm can generate random numbers with a Gaussian distribution [118]. These random numbers will have the mean equal to zero and the standard deviation equals to unity. Therefore, shifting and normalisation are required to put the generated distribution to the suitable blade distribution. From this point, there may be different ways to select the blades to be assembled. The first way applies the same procedure as by Sanliturk, where the standard deviation of the blade population is limited to a design value, see Figure 3.6. There are a total of 25,200 samples and the standard deviation of the blade cantilever natural frequencies is 5.6 Hz for this example.

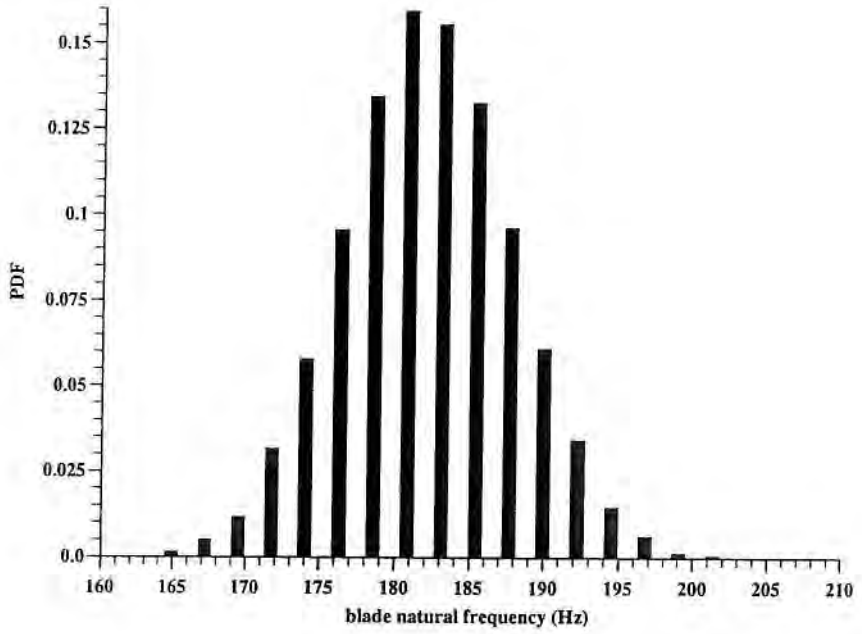

Figure 3.6 Normal distribution of blade cantilever natural frequency with standard deviation about 5.6 Hz

A 36-bladed disc is used to find the forced blade responses under a 6 engine-order of excitation. Seven hundred 36-bladed discs have been selected as samples and the blades, whose distribution has already been shown in Figure 3.6, are assembled arbitrarily around the discs. Since there are about 25200 data,

a standard practice to present these results is to plot the blade responses against the blade cantilever natural frequencies as shown by Griffin and Sanliturk. On such a graph, the 'normalised maximum response' refers to the peak value of the response of an individual blade divided by the corresponding tuned resonant response. The 'normalised blade-alone frequency' is the blade cantilever natural frequency divided by the mean blade-alone natural frequency. Figure 3.7 shows the response scatter plot for the first selection procedure.

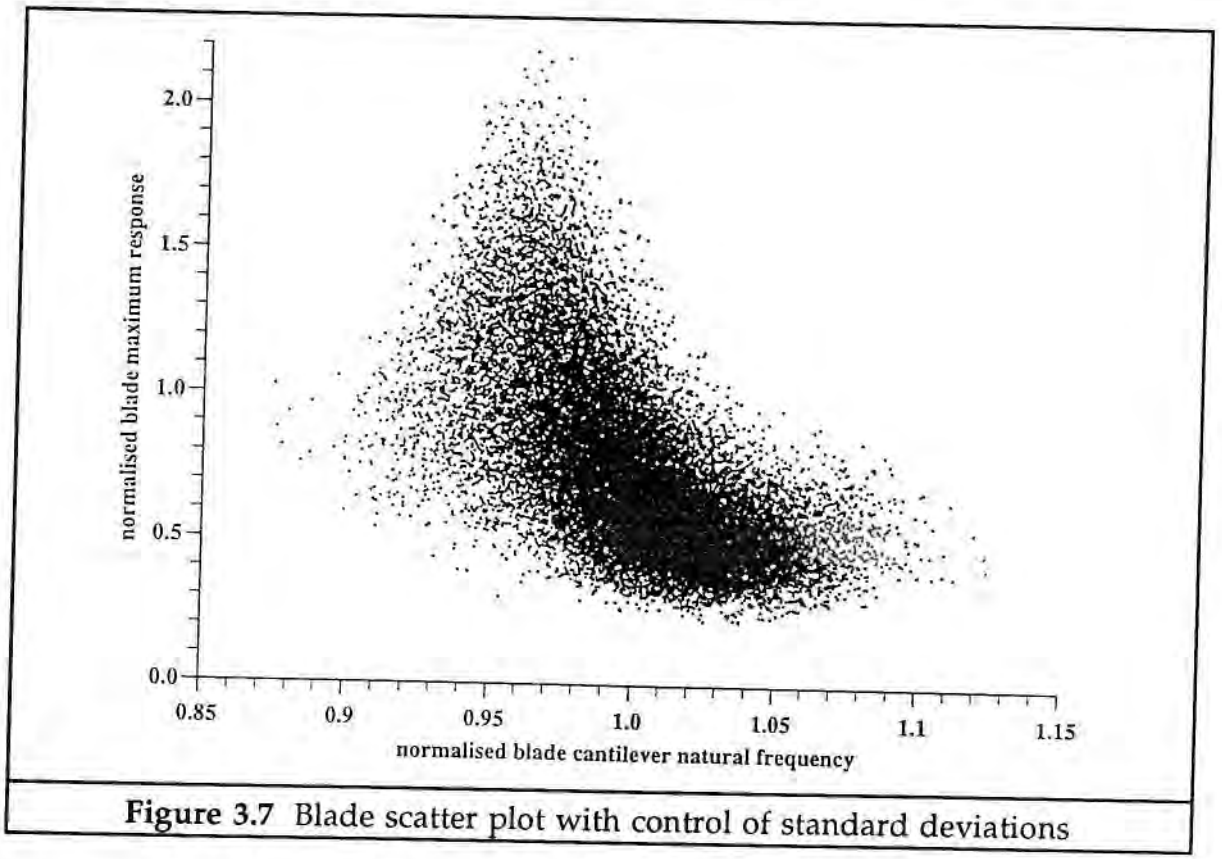

Figure 3.7 Blade scatter plot with control of standard deviations

The second selection involves the 'culling' selection procedure. This process also uses a Gaussian distributed population but the selection of blades is based on a tolerance on the blade natural frequency. A limit Δ_{lmt}, which can be defined by the user, is set inside the program so that a number outside this limit will be rejected by the program and then another one will be re-selected. The selected number, say Δ, is then perturbed to the mean blade-alone natural frequency

$$\text{blade-alone nat. freq.} = (1 + \Delta) \times \text{mean blade-alone nat. freq.}$$

If Δ is a normal distribution having zero mean and unit standard deviation, the distribution of the new blade selection is defined as follows:

$$p(\Delta) = \begin{cases} \frac{1}{\sqrt{2\pi}} \exp\left(-\frac{1}{2}\Delta^2\right); & \text{for } -\Delta_{lmt} < \Delta < +\Delta_{lmt} \\ 0; & \text{otherwise} \end{cases} \quad (3.7)$$

By doing this, the response plot of those selected blades shows a clear cutoff at the edges of the limit. Figure 3.8 shows the response scatter plot for another 700 different sets of 36-bladed discs using the second blade selection method.

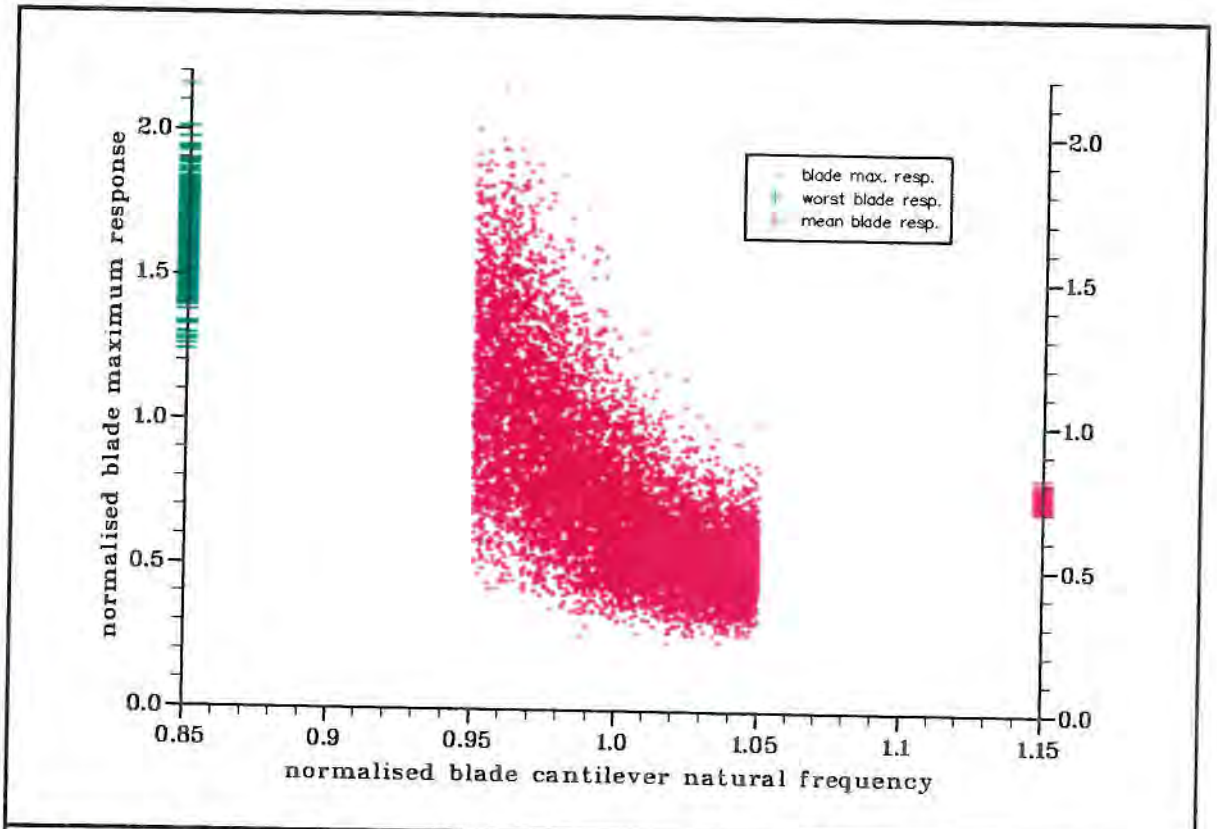

Figure 3.8 blade scatter plot with control on blade-alone natural frequency

In this case, the range of random mistuning can be defined as follows:

$$\% \text{ of scatter } (\Delta) = \frac{(\text{max. blade nat. freq.} - \text{min. blade nat. freq.}) \times 100\%}{\text{mean blade nat. freq.}} \quad (3.8)$$

Furthermore, Figure 3.8 also shows the values of the response level of the most critical blade and the mean response level of each bladed disc. These two quantities are marked in green and brown colours respectively. The critical

blade responses of a row are plotted on the left-hand y-axis while the mean responses of a row are plotted on the right-hand axis. Figure 3.9 shows the plot of response levels versus excitation frequency for the same blades.

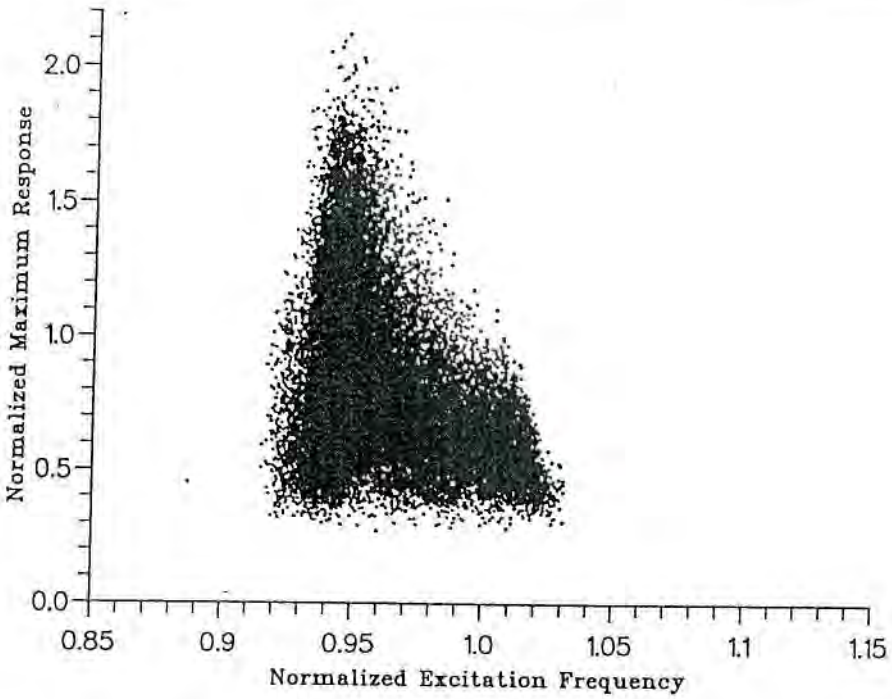

Figure 3.9 Normalised maximum response versus excitation frequency for frequency scatter of 10%

3.6 BLADE ARRANGEMENTS

3.6.1 Maximum Response Investigation

Blade mistuning of turbomachinery is small manufacturing tolerances leading to some blades vibrating more vigorously than others. These blades were named as 'rogue blades' [1] and have a greater chance of major failure. A study of the peak responses of a specific mistuned bladed system is shown here. This study involves 40 different builds, each of which is a different arrangement of one particular set of blades around a rotor. This particular set of blades also belongs to one of the combinations of the 700 randomly assembled bladed disc as shown in Figure 3.8. Figure 3.10 shows a particular arrangement of this set of blades. Figure 3.11 shows a typical peak response level versus individual blade natural frequency plot. The frequency scatter is specified at 10% of cantilever natural frequency and the assemblies are under 6 EO excitation.

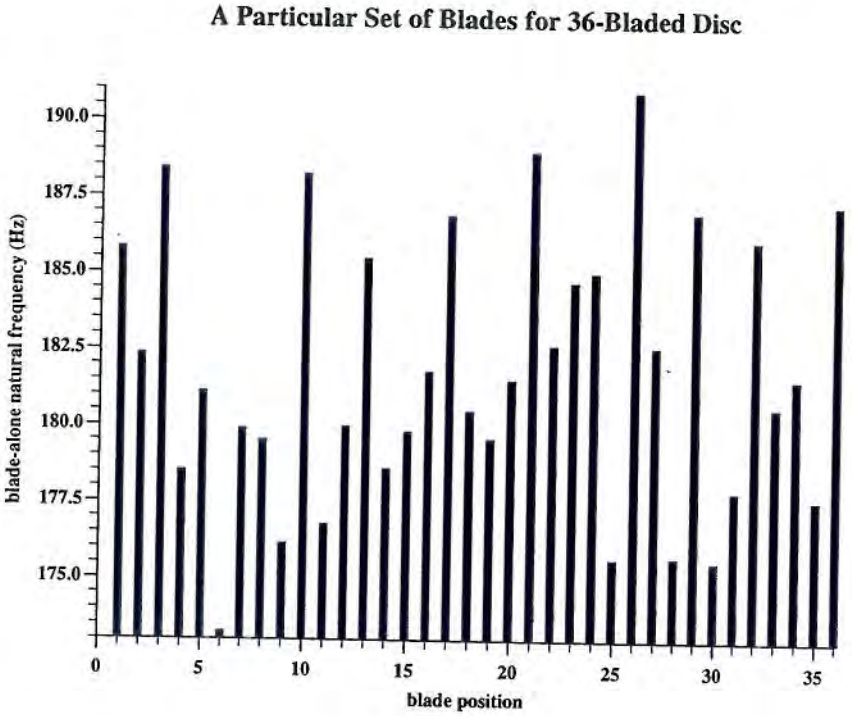

Figure 3.10 blade cantilever natural frequency a particular set of blades

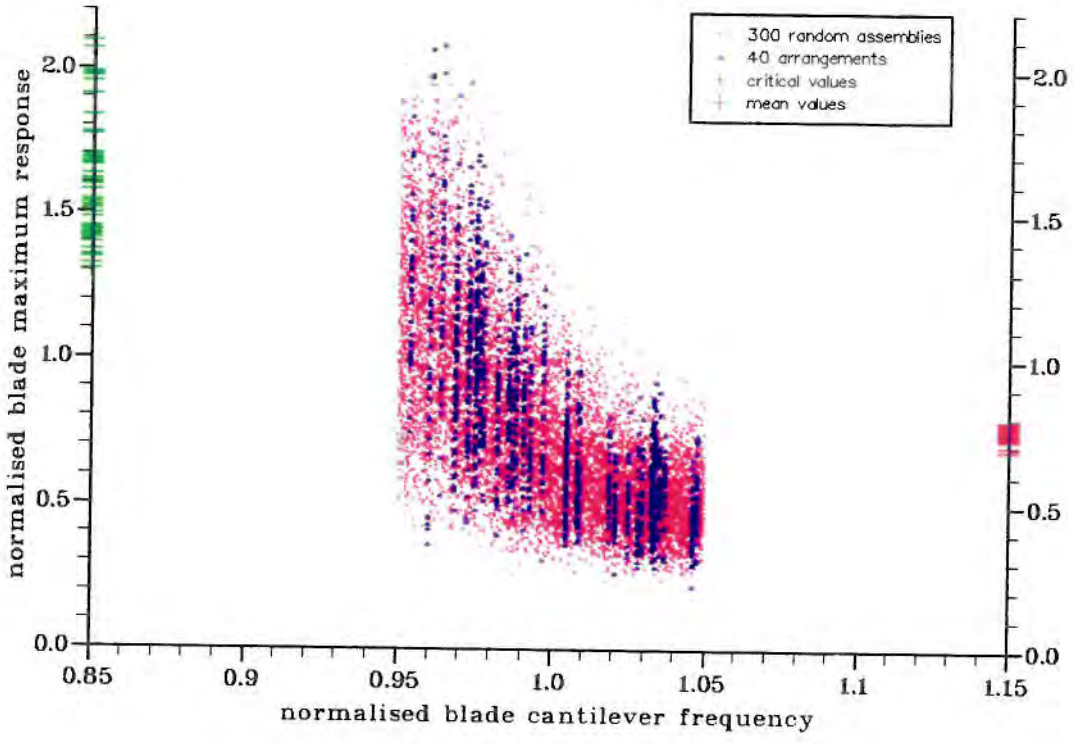

Figure 3.11 40 different combinations of a particular set of blades

In this colour diagram, the background red data are the results of all the blade responses of 300 random assemblies of 36-bladed discs. The blue data represent the 40 different combinations made from one particular set of blades as shown in Figure 3.10, but each assembly has the blades re-arranged into different positions around the rotor. The green data in the diagram are the maximum peak responses of each arrangement and the brown data are the mean response levels of each arrangement. From these results, one can observe that the maximum response levels display a remarkable range with the assemblies having a peak blade response factor of between 1.3 and 2.1. On the other hand, the mean response level scatter lies within quite a narrow band, mostly around the value of 0.7-0.8. These results show a clear picture explaining the 'rouge blade' phenomenon which is a direct result of the blade distribution arrangement on the rotor wheel.

Furthermore, this information may also be useful for experimental engineers since, in the past, all experimental measurements were based on the measurement of the highest blade response. This value can lie within a wide range and small number of samples from strain-gauge results is therefore highly unreliable. However, from the results of the mean responses level, different assemblies may give a value which is only varying in a narrow range and so all values are close to the mean of the whole population. One can use the mean values of blade responses to interpret a test result and it seems to be a better way than to find the maximum peak response blades directly.

Furthermore, the probability density function (PDF) of the critical blade responses and the mean blade responses can be found empirically and are shown in Figures 3.12 and 3.13. The 40 critical peak response axis is divided into 6 intervals. The occurrences are counted within each interval and then normalised by total number of peak responses. Here, it is interesting to see that the PDF of the critical responses level looks similar to the distribution of blade response, as shown in Figure 3.8. From these two diagrams, the PDF of the mean response level has a standard deviation about 0.02, while the PDF of the critical peak responses has a standard deviation about 0.24 and so the distribution has a quite wide bandwidth. It is therefore quite sensible to use the mean of a particular assembly and to multiply this by a factor to predict the worst possible peak response.

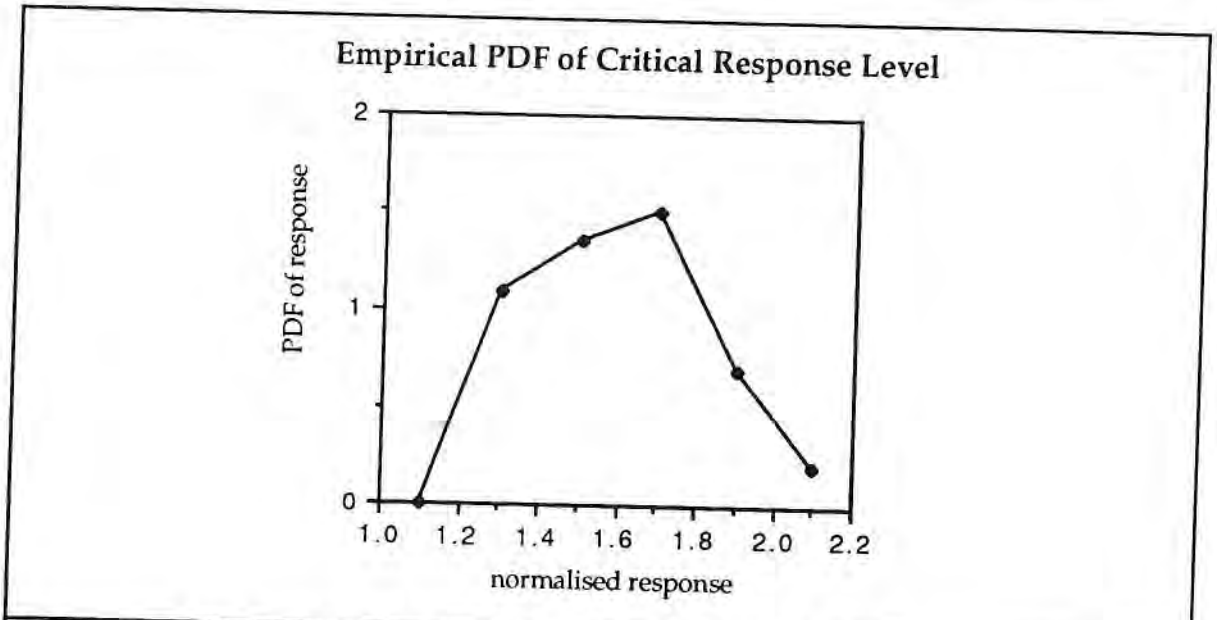

Figure 3.12 Empirical PDF of the critical blades of the 40 arrangements

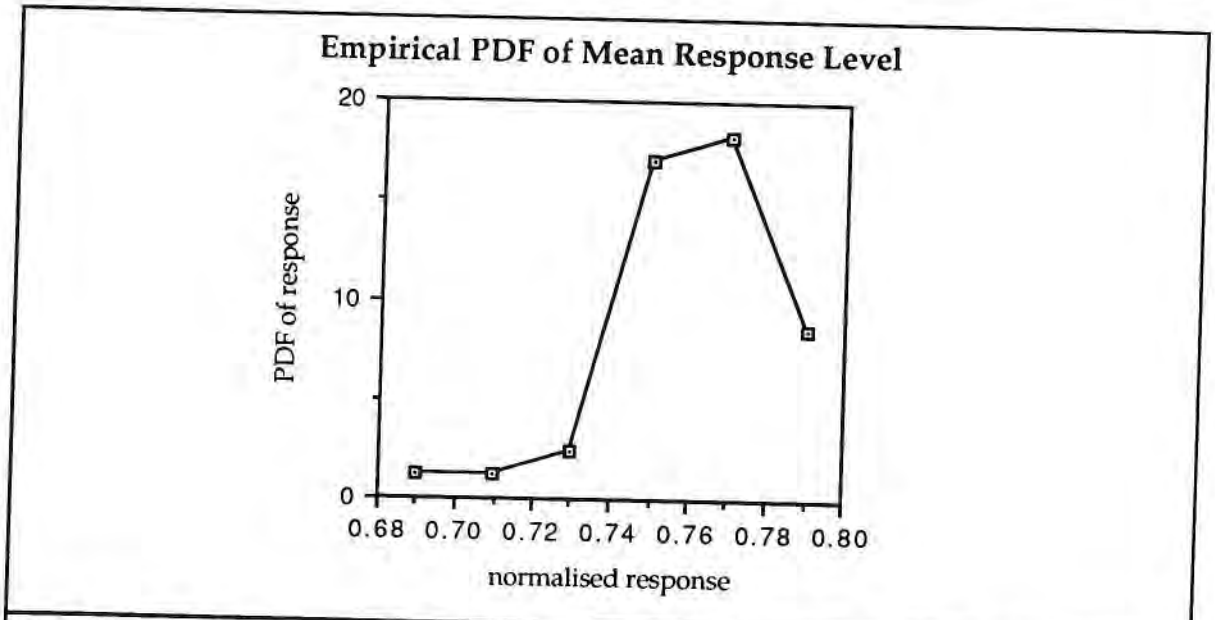

Figure 3.13 Empirical PDF of the mean assembly blades of the 40 arrangements

3.6.2 Optimal arrangements

The blade arrangement studies shown above might use to help avoiding excessive blade vibration by controlling the blade selection process. In this case, it is essential to know the best and the worst arrangements since they are important factors in practice. From the 40 arrangements, one can find some critical arrangements with some worst blade responses over the factor of 2. Figure 3.14 is a critical arrangement of blades around the wheel and this pattern leads to one of the blades suffering a higher response than all the other combinations.

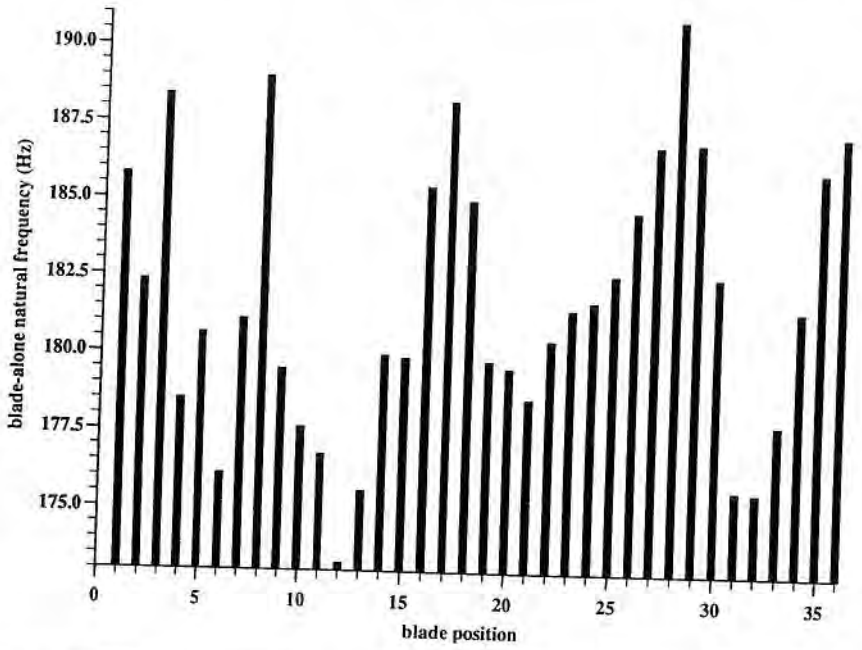

Figure 3.14 Blade cantilever frequency distribution for the critical case

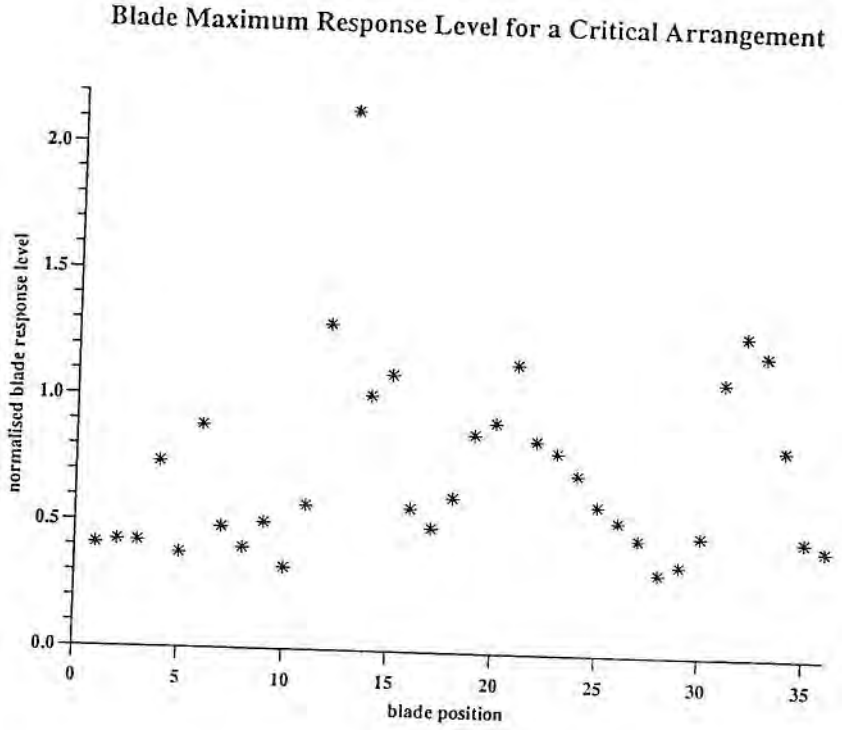

Figure 3.15 Blade maximum response level vs. blade position for the critical arrangement

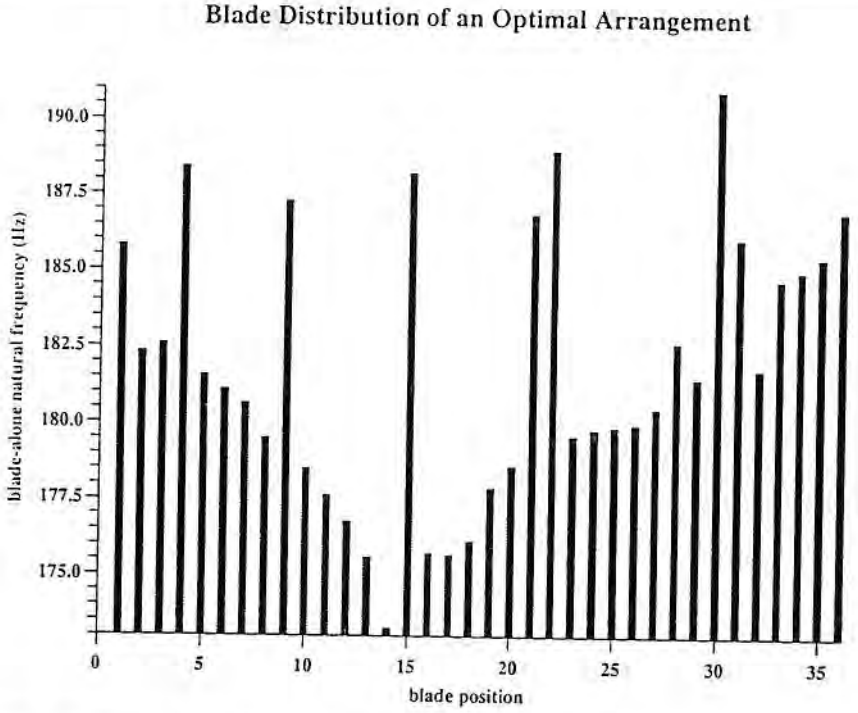

Figure 3.16 Blade cantilever frequency distribution for the optimal case

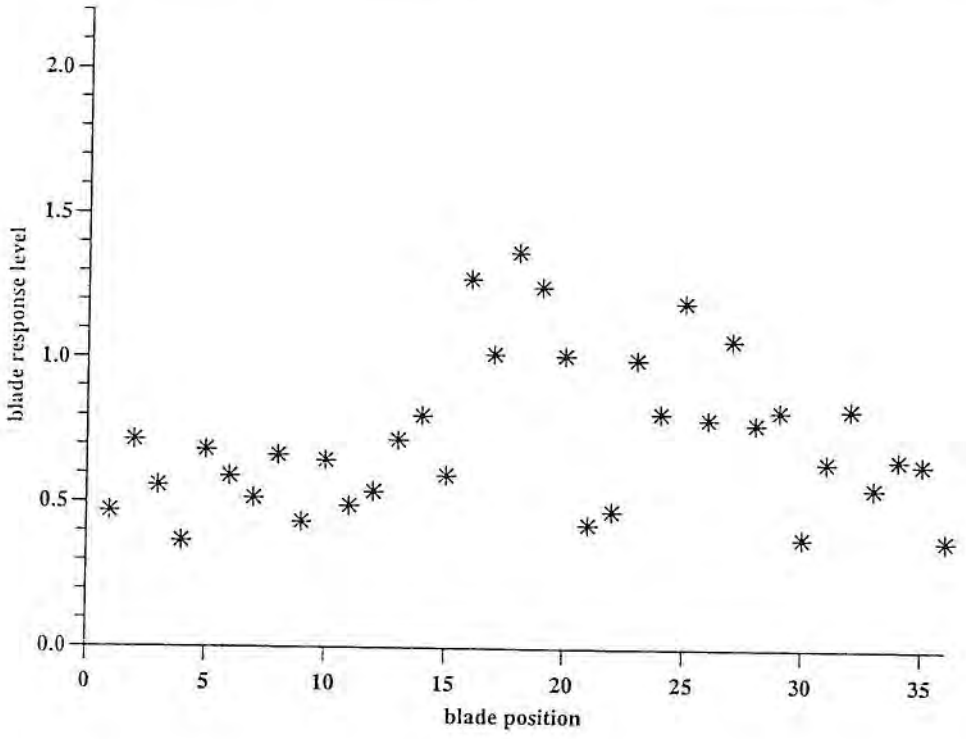

Figure 3.17 Blade maximum response level vs. blade position for the optimal arrangement

Recalling the tuned case, the responses of all blades around a rotor should have identical amplitudes. However, Figure 3.15 shows the normalised response levels scattering on a range between 0.3 and 2.1 for this particular set of blades. In this row, the worst blade locates at the number 13th slot and this blade has the amplitude over 100% greater than a tuned blade response. The rest of the blades have responses scattered around the tuned response level. This particular high-level blade response is usually termed a 'rogue blade' in the industry.

Furthermore, Figure 3.16 shows another arrangement of blades which is one of the optimal blade frequency arrangements. These blades are the same set of blades but their positions on the row are different from the set shown before in Figure 3.14. Again, Figure 3.17 shows the response levels of this set of blades but the worst blade has its amplitude only 40% greater than a tuned blade response. From these graphs, it is seen that one may reduce the worst response levels by re-arranging the same set of blades to different positions around the rotor.

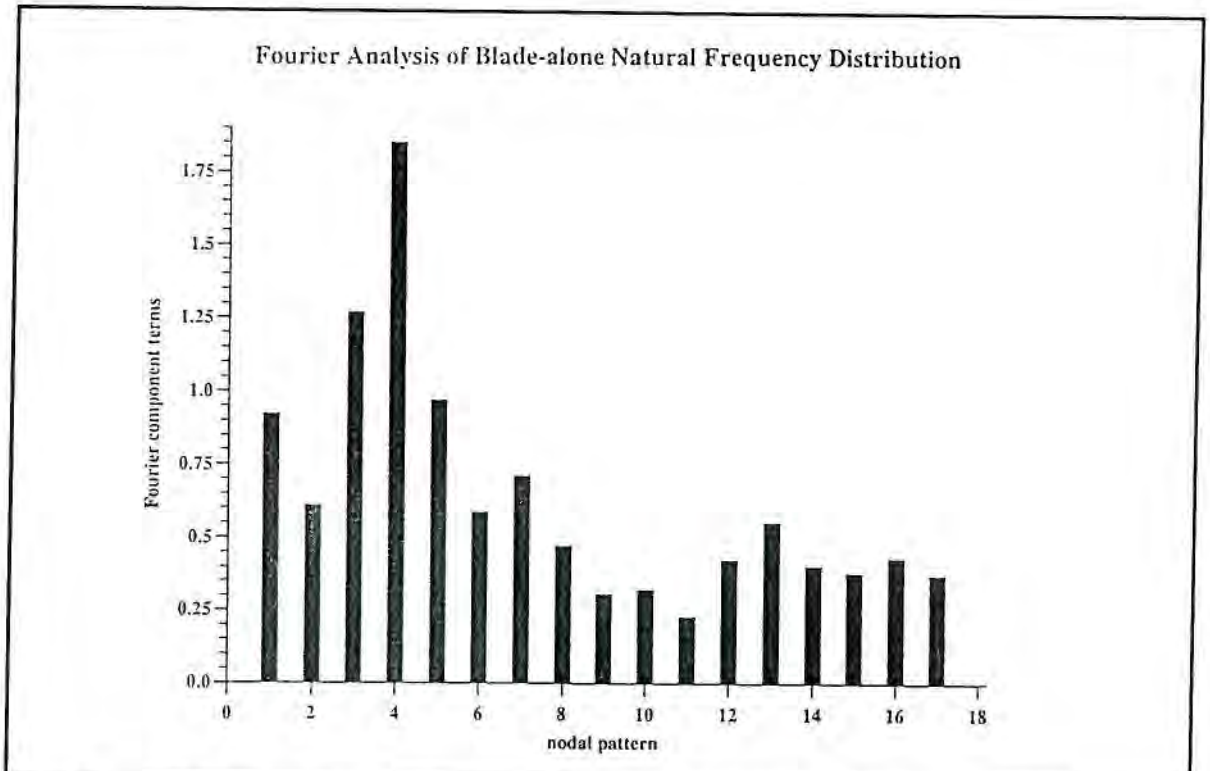

Figure 3.18 Discrete Fourier components of the blade cantilever natural frequencies for the critical arrangement

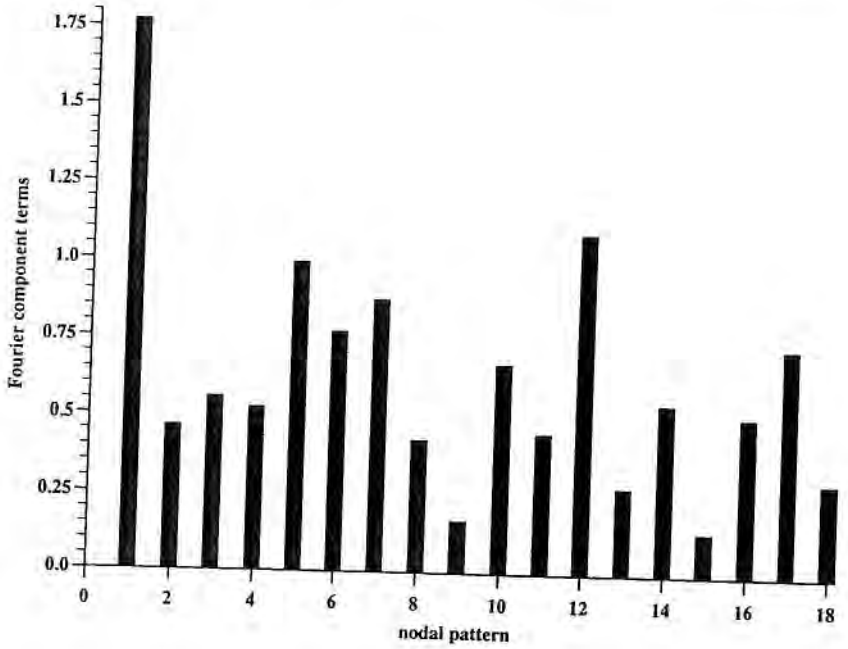

Figure 3.19 Discrete Fourier components of the blade cantilever natural frequencies for the optimal arrangement

If the arrangements of blades show an effect on the levels of blade responses, the patterns of the blade cantilever natural frequencies of a group of blades must be the source attributed to the changes. This is because the difference between a critical-blade response and an optimal-blade response set depends on how the blades are arranged. The discrete Fourier transform (DFT) analysis reveals if any particular nodal diametral component dominates for a given set of data. In other words, the discrete Fourier analysis shows which particular diametral patterns exist in a given set of random blade properties. This method is applied to the two arrangements shown above. Figure 3.18 shows the DFT components of all the possible diametral orders for the critical arrangement while Figure 3.19 shows the DFT components of diametral patterns for the optimal arrangement.

Next, the blade response patterns for these two arrangements are studied. The responses under a 6 engine-order of excitation are complex values whose real and imaginary parts represent the forward and the backward waves. Figure 3.20 and Figure 3.21 show the DFT components of the blade responses for the critical and the optimal arrangements, respectively. Both the forward and backward wave components are included for each case.

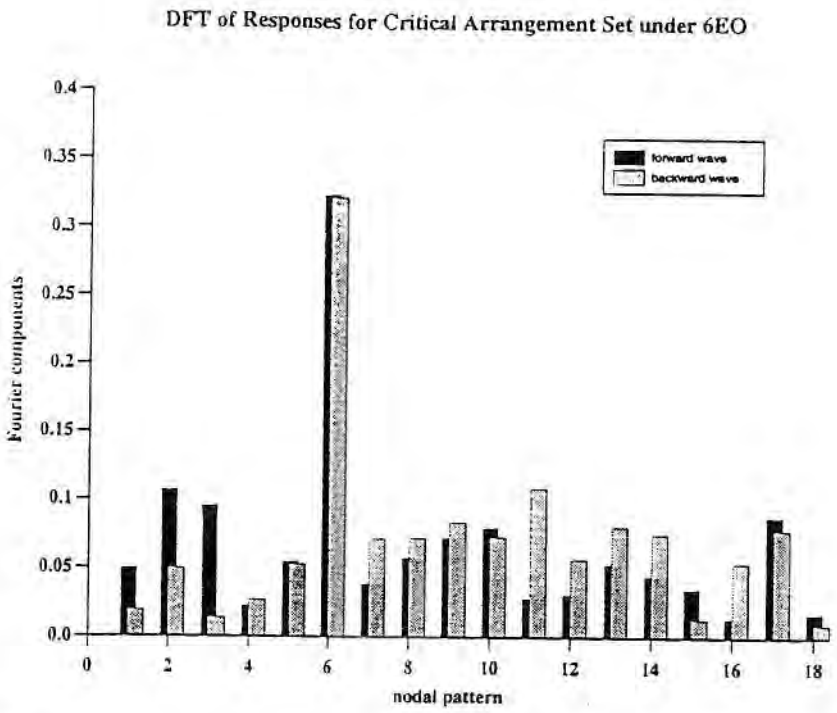

Figure 3.20 Discrete Fourier components of the blade responses for the critical arrangement

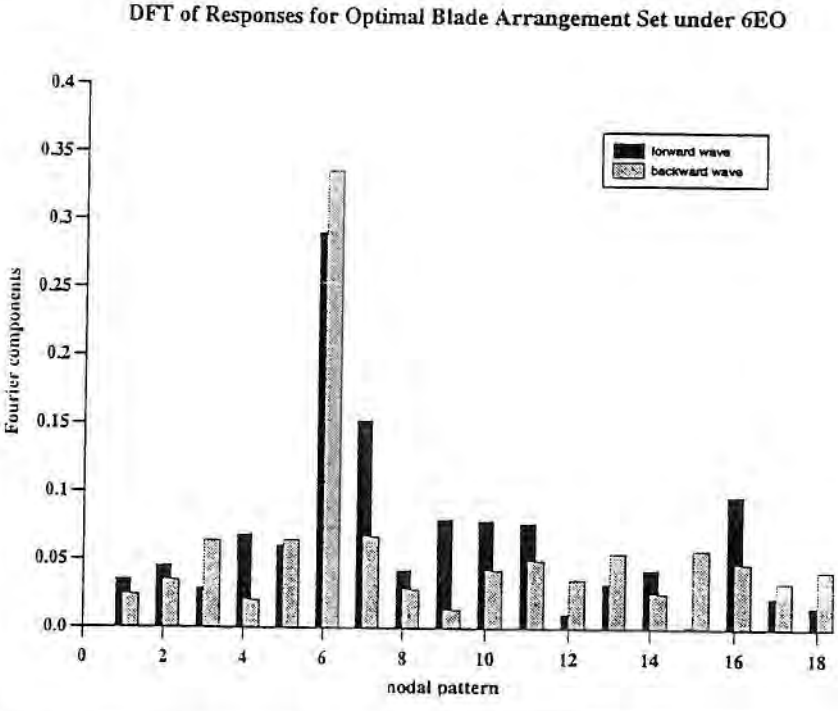

Figure 3.21 Discrete Fourier components of the blade responses for the optimal arrangement

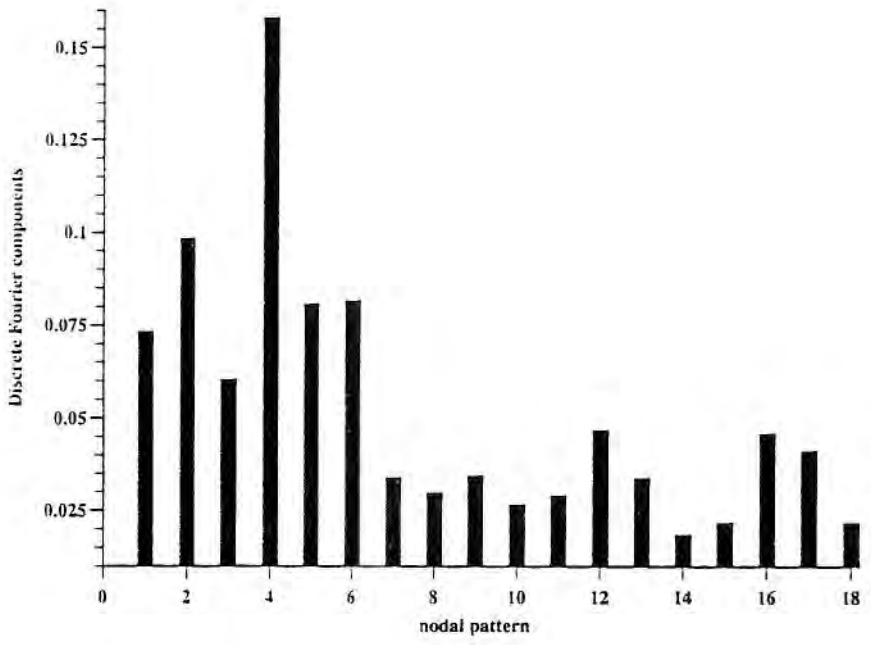

Figure 3.22 Discrete Fourier components of the modulus of the blade responses for the critical arrangement

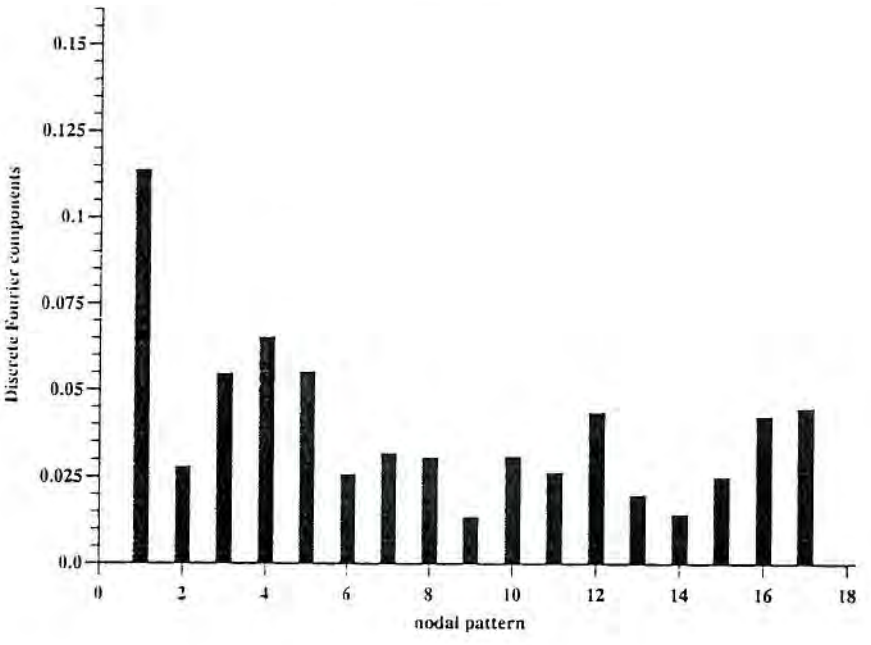

Figure 3.23 Discrete Fourier components of the modulus of the blade responses for the optimal arrangement

Nevertheless, the blade peak responses were often calculated based on the modulus or the absolute value of each blade maximum response. These values were widely used by Griffin and Sanliturk to show the responses increased due to mistuning. If, however, the DFT analysis is applied to the moduli of the blade responses, the component patterns would look like those shown in Figure 3.22 for the critical arrangement of blades and in Figure 3.23 for the optimal arrangements. From these two graphs, the main change from the analysis of individual wave responses is the dominant components of the moduli of the responses are no longer the 6th ND. The dominant component for the moduli of the responses changed to some other pattern. These responses patterns look rather like the patterns from the blade-alone natural frequency

3.6.3 Correlation studies of Blade Arrangements

The study of the two arrangements shown above leads to an important result that the arrangements display two different levels of maximum responses by re-arranging blades only to different slots on the row. This idea prompts a suspicion that the blade arrangement pattern may have something to attribute to the highest response level. One method to examine any influence due to a blade pattern on the blade responses is using the correlation techniques.

Correlation is a data comparison technique which is widely used in science and engineering. There are several approaches to present the correlation of two sets of data. The simplest approach is to plot the two sets of data, say x(i) and y(i), against each other and then to spot the correlation visually. Normally, each set of data is scaled or normalised to a reference value so that a one-to-one correlation means that the two sets of data plot against each other will be lie about a 45° diagonal. Here, the normalisation is shown as follows:

$$(x_i)_{normalised} = \frac{x_i - x_{min}}{x_{max} - x_{min}}, \quad (y_i)_{normalised} = \frac{y_i - y_{min}}{y_{max} - y_{min}} \qquad (3.9)$$

The second method is to measure the absolute difference of each corresponding element from both sets of data as follows:

$$\% \text{ correlation} = \left(\frac{2}{|(x_i)_{normalised} - (y_i)_{normalised}| + 1} - 1 \right) \times 100 \qquad (3.10)$$

A perfect correlation of a one-to-one element should be 100 % while 0 % means no correlation between the two data for that particular element. Finally, there is also a global comparison for two sets of data, x(i), y(i), defined by a linear correlation coefficient (corr) and shown as follows:

$$corr = \frac{\sum_{i=1}^{m} (x(i) - \bar{x})(y(i) - \bar{y})}{\sqrt{\sum_{i=1}^{m} (x(i) - \bar{x})^2} \sqrt{\sum_{i=1}^{m} (y(i) - \bar{y})^2}} \qquad (3.11)$$

where $\bar{x}$ and $\bar{y}$ are the mean value for x(i) and y(i).

Since the blade maximum responses are the peak responses for the engine-order frequency response sweeping through a wide frequency range, correlation has to be at a particular excitation frequency. There exists no direct relation between blade response and the blade-alone natural frequency in the case of mistuning because the blade resonances are different for a rotor. For the critical blade arrangement as shown in Figures 3.14 and 3.15, the worst blade occurs at exciting frequency of 172.8 Hz.

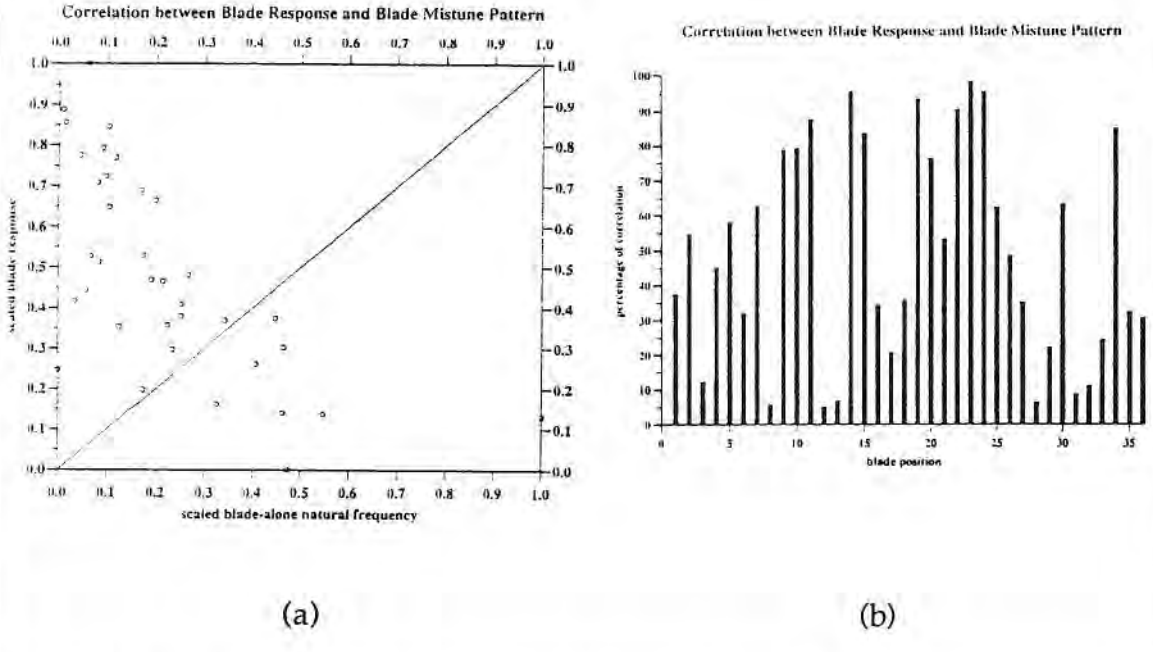

Figure 3.24 Correlation of responses and blade alone natural frequency

Figures 3.24(a) and 3.24(b) present the one-to-one correlation graph for the critical blade responses at 172.8 Hz and blade-alone natural frequencies. In Figure 3.24(a), one might be able to see a negative correlation since most data lie about a slope of -45°. This suggests that the phases between the responses and the blade-alone natural frequencies are different by an angle of 180°. Furthermore, the distribution of data in Figure 3.24(a) might also imply a inverse squared-root correlation since the data displays an inverted quadratic trend. To find this relation, it is possible to draw the logarithm values of the responses against the logarithm values of the blade-alone natural frequency.

From this graph, Figure 3.25, a least-squares fit is used to find the approximate slope for the data and empirically the value tends to be close to the range of -2 to -2.5. In theory, the blade stiffness is, say, proportional to the squared blade-alone natural frequency and the blade responses are proportional to the inverses of the blade stiffness. Hence, a correlation may exist at the level of blade stiffness which correlates with the inverted blade responses and the blade-alone natural frequency squared as shown in Figures 3.26(a) and 3.26(b).

From these studies, a correlation between the blade response and the blade-alone natural frequency suggests that the mistuning of the system has a direct influence to the critical blade response.

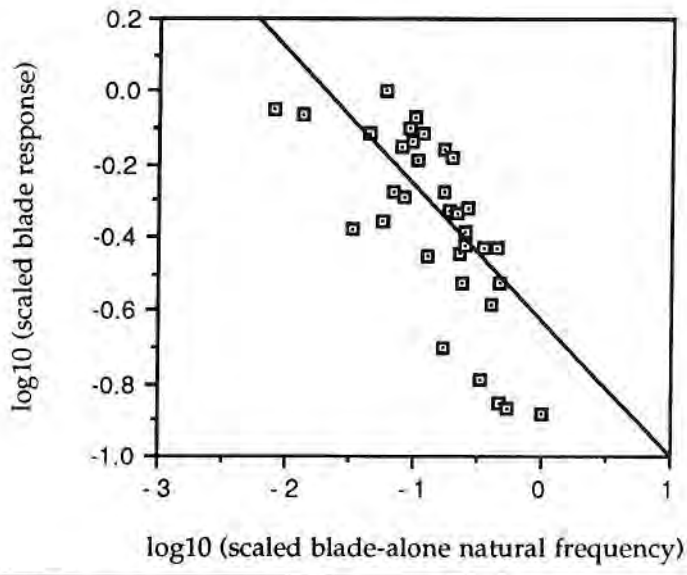

Figure 3.25 Relation graph of the blade response and blade-alone natural frequency

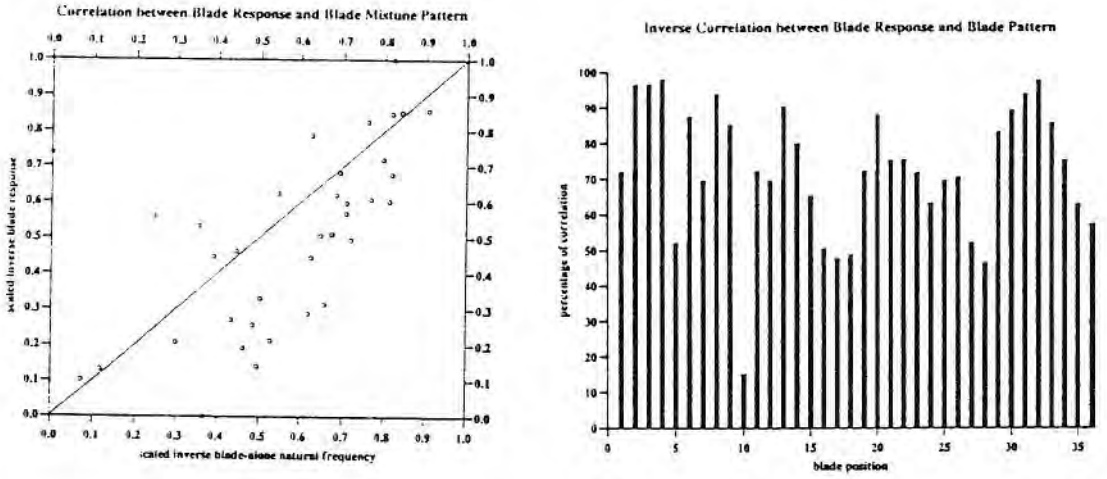

(a) (b)

Figure 3.26 Correlation of the inverted responses and blade-alone natural frequency squared

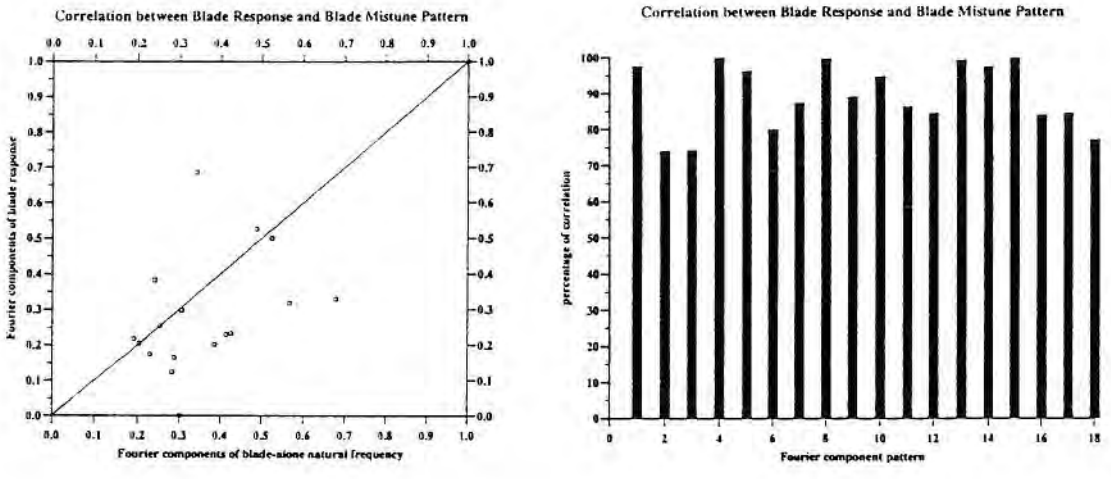

(a) (b)

Figure 3.27 Correlation of the discrete Fourier index for the responses and blade-alone natural frequency

Moreover, if the two sets of data are the Discrete Fourier components of the responses and the blade-alone natural frequency respectively, these two sets of data represent the Fourier indices of the patterns of the data. The correlation between these two sets of data are surprisingly good as shown in Figures 3.27(a) and Figures 3.27(b). These suggest that for a particular exciting frequency, in this case 172.8 Hz, the Fourier indices for both the response and the blade-alone natural frequency have a good correlation. Of course, the difference between the Fourier analysis and the analysis above for direct correlation of the response and the blade-alone natural frequency is the phase influence. Nevertheless, this evidence demonstrates that how the blades are arranged directly affects the response and the Fourier index pattern of the arrangement has most significant effect to the blade response.

The second study on correlation is the case of the optimal arrangement. The worst blade response in this case occurs at the exciting frequency of 173.8 Hz. The response level is about 1.4 times the tuned level, as can be seen from Figure 3.17. Figures 3.28(a) and 3.28(b) are the correlation diagrams showing the optimal blade responses and blade-alone natural frequencies at the exciting frequency of 173.8 Hz.

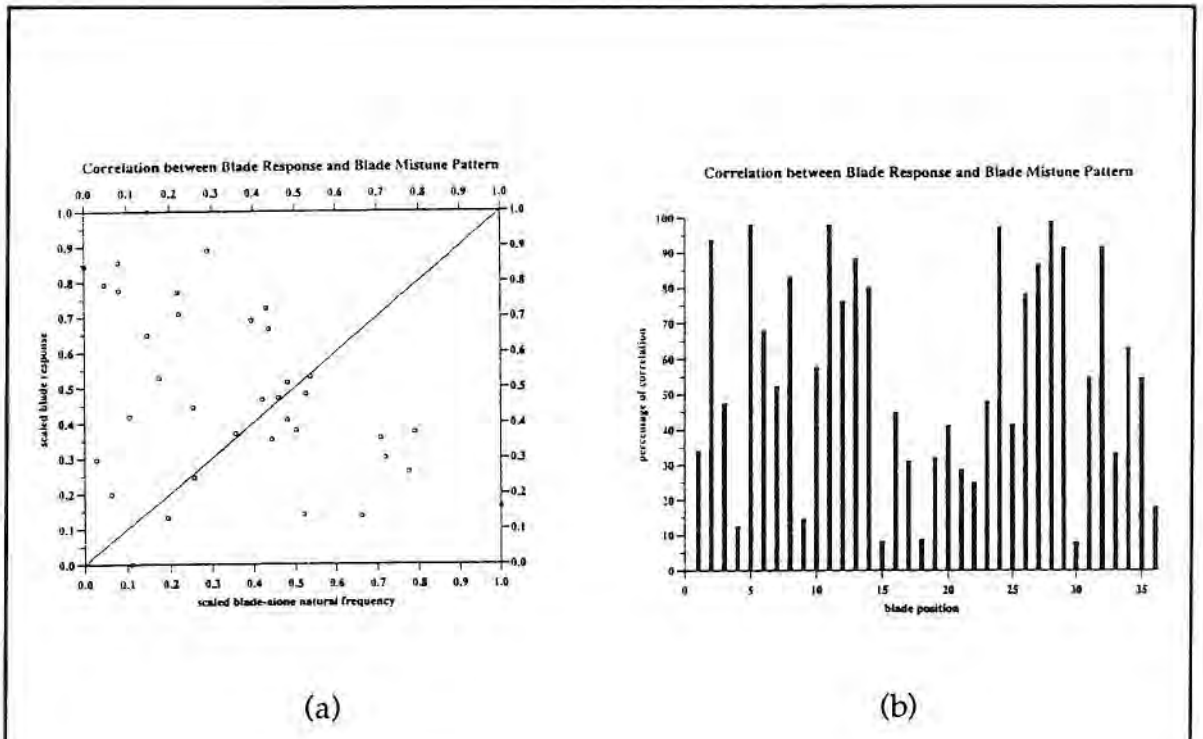

Figure 3.28 Correlation of responses and blade alone natural frequency

The correlation of the Discrete Fourier components for the optimal arrangement is also shown for exciting frequency at 173.6 Hz. Figures 3.29(a) and 3.29(b) are the diagrams showing the local correlation of every blade. Again, there is a correlation which exists for the Fourier indices of the blade-alone natural frequency and the Fourier indices of the blade responses. This further confirms the influence on blade responses of the blade arrangement patterns. The Fourier indices of the blade responses resume similarly to the Fourier indices of the blade-alone natural frequency.

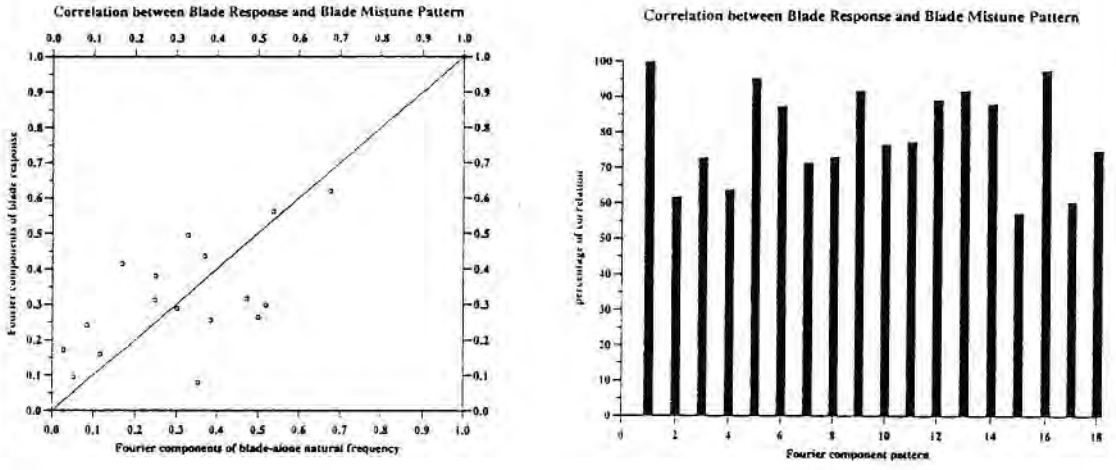

(a) (b)

Figure 3.29 Correlation of the discrete Fourier index for the responses and blade-alone natural frequency

Finally, the global correlation, as shown in equation (3.11), for the Discrete Fourier components on both blade response and blade-alone natural frequency, is plotted against a range of excitation frequency. This range of excitation frequencies covers all the possible maximum peaks of blade responses for both critical and optimal arrangements. In Figure 3.30, each point is a set of data of correlation coefficients for the Fourier indices of blade response and the blade-alone natural frequency as shown before. Generally, the critical arrangement shows more influence over all the excitation frequency range than the optimal one. The correlation studies made here

show agreement that the arrangements of blades around a disc are direct factors to cause the absolute peak responses increased or decreased.

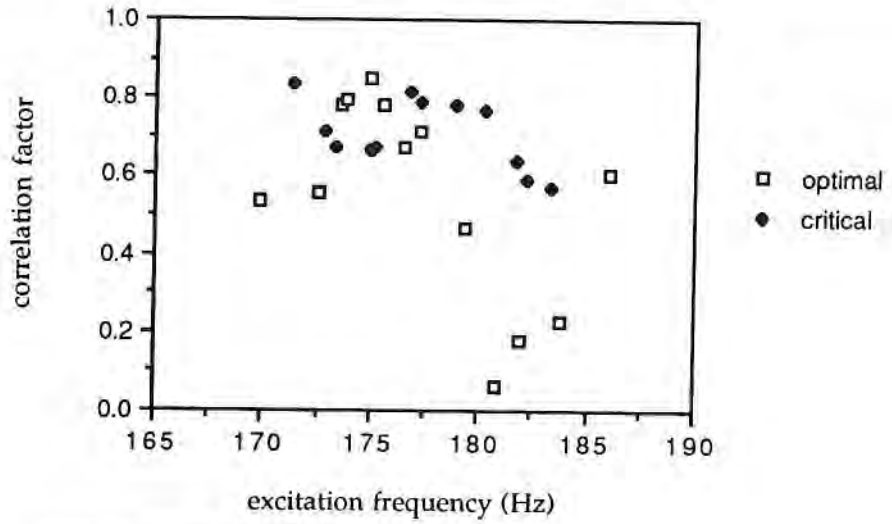

Figure 3.30 Global correlation of the Fourier indices for both arrangements over the exciting frequency range of 172 Hz to 186 Hz

Further numerical simulations demonstrate the critical nodal diameter of a pattern. Some special mistuning patterns are used here. These patterns consist of pure cosine variations for the blade-alone natural frequency. Each individual blade-alone natural frequency is obtained from the equation as follows:

$$f_i(\theta) = \bar{f} + \Delta f \cos(in\theta) \, , \, i = 1,2, \ldots , N \qquad (3.12)$$

where $\bar{f}$ is the mean blade-alone natural frequency and Δf is the amount of the mistuning range. In this study, the range of mistuning is selected to be 10% around the mean value which is consistent with the previous studies of the scatter plots. The diametral pattern n is the variable to be studied on the effect of maximum blade response and θ is the interblade phase angle. Figure 3.31 shows the worst blade response as the nodal diameter n increases. Here, the diametral pattern which leads to the worst blade response is about the 4th diametral pattern for the 6 EO excitation case. A second critical case can be found from Figure 3.31 and is at the 17th diametral pattern. This diametral pattern is actually around to the second maximum condition for $n\theta = 135^o$. Furthermore, different engine-order of excitations on the same blade

distribution also show that the critical nodal diameters are around some critical value.

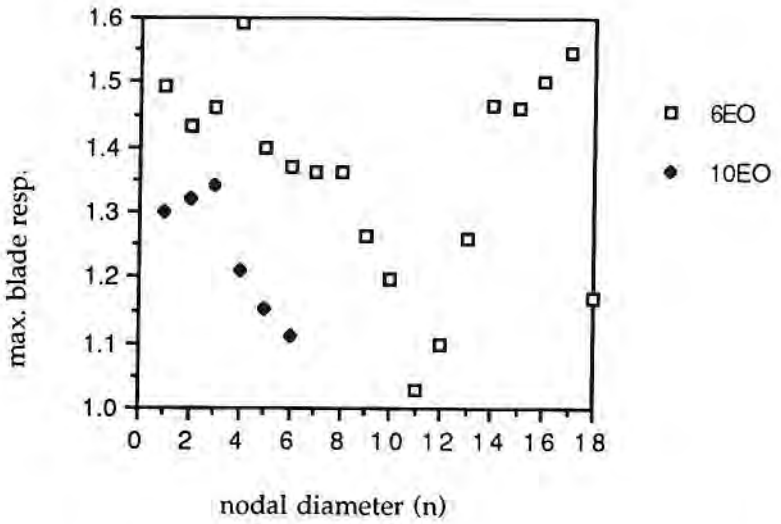

Figure 3.31 Worst blade responses change as the nodal diameter of the distribution pattern (equation 3.19) changes

To sum up, the critical blade responses depend upon the interblade phase angle of the blade-alone natural frequency distribution. The worst case of blade response would happen if the arrangement of the blade-alone natural frequency has a diametral pattern about 45°. A discrete Fourier transform is a very useful tool to find the diametral patterns. The critical diametral for a particular distribution can be found as follows:

$$n_{critical} = \frac{45^o}{\theta} = \frac{45^o \times N}{360^o} = \frac{N}{8}$$

As a result, the number of blades around the rotor is the only factor affecting the critical nodal diameter of a blade distribution. During these studies, it has been noticed that the optimal arrangement often has a dominant low number of nodal diameters. This is because a low diametral pattern, such as 1 ND, can hardly be the worst case unless for the special 8-bladed assembly. Figure 3.32 shows the same set of blades as the critical and the optimal arrangements, but the pattern has been deliberately selected to a 1 ND type. Figure 3.33 shows the absolute blade responses of this blade distribution.

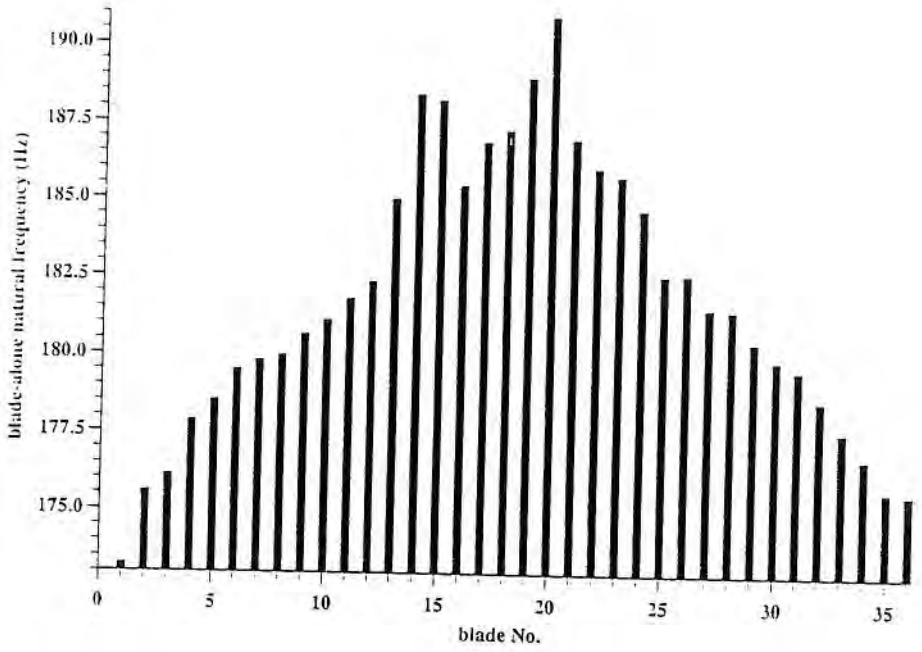

Figure 3.32 Blade arrangement with 1 ND as the dominant component for the blade-alone natural frequency

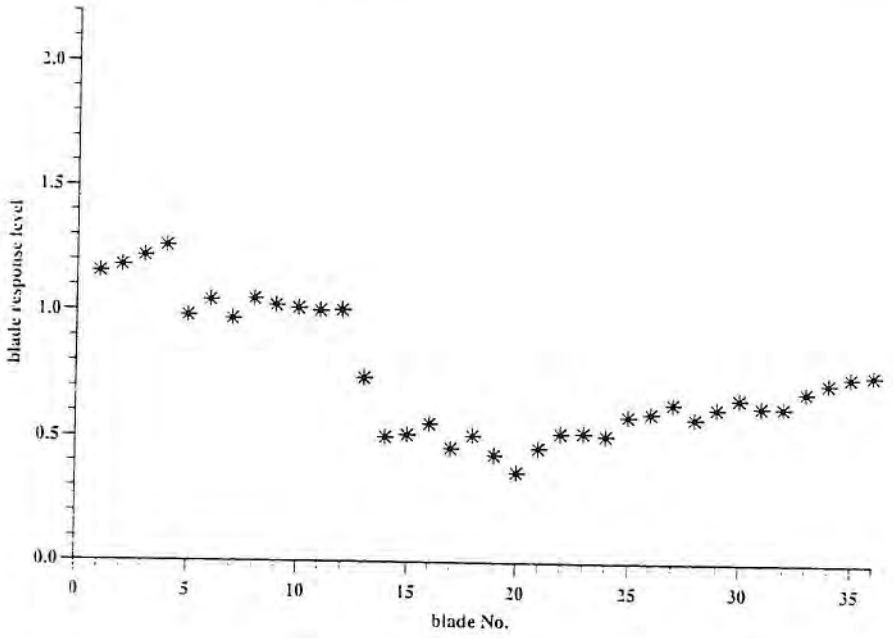

Figure 3.33 Blade response level for the arrangement shown in Figure 3.37

3.6.4 Reliability of Small Samples from Experiments

The reliability of results obtained from small samples is important for practical engine test engineers, since the number of stain gauges available is limited. Only a few blades are strain-gauged. Very often, the blade which suffers the highest stress cannot be picked in advance. From the maximum response studies, such as those shown in Figure 3.15, one can see that there are only a few blades having high responses and most of the rest of the blades are scattered around the tuned level. The worst blade is hence difficult to select by chance. However, from Figure 3.11, the means for different assembly builds are close to each other. This effect, as shown on the right-hand y-axis in Figure 3.11, is quite different from the peak or critical responses shown on the left-hand y-axis. This means that no matter how one re-arrange the blades on the wheel, the mean of their response will not change by a large amount.

Next, the reliability of samples is investigated as the number of available samples decreases. Figure 3.34 shows the scatter of means by selecting the i highest response blades (as shown by red marks) and i lowest response blades (as shown by blue marks), for i is the number of samples desired.

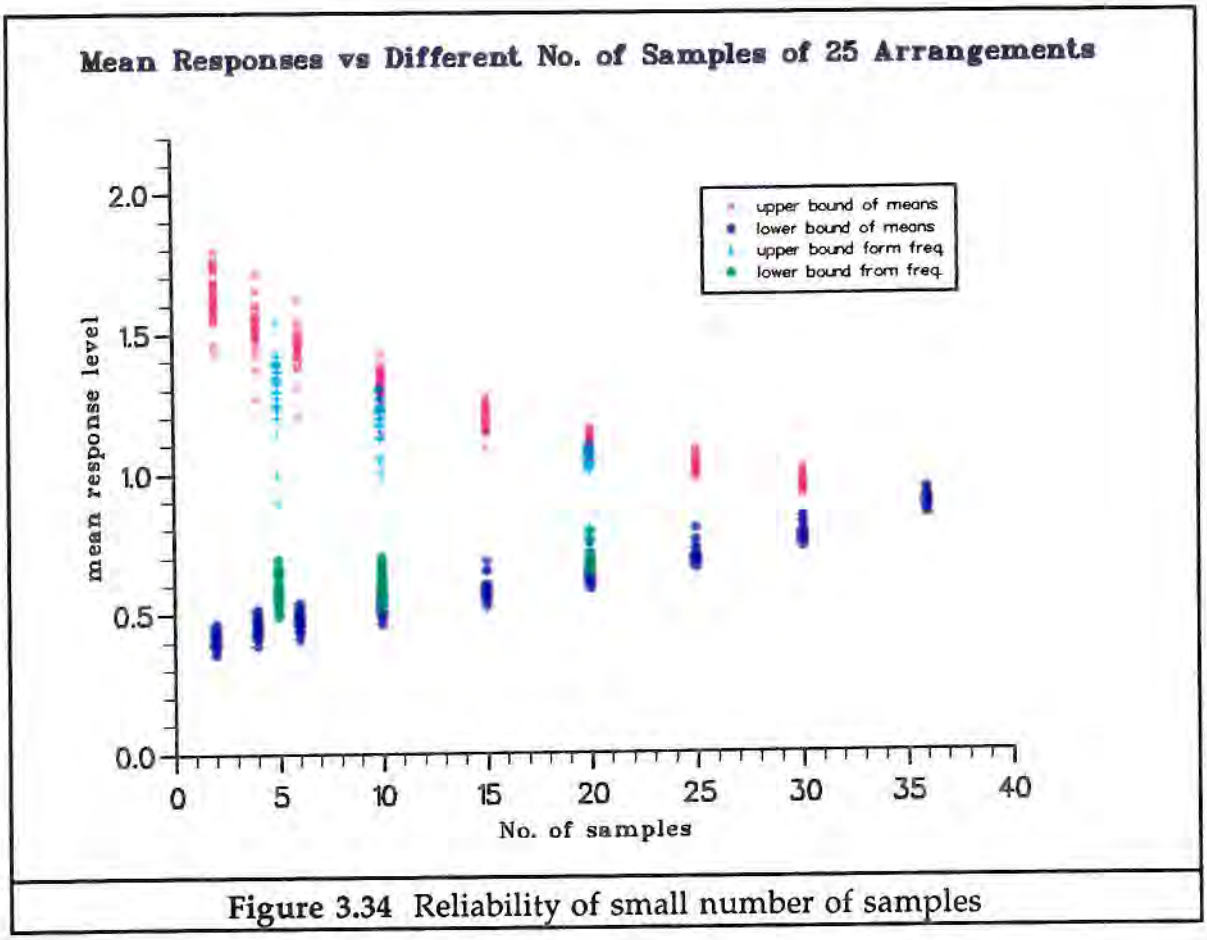

Figure 3.34 Reliability of small number of samples

Meanwhile, the *i* highest frequency blades (as shown by light-blue marks) and *i* lowest frequency blades (as shown by green marks) are also presented. From this graph, the upper and lower bounds from small samples are clear. The profiles by selecting the highest or lowest blade natural frequencies seem to be underestimates of the possible highest or lowest responses. This is because the high- or low-frequency blades may not all necessarily give the high or low responses, but most likely, some critical blades can be picked by selecting some high frequency and some low frequency blades. However, it still can be seen that for very small numbers of strain gauged blades (samples), the reliability of predictions of the worst blade is very poor since the range between the maximum blades and minimum blades is large. As the number of stain gauges increases, the bounds between the high-frequency and low-frequency blades get closer and finally overlaps.

3.7 CONCLUDING REMARKS

This chapter has presented some studies on mistuning effects of a bladed disc system. The purpose of these studies was to demonstrate some mistuning phenomena in a way that are explained for the first time in the literature. The numerical results from the studies lead to the following observations.

- The blade cantilever natural frequency is the preferable parameter to use for mistuned bladed discs. This ensures that the changes agree with realistic mistuned systems. This type of mistuning has been classified as the frequency mistuning. Another class of mistuning can be also identified as the damping mistuning due to changes in the damping levels applied on different blades on a rotor. The blade selection processes have also been discussed in this chapter and the simple 'culling' process is adopted for further analysis.

- The scatter of the peak blade responses between the upper and lower bounds has been found to be an effect due to different blade arrangements around the rotor. The critical blade responses were examined and the results showed that such high- stressed blade, or namely the 'rogue blade' is dependent on the arrangement of the blades around the rotor. Therefore, the high stress on a particular blade can be avoided by re-arranging the blades around the disc.

- Further studies of the relationship between the blade-alone natural frequencies and the blade responses show correlation on the discrete Fourier transform components from both sets of data. Therefore, the blade arrangements depend on the diametral components in an arrangement. Theoretically, the critical diametral pattern has been found as $n_{critical} = \frac{N}{8}$. Numerical results showed agreement in that by avoiding this condition with arrangements of blades around a rotor.

- Finally, the reliability of small samples was also studied. The result shows that a large number of samples are required in order to get reasonable confidence from the result of strain gauge tests to predict the highest response blade. However, the mean from a limited set of test data could be a better parameter to represent the mean of the whole assembly.

CHAPTER 4

MISTUNING EFFECTS ON COUPLED BLADED DISC RESONANT RESPONSES

About this chapter

In the previous chapter, both frequency and damping mistuning types have been defined. Some numerical examples have been presented to show the mistuning behaviour of a bladed disc system. In this chapter, further investigations are presented concerning the factors which affect the mistuning characteristics of a bladed disc. One significant factor is the disc-to-blade coupling effect. Recently, there have been studies of mode localisation effects for disordered periodic structures. A major objective for these studies was to examine the influence of coupling between the sub-systems in a periodic structure and a bladed disc system is just a particular type of these periodic structures.

Due to the influence of disc flexibility, the bladed disc system as a whole behaves differently to blade-alone or disc-alone characteristics. There are two factors which can affect this coupling. First, the mass effect can be considered by blades coupled with different discs in which disc-alone natural frequencies are almost the same but in which the two components are made from different materials. Second, a frequency effect occurs when the disc dimensions are changed but with the disc material remains the same. This chapter examines both of these effects and a new bladed disc coupling factor used here gives a general description to a bladed disc system.

Furthermore, different amounts of frequency mistuning on blades also seem to have an impact on the blade responses. A 3-dimensional presentation of the coupling factor and the amount of mistuning versus the worst response provides a more general approach for understanding the mistuning behaviour in a bladed disc system.

4.1 INTRODUCTION

The failure of many turbomachinery blades is the result of excessive blade vibration levels, which are often due to resonance conditions of the bladed disc. Therefore, many studies have been made on the parameters such as the natural frequencies, modeshapes, modal damping, and resonant responses. Apart from these parameters, there are also factors causing the above parameters to vary from case to case. Clearly, mistuning is one of these factors. Nevertheless, due to the coupling effect between blades and disc, the bladed disc system as a whole behaves differently to the blade-alone or disc-alone characteristics. Practical experience shows that some types of bladed disc are more sensitive to mistuning influences than others, since all bladed discs have mistuning among the blades. This suggests that the coupling factor between blade and disc may cause the blade response levels to vary differently between different bladed discs. This chapter concentrates on the effects from the factors, such as the amount of mistuning and the disc coupling effect of a bladed disc system.

The influence of a disc on blade vibration was first discussed by Armstrong et al. [5]. They showed the characteristics of the natural frequencies of bladed discs and gave correlation between both experimental results and theoretical calculations. Some parameters which affect the coupling, such as the blade length to disc radius ratio, were also identified, although the coupling effect was not defined in a general form. Later, modelling the disc effect on turbomachinery blade vibrations has been reported by Wagner [148], Dye and Henry [28], and Ewins [34], amongst others. They also showed the blade mistuning effect by taking into account the disc flexibility. Ewins, in 1969 [31], also published a paper on the study of double modes with detuning. The most significant part of the paper is the introduction of a detuning parameter which is a ratio of the percentage of detuning to the percentage of damping. This parameter described the coupling effect in a more general form than that used by Armstrong and others.

Meanwhile, research studies on continuous beams and plates, which started even earlier, showed that the normal modes of repeated structures varied drastically from their usual shapes with the introduction of random imperfections within each segment. In 1977, P. W. Anderson and N. Mott

shared the Nobel prize in physics for their contribution to work on the localisation phenomenon in lattice structures. Their research work dated back twenty years, when they explained how an "ordered" crystal lattice might change its conductivity abruptly by the addition of a small amount of impurities or imperfections. Their explanation was based on the theory that the state vectors or eigenmodes of the Schodinger equation, which described the transport properties of the solid, become localised when impurities were added [115]. In 1982, Hodges demonstrated this mode localisation phenomenon in structural dynamics by using a simple pendulum model [55]. He showed that the dynamic behaviour of a nearly-perfect structure changed due to the coupling effect between the substructures. Since each substructure was coupled with the adjacent substructures, it was subjected to some coupled elasticity from the adjacent substructures. Later, Pierre [116] and others defined a coupling parameter for bladed discs which is a "coupling frequency" divided by the individual substructure natural frequency. This coupling frequency was the natural frequency of the adjacent substructure as on its own. However, his bladed disc model was insufficient to define the general practical case because the model used by Pierre and others consisted only of a single-degree-of-freedom and grounded oscillators coupled to each other through springs. This model might better represent blades coupled by shrouds on a very stiff disc but the actual blade-to-disc coupling effect was not simulated. Therefore, a new coupling factor is suggested here as a function of the ratio of the bladed disc natural frequency (or the assembly natural frequency) to the blade-alone natural frequency. Numerical results show that this new coupling factor defines the bladed disc coupling in a more general way than the previous version.

4.2 MODE LOCALISATION OF VIBRATING PERIODIC STRUCTURES

Structures made up of repeated identical sections are termed periodic structures and they include continuous structures of beams, plates or shells such as aircraft fuselages, cyclic-symmetric structures such as bladed discs and space reflectors, and pendula, amongst the others [115]. Since no material is completely homogeneous and no components are manufactured exactly the same, imperfections among the structural components are inevitable, and so the actual structures are all nearly, rather than exactly, periodic. However, the vibration characteristics of such a nearly periodic structure can be severely influenced by the presence of small changes in the parameters. A 2-DOF

coupled oscillator is the first example to demonstrate the localisation phenomenon.

4.2.1 Coupled 2-DOF Oscillator

The following 2-DOF oscillator is taken from a Cargill's report [17] and the following shows a different study from Cargill for this model using a linear perturbation analysis. The purpose of showing this example is to give some explanations of the physics of mode localisation effects. The coupled pendula and the mass-spring system are shown in Figure 4.1.

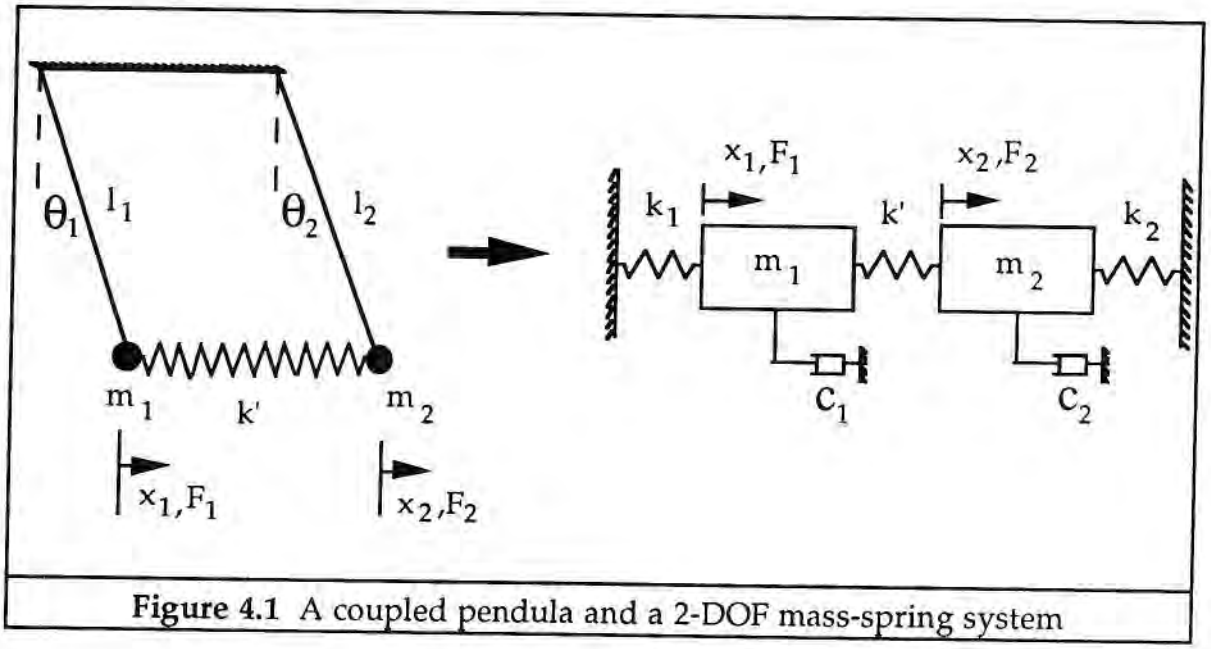

Figure 4.1 A coupled pendula and a 2-DOF mass-spring system

For the pendula, assuming both strings are identical and extensible. Mistuning is only introduced by different masses. Suppose x_1 and x_2 are the displacements for the masses 1 and 2. The extension of a string 1 can be found as follows:

$$l'_1 - l_1 = x_1 \sin\theta$$

The string tension $$T = \left(\frac{l'_1 - l_1}{l_1}\right) EA = \left(\frac{EA}{l_1}\sin\theta\right) x_1$$

For dynamic equilibrium of the mass 1 $$m\ddot{x}_1 + T\sin\theta - k'(x_2 - x_1) = 0 \quad (4.1)$$

or $$m\ddot{x}_1 + \left(\frac{EA}{l_1}\sin^2\theta\right) x_1 - k'(x_2 - x_1) = 0$$

where k′ = coupling spring constant and one can also let $k_1 = \left(\frac{EA}{l_1}\sin^2\theta\right) + k'$. Likewise, the equation of motion of mass 2 can also be found in a similar way. The equations of motion of such a system can be written as follows:

$$m_1\ddot{x}_1 + c\dot{x}_1 + k_1x_1 = k'x_2 + F_1 \qquad (4.2a)$$

$$m_2\ddot{x}_2 + c\dot{x}_2 + k_2x_2 = k'x_1 + F_2 \qquad (4.2b)$$

If ω_0 is the natural frequency of each individual substructure and is identical for each of the subsystems, the coupling of the whole structure can be seen to be through the spring k′ only. If $k_1 = k_2 = k$, putting $\frac{k'}{k} = \kappa$ and $\frac{F}{k} = f$ and using the harmonic transforms of $x = \hat{x}e^{j\omega t}$, and $f = \hat{f}e^{j\omega t}$, equations (4.2a) and (4.2b) become the following:

$$(1 - \frac{m_1\omega^2}{k} + \frac{jc\omega}{k})\hat{x_1} - \kappa\hat{x_2} = \hat{f_1} \qquad (4.3a)$$

$$(1 - \frac{m_2\omega^2}{k} + \frac{jc\omega}{k})\hat{x_2} - \kappa\hat{x_1} = \hat{f_2} \qquad (4.3b)$$

Supposing that the mass m_0 is the mean mass for the system or when the system is tuned, by applying a linear perturbation analysis (details of the principle can be found in Appendix IV), the mistuning parameter is assumed to be small perturbations on the masses m_1 and m_2 so that the rest of the system variables are defined as follows:

$$m_1 = m_0 - \varepsilon m_1 + \ldots, \qquad m_2 = m_0 - \varepsilon m_2 + \ldots$$
$$\omega = \omega_0 + \varepsilon\omega_1 + \ldots, \qquad \omega^2 = \omega_0^2 + \varepsilon\omega_2^2 + \ldots$$
$$\hat{f_1} = \hat{f_0} + \varepsilon\hat{f_1} + \ldots, \qquad \hat{f_2} = \hat{f_0} + \varepsilon\hat{f_2} + \ldots$$
$$\hat{x_1} = \hat{x_1} + \varepsilon\hat{x_{11}} + \ldots, \qquad \hat{x_2} = \hat{x_2} + \varepsilon\hat{x_{21}} + \ldots$$

By substituting the above terms into equations (4.3a) and (4.3b) and by equating the coefficients of the first perturbation term ε only, the following set of equations can be deduced as follows:

$$(1 - \frac{m_0\omega_0^2}{k} + \frac{jc\omega_0}{k})\hat{x_1} - \kappa\hat{x_2} = \hat{f_0} \qquad (4.4a)$$

$$(1 - \frac{m_0\omega_0^2}{k} + \frac{jc\omega_0}{k})\hat{x_2} - \kappa\hat{x_1} = \hat{f_0} \qquad (4.4b)$$

$$\left(\frac{m_1\omega_0^2}{k} - \frac{m_0\omega^2}{k} + \frac{jc\omega}{k}\right)\hat{x_1} - \kappa\hat{x_2} = \hat{f_1} \tag{4.4c}$$

$$\left(\frac{m_2\omega_0^2}{k} - \frac{m_0\omega^2}{k} + \frac{jc\omega}{k}\right)\hat{x_2} - \kappa\hat{x_1} = \hat{f_2} \tag{4.4d}$$

Clearly, the first two equations are the generating solutions from perturbation. If mistuning exists on the masses only, the stiffnesses k_1 and k_2 would be both equal to k and the amounts of damping for both masses are the same as well. One can introduce the following conditions for simplifying equations (4.4c) and (4.4d).

$$m_0\omega_0^2 = k, \quad \frac{m_1-m_2}{2m_0} = \Delta, \quad m_0 = \frac{m_1+m_2}{2},$$

$$\omega^2 = \omega_0^2(1-p), \qquad \text{and} \qquad \frac{c\omega}{m_0\omega_0^2} = \delta$$

The system of equations can then be reduced to the following form as follows:

$$\begin{bmatrix} p + j\delta + \Delta & -\kappa \\ -\kappa & p + j\delta - \Delta \end{bmatrix} \begin{Bmatrix} \hat{x_1} \\ \hat{x_2} \end{Bmatrix} = \begin{Bmatrix} \hat{f_1} \\ \hat{f_2} \end{Bmatrix} \tag{4.5}$$

Assuming the damping and the forces are zero, the undamped normal mode analysis of equation (4.5) would result to two possible families of characteristic frequencies as follows:

$$p = \pm\sqrt{\Delta^2 + \kappa^2} \tag{4.6}$$

Obviously, p is the frequency parameter and Δ is often referred as the disorder factor or mistuning factor, and can be a variable. A plot of the frequency parameter p against the disorder factor Δ is called the locus of the eigenvalues and Figure 4.2 displays such a graph for the 2-DOF oscillator.

Some observations from Figure 4.2 and equation (4.6) can immediately lead to some useful conclusions. The two curves shown in Figure 4.2 would never cross each other if the system is coupled and they veer away as the parameter Δ increases. This phenomenon is known as *Curve Veering* and many recent research works provide a vast literature on this. For example, Pierre [116] gave very clear explanations of the behaviour of curve veering using various examples. Furthermore, if κ is increased, the curves will separate further as

shown in Figure 4.2. In this case, the system is said to be strongly coupled since κ is the ratio between the coupling spring stiffness and the string stiffness in Figure 4.1. However, if the system is decoupled this implies that κ is equal to zero, and the two curves will then cross at point where Δ equals zero. The coupling separates the modes into the two separate families.

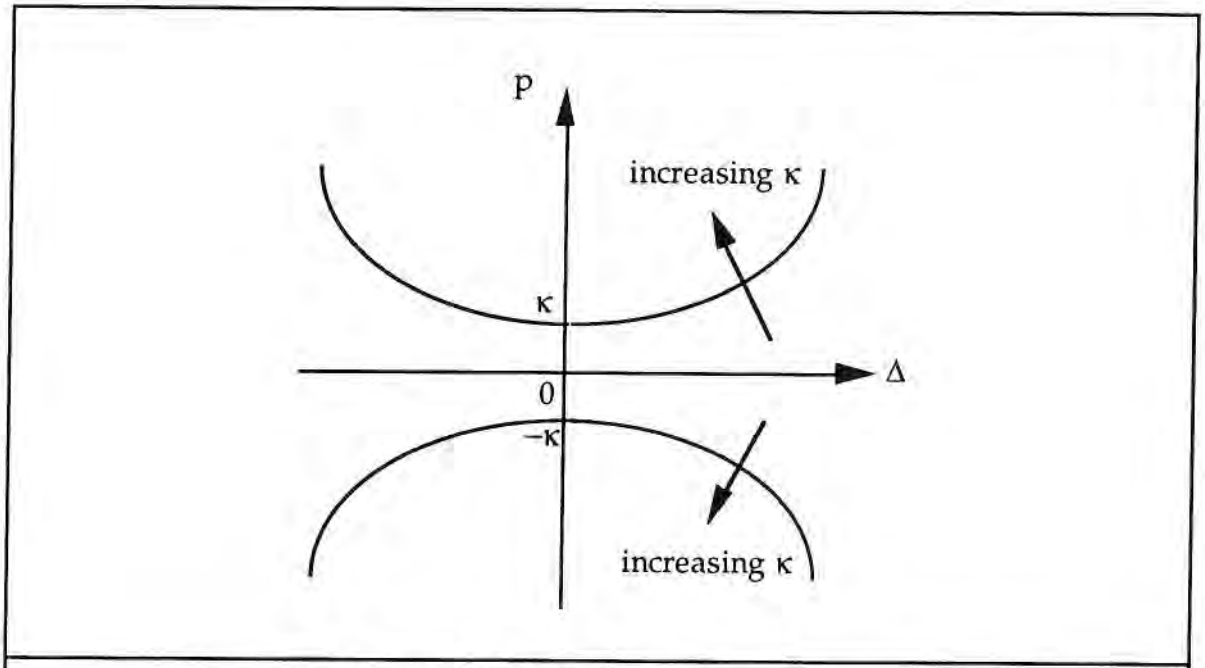

Figure 4.2 Loci of the eigenvalues

4.2.2 Forced Response Analysis of the 2-DOF Oscillator

The forced response solution to equation (4.5) can be performed as follows:

$$\begin{Bmatrix} \hat{x}_1 \\ \hat{x}_2 \end{Bmatrix} = \begin{bmatrix} p + j\delta + \Delta & -\kappa \\ -\kappa & p + j\delta - \Delta \end{bmatrix}^{-1} \begin{Bmatrix} \hat{f}_1 \\ \hat{f}_2 \end{Bmatrix} \tag{4.7}$$

The force vector to simulate the engine-order type of excitation expresses its form as follows:

$$\begin{Bmatrix} \hat{f}_1 \\ \hat{f}_2 \end{Bmatrix} = f \begin{Bmatrix} \cos n0^o + j \sin n0^o \\ \cos n180^o + j \sin n180^o \end{Bmatrix} \tag{4.8}$$

where n is an integer number indicating the engine order and $j = \sqrt{-1}$. Therefore, the system is under an equal magnitude but different phase excitation. Furthermore, the force, $\hat{f}_2$, will be positive if the integer, n, is even

and it will be negative if n is odd. To simplify the equations, let $q = p + j\delta$. Then, the possible responses may have the form as follows:

$$\begin{Bmatrix} \hat{x}_1 \\ \hat{x}_2 \end{Bmatrix} = \frac{1}{|\det|}\begin{bmatrix} q - \Delta + \kappa \\ \kappa + q + \Delta \end{bmatrix} \quad \text{or} \quad \begin{Bmatrix} \hat{x}_1 \\ \hat{x}_2 \end{Bmatrix} = \frac{1}{|\det|}\begin{bmatrix} q - \Delta - \kappa \\ \kappa - q - \Delta \end{bmatrix}$$

where $|\det| = (q - \Delta)(q + \Delta) - \kappa^2 = q^2 - \Delta^2 - \kappa^2$

If we take any of these equations, there are three possible variables q, Δ, κ in the equation and all these variables may affect the response magnitude. Therefore, the values of Δ and κ have to be fixed and the response equation can be differentiated with respect to q to find the conditions for maximum response. These conditions are evaluated as both the mistuning amount Δ^* and the spring ratio κ^* are fixed for a particular frequency parameter study.

$$q = \kappa^* - \Delta^* + j\sqrt{2\kappa^*\Delta^*} = p + j\delta \tag{4.9}$$

Therefore, the absolute values of the frequency parameter are

$$p = \pm\sqrt{\kappa^{*2} + \Delta^{*2} - \delta^2} \tag{4.10}$$

for maximum responses to be encountered. Since the mistuning factor Δ^* is a small value and δ can be assumed to be small as well, the frequency parameters are approximate to $\pm\kappa^*$ for the case of maximum responses. From Figure 4.2, these points locate closely the vertex of the locus of the eigenvalues. Therefore, the worst effect from mistuning happens when the frequency parameter close to the vertex of the eigenvalue locus.

4.3 BLADED DISC COUPLING INFLUENCES

4.3.1 Bladed Disc Coupling Factor

From the 2-DOF oscillator study, there are many parameters causing the response magnitudes to vary. For a multi-degree-of-freedom system, there are even more factors and this is more complicated for analysis. Therefore, the direct approach mentioned in Chapter 3 is adopted here again. The mathematical model of a shroudless bladed disc represented in matrix form can be shown as follows:

$$[\mathbf{M}]\{\ddot{x}\} + [\mathbf{C}]\{\dot{x}\} + ([\mathbf{K}] + j[\mathbf{D}])\{x\} = \{f\} \tag{4.11}$$

where [M] is the mass matrix, [C] is the viscous damping matrix, [K] is the stiffness matrix, [D] is the hysteretic damping matrix, and j is $\sqrt{-1}$. These equations of motion can be re-written as follows:

$$\ddot{x}_i + 2\zeta_i\omega_{b_i}\dot{x}_i + \omega_{b_i}{}^2(x_i - y_i) + i\eta\omega_{b_i}{}^2x_i = q_i(t) \tag{4.12a}$$

$$\frac{M_i}{m_i}\ddot{y}_i - (1 + j\eta)\,\omega_{b_i}{}^2x_i + (\omega_{n_i}{}^2 + 2\frac{K_d}{m_i} + \frac{K_G}{m_i})\,y_i - \frac{K_d}{m_i}y_{i-1}$$

$$- \frac{K_d}{m_i}y_{i+1} = 0 \tag{4.12b}$$

so that ω_b is the blade cantilever natural frequency and q(t) = f(t)/m.

The approach for the analysis of the multi-degree-of-freedom system is similar to the study of the 2-DOF example shown above. First, it is appropriate to find a coupling factor relating the blade substructure natural frequency to the assembly natural frequency. This coupling factor is equivalent to the frequency parameter p in the previous 2-DOF oscillator. Let $x = Xe^{j\omega t}$, and $q(t) = Qe^{j\omega t}$, etc. equation (4.12a) can be written as follows:

$$(\omega_{b_i}{}^2 - \omega_{s_i}{}^2)\,X_i + 2j\zeta_i\,\omega_{b_i}\omega_{s_i}X_i - \omega_{b_i}{}^2Y_i + j\eta\omega_{b_i}{}^2X_i = Q_i \tag{4.13}$$

By neglecting the damping, it can be found that the coupling to the disc deflection Y is duly coming from the blade cantilever natural frequency. Since there is no excitation applied to the disc, apart from the coupling effect from the blade, the ratio between the blade deflection and the disc deflection is related by a factor α as follows:

$$\alpha_i = \frac{\omega_{b_i}{}^2 - \omega_{s_i}{}^2}{\omega_{b_i}{}^2} = 1 - \frac{\omega_{s_i}{}^2}{\omega_{b_i}{}^2} \tag{4.14}$$

For a tuned bladed disc, ω_b is the same for every blade. The blade deflections are just the disc rim deflection multiplied by the coupling factor and this factor is the same for all the blades. In other words, the blade configuration simply

reproduces the same nodal diametral pattern as the disc rim. However, in the mistuned case, the blade cantilever natural frequency will be different from blade to blade and the coupling factor for the mistuned case will also vary from blade to blade. The differences between the blades will transfer to the disc deflections. These will cause the disc modes to split because the disc is cyclically symmetric. Under this condition, the disc deflections lose their normal patterns because of the blade mistuning and hence the coupling between each blade and the disc will not be the same for every blade any more.

The disc-alone natural frequencies can be evaluated analytically by using the lumped mass-spring system as shown in Figure 4.3. The natural frequency for a particular mode of the model can be written, as shown by Afolabi [1]:

$$\omega_d^2 = \frac{1}{M}\left[K_G + 4K_d \sin^2\left(\frac{\psi}{2}\right)\right] \qquad (4.15)$$

where ψ is the interblade phase angle; $\psi = \frac{2\pi n}{N}$; n is the number of nodal diameters and N is the number of masses discretized around the disc. The detailed derivation of equation (4.15) can also be found from Sinha and Griffin [129].

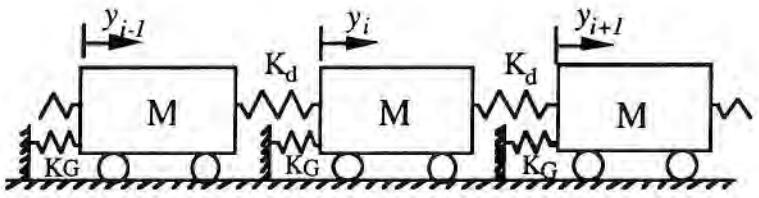

Figure 4.3 Disc model

The coupling influence between the blades and the disc has been mentioned in Chapter 2. Practically, there are two factors which may judge the strength of the coupling from a disc to the blades. First, the frequency of different discs may be the same by keeping the dimensions unchanged but varying the disc mass to simulate different materials for the disc. This type of effect can be termed the *mass ratio effect* between blades and the disc. Second, the disc-alone natural frequency may change by varying the disc dimensions while the different discs are made of the same material. This may be termed as a *frequency ratio effect* between the blades and the disc. Both effects have been

studied in the following sections and the mass ratios and frequency ratios are adjusted by using equation (4.14) with different values of stiffness.

4.3.2 Mass Ratio Effect

From a knowledge of structural dynamics, it is known that a disc made of steel has similar natural frequencies to those of a disc made of aluminium or plastic if all the disc dimensions are kept the same. This is because the properties of materials have linear relations between strength and densities. Obviously, the properties which vary among the three discs are the disc stiffness and disc mass. However, the dynamic response may be very different among the three discs because of the inertia effect. From this point of view, a disc-to-blade mass ratio WR can be defined as follows:

$$WR = \frac{\text{disc mass}}{\text{single blade mass}} \tag{4.16}$$

In this study, comparison is made between discs having mass values equal to 0.1M, 0.3M, M, 3M, 10M, where M is the 'standard' or the 'reference' disc mass value shown in Table 4.1.

Blade properties:

$m = 0.05$ kg $k = 65384.16$ N/m $\eta = 0.2$ % $\zeta = 0.4$ %

Disc properties (mass ratio WR variation):

$M_{ref} = 0.18$ kg,	$K = 941532.0$ N/m,	$K_G = 65.384$ N/m,	WR = 1
$M_1 = 0.018$ kg,	$K = 94094.4$ N/m,	$K_G = 65.384$ N/m,	WR = 0.1
$M_2 = 0.06$ kg,	$K = 313800$ N/m,	$K_G = 65.384$ N/m,	WR = 0.33
$M_3 = 0.54$ kg,	$K = 2824610$ N/m,	$K_G = 65.384$ N/m,	WR = 3
$M_4 = 1.8$ kg,	$K = 94159673$ N/m,	$K_G = 65.384$ N/m,	WR = 10

Disc properties (frequency ratio FR variation):

$M_{ref} = 0.18$ kg,	$K = 941532.0$ N/m,	$K_G = 65.384$ N/m,	FR = 1
$M_1 = 0.18$ kg,	$K = 94153.2$ N/m,	$K_G = 65.384$ N/m,	FR = 0.1
$M_2 = 0.18$ kg,	$K = 235383$ N/m,	$K_G = 65.384$ N/m,	FR = 0.25
$M_3 = 0.18$ kg,	$K = 3766128$ N/m,	$K_G = 65.384$ N/m,	FR = 4
$M_4 = 0.18$ kg,	$K = 9415320$ N/m,	$K_G = 65.384$ N/m,	FR = 10

Table 4.1

The stiffness of each disc is calculated by using equation (4.15) and is chosen so as to keep the disc frequencies constant for every case. The eigenvalues of the bladed system are solved so that the natural frequencies of the bladed disc can be evaluated and the results are plotted in Figure 4.4 as natural frequencies versus nodal diameters.

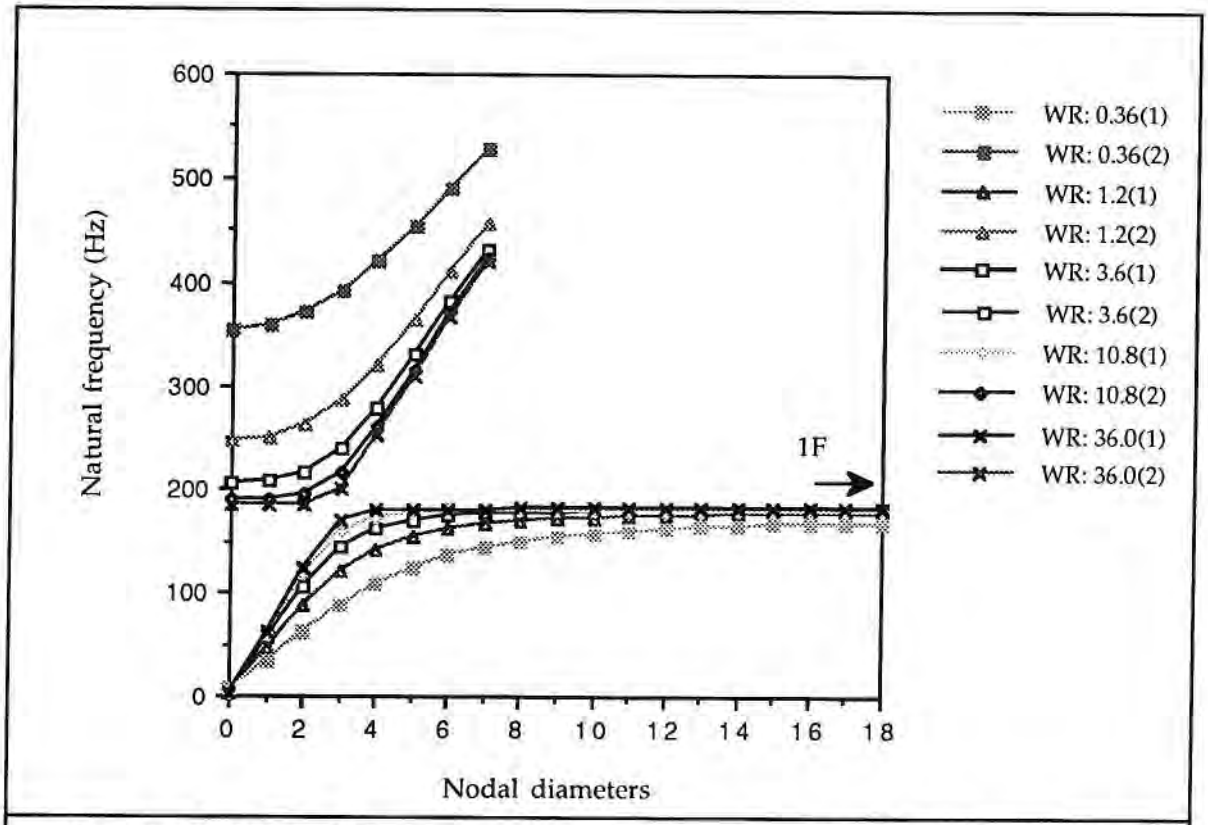

Figure 4.4 Natural frequency diagram for various disc/blade mass ratio

This graph shows the tuned system natural frequencies of the first family and part of the second family for the five different bladed discs. They show that as the disc becomes stiffer, the gap between the first and second family gets smaller. This phenomenon is the curve veering effect and this result agrees well with the 2-DOF oscillator study. It can also be observed that as the disc becomes stiffer, the loci of the natural frequencies between the two families veer away from each other after getting very close together. Although this shows that the disc stiffness affects the natural frequencies of a bladed disc system, the influence of mistuning on bladed disc response to forced vibration still needs to be established.

Some numerical simulations of blade response under a wide range of engine order excitations are shown next. The 36-bladed disc model is used and the

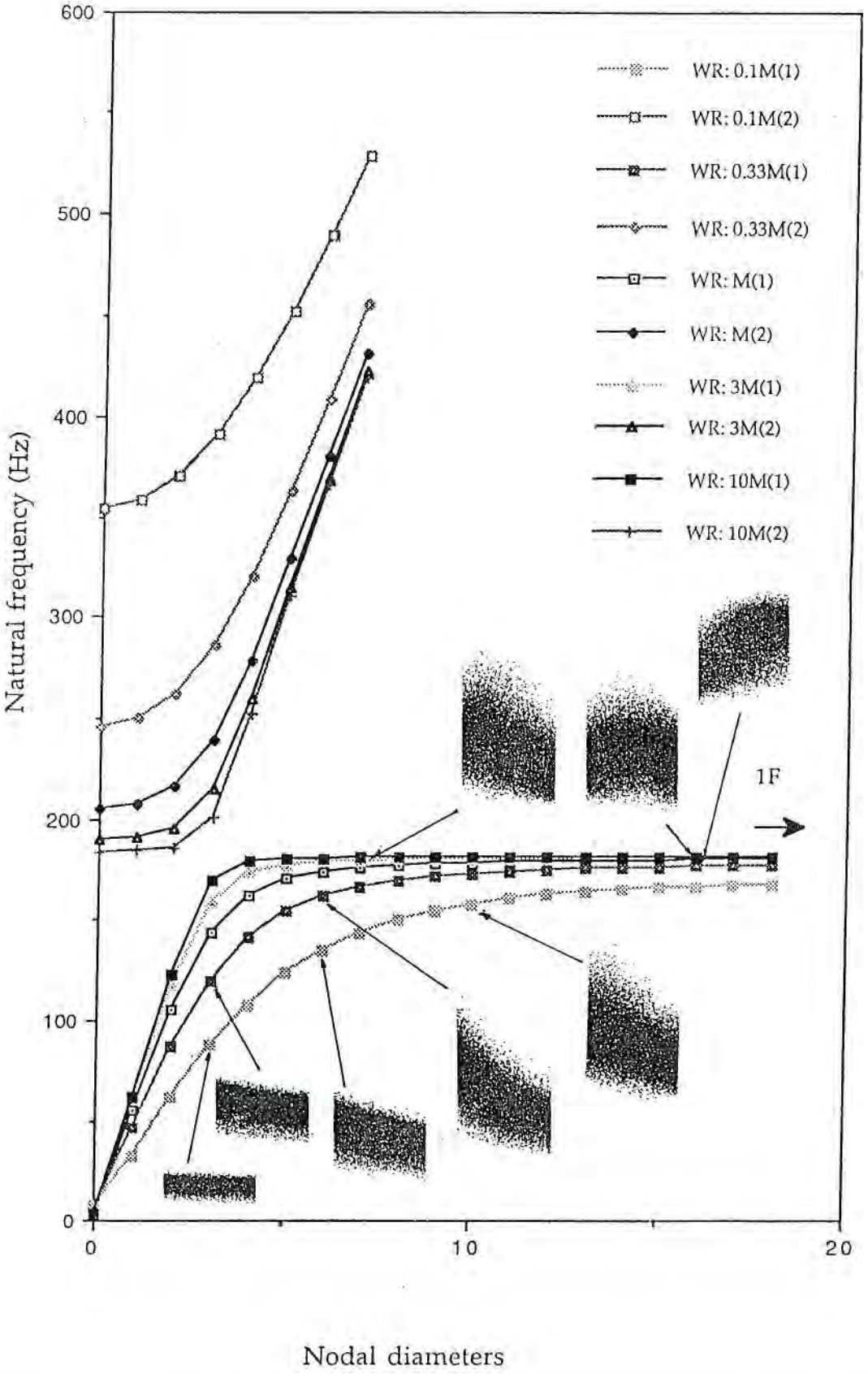

Figure 4.5 Disc coupling of various mass ratio with constant natural frequency

blade forced responses are evaluated by solving equation (4.11). Random blade parameters are selected by using a random number generator and by specifying the frequency scatter of a 10% culling process. The statistical study is obtained by repeatedly calculating the peak blade responses of the 36-bladed disc for up to 700 sample cases. Figure 4.5 shows the results from some of these calculations for particular engine orders. From these plots, one can find that the disc flexibility is only effective within the region of curve veering. For the blade-dominated region, that is for modes of the bladed disc with many nodal diameters, the disc flexibility hardly has any influence on the blade response.

4.3.3 Frequency Ratio Effect

Another influence of disc coupling occurs when different disc dimensions are used but keeping the material the same for all discs. This results in a change of the disc-alone natural frequencies, and the disc-to-blade frequency ratio FR can be defined as follows:

$$FR = \frac{\omega_d}{\omega_n} \tag{4.17}$$

where ω_d is the disc-alone natural frequency and
ω_n is the blade cantilever natural frequency.

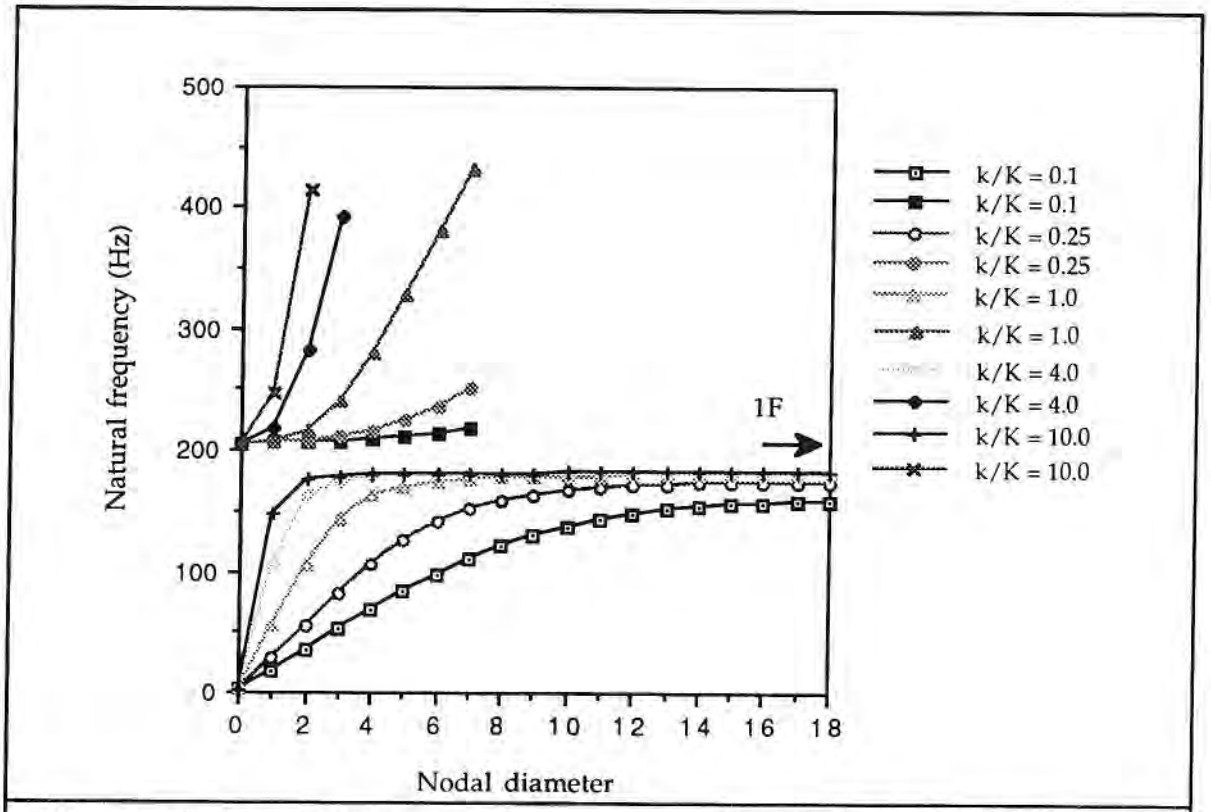

Figure 4.6 Natural frequency diagram for various disc/blade stiffness ratio

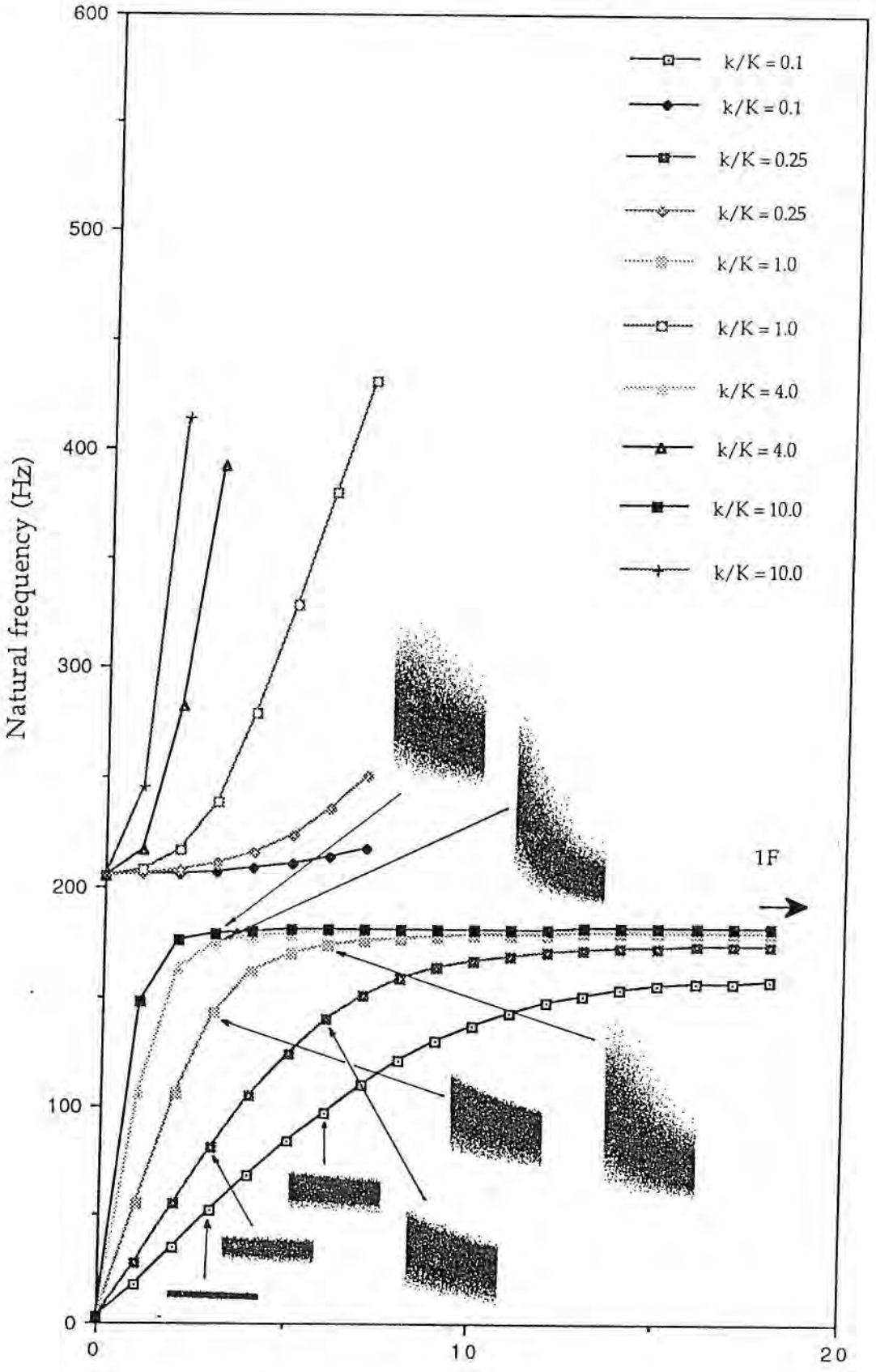

Figure 4.7 Disc coupling of various frequency ratio

To demonstrate this effect, discs with different dimensions are studied. These changes of dimensions are calculated by keeping the mass ratio constant while the disc stiffness is varied in the range from $0.1K_d$ to $10K_d$, where K_d is the standard or the reference value shown in Table 4.1. Again, the eigenvalues of the bladed systems are solved first and Figure 4.6 shows the natural frequencies of the bladed discs against number of nodal diameters. Here, the graph presents a different disc coupling effect from that in Figure 4.4. The two families of modes for a particular bladed disc configuration do not get closer when the disc becomes stiffer: instead, both curves become steeper. The minimum gaps between the curves for all the different discs stiffness are almost identical.

Next, numerical studies of the forced responses for the mistuned 36-bladed system are again investigated for this case. The bladed disc responses are evaluated for different frequency ratios (FR) and each of these ratios can be considered to represent a particular bladed disc mode. For all cases, a 10% frequency scatter is applied randomly and 700 different assemblies are picked from a large blade population. Different engine order excitations are applied so that responses in various diametral modes can be evaluated. The resulting plots are shown in Figure 4.7 and one can notice the same effect on response due to disc coupling as that shown earlier in Figure 4.5 for which the disc flexibility only affects the blade responses within the curve veering part on the frequency versus nodal diameter characteristic. For higher numbers of nodal diameters, the maximum peak responses remain unchanged for different degrees of disc coupling.

4.3.4 Blade and Disc Coupling Effect

The above studies show two of the extreme cases for shroudless blades assembled on different discs. In practice, real bladed disc coupling effects will lie in between these two extreme categories. Figure 4.8 shows all the peak responses of a 36-bladed disc with different disc couplings. The coupling factor from equation (4.14) is used here to define the disc flexibility influence for a particular assembly mode as follows:

$$CR = 1 - \frac{\omega_{as}^2}{\omega_n^2} \qquad (4.18)$$

where ω_{as} is the bladed disc assembly frequency and
ω_n is the blade cantilever natural frequency.

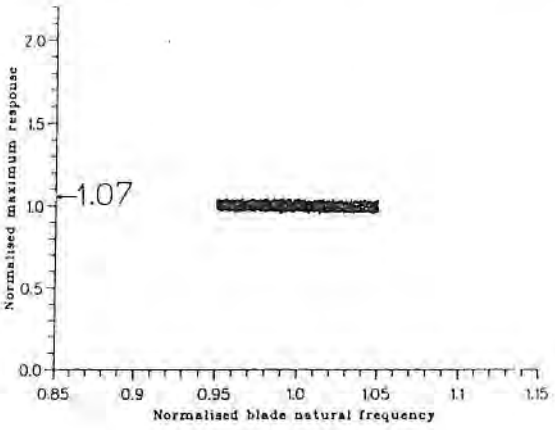

CR = 0.918

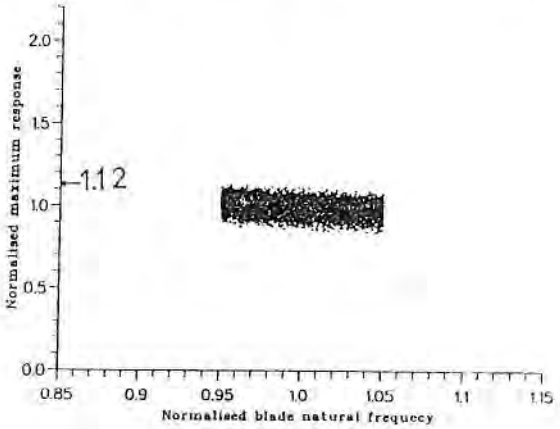

CR = 0.801

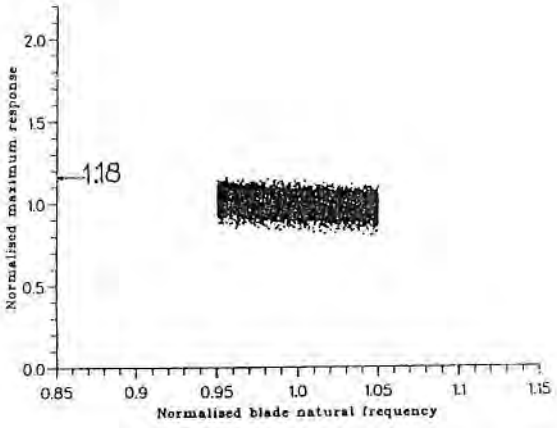

CR = 0.768

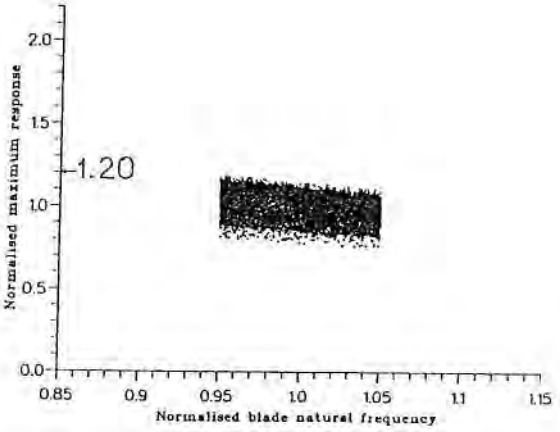

CR = 0.712

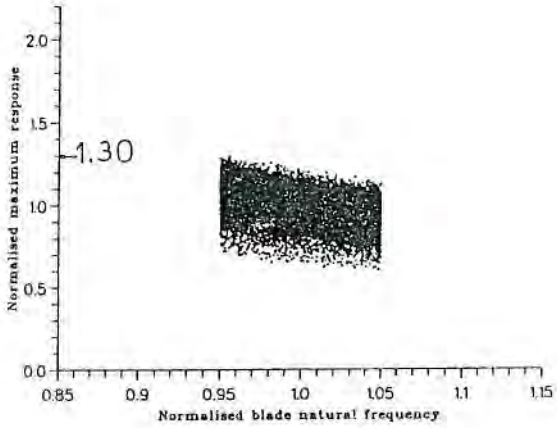

CR = 0.566

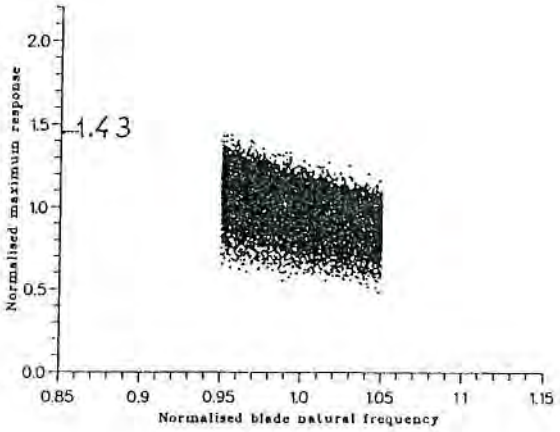

CR = 0.446

Figure 4.8 Maximum blade responses plots for different CR values

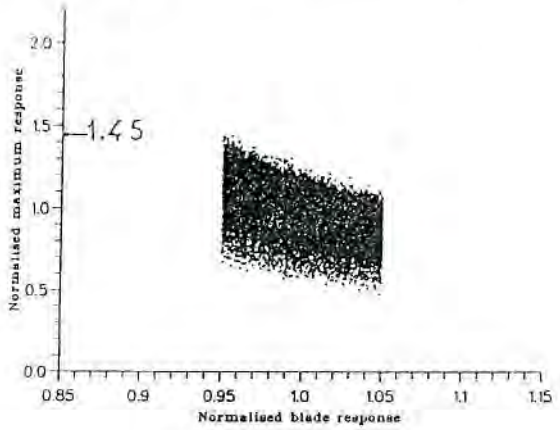

CR = 0.406

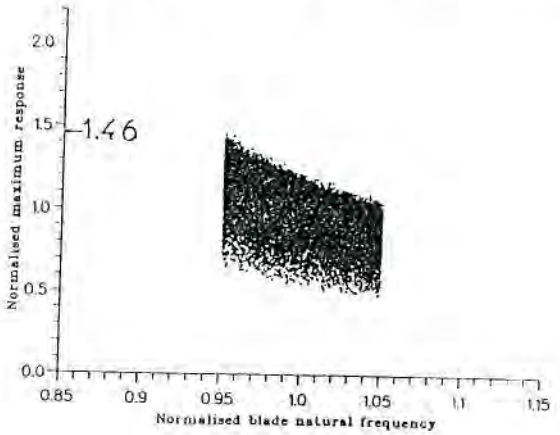

CR = 0.281

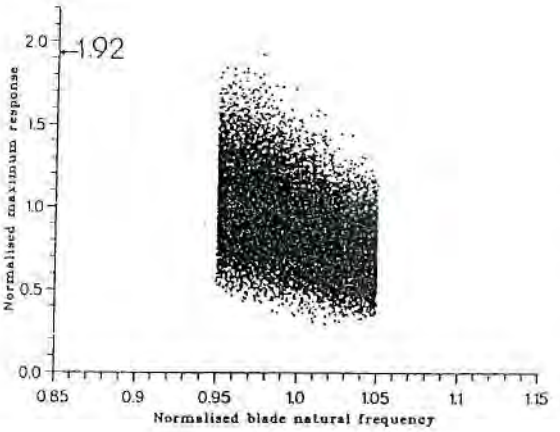

CR = 0.243

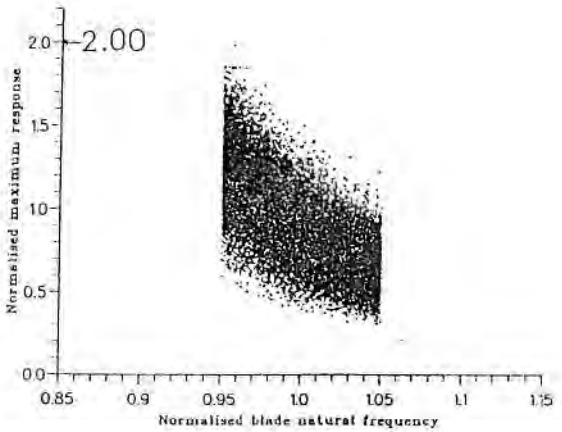

CR = 0.197

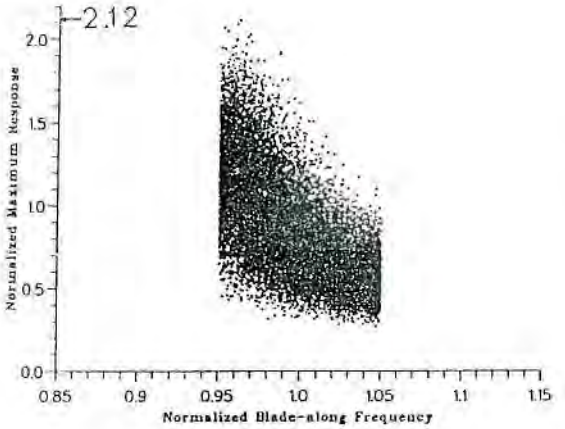

CR = 0.076

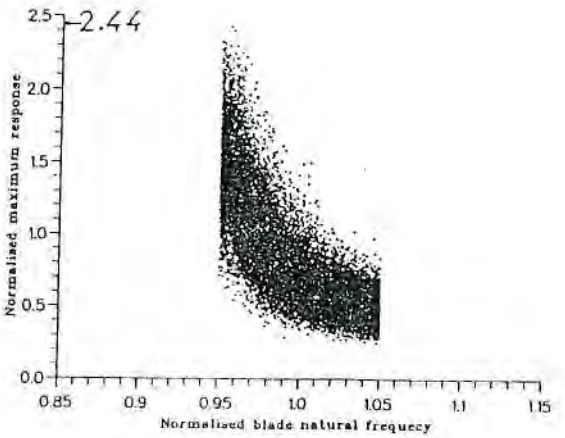

CR = 0.082

Figure 4.8 Cont.

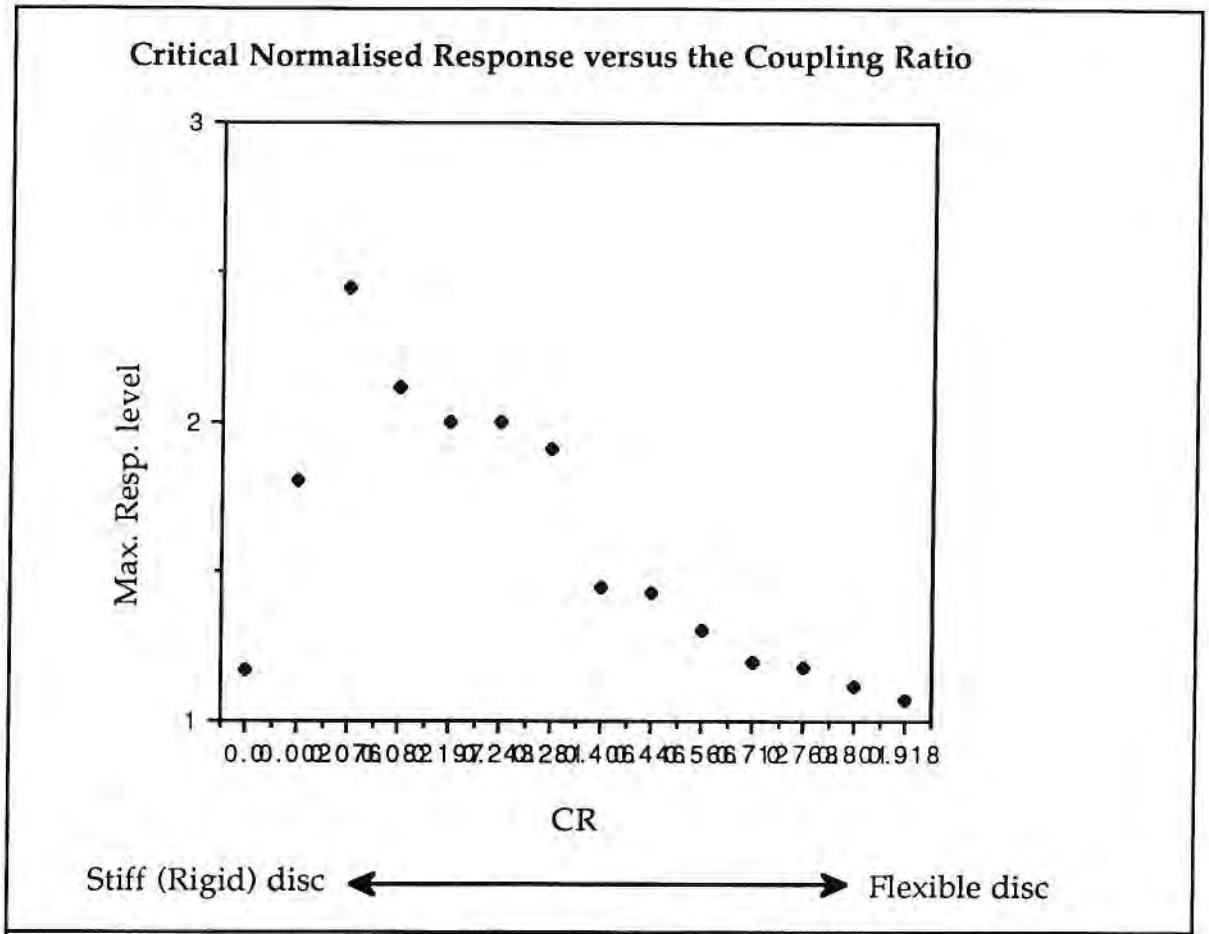

Figure 4.9 Critical blade response level vs. the coupling factor for the first blade mode of the 36-bladed disc

Figure 4.9 shows the normalised maximum peak response versus the coupling ratio, CR. The amount of mistuning added to the blades for each bladed disc is 10 % random variation about the blade-alone natural frequency. The normalised maximum peak response is the highest of all the possible blade responses of a 36-bladed disc. This peak response is the absolute maximum response and it might not occur in many blade combinations. This diagram shows an relationship between the maximum peak responses and the bladed disc flexibility. The graph shows that the blade peak response has a steep increase for weak coupling, that is, for a stiffer disc. The critical blade response climbs to a maximum factor of nearly 2.5 at a coupling factor about 0.04. If the disc becomes softer, that is strong coupling, the blade peak response has a gentle decrease. Nevertheless, a large quantity of data is required to yield a reliable result, since the calculations rely on a simulation method. The process may hence become expensive and take a long time to produce one such graph.

Another feature noted in this study is the worst case for a particular bladed assembly under different engine orders. Sanliturk [125] showed that the critical blade of an assembly varies if different engine orders of excitation are applied. He showed that a particular order, the 6th engine order in his specific case study, will produce a critical blade which will be higher than any other critical blade excited by other engine orders. In the present study, it is found that such a worst condition always happens around the "corner" of the eigenvalue loci and it is directly related with the coupling effect from the disc (near the curve veering region). This can be observed clearly from either Figure 4.4 or Figure 4.6 where different builds of assemblies are seen to have the same characteristics despite the different coupling effects. The observations obtained here match well with the study 2-DOF oscillator. The worst possible response happens close to the vertices of the loci of eigenvalues and these vertices represent the 'corners' of the natural frequencies versus nodal diameter plot.

For flexible discs, the worst critical blade case occurs at a larger number of nodal diameters than at lower nodal diameters for the rigid disc coupling. One reason suggested for this is that as the bladed disc natural frequency tends towards the blade-alone cantilever natural frequency, the blade response tends to be a maximum while at the same time the disc coupling still has a strong effect on the system. After these critical areas, the disc is more rigid and hence the vibration is blade-dominated. The blade critical amplitudes in this region will decrease for larger nodal diameter excitations. In theory, when the disc becomes infinitely rigid, the blade should vibrate more like an independent system. However, it is found in this study that this is not always the case and small disc coupling exists even when the disc is very rigid compared to the blades.

Finally, Pierre [115] also used a "localisation factor" which is the amount of mistuning divided by a coupling ratio. According to him, this coupling ratio is the substructure frequency divided by the adjacent substructure frequency. However, the scatter of the blade responses for different amounts of mistuning will be discussed below where it will show that for small amounts of mistuning, the responses are scattered around the tuned position. If the amount of mistuning becomes large, the response scatter would reach a

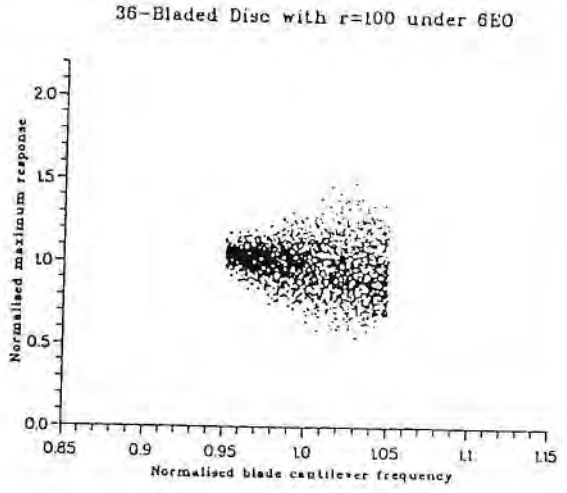

Mass ratio increased by 100 times

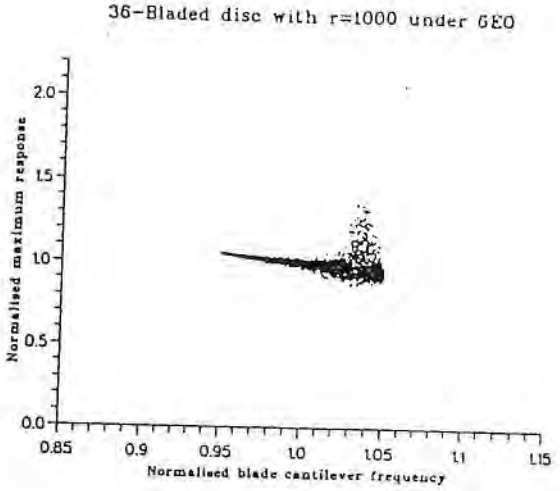

Mass ratio increased by 1,000 times

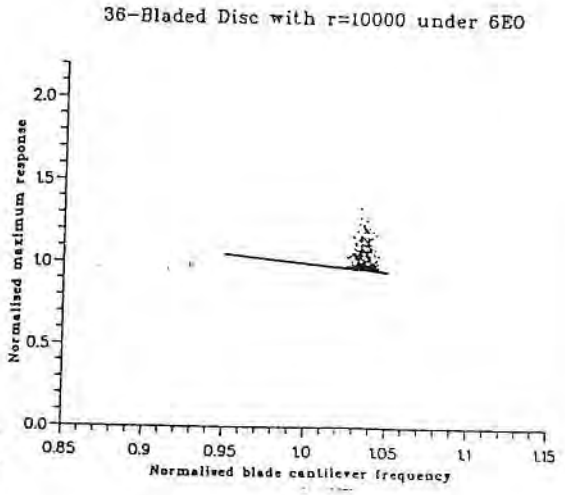

Mass ratio increased by 10,000 times

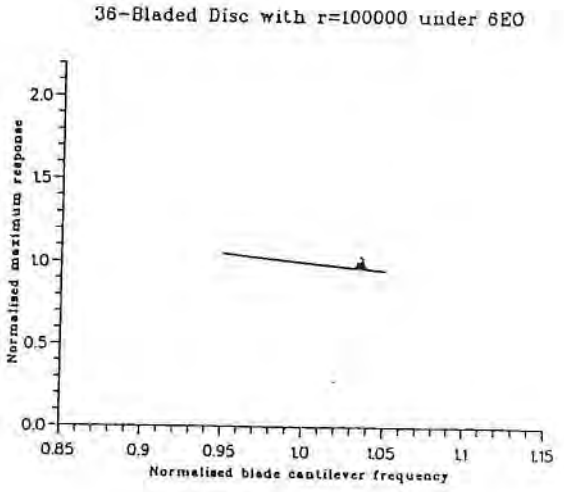

Mass ratio increased by 100,000 times

Figure 4.10 Weak coupling effects as the disc mass increases

maximum value at an upper bound. After this condition is reached, the peak values do not demonstrate any rapid changes with even greater mistune, a result which shows that the localisation factor defined by Pierre may not be a particularly useful parameter. Furthermore, the numerical model used by Pierre is more like a packet of grounded blades connected by a continuous shroud than a bladed disc. Practically, it is believed that such a model cannot represent the bladed disc system in a general way and it is felt that the new coupling factor introduced in this thesis describes the coupling effect in a more general form.

4.4 WEAK COUPLING EFFECT

Theoretically, a bladed disc vibrating in a mode with a large number of nodal diameters can be thought of as a rigid disc and, when the disc is almost rigid, little coupling exists between the blades. This is known as 'weak coupling'. However, mistuning is sensitive even for weak coupling. This fact has been reported by many researchers in studies of the effects of localisation phenomena for nearly-periodic structures [55, 56, 115]. So far, little work has been shown on a bladed disc model. In the present study, weak coupling effects of the 36-bladed disc are examined. From Figure 4.9, the peak value for the coupling ratio equal to 0.04 can be regarded as the worst case. From there to the left, the coupling ratio approaches zero and the system can be classified as weakly coupled between the blades and the disc. It has been found that for weakly coupled systems, the maximum peak response level drops slowly as the coupling ratio approaching 0.0. Figure 4.10 shows some of the results observed by increasing the mass ratios. It is clear that the disc has to be very rigid for the maximum peak response to drop to a low level. Furthermore, the high frequency blades seem to suffer the worst response when the disc coupling is weak as can be seen from Figure 4.10.

4.5 INFLUENCES OF AMOUNT OF MISTUNING

More numerical studies were followed using the blade selection procedure defined in chapter 3. Figures 4.11-4.13 show graphs of response versus frequency; normalised maximum responses versus normalised blade-alone frequency and normalised maximum responses versus normalised excitation frequency. The blade-alone natural frequency scatters of the studied cases are of limits 2%, 10% and 20%, respectively. Figures 4.11(a), 4.12(a), and 4.13(a) are the plots of the individual blade responses versus the frequency range specified.

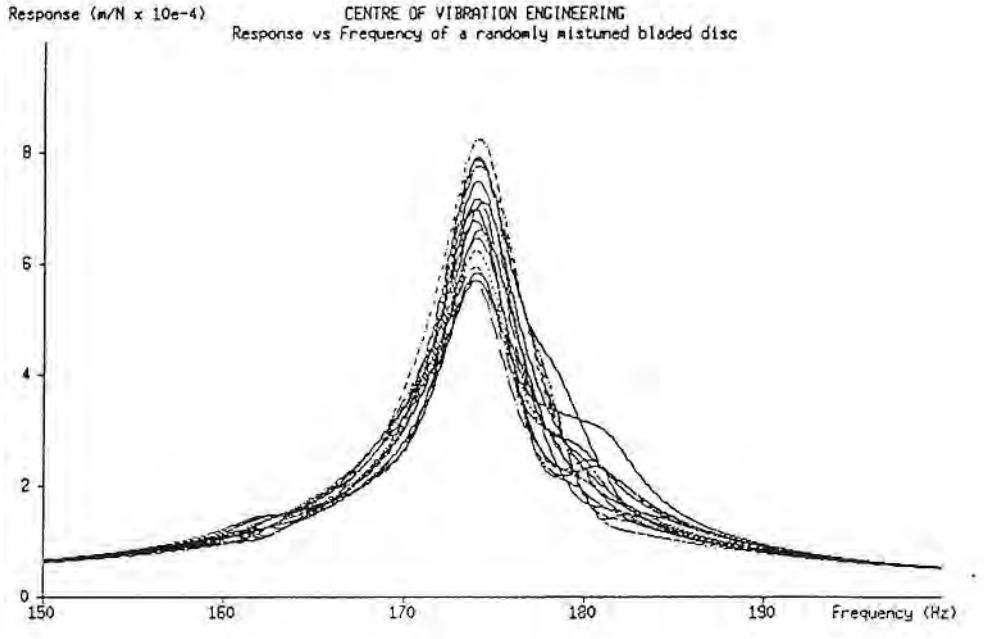

Figure 4.11(a) Response versus frequency plots for frequency scatter of 2%

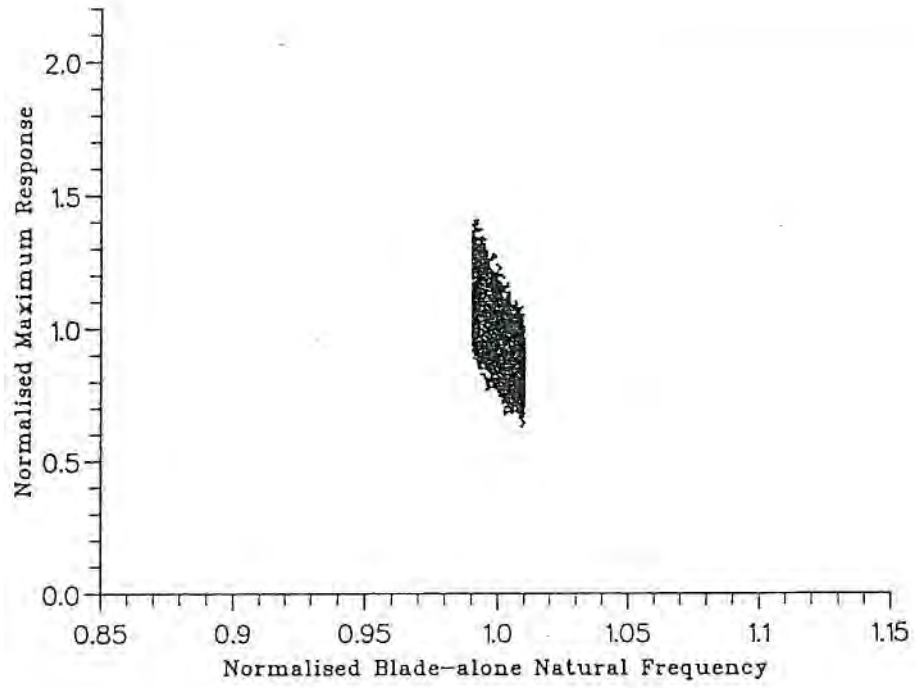

Figure 4.11(b) Normalised maximum response versus blade-alone natural frequency for frequency scatter of 2%

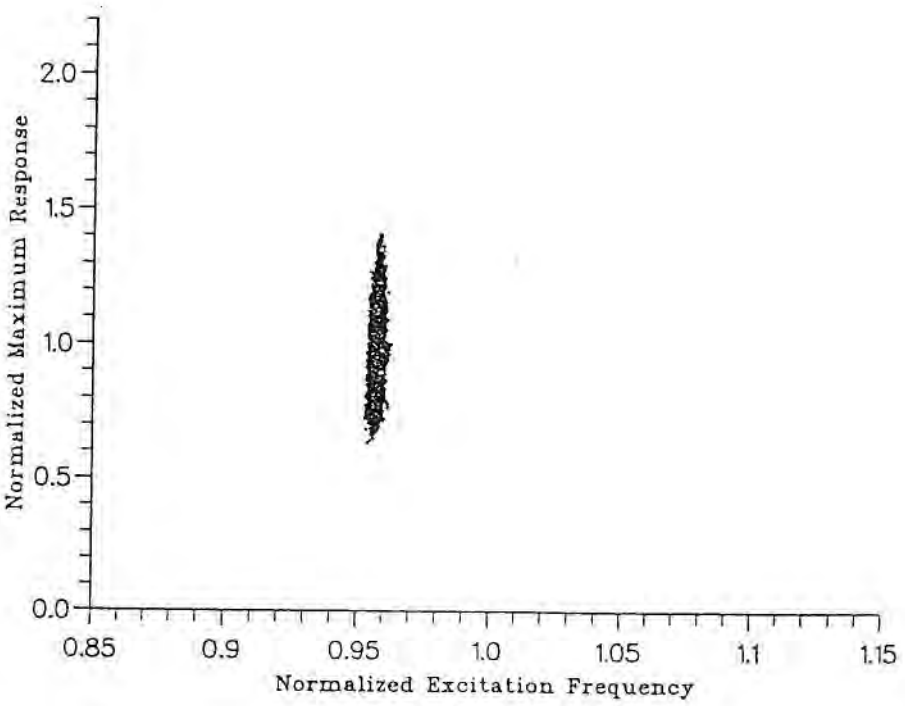

Figure 4.11(c) Normalised maximum response versus excitation frequency for frequency scatter of 2%

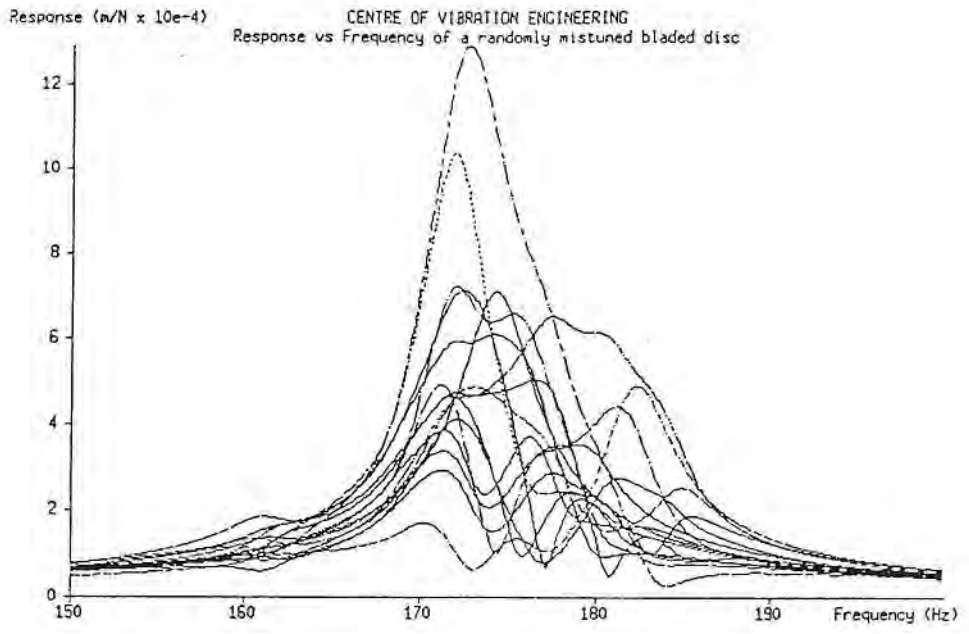

Figure 4.12(a) Response versus frequency plots for frequency scatter of 10%

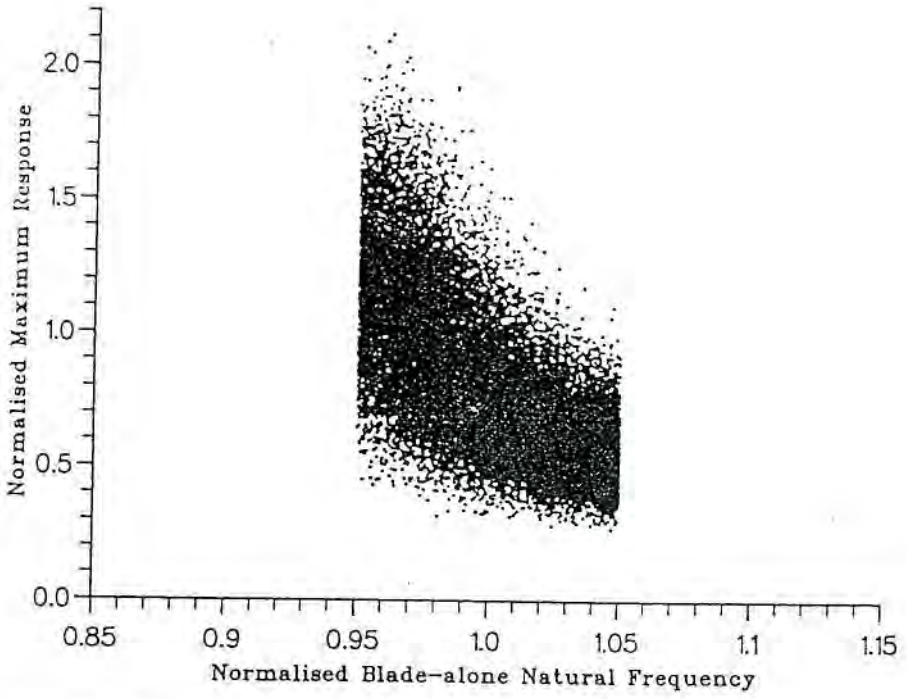

Figure 4.12(b) Normalised maximum response versus blade-alone natural frequency for frequency scatter of 10%

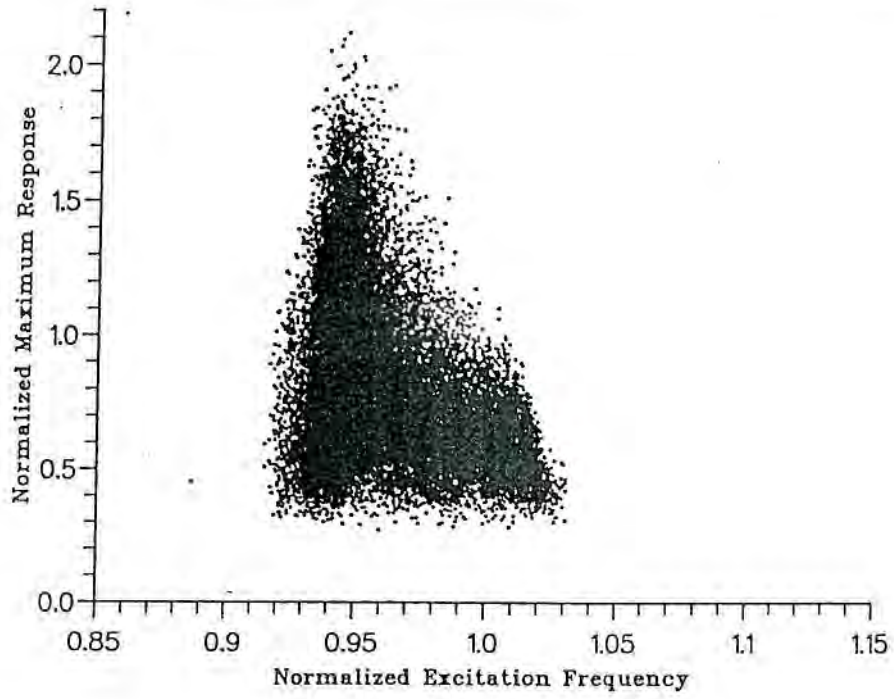

Figure 4.12(c) Normalised maximum response versus excitation frequency for frequency scatter of 10%

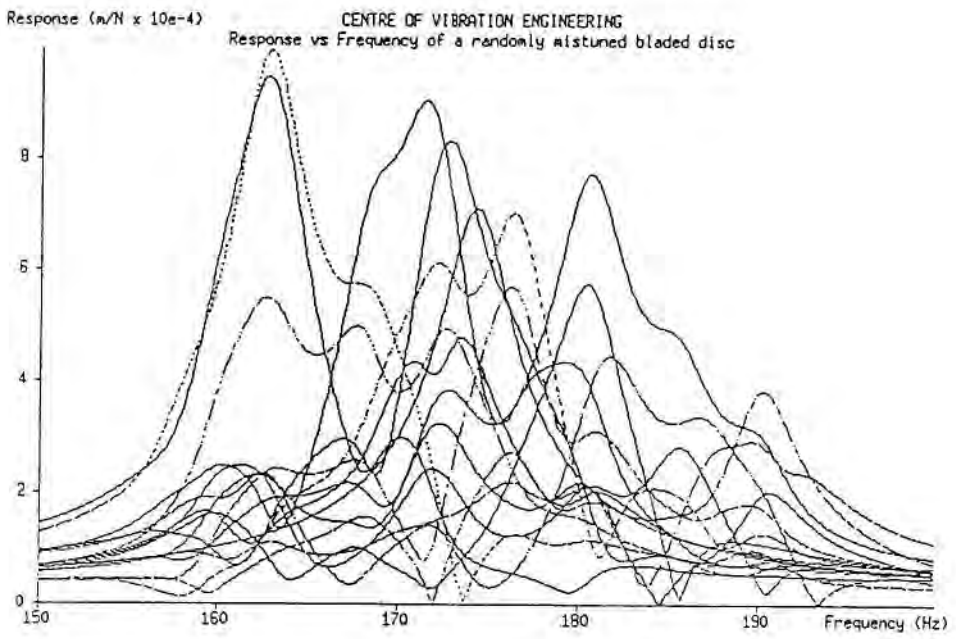

Figure 4.13(a) Response versus frequency plots for frequency scatter of 20%

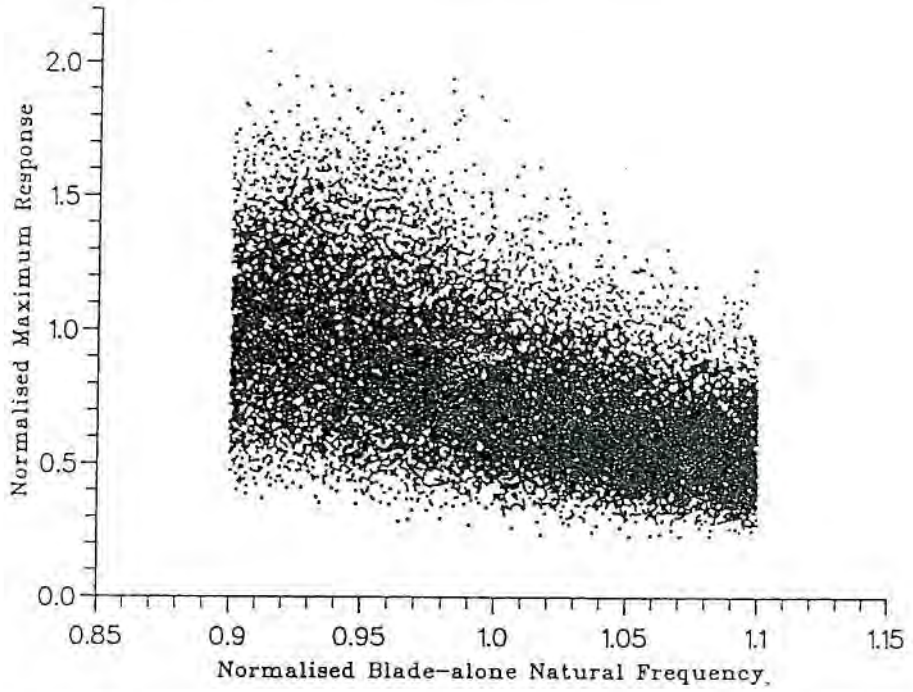

Figure 4.13(b) Normalised maximum response versus blade-alone natural frequency for frequency scatter of 20%

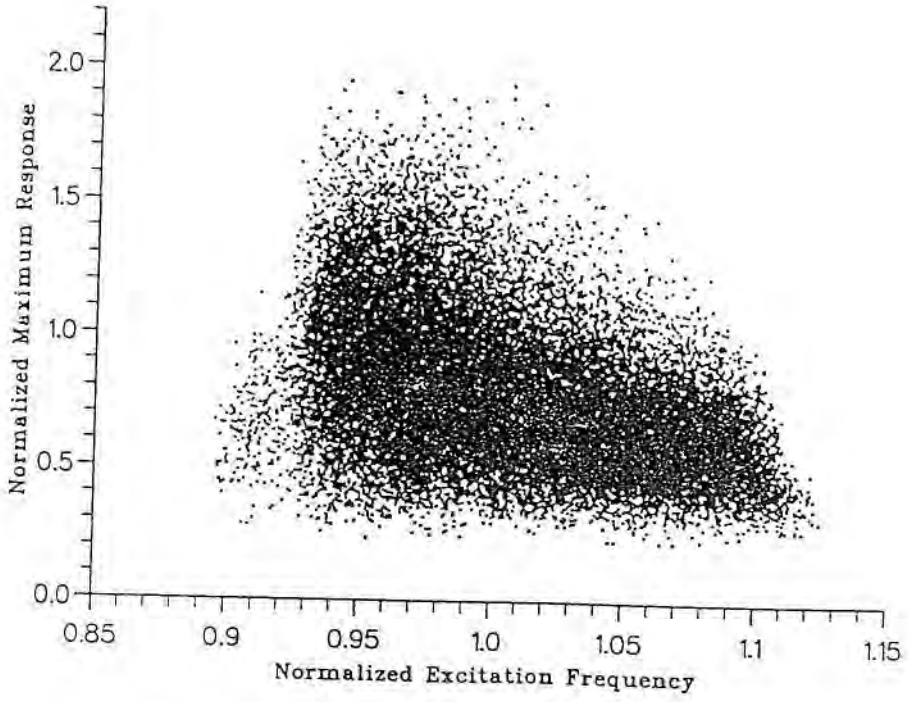

Figure 4.13(c) Normalised maximum response versus normalised excitation frequency for frequency scatter of 20%

These show that all the peak responses are within the specified frequency range. From the diagrams of 4.11(b), 4.12(b), and 4.13(b), the peak responses of 700 combinations of blade responses of a 36-bladed disc are shown against the normalised blade-alone natural frequency. Figures 4.11(c), 4.12(c), and 4.13(c) are the plots of the normalised blade responses versus the normalised excitation frequency. Here, the 'normalised excitation frequency' is the exciting frequency at the maximum response point divided by the blade-alone natural frequency. From the above graphs, Figure 4.11(b) agrees well with the results for a 2% culling shown by Griffin [50].

Furthermore, it seems that the profile (or envelope) of the response plots changed as the degree of mistuning changed. By increasing the percentage of mistuning, the envelope starts with a deep and sharp boundary with small mistuning and then to a flatter and gentle curve with 20% mistuning. This also agrees with Griffin's finding "*The scatter in blade frequencies increased the variation in blade amplitudes also increased up to a certain point and then levelled off*".

4.6 MISTUNING PARAMETERS PLOT

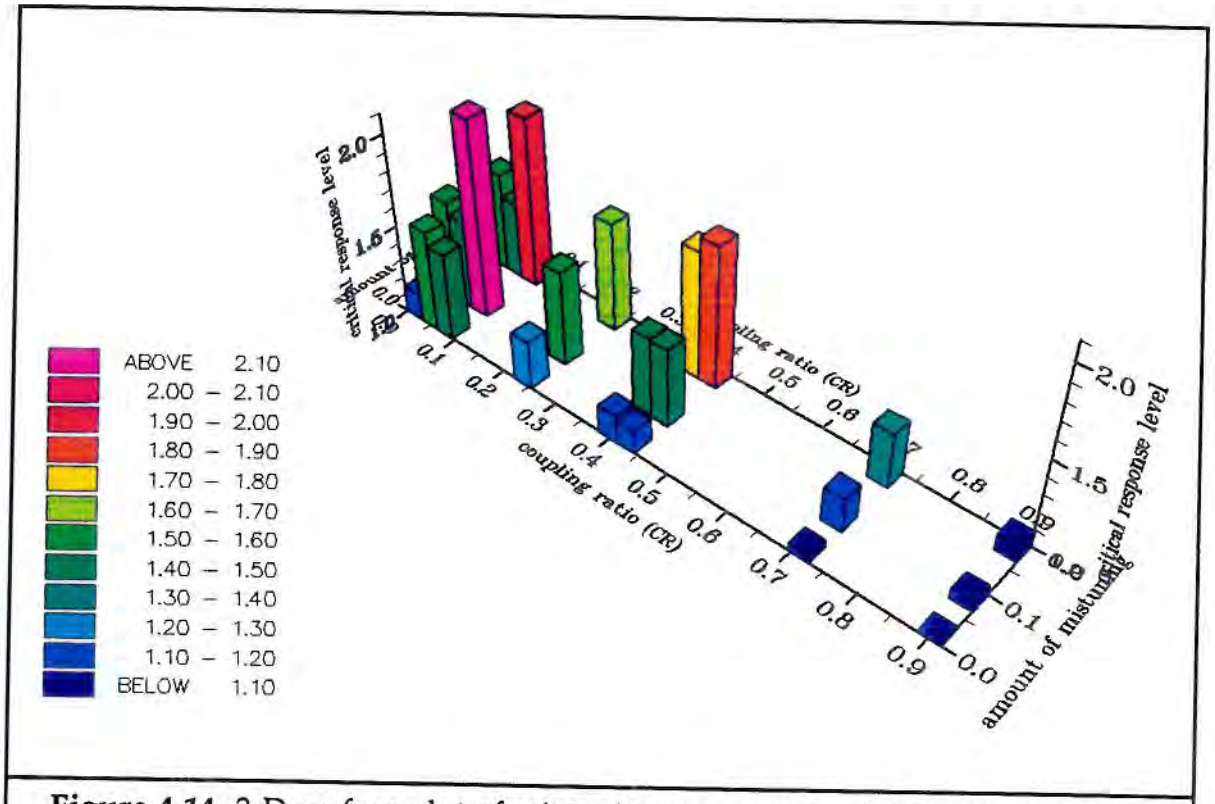

Figure 4.14 3-D surface plot of mistuning parameters of the 36-bladed disc

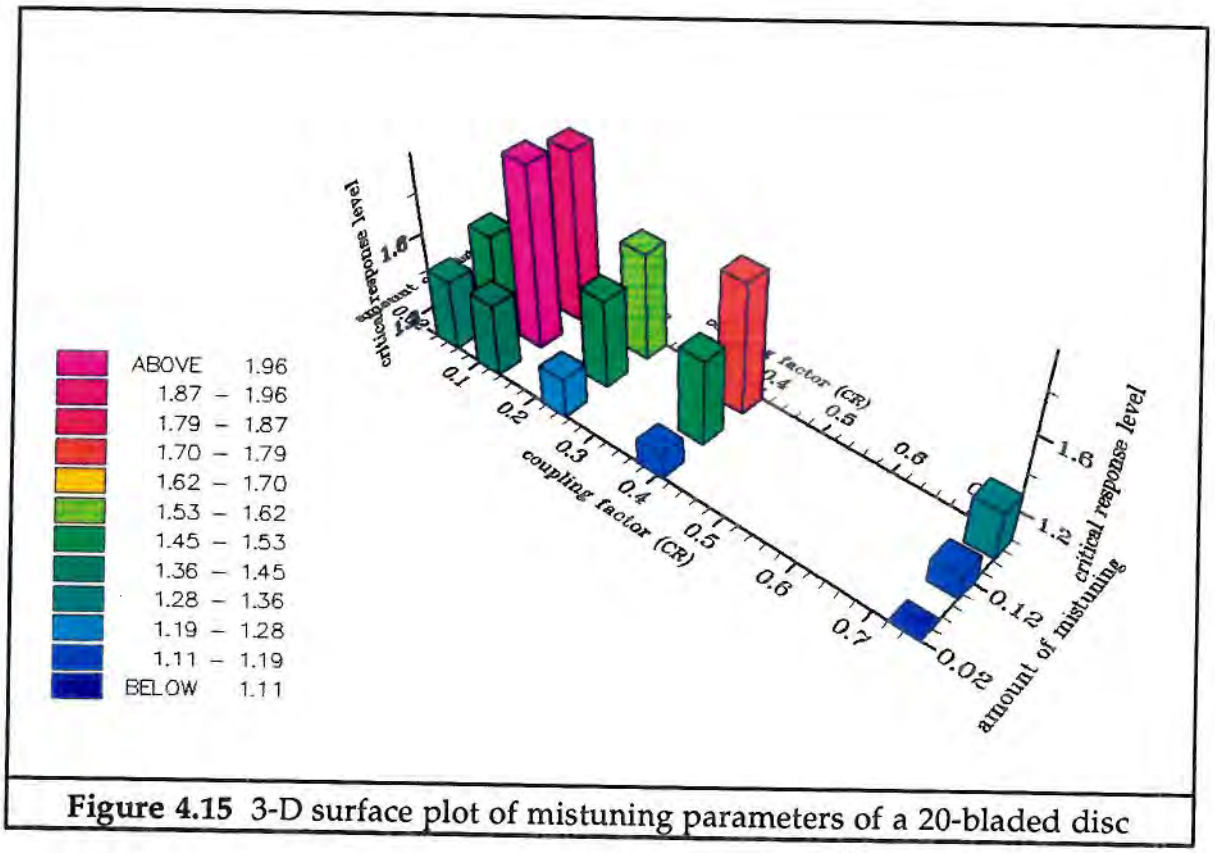

Figure 4.15 3-D surface plot of mistuning parameters of a 20-bladed disc

The parameters which influence the mistuning effects on the response levels are displayed on a 3-D surface plot. Figure 4.14 shows a 3-D parameter plot for a mistuned 36-bladed disc. This graph shows the effect of the coupling ratio and the amount of mistuning against the peak response level. The grids actually show the critical response levels at coupling ratios with certain amounts of percentage of mistuning. Figure 4.15 shows the same 3-D plot for a mistuned 20-bladed disc. From these two graphs, the worst mistuning effects are seem to be located where the coupling is getting weak and where the mistuning amount is around 8-12% in frequency scatter between the maximum and minimum blades.

4.7 CONCLUDING REMARKS

This chapter investigated some factors which have a significant influence on a mistuned bladed disc system. Generally, for frequency mistuned systems, the coupling factor and the amount of mistuning are found to be the important parameters to mistuning effects. Practically, these factors will be very useful for designers and test engineers to identify the severity of blade response due to mistuning. A model of a 2-DOF periodic oscillator was first used to demonstrate the features of curve veering in eigenvalue loci. Some factors affecting the response magnitudes were obtained from a perturbation analysis. This simple example provided the main idea for a numerical study of a 36 bladed disc. From this study, the following comments are made.

- Disc coupling effects are mainly due to two factors; the mass effect and the frequency effect. The mass effect refers to discs of different materials but similar dimensions and results in the natural frequency loci getting closer as the disc gets more rigid. The frequency effect refers to discs made of the same material but with different dimensions. This effect seems to push the natural frequency loci to be steeper but with the veering gap not changed so much. Some forced response studies are shown for some of the resonant points. The outcome shows that the coupling effect is only significant along the veering part of the natural frequency loci on the frequency diagram. After the turning point, the disc coupling effect becomes less as the disc is getting more rigid.

- In the case studies shown here, the forced response analysis always shows that there is a blade maximum response close to the turning point of the

natural frequency locus for a specific mistuned bladed configuration. Both the analytical 2-DOF oscillator and the 36-bladed disc simulations point to the same conclusion.

- The amount of frequency mistuning in the system and its specific distribution is also important, as can be seen from the peak response distribution changes as the amount of frequency scatter varies.

- The response scatter and the critical responses have been found to be dependent upon the coupling effect between the blades and its disc or shrouds. A new disc-to-blade coupling ratio has been defined as a function of the ratio between the assembly frequency of the system and the blade-alone natural frequency. Numerical results suggest that this factor can describe the coupling effects in a general way. The absolute critical blade of a population versus the coupling ratio is shown and some part of the curve in figure 4.9 shows an inverse exponential shape. This suggests that for some maximum responses it might be possible to modify the disc a little so that a different coupling ratio is obtained and the critical response is thereby reduced by some degree.

- There also exists a relationship between the coupling ratio, the amount of mistuning and the critical response level. These parameters can be shown in a 3-D surface plot. From this plot, it can be observed that the mistuning effect will be worst at a particular coupling ratio and amount of mistuning. Usually, this point is found near the median to weak coupling range with a mistuning scatter of around 8 to 12 %. Further mistuning will result the system changing and the effect cannot be classified as mistuning. It is unfortunate that the 3-D plots depend on the blade number, which suggests that for different blade numbers different plots have to be obtained.

CHAPTER 5

EFFECTS OF DAMPING MISTUNING ON THE VIBRATION CHARACTERISTICS OF BLADED DISCS

About this chapter

It is always the case that damping affects the forced resonance response of a bladed system and very often variations of damping will exist between the blades, the so-called *damping mistuning* effects. This chapter describes a study of mistuned bladed disc vibration concerning these damping mistuning effects. The non-proportional dampers which connect each blade to ground are considered here. A simple analytical study shows that non-proportional damping may lead to complex modes for a bladed disc assembly. These complex modes will then cause variations on blade responses even when there is no frequency mistuning between the blades.

Numerical studies on the blade responses from damping mistuning are shown using the same 36-bladed disc model as used before. These new studies include the damping variation effects from some common mistuning patterns, such as the single-blade mistune pattern and the random mistune pattern. Furthermore, damping together with a random frequency mistuning is also examined. All these investigations show slight localised effects on responses with the presence of a damping mistuning pattern.

Finally, a case study investigates the coupled damping between blades which may be considered to represent under-platform dampers arranged in a specific way, such as the so-called *rainbow arrangement* for practical rotors. Numerical results based on this study show surprisingly influences due to the coupling effects over the damping mistuning effects. It also shows that one can use a complex mode criterion to judge the damping mistuning effect.

5.1 INTRODUCTION

Damping is always an important factor in structural dynamics since all real structures exhibit some energy dissipation or damping when set in motion. In many cases, the differences between real systems and their numerical simulations are the result of inadequate treatment of damping. In the past, uniform damping has often been assumed to exist around the blade row, and mistuning effects were usually confined to the small blade-to-blade variations in either mass or stiffness that cause the blade-alone natural frequencies to vary between the blades on the row. Variations among the dampers in a bladed disc have not previously been considered.

There are three main types of damping in bladed disc assemblies. The viscous damping is a frictional effect between the structure and the surrounding air, while hysteretic damping (material damping) is a result of internal resistance from the material itself. Finally, friction damping can exist between the blade root, caused by blade root rubbing or by the action of friction damping devices. Viscous damping was possibly the first damping model to be used by structural engineers when they studied resonance of a dynamic system. The hysteretic damping model was then introduced by Myklestad in the early 50s [107]. Later, Bishop showed the analogues between the hysteretic and viscous damping [10], and demonstrated the study of a damped multi-degree system by using hysteretic damping [11].

Since mistuning studies examine vibrating blade responses through their resonances, damping must be added to the blades in order to avoid numerical singularity at the resonances and to make the studies physically meaningful. For example, the lumped-mass bladed disc models used by Wagner [148] and Dye and Henry [28] had a viscous damper for each blade. The receptance model used by Ewins [34] had hysteretic damping added to the blades. Muszynska and Jones later made quite a comprehensive study of friction damping effects [102, 103]. Furthermore, Afolabi, in 1982 [1], considered the blade material to be non-homogenous and, therefore, he considered variations of hysteretic damping added as a complex part of the stiffness matrix. However, this type of damping is only a displacement-dependent term in the equation of motion. The viscous dampers between blades, which will be velocity-dependent terms in the equation of motion of the system, have been simulated uniformly for all the

blades around a disc. The mistuning effects from non-uniform or mistuned viscous dampers have not yet been studied, as far as the author has established. Particular examples from these mistuning effects could arise as sudden aerodynamic changes on the blades when the engine is under running conditions and the non-linear friction damping between blades. In all these cases, the variation between blade dampers could be quite large.

However, the most common type of damping mistuning is probably the variation of the friction forces at the blade roots or the contact between the blade platforms and the friction dampers. It is practical to use under-platform dampers to cure excess resonant vibration levels of blades. However, the actual mechanism of friction damping is a very complicated subject and a lot of research is being undertaken at the present time now. A detailed description of the non-linear algorithms is beyond the scope of this thesis so that only linear or quasi-linear equations are considered. This chapter focuses on studies of damping mistuning such as the complex mode effect and the coupled damping effect between blades. The latter can be even used to model the effect of under-platform dampers. A case study of 'rainbow damper test' presents an analysis of the linear system or quasi-linear system on damping mistuning effects. The main objective of this study is to understand the behaviour of mistuned damping devices used in practical turbomachines.

5.2 THEORETICAL BACKGROUND

The mathematical model used to represent a bladed disc assembly is the same as that used in the previous two chapters. A 36-bladed system consists of 36 lumped masses to represent the first bending modes of the blades on a cyclically symmetrical disc which is itself modelled by 36 masses. Later, a modified model comprising 92 blades to represent a HP (high pressure) turbine rotor with two lumped masses for each blade is used. The equations of motion of either model can be written as sets of simultaneous equations and in matrix form as follows:

$$[M]\{\ddot{x}\} + [C]\{\dot{x}\} + \left([K] + j[D]\right)\{x\} = \{f\} \qquad (5.1)$$

where [M], [K], [C] and [D] are mass, stiffness, viscous and hysteretic damping matrices as defined in the previous chapter.

5.2.1 State-space Formulation

If the elements in the damping matrix [C] are for proportional damping, equation of motion (5.1) can be decoupled by the real eigenvectors for the undamped system. In other words, the damping matrix is a linear combination of the mass and the stiffness matrix (that is, $[C] = \alpha[M] + \beta[K]$ for α and β constants). This damping representation is also known as Rayleigh damping or diagonal damping. By definition, each proportionally-damped element in a system has a phase relationship of either 0 or 180 degrees, that is exactly in or out of phase. However, in reality, damping is not uniformly distributed around a structure. If the damping distribution is not proportional to the structural properties, it is known as a non-proportionally damped system [42]. In this case, equation (5.1) cannot be decoupled by the matrix of real eigenvectors. Frazer, Duncan and Collar [48] first expanded the problem to a 2N state-space equation, in 1932, by introducing an auxiliary condition of the form as follows:

$$[\mathbf{M}]\{\dot{x}\} - [\mathbf{M}]\{\dot{x}\} = \{0\} \tag{5.2}$$

After that, many different forms of equations have been formulated according to different researchers. The following form is adopted from Ewins [42]. The advantage of this version of the equation is that the system matrices are symmetric so that a general LU decomposition can be applied for further reduction to the general eigenvalue form. By combining equations (5.1) and (5.2), one can easily derive the equation as follows:

$$\begin{bmatrix} \mathbf{C} & \mathbf{M} \\ \mathbf{M} & \mathbf{0} \end{bmatrix} \begin{Bmatrix} \dot{x} \\ \ddot{x} \end{Bmatrix} + \begin{bmatrix} \mathbf{K} & \mathbf{0} \\ \mathbf{0} & -\mathbf{M} \end{bmatrix} \begin{Bmatrix} x \\ \dot{x} \end{Bmatrix} = \begin{Bmatrix} \mathbf{f} \\ \mathbf{0} \end{Bmatrix} \tag{5.3}$$

or

$$[\mathbf{A}]\{\dot{y}\} + [\mathbf{B}]\{y\} = \{\mathbf{p}\} \tag{5.4}$$

where

$$[\mathbf{A}] = \begin{bmatrix} \mathbf{C} & \mathbf{M} \\ \mathbf{M} & \mathbf{0} \end{bmatrix}, \quad [\mathbf{B}] = \begin{bmatrix} \mathbf{K} & \mathbf{0} \\ \mathbf{0} & -\mathbf{M} \end{bmatrix}, \quad \{\mathbf{p}\} = \begin{Bmatrix} \mathbf{f} \\ \mathbf{0} \end{Bmatrix}$$

Here, both [A] and [B] are symmetrical but non-positive definite matrices.

5.2.2 Tuned System

The identification of non-proportional damping values for multi-degree-of-freedom systems is one of the most difficult modelling tasks in structural dynamics, because such systems are coupled. Many researchers in the past have tried to formulate a general damping rule for multi-degree-of-freedom damped systems [91, 144]. So far, the most commonly-used analysis of damping is based on a single-degree-of-freedom analysis, see Figure 5.1 and Appendix VI This analysis is valid only for lightly-damped structures whose damped resonant frequencies are very close to the undamped natural frequencies.

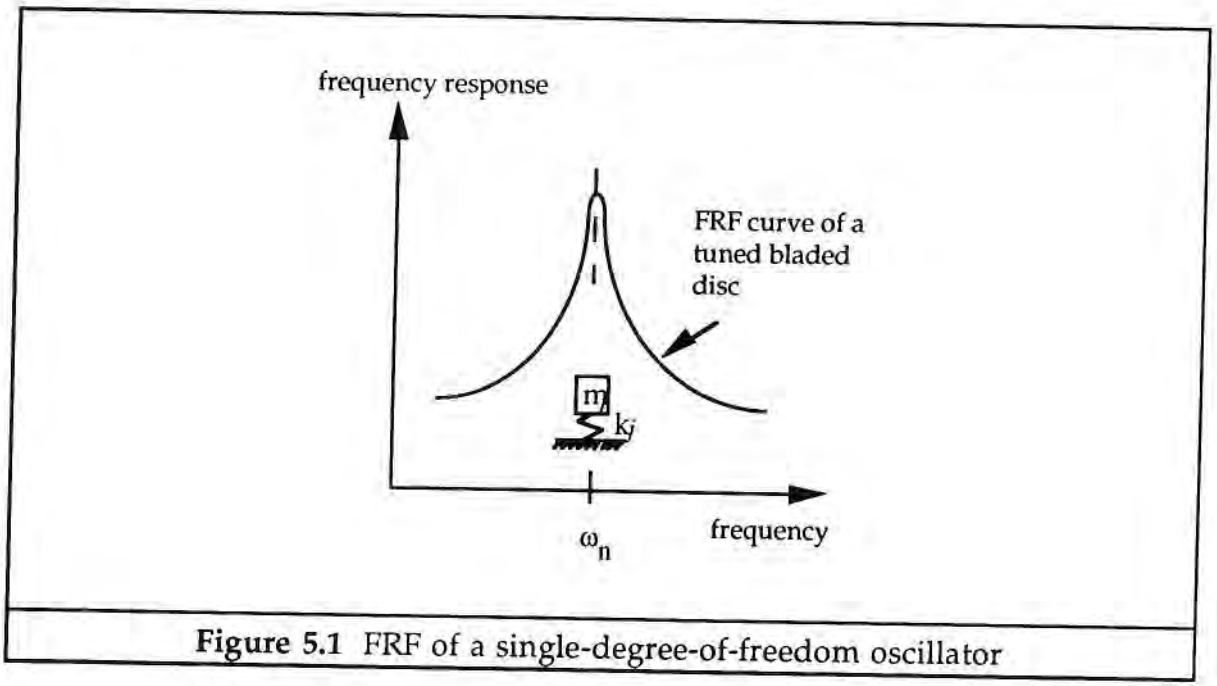

Figure 5.1 FRF of a single-degree-of-freedom oscillator

For a tuned bladed disc model such as the one shown in Figure 3.1, the damping matrix will be in the form as follows:

$$\{\phi\}_r^T[C]\{\phi\}_r = \begin{cases} 2\zeta_r\omega_r\,; & \text{for odd number diagonal terms in [C]} \\ 0\,; & \text{otherwise} \end{cases} \qquad (5.5)$$

for which $\{\phi\}_r$ is the rth mass-normalised eigenvector and ζ_r are the damping coefficients. For a uniformly damped system, the coefficients ζ_r are identical. The damped eigenvalue, s_r, can be expressed as follows:

$$s_r = \omega_r(-\zeta_r \pm j\sqrt{1 - \zeta_r^2}) \qquad (5.6)$$

The numerical model adopted for this study is the 36-bladed disc model used in the previous chapter. The structural parameters for the tuned model are shown in Table 5.1. The hysteretic damping ratio or the loss factor η can be defined as $k^* = (1 + j\,\eta)k$. Theoretically, the hysteretic damping ratio can be shown to be related to a viscous damper at resonance [108] as $\eta = 2\zeta$. Furthermore, there are two other terms for quantifying the damping levels in a lightly damped structure (see Appendix V for details) shown as follows:

a) the logarithmic decrement (or log dec.) $\delta \approx 2\pi\,\zeta_r$ and

b) the Q-factor $Q \approx \dfrac{1}{2\,\zeta_r}$

m = 0.05 kg	k = 65384.16 N/m	
M = 0.18 kg	K = 941532.0 N/m	K_G = 65.384 N/m
η = 0.2 %	$\zeta \approx$ 0.5 %	Q ≈ 80

Table 5.1 Structural Parameters

5.2.3 Complex Modes

Complex modes are effects of phase differences being neither 0° or 180° which normally associate with proportional damping distributions. Complex modes are hence direct results from the non-proportional damping. In modal analysis, the state-space equation provides a general method to deal with systems including both hysteretic and viscous damping and when the damping is non-proportional. The numerical solution to the state-space equation as shown by equation (5.4) can be obtained by assuming a complex harmonic solution $\{y\} = \{Y\}e^{st}$ and thus the complex eigenvalue problem can be formed by letting $\{p\} = 0$ as follows:

$$-s_r\,[\,\mathbf{A}\,]\,\{Y\} = [\,\mathbf{B}\,]\,\{Y\} \qquad (5.7)$$

and this equation leads to s_r, $\{\theta\}_r$ and r = 1,2, ... 2N.

Since the matrices **[A]** and **[B]** are non-positive definite, not all eigensolvers can solve equation (5.7). It is convenient and necessary to transform equation (5.7) from the general form to the standard form of eigenequation by factorising the [A] matrix using the general LU decomposition:

$$[\mathbf{A}] = [\mathbf{L}][\mathbf{U}]$$

such that,

$$-s_r [\mathbf{I}] \{Y\} = [\mathbf{L}]^{-1}[\mathbf{B}][\mathbf{U}]^{-1} \{Y\} \tag{5.8}$$

The complex QR algorithm is one of the routines which can solve the above equation and the complex QR algorithm from NAG library F02AKF is used in this study. The eigenvectors obtained from the state-space equation consist of two parts; the displacements and the displacements divided by s_r (i.e. the velocities). By properly selecting the eigenvectors and then normalising by the mass matrix of the system, mass-normalised mode shapes can be obtained. To validate the computer program, numerical examples are taken from reference [42] and are re-calculated here using the state-space equation. The results are also included in Appendix V, where one can see excellent agreement between the normal eigenvalue method and the state-space method.

For quite a long time, researchers were looking for some explanations on the complex mode effects in structural dynamics, and searching for factors which affect the complex modes in a dynamic system. Recently, in 1991, Lin [90] applied a perturbation theory to show that damped modes become complex if there exist close modes. Imregun and Ewins, in 1995, further pointed out numerous practical examples in which complex modes can be found and they also showed some of the factors which cause modes to become complex [67]. Nevertheless, the following analysis examines the complex mode effects from the phases of a pair of modes, since the phases of the complex eigenvalues s_r and the eigenvectors $\{\Psi\}_r$ are the major interest in the studies of complex modes. If a 2-degree-of freedom system can represent a lightly damped but tuned bladed disc system, two of the single-degree-of freedom systems are used to represent the situation of complex modes. Considering each mass-spring-damper oscillator, the equation of motion has the following form:

$$m_i \ddot{x}_i + c_i \dot{x}_i + k_i x_i = f_i$$

The response of this equation of motion under a unit-amplitude harmonic force will be in the form as follows:

$$X_i = \frac{1}{-\omega^2 m_i + j c_i \omega + k_i} \tag{5.9}$$

The phase for the response is then defined as follows:

$$\tan \theta_i = \frac{-c_i \omega}{k_i - \omega^2 m_i} = \frac{-2\zeta_{ri}\, \omega_{ri}\, \omega}{\omega_{ri}^2 - \omega^2} \tag{5.10}$$

The differences in phases between two of these modes are (for example, the two modes of a double mode) thereforeapproximatedin the form as follows:

$$\Delta(\tan \theta) = \frac{-2\zeta_{r1}\, \omega_{r1}\, \omega}{\omega_{r1}^2 - \omega^2} - \frac{-2\zeta_{r2}\, \omega_{r2}\, \omega}{\omega_{r2}^2 - \omega^2} \tag{5.11}$$

In the special case, where $\omega_{r1} = \omega_{r2} = \omega_n$ (no frequency mistuning), equation (5.11) can be simplified as follows:

$$\Delta(\tan \theta) = \frac{2(\zeta_{r2} - \zeta_{r1})\, \omega_n\, \omega}{\omega_n^2 - \omega^2} \tag{5.12}$$

For a tuned bladed disc, the blade masses and blade stiffness are identical on a rotor and ζ_{r1} and ζ_{r2} are the same. Hence the change of the phase between the two blades will be zero. In this sense, the modes are real and the damping is proportional.

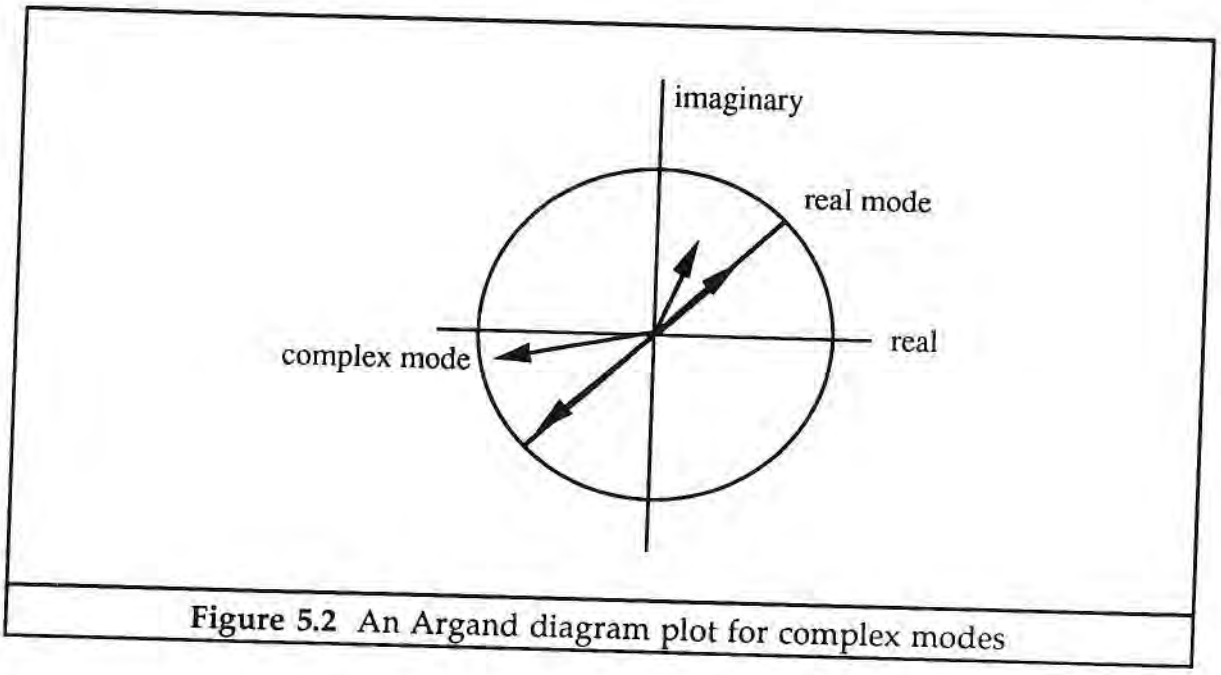

Figure 5.2 An Argand diagram plot for complex modes

One way to present the phase properties of a complex mode shape is to use the Argand diagram. In the past, this method was usually used to present the

phases of complex eigenvalues. Figure 5.2 shows the eigenvectors plotted in an Argand diagram which can be used to demonstrate the complexity of a mode. In this diagram, each eigenvector element can be plotted with its imaginary part versus its real part. Theoretically, the phase between the motions of the two blades is either 0 or 180 degrees for real modes. On the Argand diagram, the magnitudes from these modes will lie along a straight line as shown in Figure 5.2.

However, the phases for complex modes will not lie in a straight line on the Argand diagram since the phase between the two elements is not 0° nor 180°. In this case, the damping magnitudes between the blades are no longer proportional to the blade mass and stiffness matrices. This is important because even when there is no blade frequency mistuning present in a bladed disc, complex modes may still occur if the damping is unevenly distributed for all the blades around the rotor. The reason for this is that the non-proportional damping can cause the two damped frequencies to be different, as equation (5.8) shows the relation between the damped frequency and the damping factor. Moreover, in equation (5.12), the frequency parameters are second-order effects and hence comparatively larger than the damping factors. The difference between the two damping values may have to be large to have any significant changes for complex modes since $\Delta(\tan\theta)$ is directly proportional to the change of damping. It is therefore essential to stress that the definitions for damping mistuning are unlike the frequency mistuning when only small changes exist in the properties from blade to blades. Damping mistuning may have major, first-order, variations from blade to blade.

The last case to be studied is when the two natural frequencies are not equal and Equation (5.12) is no longer valid. From equation (5.11), it is not so easy to predict the phase change effects and the results will be case-dependent. Since the value of ζ is much less than the value of ω, the change due to the blade natural frequencies variation with constant damping may not be significant for causing complex modes. However, full simulations must be carried out for the whole mistuned assembly in this case. An Argand diagram to show the complex modeshapes is still useful since it indicates how complex is each mode for the system.

The Argand diagram used in this study has a reference diametral line showing the mean of all the eigenvector elements [64] and the magnitude of each

element from a eigenvector is normalised by the maximum value in the vector. If most of the eigenvector elements are near or close to the red line, it is said that the modes are real or close to real. If, however, the plots of eigenvector elements scatter around the red line, the modes are then defined as complex. Imregun and Ewins [67] also defined two modal complexity factors to quantify the complex mode effect. Finally, these ideas of complex modes are shown in Appendix V using the 3-degrees-of-freedom system from reference. The numerical results from a free vibration analysis show strongly complex modes if non-proportional damping exists together with close natural frequencies for a vibrating system.

5.2.4 Forced Response of a Non-proportionally Damped Bladed Disc

The theory of forced response analysis by complex modal analysis has been detailed by Ewins [42]. For a bladed disc response, the excitation on the ith blade by an nth engine order (nEO) excitation force pattern can be written as follows:

$$f_i = A_i \exp[j(i-1)\psi], \qquad \psi = 2\pi n/N \tag{5.13}$$

where A_j is the amplitude of the force, ψ is the interblade phase angle, j is $\sqrt{-1}$, $n = 0, 1, 2, \ldots, (N-1)$ is the engine order (EO) of excitation, and N is the number of blades in the row. For simplicity, the amplitude of the force is taken to be unity but the force on each blade is different by the interblade phase angle between the adjacent blades. The force vector can be written as follows:

$$\{p\} = \{1, e^{j\psi}, e^{j2\psi}, \ldots, e^{j(N-1)\psi}, 0, 0, \ldots, 0\}^T_{1x2N}$$

By assuming a harmonic transform,

$$\{y\} = \begin{Bmatrix} x \\ \dot{x} \end{Bmatrix} = s\{Y\}e^{st} = j\omega \begin{Bmatrix} X \\ i\omega X \end{Bmatrix} e^{j\omega t}; \qquad \text{for } s = j\omega \tag{5.14}$$

one can write the state-space equation (5.4) as follows:

$$(i\omega[\mathbf{A}] + [\mathbf{B}])\{Y\}e^{j\omega t} = \{p\}e^{j\omega t} \tag{5.15}$$

The forced response of such a damped system can be written in modal summation form as follows:

$$\{Y\} = \sum_{i=1}^{2N} \frac{\{\Theta\}_r \{\Theta\}_r^T \{p\}}{j\omega - s_r} \qquad (5.16)$$

and $\{\Theta\}_r$ contains the *A-matrix normalised* eigenvectors. s_r is the damped eigenvalue of equation (5.8) and is equal to $j\omega$. A proof of equation (5.16) from the state-space form is given in Appendix V. However, if the bladed disc is tuned or perfectly cyclically symmetric, the eigenvectors will give some errors to the modeshapes as experienced in the undamped case in chapter 3. During the whole study, several different packages for complex eigensolutions, applying the QR algorithm, have been tried but all of them gave the unexpected frequency responses for a tuned bladed disc comparing to the responses evaluated using the direct method. If, however, a small perturbation is added to the system, so that each pair of eigenvalues is just slightly separated from each other, the responses by the modal method are then in good correlation to those obtained by the direct method. In Chapter 3, a perturbation suggested to add to one of the stiffness elements for the undamped case. Here, for the state-space solution, the damping element is more sensitive and therefore the same perturbation is better on one of the dampers.

5.3 BLADE RESONANT RESPONSES OF DAMPING MISTUNED ASSEMBLIES

Uniform damping effects on frequency-mistuned bladed discs have been considered for quite a long time. In 1969, Wagner [148] studied the effect of damping on turbomachinery blades coupled to a flexible disc. He concluded that damping tended to average the response levels of the blades. Later, in 1969, Ewins correlated the detuning effect with the damping factors [31] and Ewins and Rao, in 1975 [37], showed that heavy hysteretic damping could have the result of a mistuned bladed disc behaving like a tuned one. These studies were based on the assumption that damping was uniform on every blade. In this chapter, some case studies will be based on damping mistuning behaviour on bladed disc assemblies. The second part of the study arises from attempts to add some coupled damping terms which can represent some characteristic of friction dampers.

Viscous damping between each blade and ground is used in the current study to simulate aerodynamic damping effects in the model shown in Figure 3.1. Variations in the aerodynamic forces are due to the non-uniform flow field,

and these forces can be considered as velocity-dependent. In practice, such forces will not be the same on each of the blades around the disc and mistuning of this type (damping mistuning) may cause different responses of the adjacent blades. The particular effects studied here are examples of (i) no damper on particular blades, (ii) double damping effect on particular blades. Two types of mistuned damping patterns have been applied to a 36-bladed disc. First, it is assumed that damping variations are added to a dimensionally-tuned bladed disc. Secondly, damping mistuning is applied to a system which already has a random frequency scatter of ± 5 per cent.

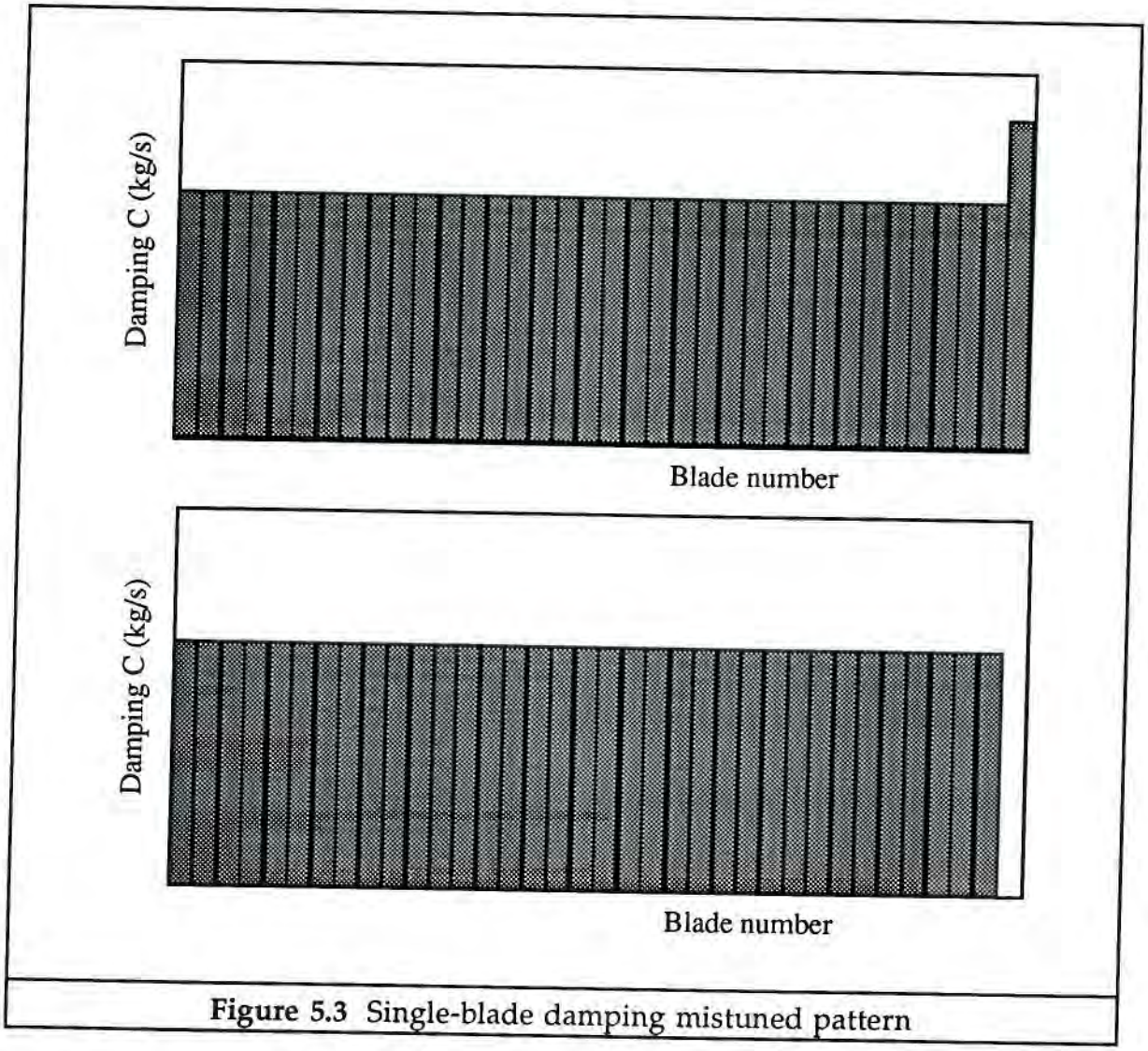

Figure 5.3 Single-blade damping mistuned pattern

In Figure 5.3, the mistuning damper is assumed to be added to the last blade. The position of a single blade in a mistuned wheel is not important since the structure is otherwise symmetrical. The stiffness and mass are the same for all the blades. The scale of the dampers is not indicated because the mistuned value could be doubled from the reference value or zero (no damping). The

reference damping value is shown in Table 5.1 in damping ratio to the critical damping value. For doubled damping, this ratio is also doubled.

In Appendix IV, a perturbation technique has been shown by which the mistuned responses can be calculated as a perturbation to the tuned system responses. Here, considering the exact form of equation (A4-12) as follows:

$$[[I] + [Z(\omega)]^{-1}[\delta Z]]\{x\} = \{x\}_o \qquad (5.17)$$

the perturbation matrix $[\delta Z]$, in the case of single damper mistuning, obviously has only one element within the entire matrix as follows:

$$\delta Z_{ij} = \begin{cases} \pm \omega c & i = j = n-1 \\ 0 & \text{otherwise} \end{cases}$$

The coefficient matrix of $\{x\}$ will therefore have the following form as follows:

$$\begin{bmatrix} 1 & 0 & \cdots & a_{1n-1} & 0 \\ 0 & 1 & \cdots & a_{2n-1} & 0 \\ \cdots & \cdots & & \cdots & \cdots \\ \cdots & \cdots & & 1+a_{n-1n-1} & 0 \\ \cdots & \cdots & & a_{nn-1} & 1 \end{bmatrix} \{x\} = \{x\}_o$$

where a_{in-1} are the coefficients after the multiplication between the inverse of the matrix $[Z(\omega)]$ and the perturbation matrix $[\delta Z]$. This is a coupled matrix so that the change of one blade will affect the whole assembly row. The peak responses of the mistuned 36-bladed disc under 6EO excitation are computed using the exact inverse method and the results are shown in Figure 5.4. The 'normalised peak response' is the peak value of the mistuned response divided by the peak value of the tuned system response with uniform damping as indicated in Table 5.1. In this diagram, it is shown that the blade with the double damping value has its response level lowered by about 1.5%, while the blade with the damper completely removed from the system has its response level increased by about 1.65%. The two sets of data display an inverse symmetry about the unit normalised response. This suggests that the missing damper does not have a drastic effect to the system. Moreover, the

neighbouring blades around the mistuned blade show a lesser effect in response than the last blade which is different from the rest. This suggests that blade-ground viscous damping has a localised effect on the system. Finally, the neighbouring blades around the mistuned blade do not necessarily show symmetry around the cascade row because the system is under a 6EO exciting force and hence the direction of the travelling wave excitation has an effect on the response.

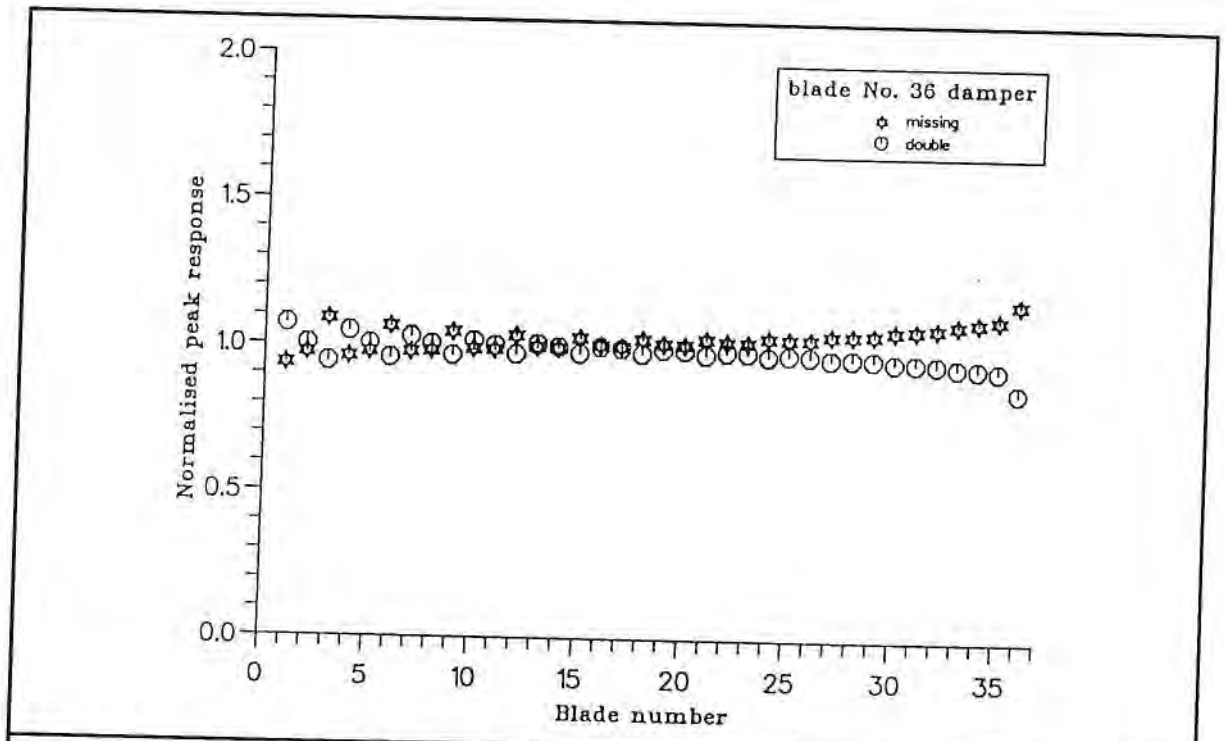

Figure 5.4 Peak 6EO responses of a 36-bladed disc with single damper mistuning solving by the direct method

Next, the perturbation technique which has been shown in Appendix IV is applied here to calculate the responses for the same mistuned bladed disc with the same damping patterns. The mistuned system responses for a perturbation is deduced by the following equation (equation A4-6) as follows:

$$\{x\} = [[\mathbf{I}] - [\mathbf{Z}(w)]^{-1}[\delta Z]\,]\{x\}_o \qquad (5.18)$$

Figure 5.5 shows a corresponding peak response calculation for the same damping mistuning patterns as used for the direct method solution in Figure 5.4. However, the perturbation technique is used this time by solving equation (18) which neglects the higher order terms in the inversion. Quite clearly, the solutions from the perturbation method are not so accurate as the direct

solution because only the first order term is considered. The error difference on blade 36 between the two methods is approximately 4.4%. Nevertheless, the approximate solution by the perturbation method can predict the same response pattern as the one shown in Figure 5.4. The purpose of this exercise is to compare the results obtained from the perturbation method and the direct method. In recent years, many researchers were showing the studies of cyclic symmetric structures using the perturbation technique. Naturally, mistuning is a perturbation to a tuned system and linear perturbation theory is available only if the higher order effects are negligible.

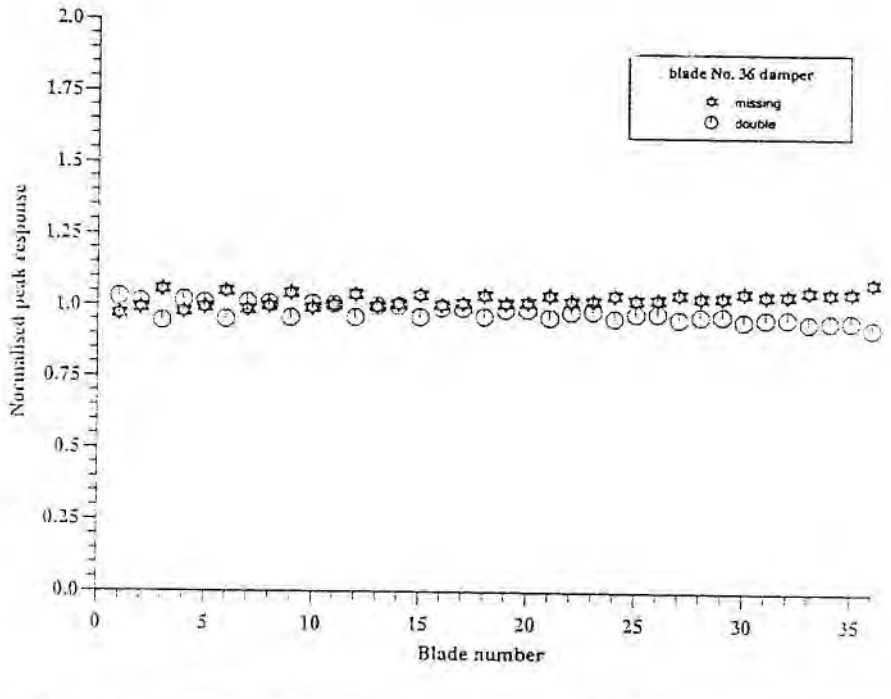

Figure 5.5 Peak 6EO responses of a 36-bladed disc with single damper mistuning solving by the perturbation method (equation 5.18)

Figures 5.6a and 5.6b show the scatter of two different randomly-distributed damping patterns. In Figure 5.6a blades No. 17 and 32 have dampers missing while in Figure 5.6b the dampers on blades No. 27, 32 are missing. The idea of comparing the two different damping distributions is to examine any relationship between the blades with no damper and the adjacent blades. From the conclusion of the single blade mistuned damping, it is shown that damping is a localised effect since a mistuned damper may affect its neighbouring blades slightly.

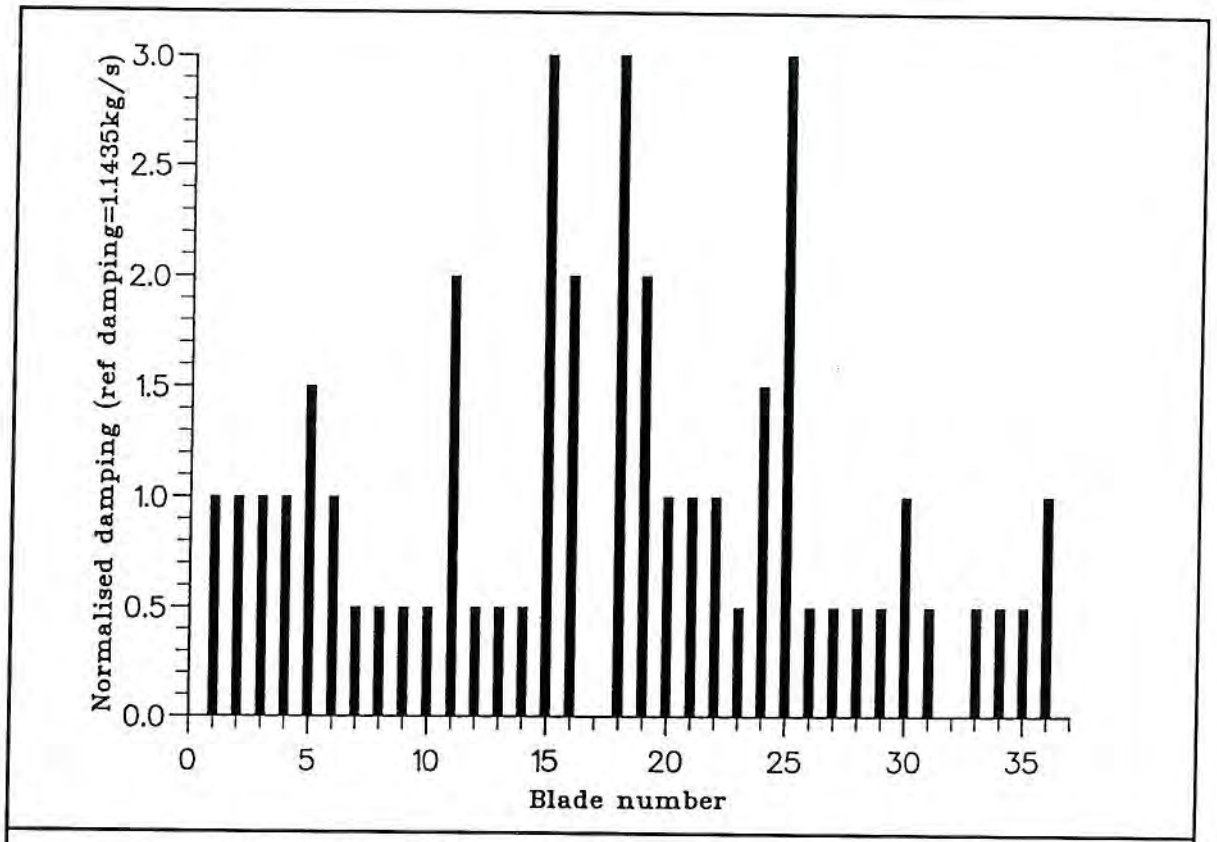

Figure 5.6a Randomly mistuned damping pattern I

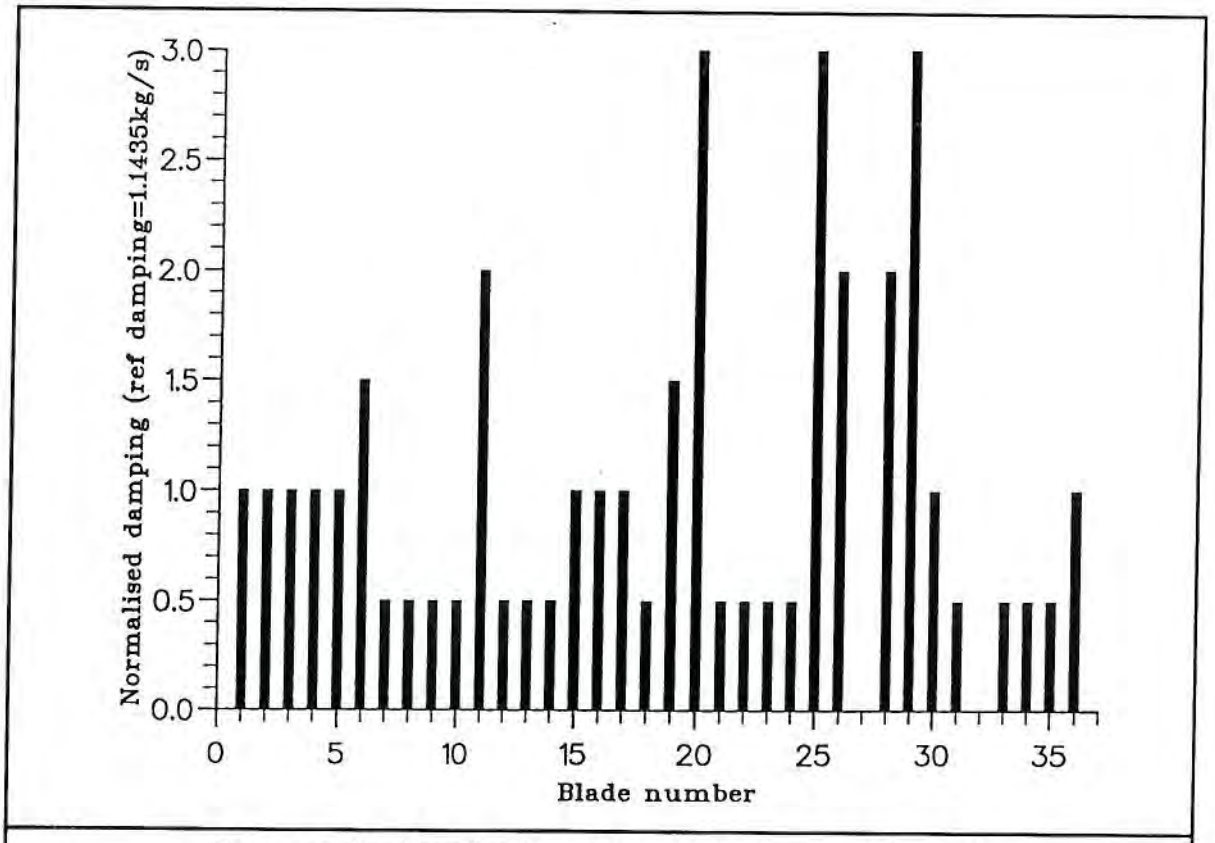

Figure 5.6b Randomly mistuned damping pattern II

In both distributions, the first missing damper is situated between two high-value dampers, while the second one is located among low-value dampers. For Distribution I, the two missing dampers are quite well separated from each other while for Distribution II, they are close to each other. The damping values shown in the Figures are normalised by a reference value which is the mean value of the distribution. The results from these random mistuning patterns are shown in Figure 5.7 as the normalised response versus blade number. The two distributions shown in the diagram are quite different from each other. It is of interest to note that neither blade with the damper missing exhibits the highest response level. Normally, it is a highly mistuned blade (over the mean) adjacent to a bunch of lowly mistuned (below the mean) blades which suffers the worst response. From Figure 5.7, Distribution I obviously gives the worst effect. This is the result that a group of several lightly damped blades together leads to a significant increase of the blade response level. The sudden loss of a damper does not necessarily imply an abrupt change on the system as well.

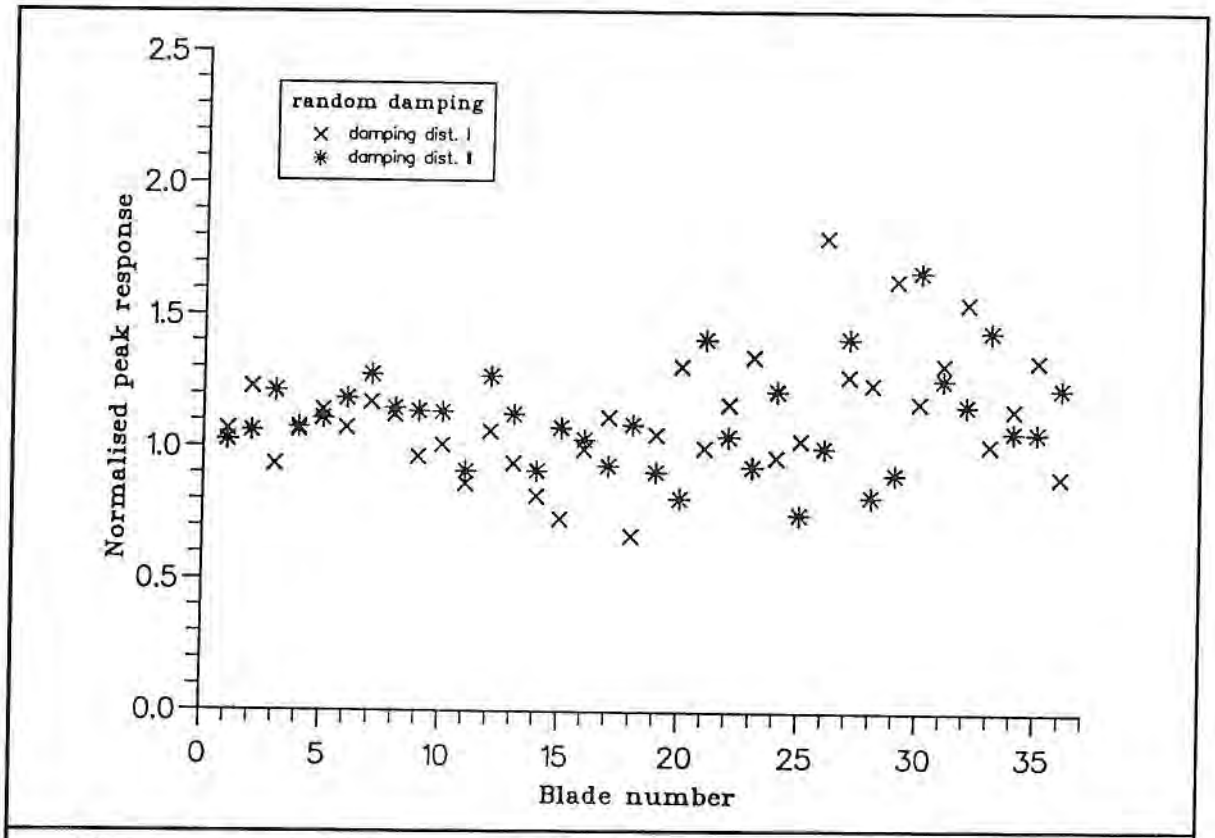

Figure 5.7 Peak 6EO responses of a 36-bladed disc with random damper mistuning

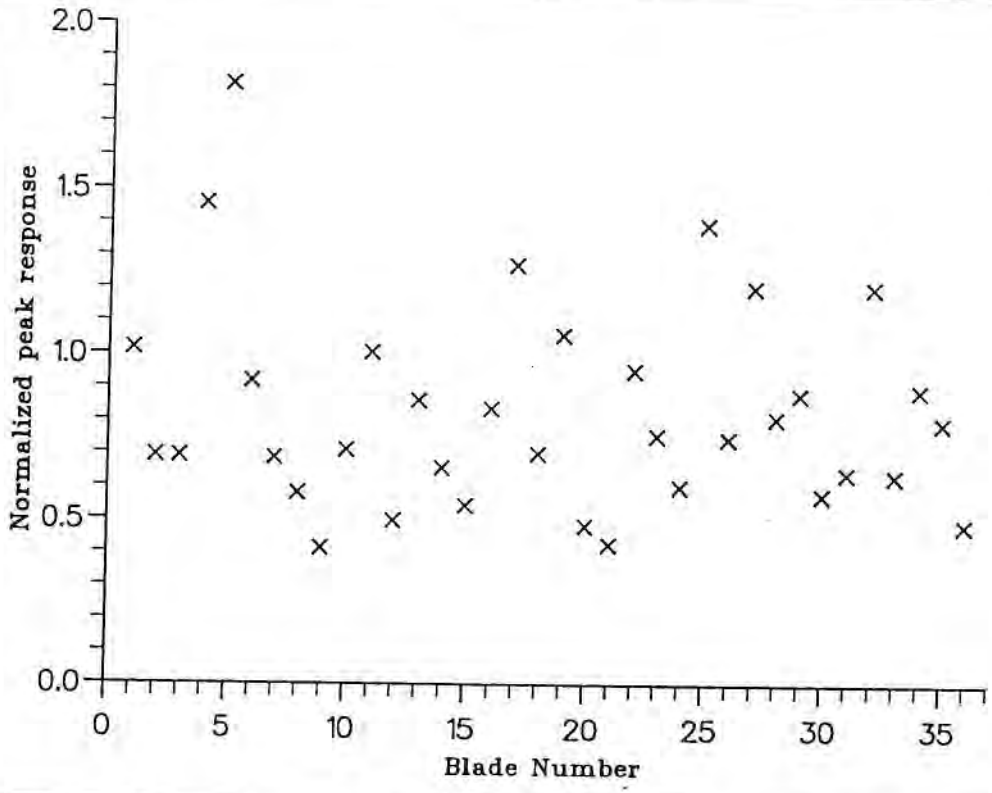

Figure 5.8 Normalised peak responses for constant damping

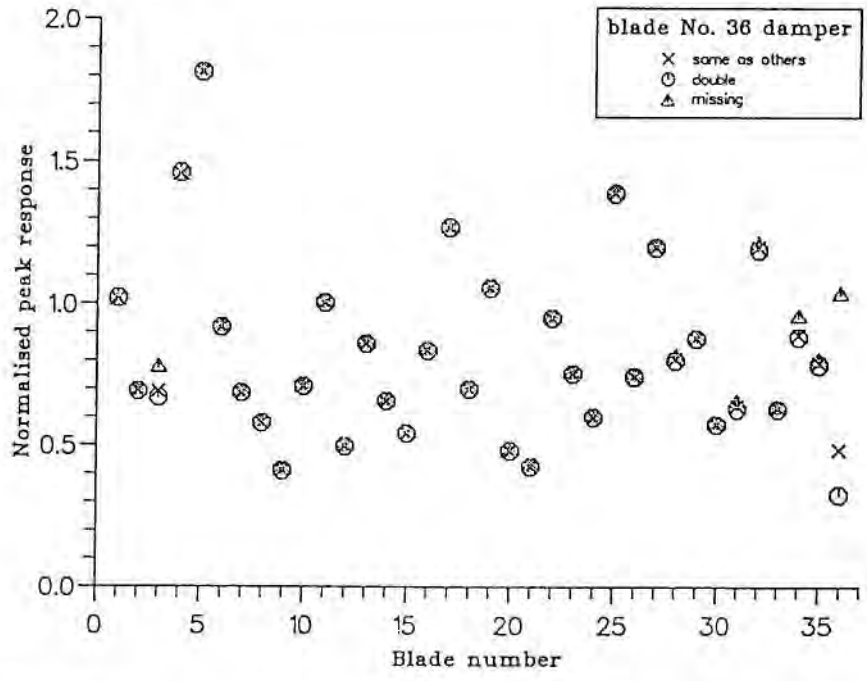

Figure 5.9 Peak responses of 36 bladed disc with single damper plus random frequency mistuning

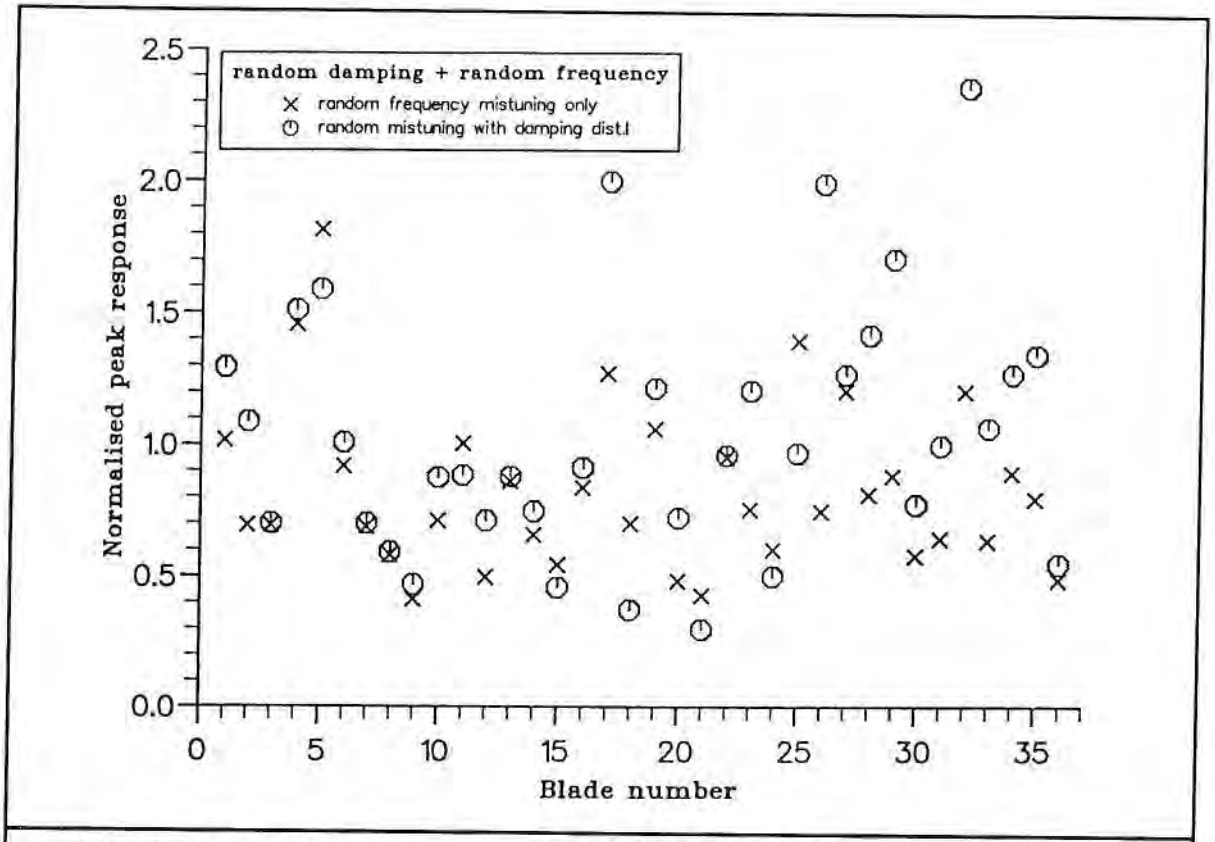

Figure 5.10a Peak responses of 36 bladed disc with random mistuning

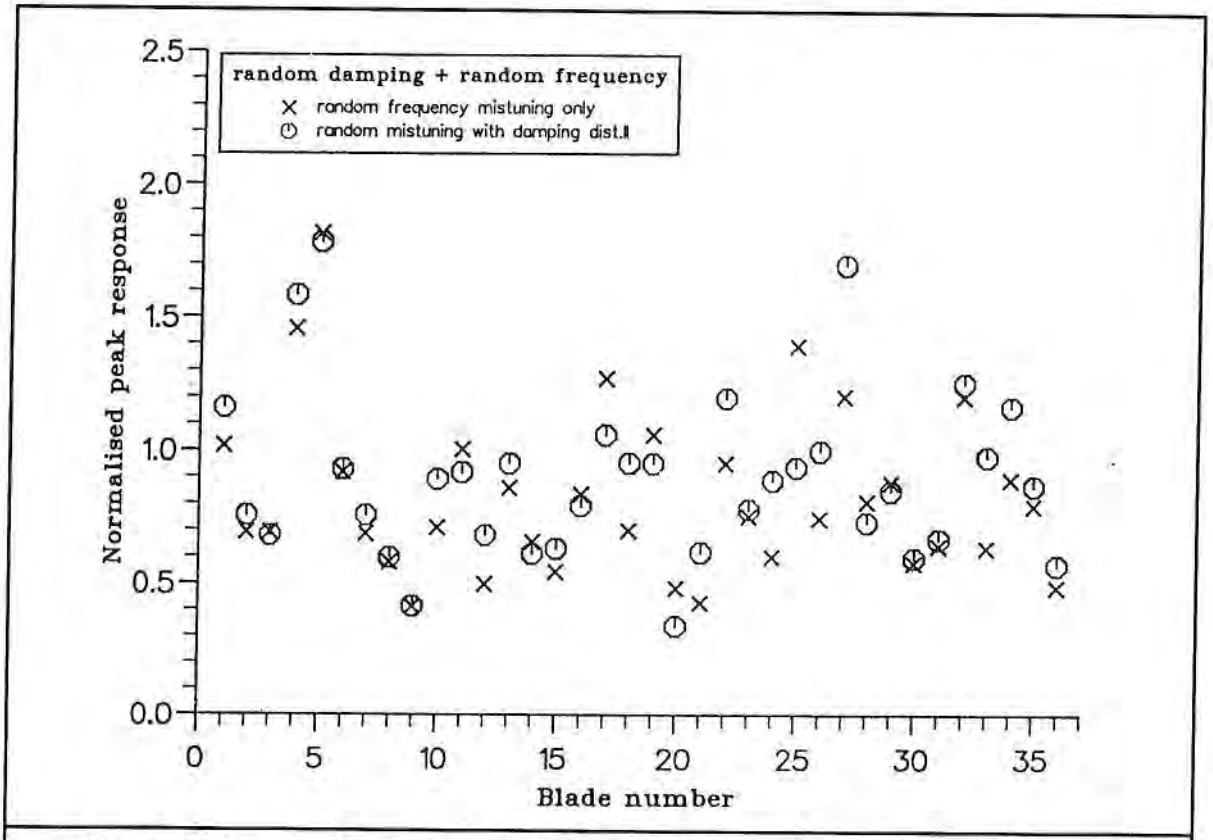

Figure 5.10b Peak responses of 36 bladed disc with random mistuning

Next, if the bladed disc has a 10% frequency scatter randomly distributed amongst blades, as those shown in Figure 3.10. The normalised peak responses for all the blades with a uniform damping value (ζ = 1.0 %) are shown in Figure 5.8 while Figure 5.9 shows the peak responses of a single damper variation versus the blade numbers. The results again suggest that the response of that specified blade has localised effect. The response goes up by a small factor on the blade which has the damper missing, but the other neighbouring blades have little influence on it. Figures 5.10a and 5.10b contain plots showing the peak responses of both random damper variations added to a 10% random frequency mistuning of the bladed disc. The first distribution shows that damping variation can have a severe effect over the frequency mistuning. The critical blades are the one with the damper missed and located among low damping values. Also, these low damper blades were located between blades with very high damping values. The second distribution shows that the damping variation does not cause very serious problem to that set of blades.

5.4 COMPLEX MODES IN DAMPING MISTUNED ASSEMBLIES

In practice, one will expect that a set of mistuned dampers will lead to non-proportional damping of the system and hence that the system mode shapes will be complex. In Appendix V, a study of the complex modes for a 3-degrees-of-freedom system is shown using the state-space equation (5.8). The Argand diagram plots of the eigenvector elements are used to illustrate the complexity of modes. Next, a 36-bladed disc is investigated using the model shown in Figure 3.1. The viscous damping elements connected between the blades and ground are associated with the non-proportional damping. By using the Argand diagram plots, Figure 5.11 shows the case of a perfectly tuned assembly with neither damping nor frequency mistuning and the results of this case indicate that all the modes are real as all the eigenvectors lie along a straight line. Complex modes can be found even when one damper is mistuned as shown in Figure 5.12. In this case, one damper has been deliberately dropped and as a result, some modes, especially those with close natural frequencies, show complex effects. Next, Figure 5.13 shows the case for a uniformly damped but frequency mistuned rotor. In this case, no complex modes are observed. This further confirms that close modes are necessary conditions to cause complex modes if they are also associated with mistuned dampers or other forms of non-proportional damping. Moreover, for non-proportionally-damped systems, close modes seem to lead to more modal

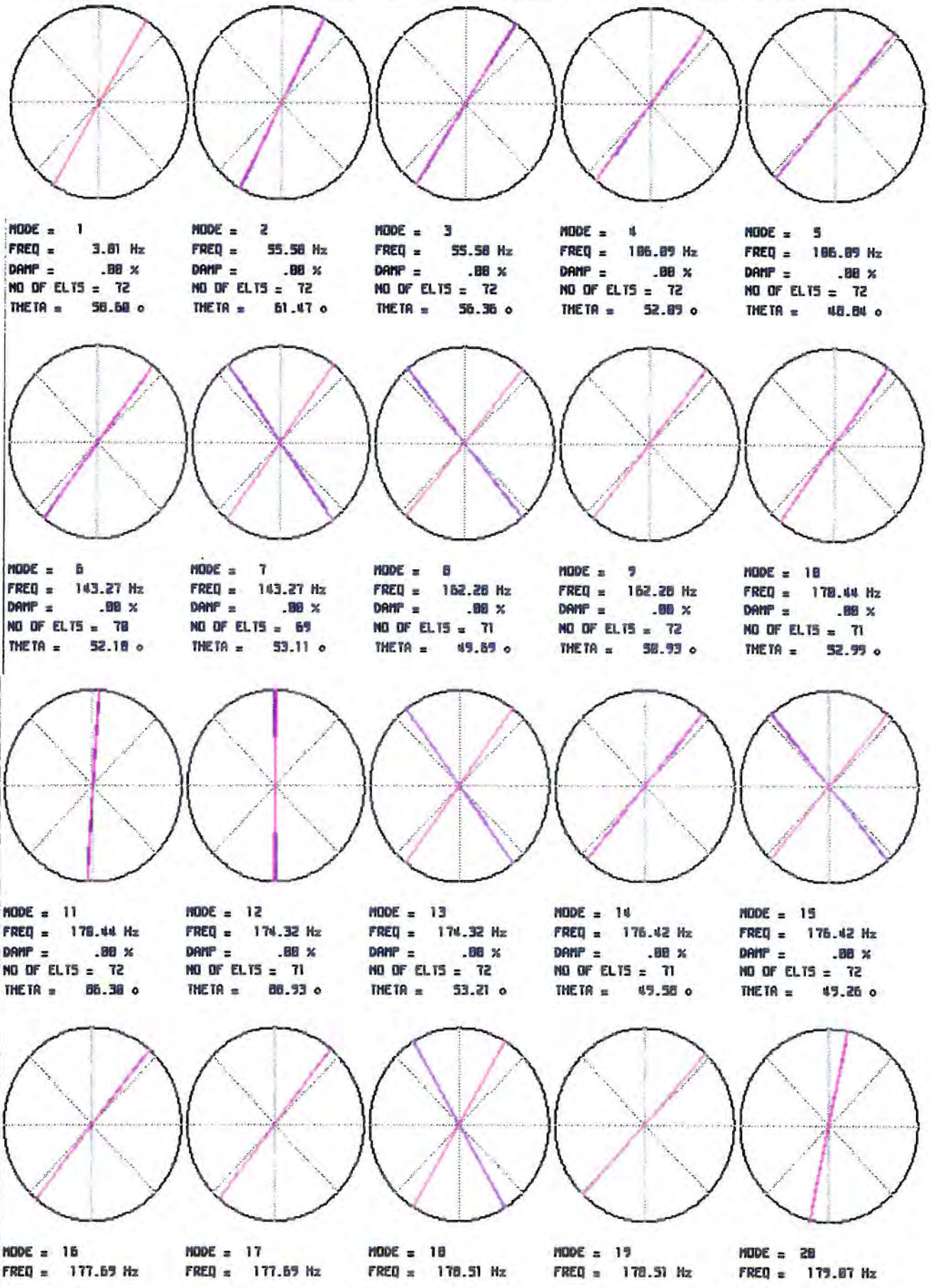

Figure 5.11 Complex modes of tuned 36-bladed disc

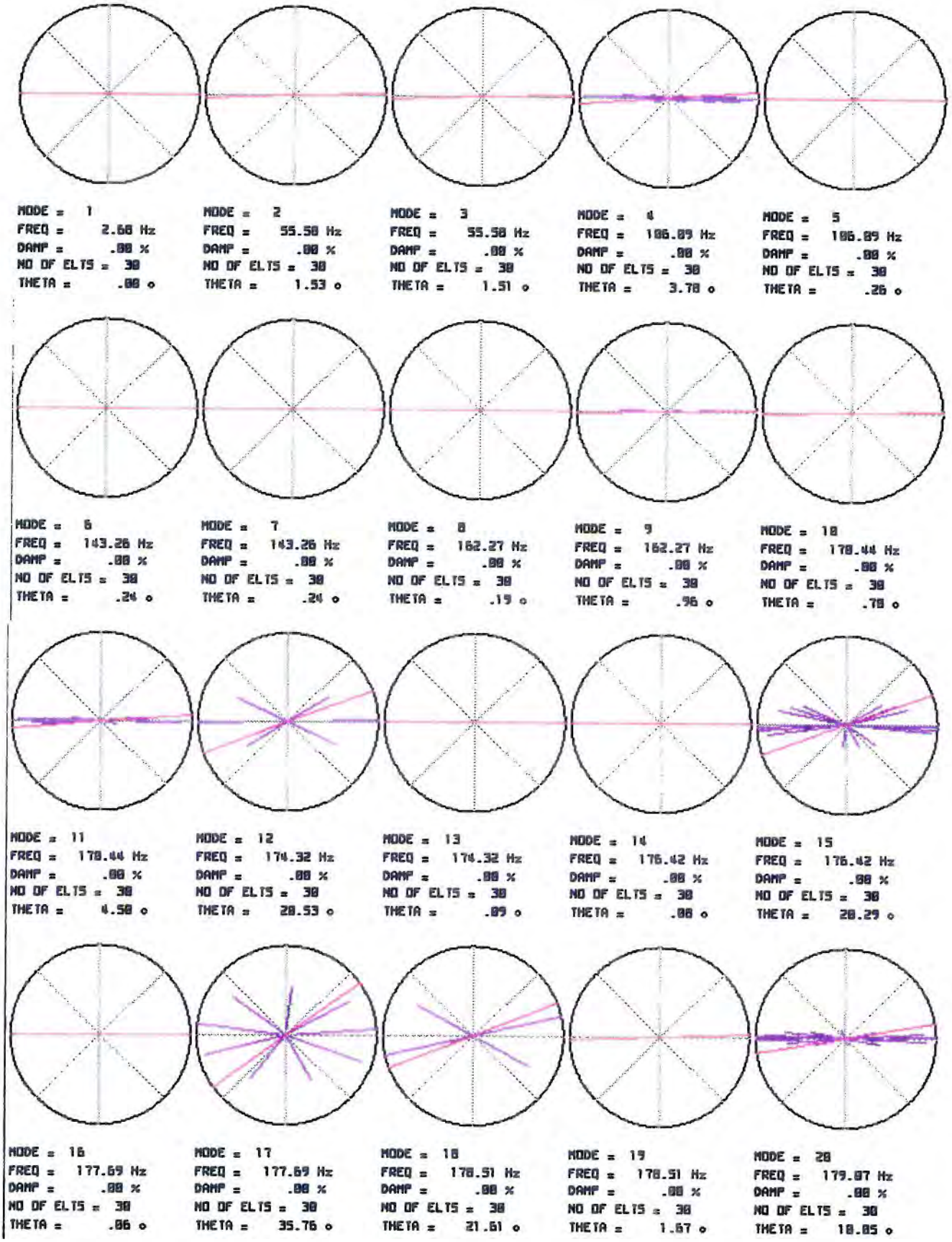

Figure 5.12 Complex modes of 36-bladed disc with single damper left-out

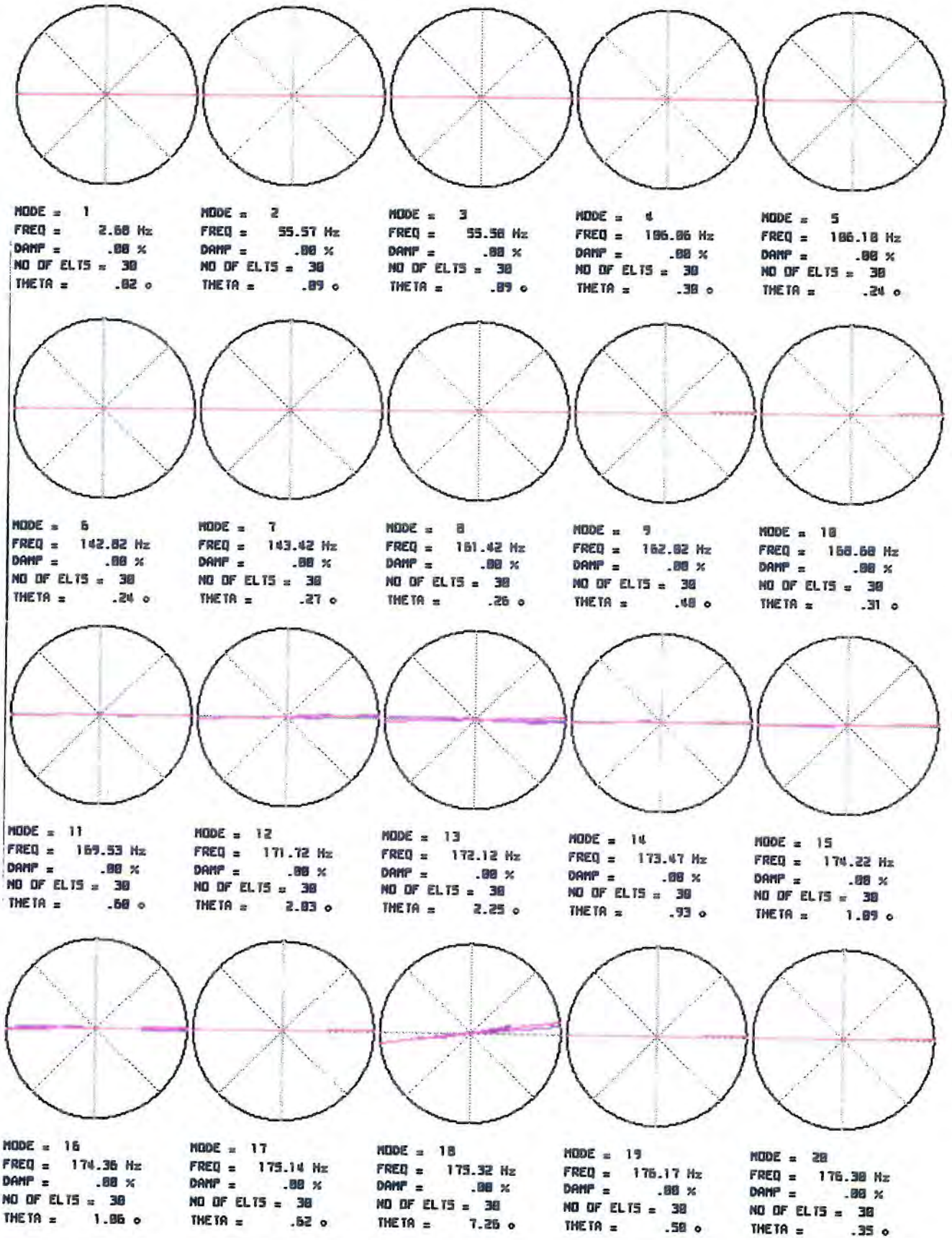

Figure 5.13 Complex modes of 36-bladed disc with 10% frequency mistuning

complexity, as shown in Figure 5.12. In this diagram, the lower modes are well-separated ones. They correspond to the lower nodal diameter patterns of the bladed disc and it can be seen that these modes are approximately real. However, when the modes are closer to the cantilever blade modes, many modes are clustered together and complex modes appear in this region.

5.5 CASE STUDY: RAINBOW TEST

The "rainbow test" is an experimental process used to test the effects of different standards of under-platform dampers. It is used to determine the optimal damping value in a fast and economical way. By this technique, different standards of damper are arranged into several sectors of a bladed assembly so that various damper effects can be found by performing a single test. This study tries to simulate the "rainbow test" effect by using a simple numerical model, which is a modified version of Figure 3.1 (see Figure 5.14).

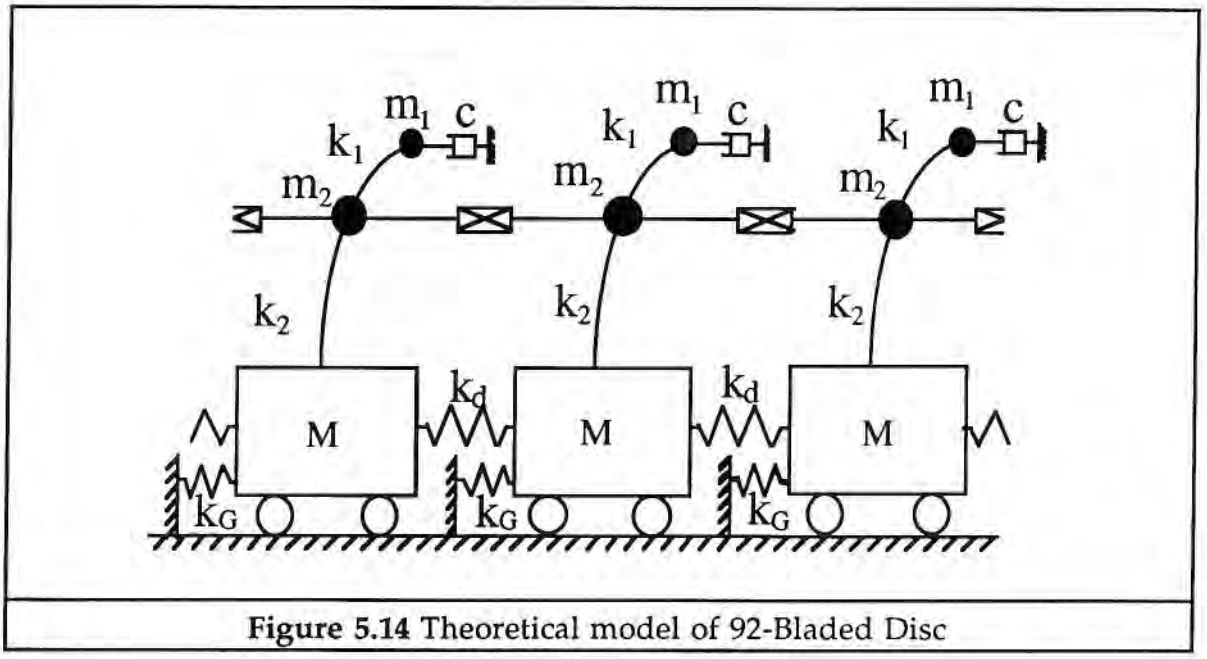

Figure 5.14 Theoretical model of 92-Bladed Disc

Each blade is now represented by two masses and springs. The tip mass represents the blade part above the platform while the second mass represents the blade section below the platform. The under-platform dampers can then be simulated by adding damping elements between the lower masses of adjacent blades. The system parameters can be deduced either from a Finite Element analysis of the whole assembly or from a modal test of the actual assembly.

5.5.1 **Identify System Parameters**

The blade and disc parameters for the specific 92-bladed disc used here are obtained from experimental data. The blade-alone natural frequency measured in a fixed root is 1076 Hz and the cantilever natural frequency measured with a fixed platform is 1326 Hz for 1F (first bending mode). Some stationary (i.e. non-rotating) bladed disc modes are also known from tests, as follows:

Modes (No. of nodal diameters)	Natural frequency (Hz, Ω = 0 from test)	Natural frequency (Hz, Ω = 0 calculated)
7 - ND	1009	1009.715
8 - ND	1019	1019.461
9 - ND	1024	1024.506
40 - ND	1037	1035.983

Table 5.2 Experimental measurements of 92-bladed disc

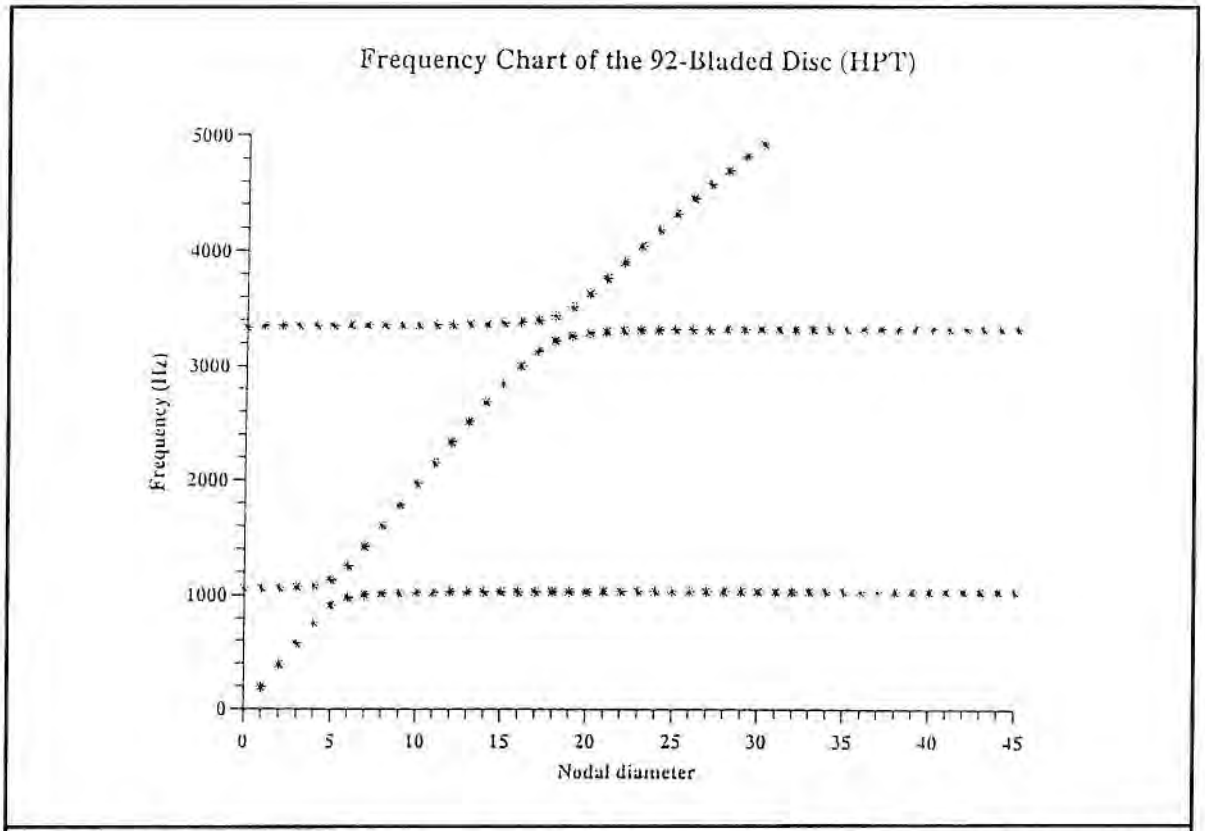

Figure 5.15 Natural frequency vs. nodal diameters for the 92-bladed disc model

From these data, suitable parameters for the lumped-mass model are found as shown in Table 5.3 and the computed natural frequency versus nodal diameter characteristics are shown in Figure 5.15. A suitable value for viscous damping can first be estimated by using equation (6) and then checked based on the half-

power point technique to find the Q-factor of the response curve. The coupled damper values, i.e. the under-platform dampers value, are then evaluated in a similar way. Without the coupled dampers, the damping of the assembly modes has been set at a Q-factor value of 200. The coupled dampers are divided into several different values. The maximum value is evaluated by a trial-and-error method until the response function gives a Q-factor value of 50. The rest of the damping values are found by simply taking fractions of the maximum value. The coupled dampers were then arranged into two different distributions, as shown in Figure 5.16.

ω range between 1000-1050 Hz		
$m_1 = 0.01$ kg	$k_1 = 645299.311$ N/m	
$m_2 = 0.005$ kg	$k_2 = 1450048.9665$ N/m	
$M = 0.28$ kg	$K_d = 95507200.0$ N/m	$K_G = 65.384$ N/m

Table 5.3 Structural Parameters for 92-bladed disc

5.5.2 **Modeshape Studies**

The two configurations of bladed discs applying the two arrangements of dampers were analysed using equation (5.8), and the mass-normalised modeshapes of the blades are shown in Figures 5.17, 5.18 and 5.19. Theoretically, the complex part of the mode shape should be relatively small in comparison with the real part for *real* modes. From the results, it seems that from the 6-nodal diameter mode up to the 8-nodal diameter mode, the imaginary parts of the modeshapes become more significant in amplitude as the number of nodal diameters increases. This effect indicates that the modes are complex. From the phase plots of these modes, it can be deduced that complex modes constitute a slight travelling wave effect in the responses. This effect gets more significant if the modes are clustered together by having close natural frequencies.

Next, the discrete Fourier components of the modeshapes were used to study further the effect of complex modes and the coupling effects. Generally, the lower diameter patterns represent relatively strong coupling while higher nodal diameter patterns represent relatively weak coupling, as described in Chapter 4. Figures 5.20, 5.21, and 5.22 show the Fourier coefficient terms. From these plots, the complex mode effect seems to become stronger after the 6

nodal diameter mode and the real parts of the modes are gradually affected by the imaginary parts. This effect can be also demonstrated from Figures 5.23 and 5.24 which are the eigenvectors plotted in Argand diagrams, with mistuned damping configurations I and II respectively. The lower modes in these graphs are clearly real modes until the natural frequencies are close to each other and the modes afterwards are complex. One interesting point to notice is that complex modes start to have significant influence after the 6 nodal diameter mode for the first blade mode family. From the frequency versus nodal diameter plot, this is exactly when the curve starts to bend. At this point, the modes are close to each other, so-called "close" modes, and a complex mode effect is expected and found.

5.5.3 Maximum Responses Studies

Finally, the maximum responses of the two damping distributions are calculated under 5th, 6th, 8th, and 36th engine-orders. In the previous Chapter, the coupling effect was shown to be significant to the blade responses. It also showed that as the number of nodal diameters gets greater, there is always a veering point on the frequency versus nodal diameter curve. By applying different engine-order excitations to the bladed disc assembly, different coupling effects can be achieved. Figures 5.25, 5.26, 5.27, and 5.28 show the individual blade responses for the tuned cases under each individual damping value in the rainbow case, together with the blade responses of the rainbow tests. Two characteristics can be seen in the results; first, the rainbow results can only predict the true responses correctly for high engine orders. For low nodal diameters, the responses behave towards the average damping level of the rainbow. Second, the two different damping distributions give different response patterns at low engine orders such as 6EO. From Figure 5.26, the high blade responses from the second rainbow arrangement seem to be sensitive to light damping as well. Below 6EO, the response pattern is more like that for real mode shapes. This is because the modes are quite well separated and so have lost the complex features.

5.6 CONCLUDING REMARKS

This chapter has shown how damped bladed disc resonance responses can be computed by applying the state-space formulation of the equations of motion. Both the mode shapes and the responses are examined for some different

bladed models. The following comments are made based on the numerical studies of these cases.

- Damping normally tends to lower the peak resonant responses of a dynamic system. However, damping mistuning may affect a bladed system in an adverse way depending on the arrangement of the blades. Generally, a damper missing from a particular blade would cause the response level of that individual blade to increase. The increase of response for such an undamped blade may have either an adverse or a beneficial effect, depending on how the damping variation and the frequency scatter is arranged. Since damping is a localised effect, frequency mistuning tends to be the more dominant effect unless a series of under-damped blades are grouped together. As a result, the discrepancies of the blade responses could be quite large because of the non-uniform viscous damping terms.

- Complex modes are only associated with non-proportional damping elements and then only if the modes are close together. This effect can be found on a bladed disc system although the modeshapes will not be significantly complex except in the case of close modes.

- From the numerical studies, it is concluded that the rainbow test is only effective for high nodal diameters forced responses. In these region, the assembly frequencies are well above the veering point on the natural frequency versus nodal diameter plot. Therefore, the real part of the modeshape has been distorted by the increasing magnitudes of the imaginary parts of the eigenvectors, as can be seen from Figures 5.20, 5.21, 5.22 and so the modes become complex. This also shows the effect of coupling from the disc and strong coupling may smear the damping mistuning effects.

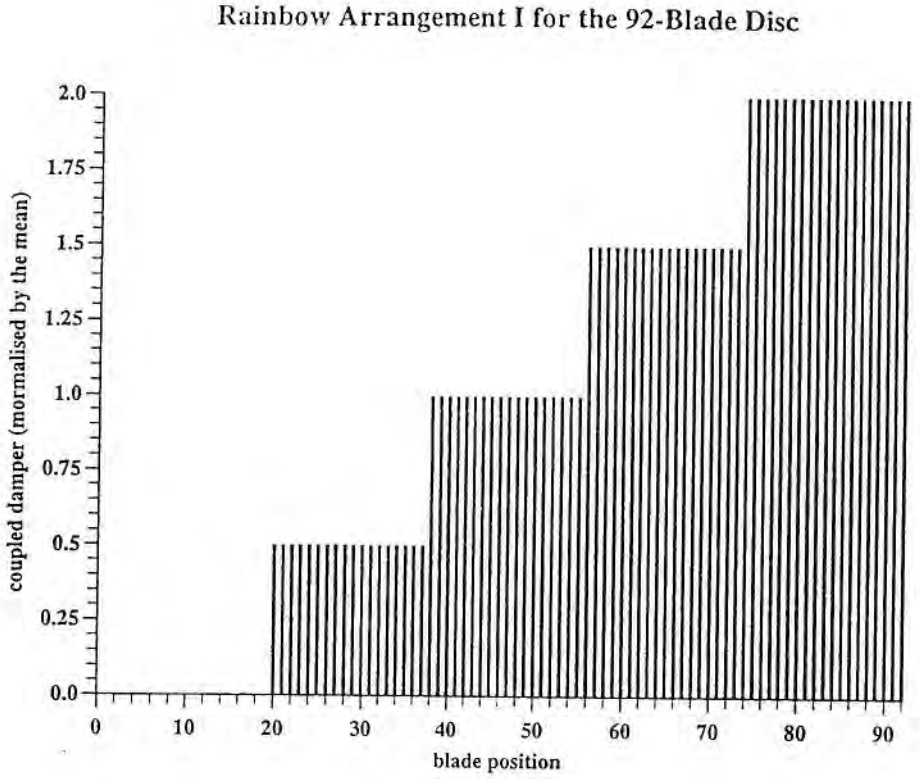

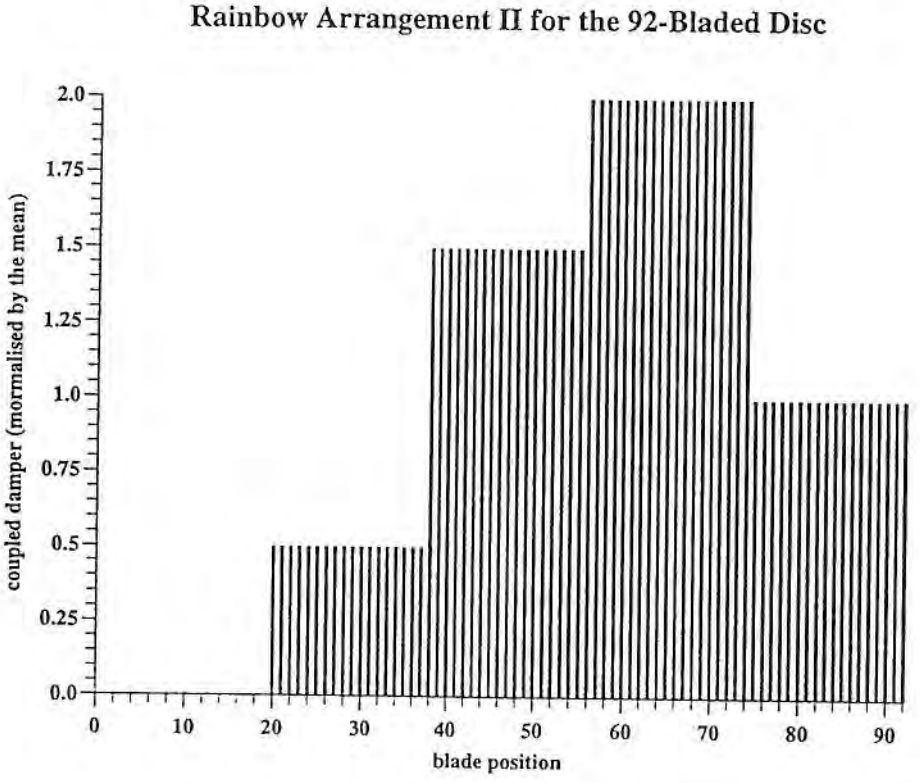

Figure 5.16 Rainbow arrangements for the coupled dampers

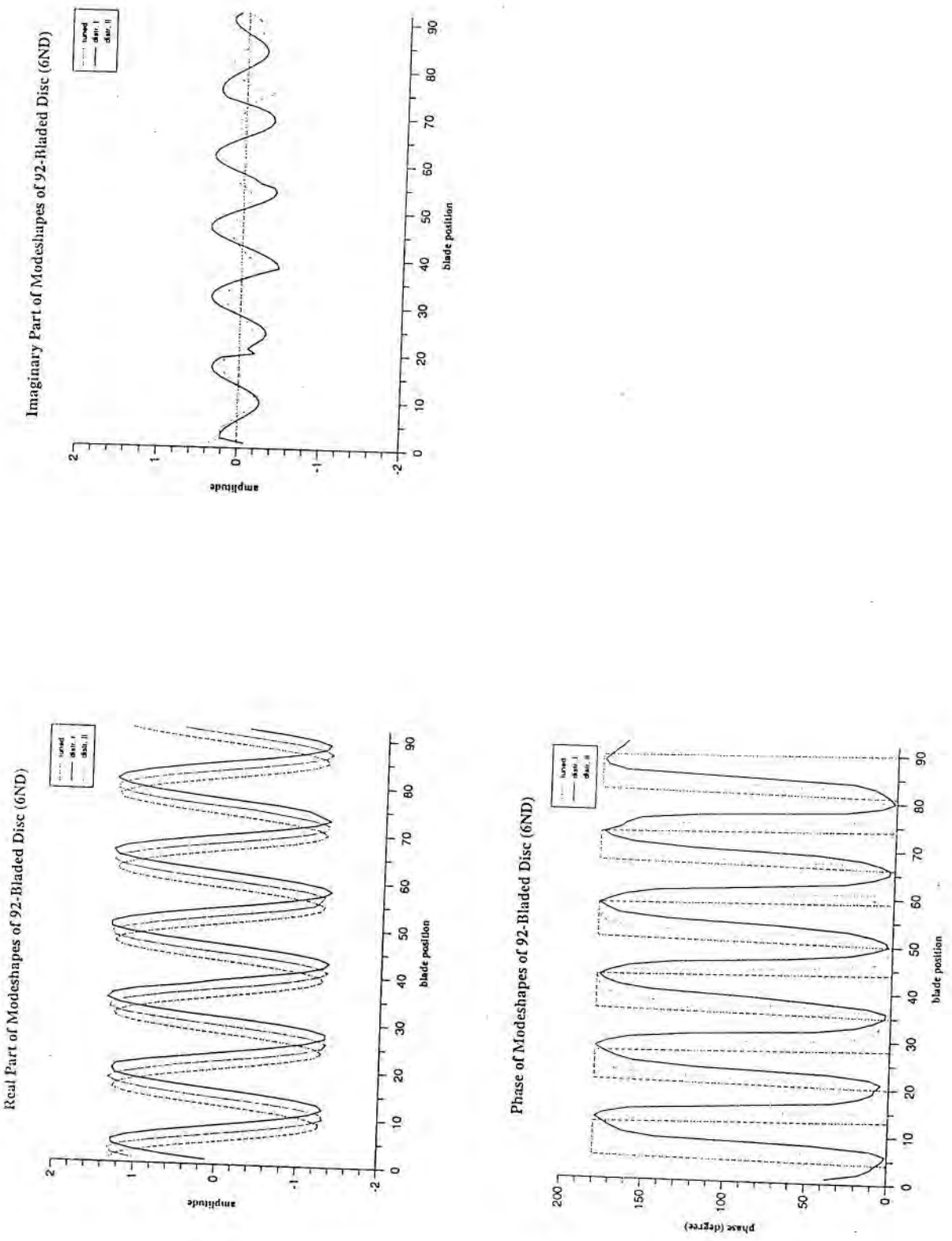

Figure 5.17 Modeshape and phase of mode 6 for the mistuned 92-bladed disc

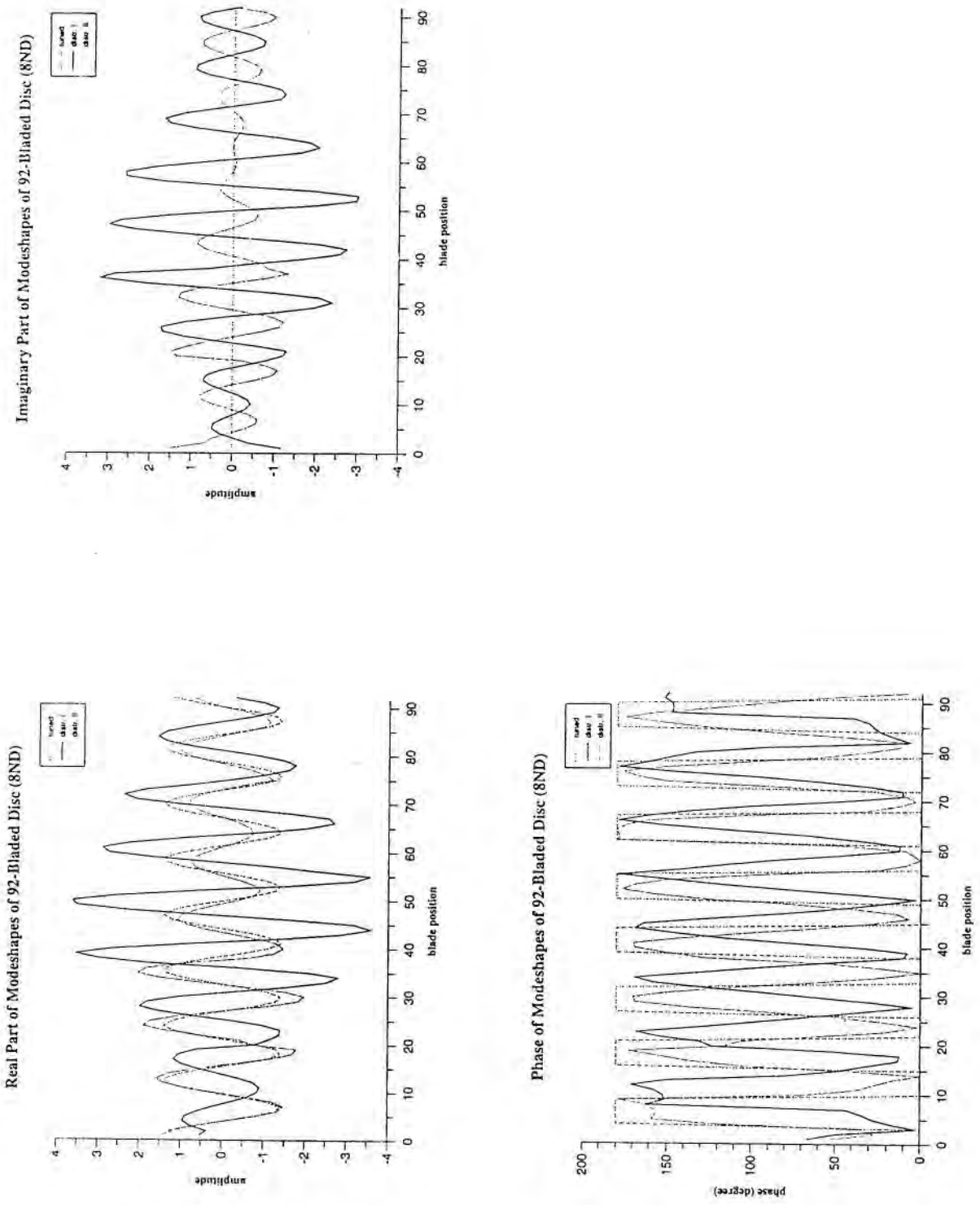

Figure 5.18 Modeshape and phase of mode 8 for the mistuned 92-bladed disc

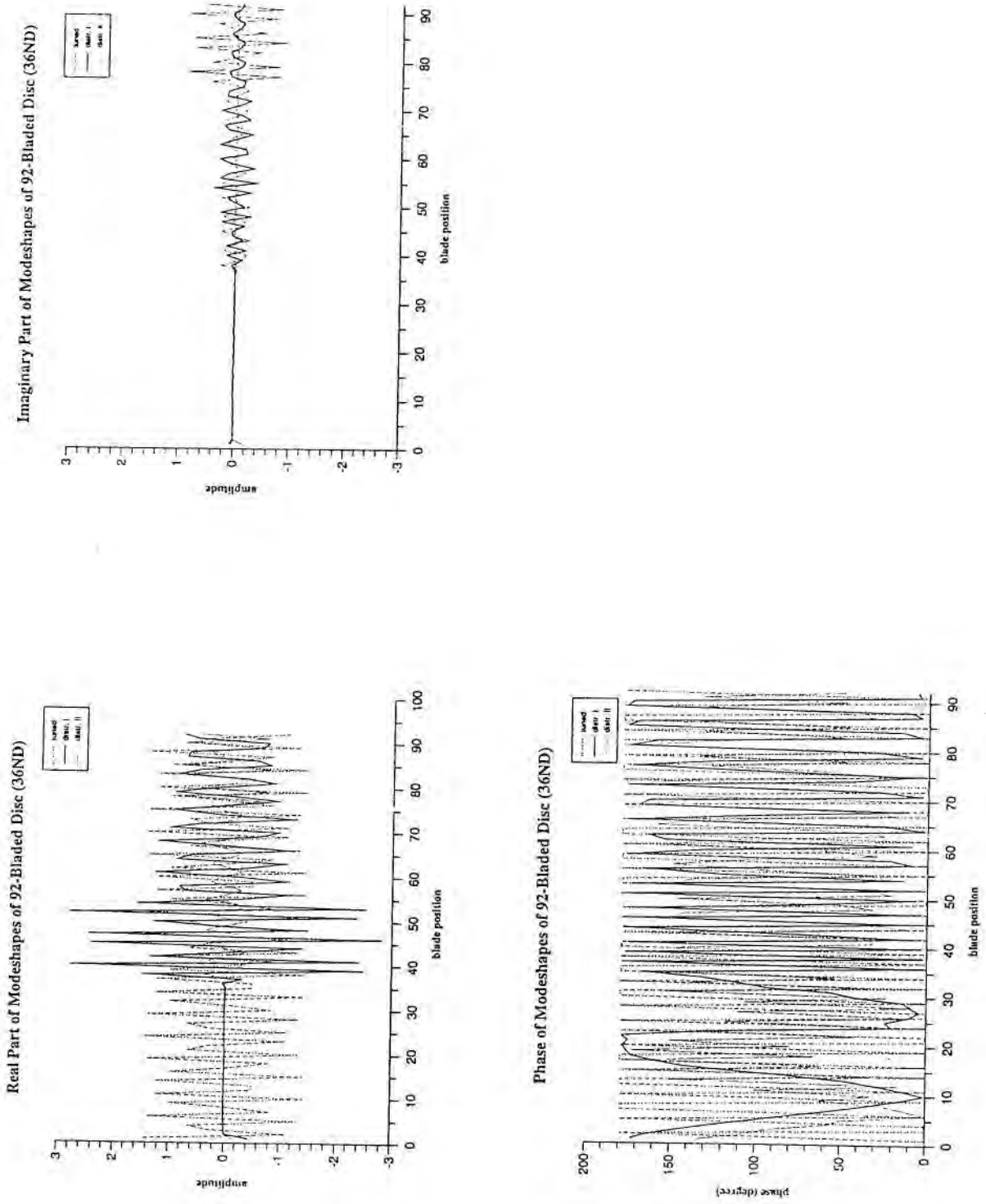

Figure 5.19 Modeshape and phase of mode 36 for the mistuned 92-bladed disc

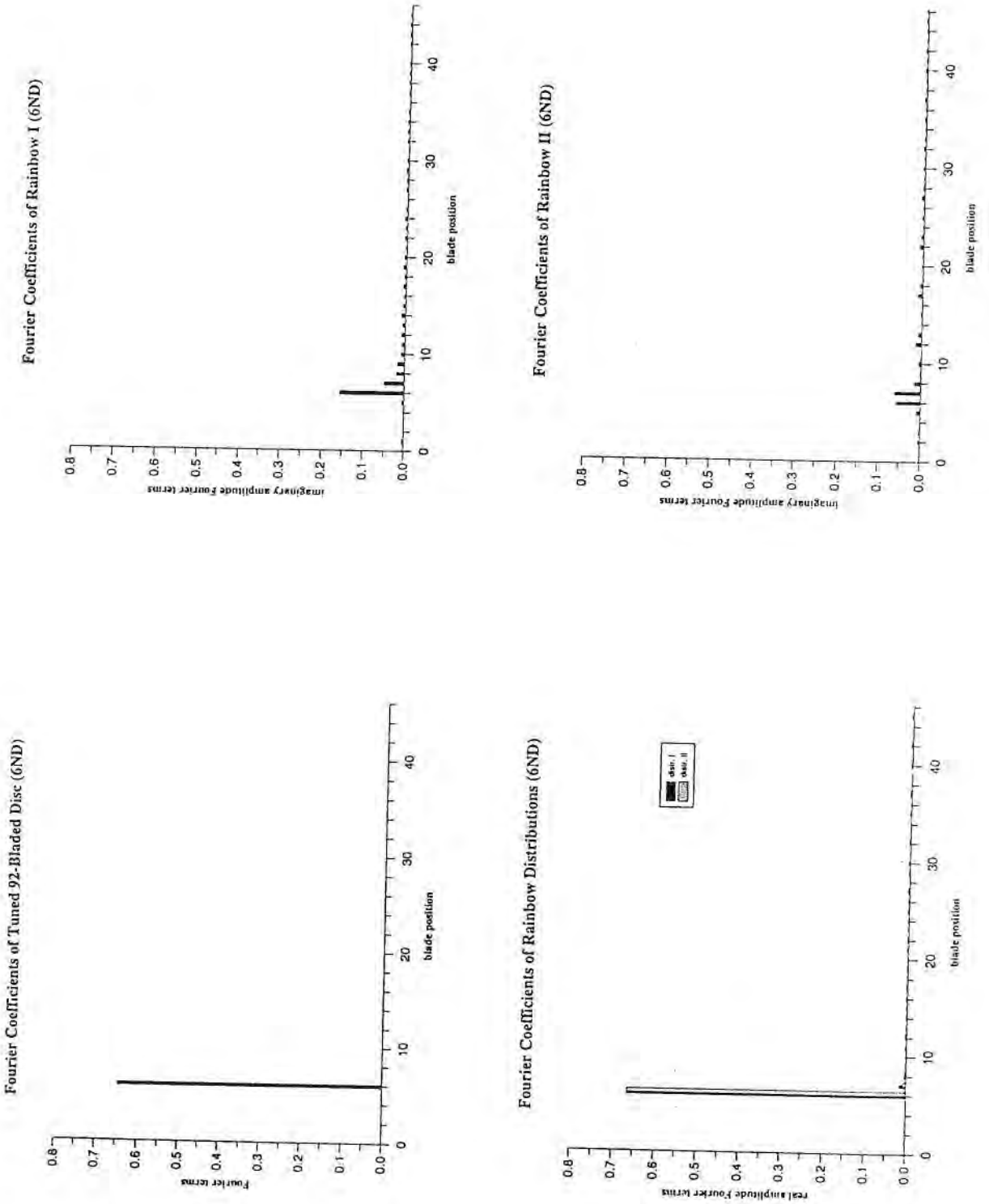

Figure 5.20 Fourier components of mode 6 for the damping mistuned 92-bladed disc

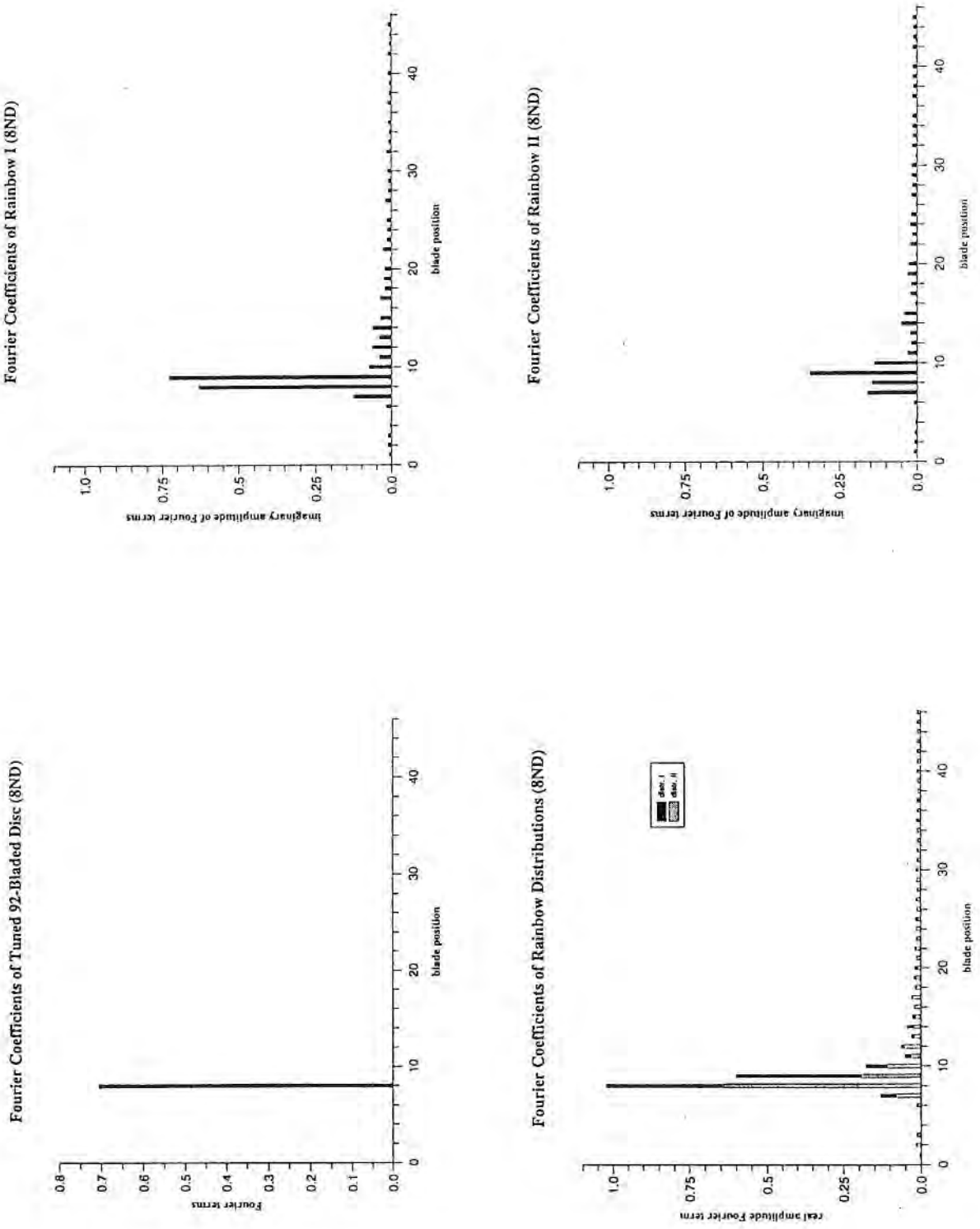

Figure 5.21 Fourier components of mode 8 for the damping mistuned 92-bladed disc

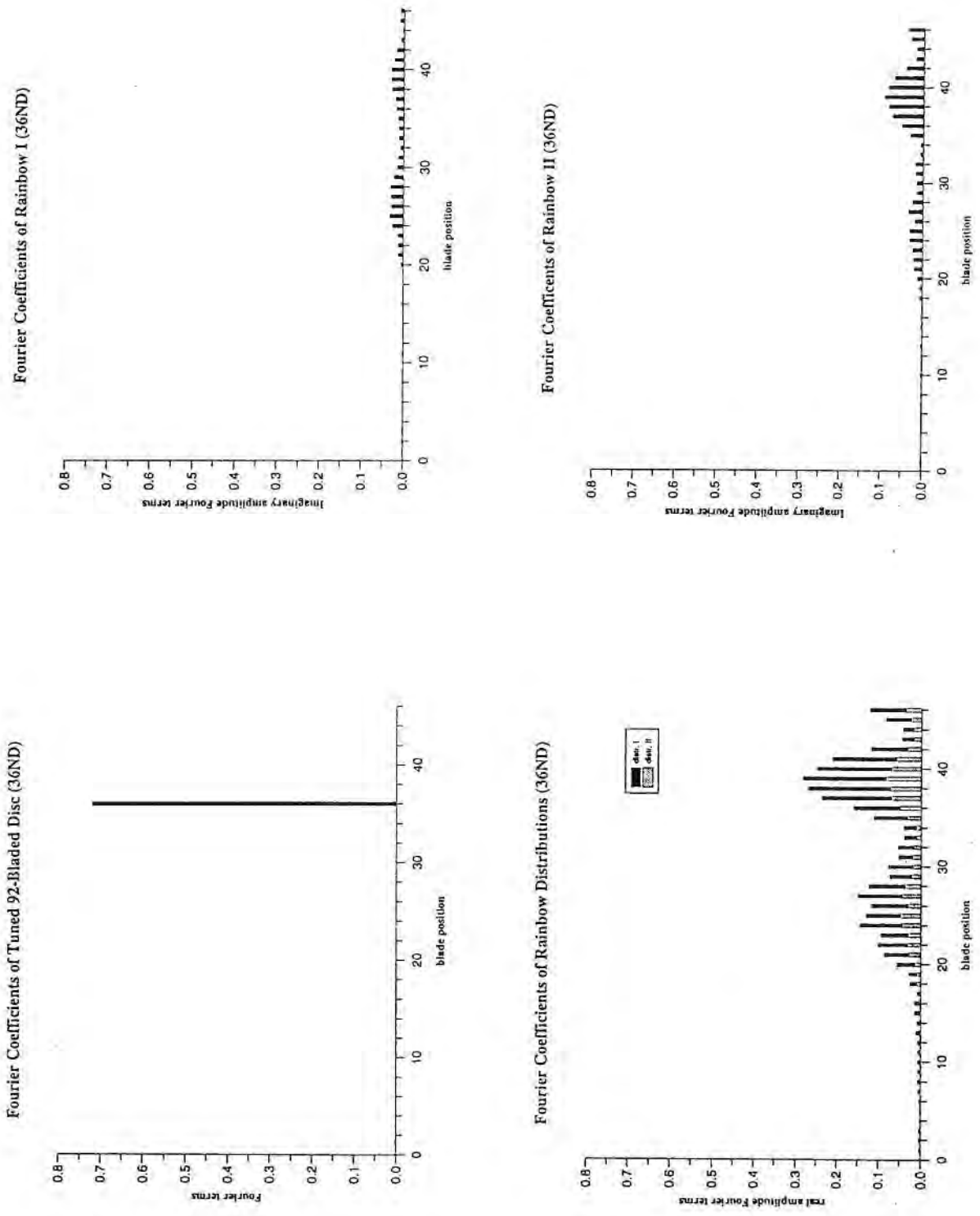

Figure 5.22 Fourier components of mode 36 for the damping mistuned 92-bladed disc

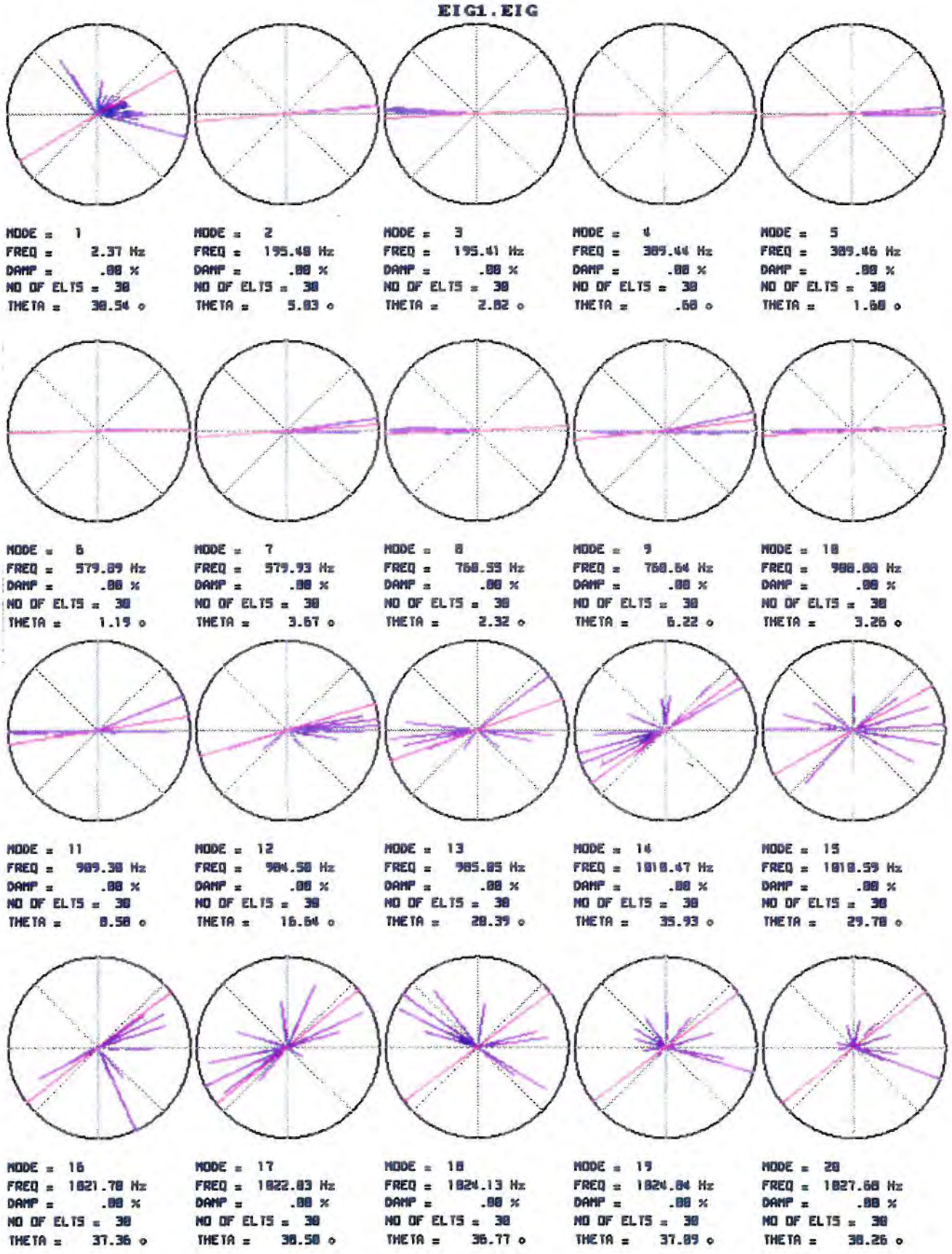

Figure 5.23 Complex mode effect for the rainbow arrangement I of the mistuned dampers

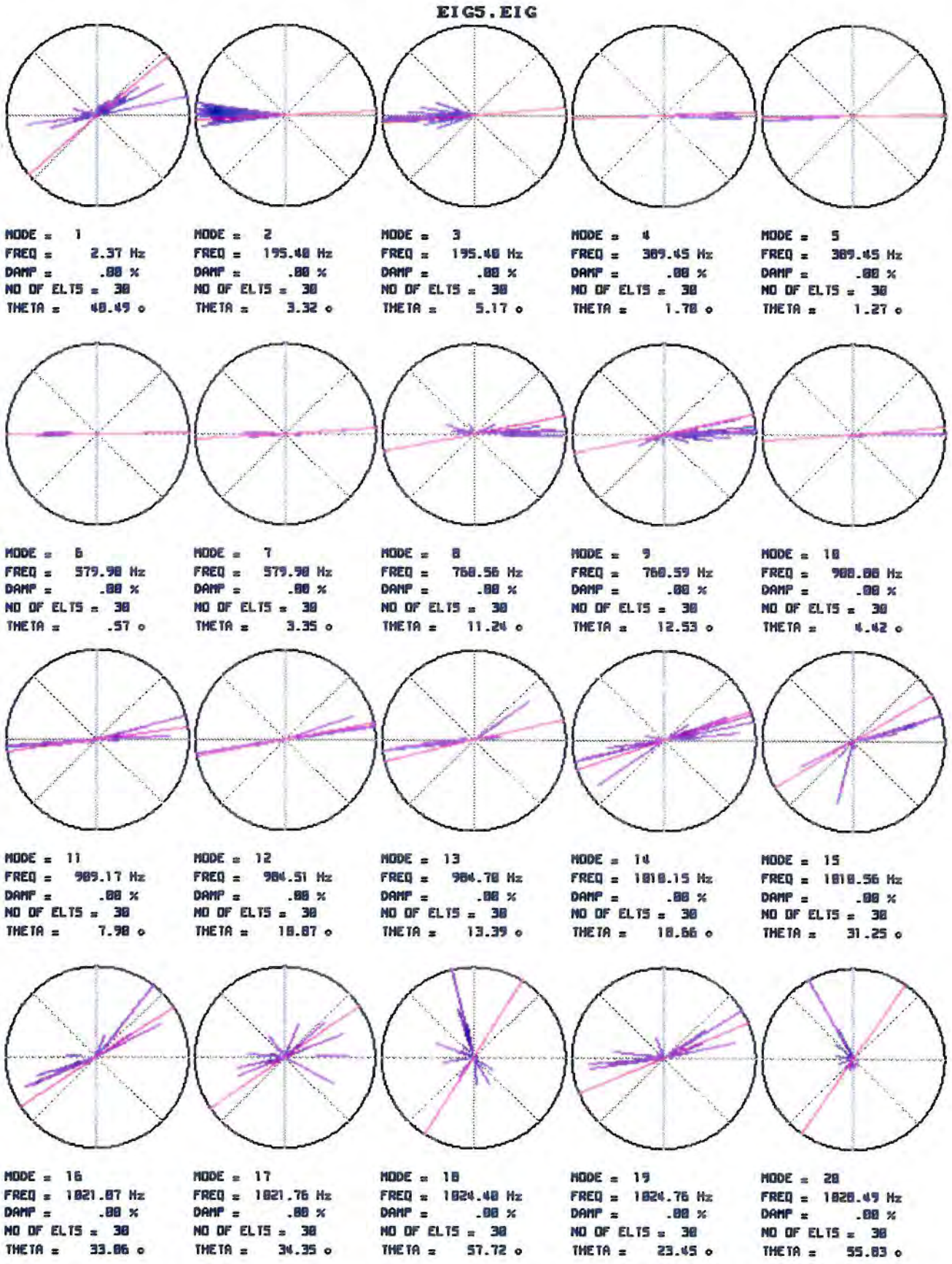

Figure 5.24 Complex mode effect for the rainbow arrangement II of the mistuned dampers

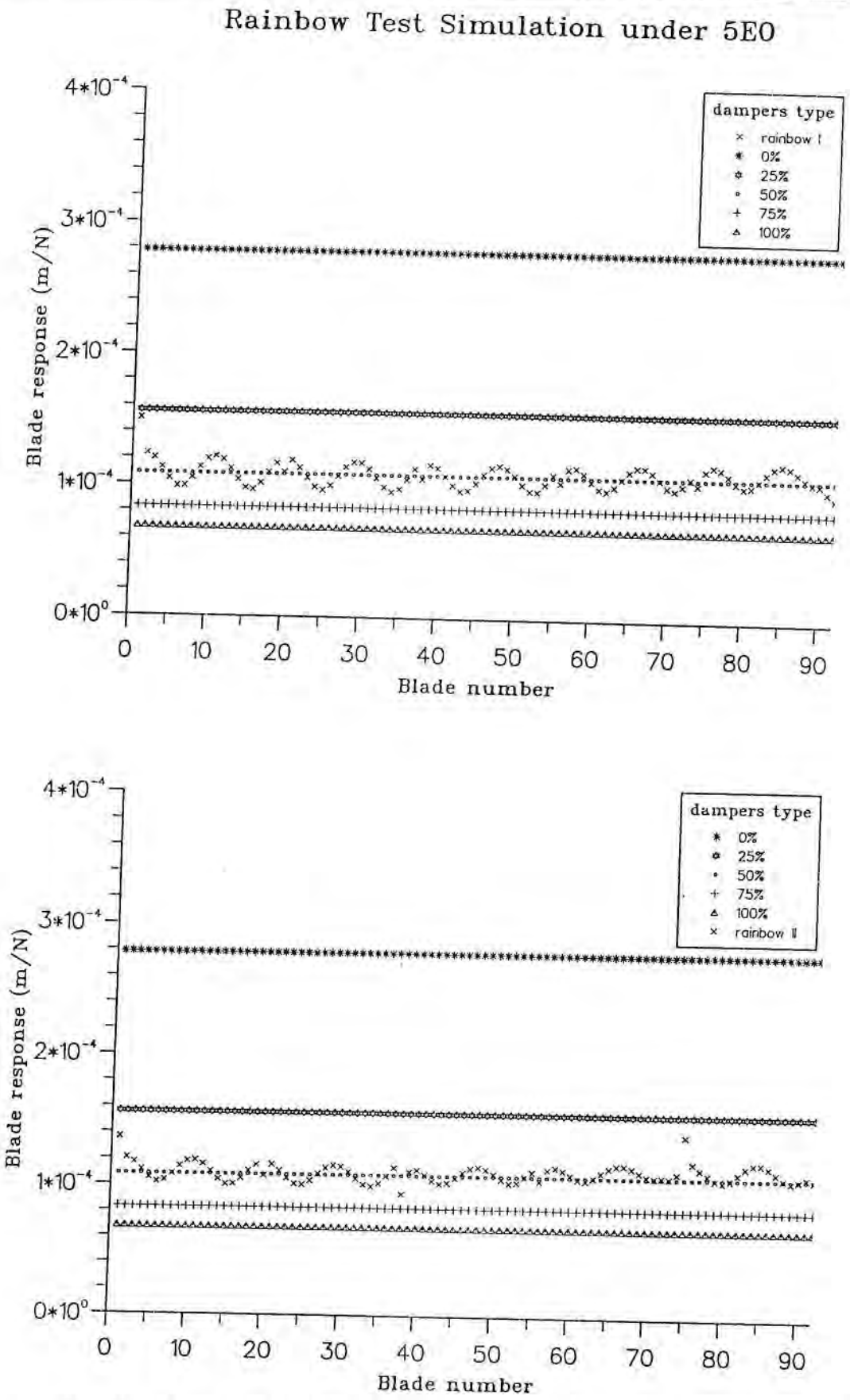

Figure 5.25 Blade amplitudes for the different coupling dampers under 5EO excitation

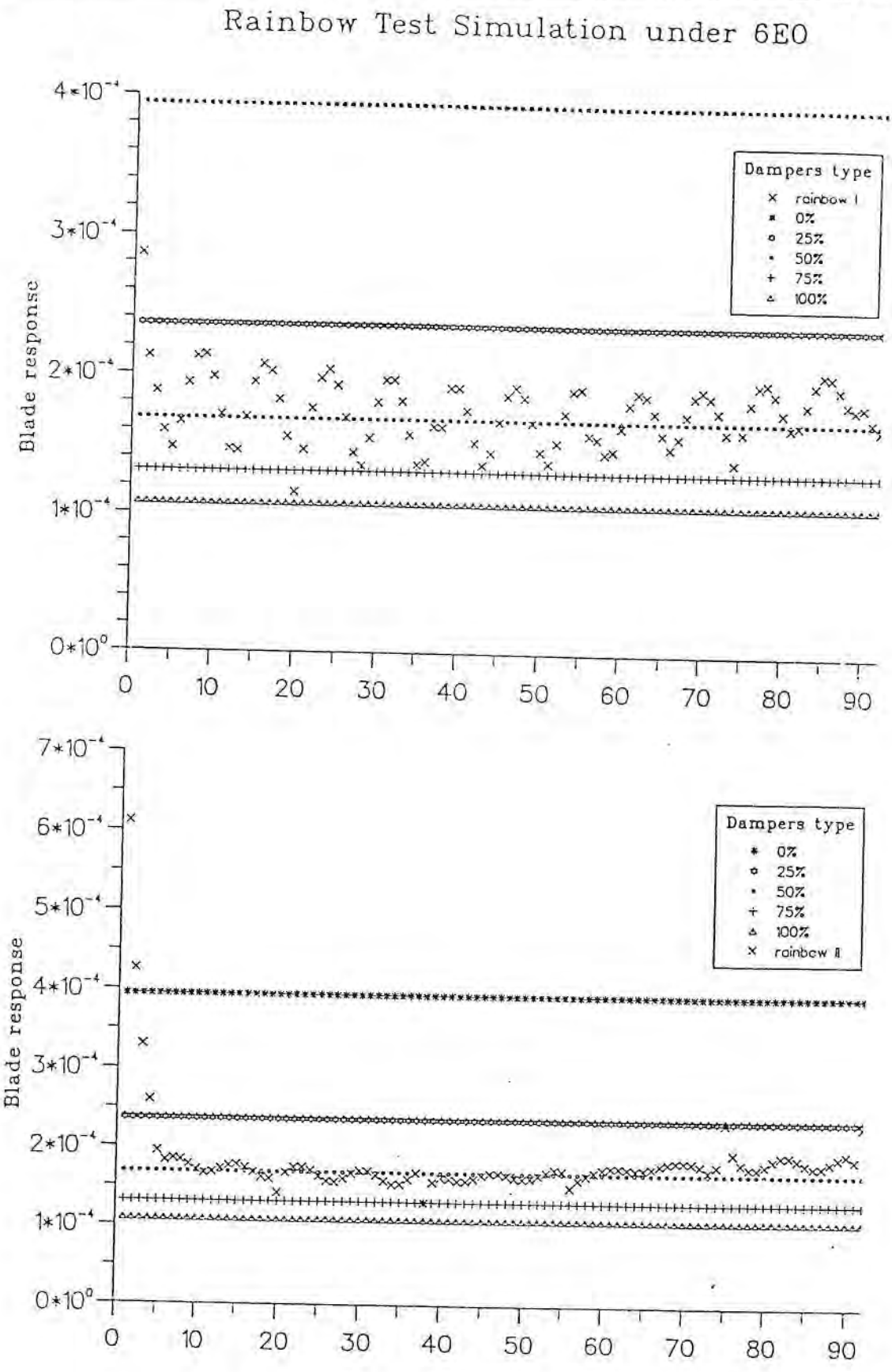

Figure 5.26 Blade amplitudes for the different coupling dampers under 6EO excitation

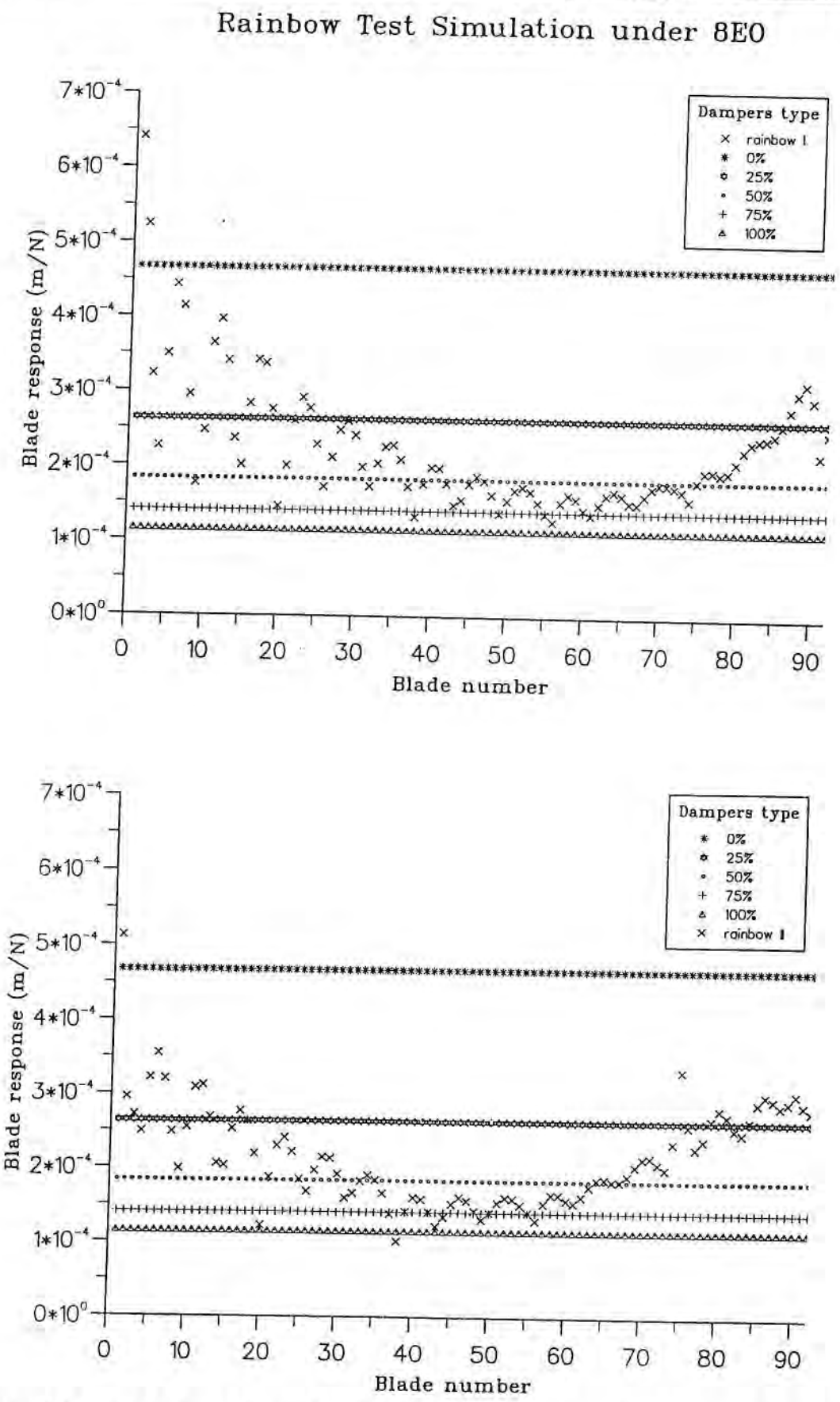

Figure 5.27 Blade amplitudes for the different coupling dampers under 8EO excitation

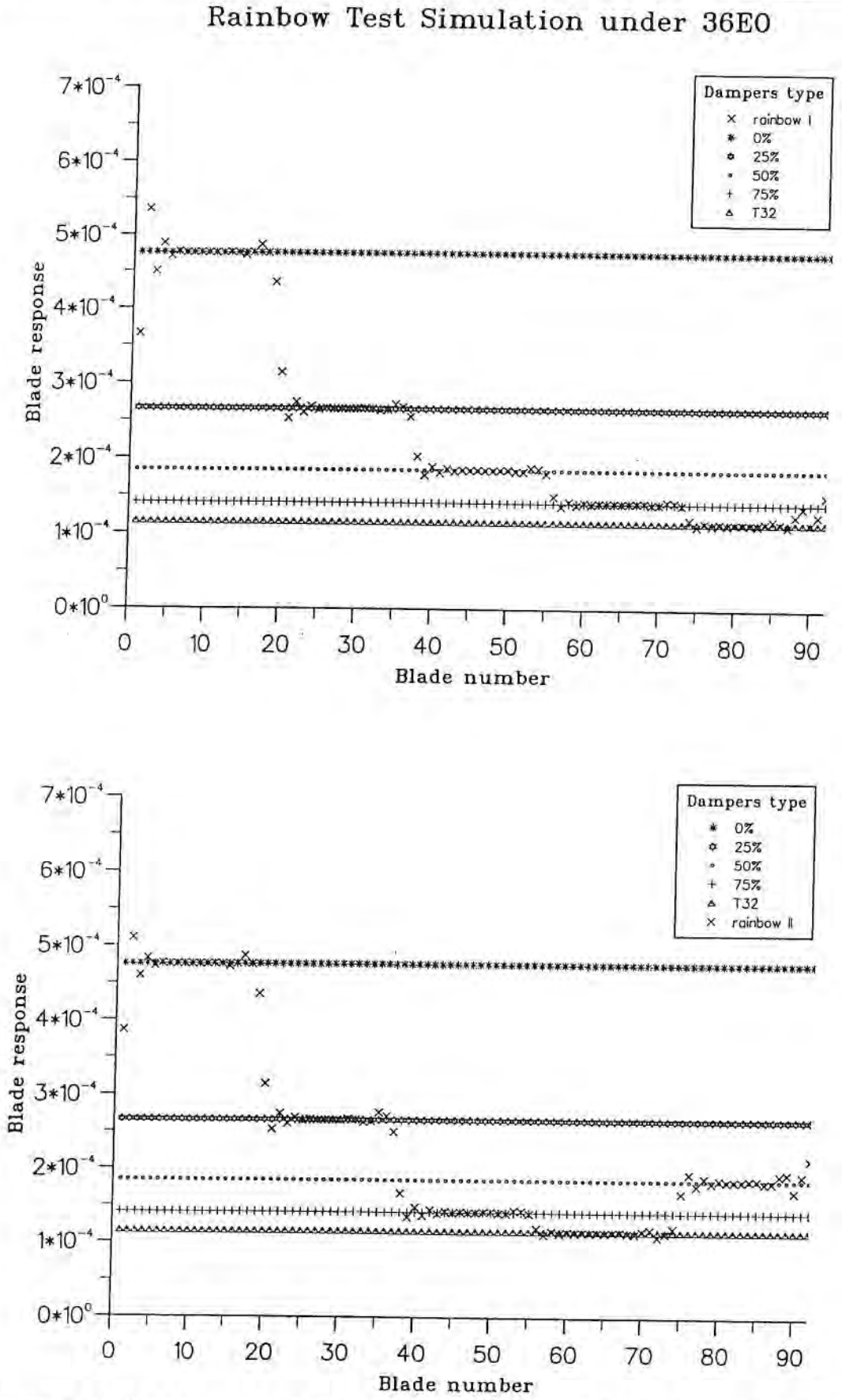

Figure 5.28 Blade amplitudes for the different coupling dampers under 36EO excitation

CHAPTER 6

PROBABILISTIC ANALYSIS OF MISTUNED BLADED ROTORS

About this chapter

This chapter describes the development and approaches of probabilistic techniques applied to mistuned bladed discs. In the past, different probabilistic techniques have been developed and in attempts to estimate the range of critical blade responses due to blade mistuning. Empirically, the probability density function (PDF) demonstrates that there is a linear relationship between the response scatter and the PDF of the response scatter. Most of the techniques shown in this chapter concentrated on finding the probability density function (PDF) of the blade responses due to some small amount of uncertain changes in blade parameters, such as mass or stiffness varying between blade to blade. The most popular analyses were the transform variable technique (TVT), the perturbation technique and the combined closed-form perturbation technique. All these techniques assumed the blade parameter as a normal or Gaussian input.

Furthermore, a technique based on the TVT method is presented in this chapter. After some studies of basic linear functions of transformation, the inverse function of transforms seems to give similar characteristics and shape of the scatter plots obtained before. Finally, a further method applies two-step transformations of the random variables from the blade parameters to system frequency, and then to the individual blade response distributions. This method may provide a simpler solution to find the PDFs for multi-degree-of-freedom systems.

6.1 INTRODUCTION

In practice, many engineering processes contain *randomness*: that is, the actual outcome is unpredictable to a certain degree. Suppose that some components with same material properties are examined by the same technique of testing and the results obtained are always the same. Then, the process is said to be *deterministic*. However, if all conditions are maintained under the same control, but the results continually differ from each other, then the process is said to be *random*. In this case, a single result cannot represent any meaningful outcome and a *statistical* description of the total possible result is required. The sources of randomness may come from two facts: the component imperfection and random uncertainty of properties. It is the first which has been considered in this study.

Usually, in vibration, the theory of random processes is applied to randomly-excited structures for a motion over a time period. This area of work is known as random vibrations. However, random responses from a dynamic structure may also arise from the structural properties being *imperfect*, since no material is perfectly homogeneous and no components are manufactured identically. Theoretically, the parametric outcome of random cases can be identified through the values of a function, and such a function is called a *random variable;* which can be either discrete or continuous. The mechanical properties of dynamic systems are subject to a certain degree of uncertainty, or *disorder*, because the physical properties are due to the inherent deterioration, or experiencing variations with time as a result of wear and tear. This type of model gives rises to a random response of the system. Bliven and Soong, in 1969 [13], presented a study of imperfect beams. Examples of such structures also include normal mode localisation of nearly periodic structures and blade mistuning of turbomachinery blades etc.

One area to apply probability ideas in engineering is the evaluation of the safety and reliability ranges of a structure, and to form associated design criteria. In chapter 3, the author has presented a detailed study of a stochastic or statistical simulation technique. This technique was reported by Griffin and Hoosac for the first time [50] in 1983. It was a direct simulation technique by assembling a large number of bladed discs with random blade mistuning on a rotor. One significant discovery from their work was the scatter profile that they found. Since then, other researchers have tried to find analytical methods for predicting the

probability density function (PDF) of a large blade population. These analytical methods have the advantage that they can save time to get the trend of the maximum response plots as shown by Griffin et al. [99, 128, 130]. However, the mathematical formulations are complex and are formidable for mistuned multiple-bladed systems.

Statistical analysis of mistuned bladed discs started in the early 1980s by Sogliero and Srinivasan [132] with a prediction method for blade fatigue failures of a mistuned bladed disc. They assumed the individual blade-alone frequency distribution to be normal and the excitation to be Gaussian white noise. They further assumed the distribution of peak responses to be a Rayleigh distribution. They estimated the expected damage and the expected time to failure for a 24-bladed disc. At about the same time, Huang [62] independently tried to formulate a perturbation expression to estimate the mean values and variances of a closely coupled bladed disc. Sinha [130, 131, 20] constructed the probability density function (PDF) of a bladed disc by assuming a normal distribution of the responses. The expected value and variance of such a normal distribution were determined by using a same technique originally developed by Huang, in 1980 [62], for a closely packed bladed system. Later, he and his co-worker Chen [20, 131] added some higher order terms into the model in order to improve the accuracy and to add nonlinear friction factors into the model. Singh reported an analytical method, in 1985 [127, 128], to determine the probability distribution of a randomly-assembled bladed disc. Later, in 1989, Wei and Peirre used the perturbation technique to find the expected value and the variance of a mistuned bladed system [155]. Recently, Mignolet and Lin [89, 99] presented a combined closed-form perturbation approach which was a modification of the model developed by Sinha. This model showed reasonable correlation with direct simulations.

Numerical studies demonstrate that the response scatter plots often had sharp boundaries or envelopes formed, as shown in Chapters 3 and 4. For some time, researchers were asking what were these boundaries. The objective here is to study the envelope from an analytical method. In this chapter, an attempt to formulate an analytical probabilistic density function of the responses scatters is presented based on the transform variable technique (TVT). However, an exact analytical equation of mistuned bladed disc is required and this is almost impossible to obtain. Nevertheless, the studies on analytical probabilistic methods show that the envelope of an inverse transformation of a normal distribution give

the similar envelope of the scatter plots. In fact, the blade parameters and the blade responses are inversely related in a dynamic formulation. Hence, the envelopes of scatter plots are direct effects due to simulations.

6.2 FUNDAMENTALS OF PROBABILITY DENSITY FUNCTIONS

6.2.1 Probability Density Functions

Probability is a measure of the chance of occurrences of one event. The set of all possibilities of an event is collectively a *sample space*, and each of the individual possibility is a *sample point*. The theory of probability relies on an experimentally observed phenomenon. A particular outcome of a hypothetical experiment or trial is called an *event*. The occurrence $O_N(N_x)$, or the relative frequency of an event, N_x, from N repetitions of experiments can be defined as follows:

$$O_N(N_x) = \frac{N_x}{N} \tag{6.1}$$

If an experiment is repeated an infinite number of times, the occurrence of the event is quite likely to oscillate about a certain constant value. Practically, this is an impossible proposition, since there is no experiment which can be performed infinitely. Therefore, a hypothesis of probability is used and is defined here as follows:

$$P(N_x) = \lim_{N\to\infty} (O_N(N_x)) = \lim_{N\to\infty} \left(\frac{N_x}{N}\right) \tag{6.2}$$

and

$$0 \leq P(N_x) \leq 1 \tag{6.3}$$

In many cases, the probability event will not be discrete constants but a continuous variable x. In this case, it is meaningless to pose a particular value for the probability of a given variable. The distribution for a continuous random variable is thus characterised by the probability density function (PDF), p(x), defined as follows:

$$p(x) = \lim_{\Delta x\to 0} \frac{P(x+\Delta x)}{\Delta x} \tag{6.4}$$

One can also define the probability density function as follows:

$$p(x) = \frac{\partial P(x)}{\partial x} \tag{6.5}$$

Hence, the cumulative probability function (CPF), P(x), can be then defined as follows:

$$P(x) = \int_{-\infty}^{x} p(x)\, dx \tag{6.6}$$

Empirically, a PDF can be found by dividing the range between the minimum and maximum values into small intervals and then counting the number of occurrences within each interval. This value can be estimated at the mid-point of each interval and the probability density function is normalised to unity [125].

$$p(x) = \frac{1}{\delta}\left(\frac{n}{N_s+1}\right) \tag{6.7}$$

where δ is the interval value,

n is the number of data items within the interval,

N_s is the total number of sampled data.

The cumulative probability function (CPF) can be defined as follows:

$$P(x) = \sum_{-\infty}^{x} N_s p(n) \tag{6.8}$$

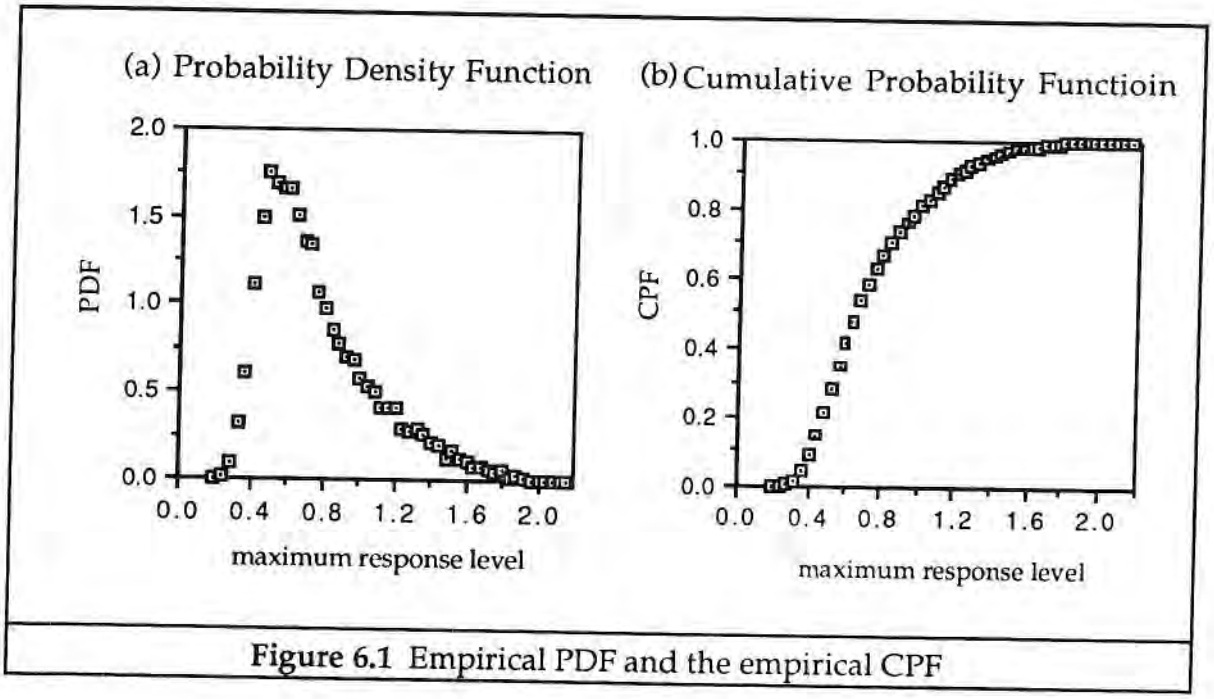

Figure 6.1 Empirical PDF and the empirical CPF

Figures 6.1(a) and 6.1(b) are the plots of the empirical PDF and the empirical CPF, respectively, of the response for blade scatter of 10% frequency mistuning under 6EO excitation, as shown previously in Figure 3.8. The PDF plot looks very similar to the envelope of the response scatter plot as shown in Figure 3.8 and the distribution of the response is clearly showing that it is not a normal distribution. This study also suggests that there is a linear relationship between the PDF and the response profile.

6.2.2 **Multiple Random Variables**

Figure 6.1(a) clearly does not represent the whole picture of Figure 3.8. Furthermore, Figures 3.8 and 3.9 show events of two random variables against the blade response levels. Figure 3.8 shows the events involving the blade response levels and the blade-alone natural frequencies while Figure 3.9 shows events of the blade response levels and the exciting frequencies. The joint probability density function of two random variables defines the probabilities of all possible pairs of the responses and the frequencies. Empirically, the PDF of two random variables can be constructed through random walk theory. Suppose the number of occurrences in the two-dimension space is $n_{ij}(x,y)$, and that i and j are the intervals along the x and y axes. The probability density function is in the form which follows:

$$p_{ij}(x,y) = \frac{n_{ij}(x,y)}{N} \tag{6.9}$$

where N is the total number of data points. Figures 6.2 and 6.3 are the three-dimensional plots of the PDF of the response against the plane of normalised frequency and normalised response. The blade scatter is 10% frequency mistuning and the assembly is subjected to a 6EO excitation. The PDF of the responses is found by dividing both frequency and response range into 30 X 30 regions and then counting the number of occurrences in each region. The volume of the distribution is normalised against the total number of data point N, which is 25200. The probability of occurrence is hence dependent on both the natural frequency and the excitation frequency. If the plots are viewed from the sides, the original diagrams of Figure 3.8 and 3.9 are obtained. For normalised blade-alone frequency plots, the highest probability seems to occur at the high-frequency blades. This agrees well with the results by Griffin and Sanliturk. Nevertheless, this empirical (or direct) simulation technique simply solves all the possible

deterministic models assembled using random numbers to simulate all possible physical changes due to mistuning.

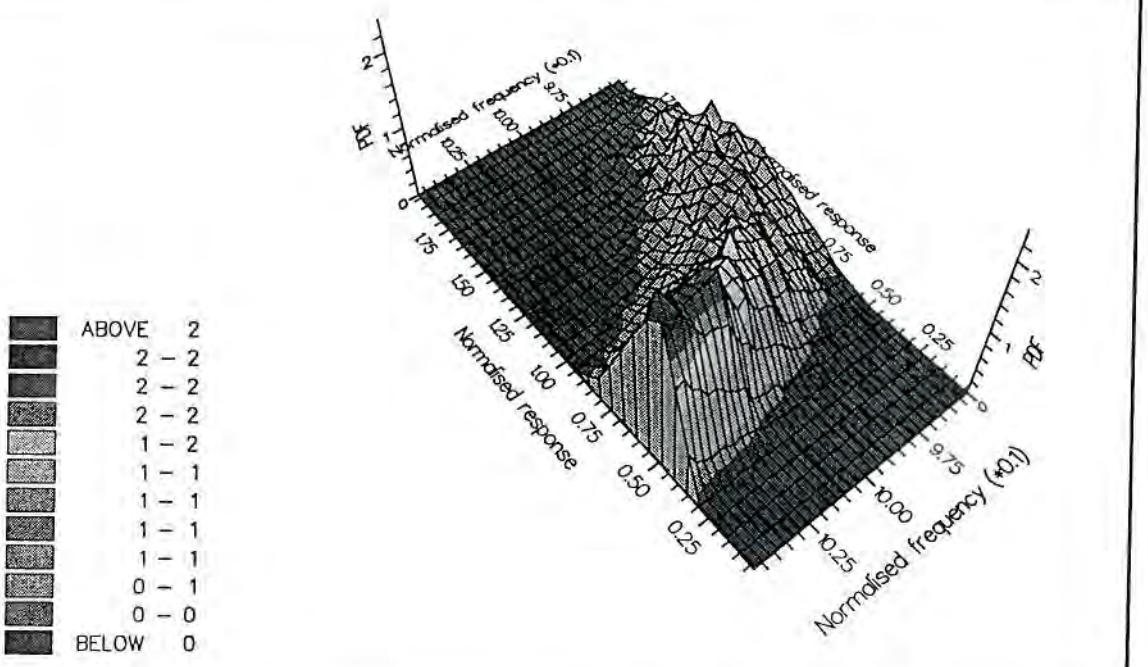

Figure 6.2 PDF versus response and blade-alone natural frequency plane for frequency scatter of 10% under 6EO

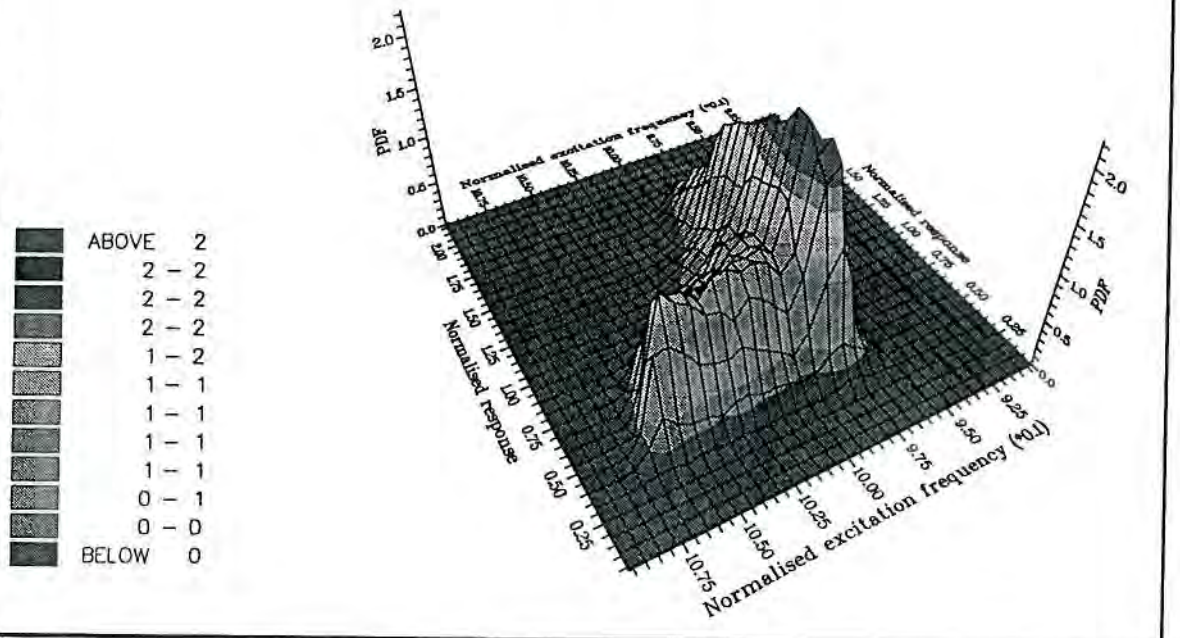

Figure 6.3 PDF versus response and excitation frequency plane for frequency scatter of 10% under 6EO

6.3 STATISTICAL INFERENCE METHOD

One way to fit the observed data with an analytical PDF is by using the statistical inference method. This method usually tries to fit a well-known PDF to the observed values. Inference methods of statistics, therefore, provide a link between the real word data and the idealised probabilistic models assumed or prescribed in a probabilistic analysis. The procedures involve the derivation of some statistical information and estimation of parameter values from observed data. These statistical parameters include the mean (expected value), variance, and kurtosis of the data. Then, one can infer an assumed function to the raw data distribution by comparing the parameters obtained from the observed data and the generated moments.

6.3.1 The Moment Method

A random distribution often relates to some parameters such as the mean and the variance. These quantities refer to the moments of the distribution. Generally, the k th moment of the PDF, $E(x^k)$, can be defined as follows, [7]:

$$E(x^k) = \frac{\int_{-\infty}^{\infty} x^k p(x)\, dx}{\int_{-\infty}^{\infty} p(x)\, dx} \tag{6.10a}$$

or

$$E(x^k) = \int_{-\infty}^{\infty} x^k p(x)\, dx \tag{6.10b}$$

This is because the denominator of equation (6.10a) is the area covered by the curve of the PDF and is equal to unity.

In the case of a discrete distribution, the integration will take the summation form as follows:

$$E(x^k) = \sum_{i=1}^{N} x_i{}^k P_i = \sum_{i=1}^{N} x_i{}^k \frac{n_i}{N} = \frac{1}{N} \sum_{i=1}^{N} x_i{}^k n_i \tag{6.11}$$

where P_i is the probability in discrete form corresponding to the relative frequency defined in equation (6.2).

Furthermore, reference [7] also describes details for generating the moments of some common continuous PDFs by the moment generating function. Since there is a relationship between the moments of a random variable and the parameters of the corresponding distribution functions, it follows that the parameters of a distribution may be determined by estimating the mean and the variance of the random variable. This method is the method of moments.

6.3.2 Some Common Probability Density Functions

After determining the moments of a distribution, a suitable distribution function is required. Reference [7] shows some common distribution functions which are useful to infer practical distributions. From Chapter 4, studies of different bladed disc configurations including the coupling ratio and different amounts of mistuning were shown. These studies displayed some different blade response scatter distributions. Among these scatter distributions, there mainly constituted some normal and, possibly, some lognormal functions. The formulae for these functions are well-defined.

- Lognormal fit

$$p(x) = \frac{1}{\sqrt{2\pi}\,\zeta x} \exp\left(-\frac{1}{2}\left(\frac{\ln x - \lambda}{\zeta}\right)^2\right) \qquad \text{for } x \geq 0 \qquad (6.12)$$

where: expected value $E(x) = \exp\left(\lambda + \frac{1}{2}\zeta^2\right)$

and variance $Var(x) = E^2(x)\,[e^{\zeta^2} - 1]$

- Normal fit

$$p(x) = \frac{1}{\sqrt{2\pi}\,\sigma} \exp\left(-\frac{1}{2}\left(\frac{x - \mu}{\sigma}\right)^2\right) \qquad \text{for } -\infty < x < \infty \qquad (6.13)$$

where: expected value $E(x) = \mu$

and variance $Var(x) = \sigma^2$

- Combined PDF fit

From Chapter 4, one may see that the shape of the scatter profile is different for different coupling factors. Some of the scatter plots look like lognormal distribution but some of the weakly-coupled scatters look more like normal ones.

Therefore, it is possible to construct a combined fit which may be suitable for fitting a range of different scatters. In this case, a third parameter is needed to measure the dispersion of the peaks according to the mean. This parameter is the coefficient of skewness, or the third moment, which provides a measure of how symmetric the variate is about its mean value.

$$p(x) = \begin{cases} \text{lognormal}; & \text{if skew} \neq 0 \\ \text{normal}; & \text{if skew} = 0 \end{cases} \qquad (6.14)$$

Figure 6.4 shows the fit of a lognormal function plot to the scatter distribution as presented in Figure 6.1(a).

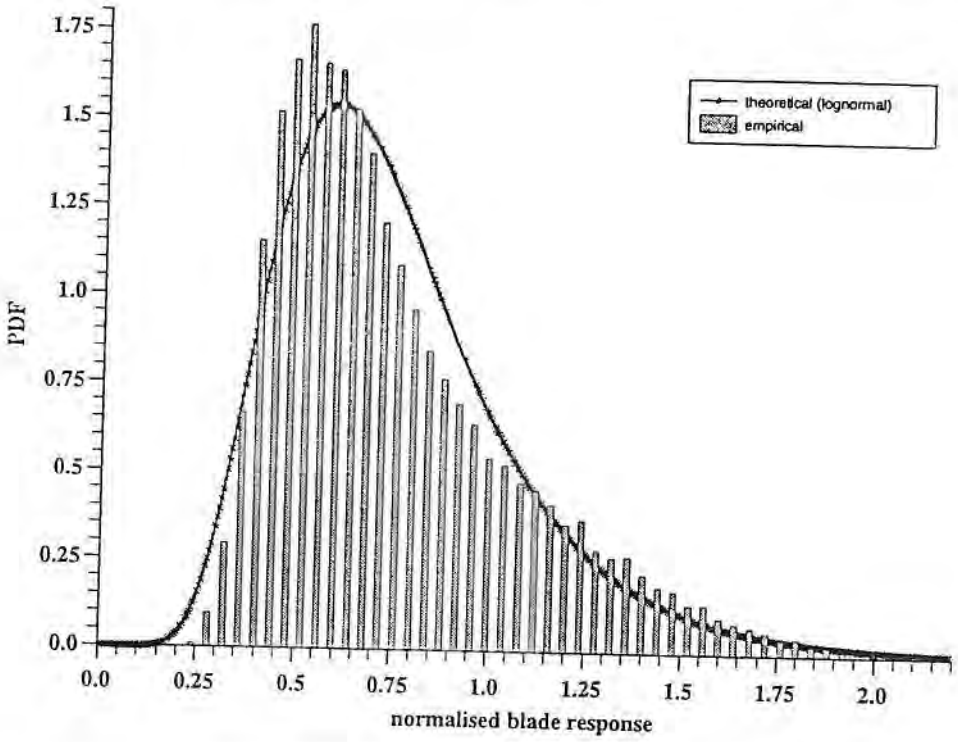

Figure 6.4 PDFs from simulation and inferred analytical one

By finding an analytical probability density function of the responses, a confidence interval may be constructed [7]. However, the PDF created by this method requires a huge amount of data. Numerically, this could be provided but it is impossible to obtain such an amount of data from experiments. Furthermore, there is no physical meaning for any of such fitted curves. A more meaningful method involving a closed-form approach is shown in the following section.

6.4 TRANSFORM VARIABLE TECHNIQUE (CLOSED-FORM APPROACH)

6.4.1 Theory

This is a traditional method of probabilistic analysis which requires one-to-one transformations of random variables. The method is just like solving differential equations by the method of a change of variables. Suppose that two random but dependent variables y and x have the explicit relationship as follows:

$$y = f(x) \text{ and } x \rightarrow p(x) \tag{6.15}$$

If the probability density distribution of x, p(x), is known, then the probability density distribution of y, p(y) can be determined without its explicit formulation. This problem is then reduced to a change of variables and a determination of the inverse function for $x = f^{-1}(y)$. This functional relationship is shown as follows:

$$p(y) = p(x)\det(J) = p\left(f^{-1}(y)\right) \det(J) \tag{6.16}$$

where **J** is the Jacobian matrix which is defined in 1-dimensional form as follows:

$$J = \frac{dx}{dy}$$

or

$$p(y) = p\left(f^{-1}(y)\right) \det\left(\frac{dx}{dy}\right) \tag{6.17}$$

Therefore, a distribution of a random variable y having a deterministic functional relationship with another random variable x can be found by a one-to-one mapping transformation of variables. Similarly, such an approach can be used for multiple random variables with multiple random dependent variables, such that the functional relationships between the variables exist as follows:

$$\begin{aligned} u_1 &= u_1 (x_1, x_2, \ldots, x_m) \\ u_2 &= u_2 (x_1, x_2, \ldots, x_m) \\ &\ldots\ldots \\ u_m &= u_m (x_1, x_2, \ldots, x_m) \end{aligned} \tag{6.18}$$

the general procedure of the joint probability density function of u can be found as follows:

$$p(u) = p[x_1(u), x_2(u), ..., x_m(u)]\det(\mathbf{J}) \tag{6.19}$$

where **J** is the Jacobian matrix which is defined as follows:

$$\mathbf{J} = \begin{pmatrix} \frac{\partial x_1}{\partial u_1} & \frac{\partial x_1}{\partial u_2} & \cdots & \frac{\partial x_1}{\partial u_m} \\ \frac{\partial x_2}{\partial u_1} & \frac{\partial x_2}{\partial u_2} & \cdots & \frac{\partial x_2}{\partial u_m} \\ \cdots & \cdots & \cdots & \cdots \\ \frac{\partial x_m}{\partial u_1} & \frac{\partial x_m}{\partial u_2} & \cdots & \frac{\partial x_m}{\partial u_m} \end{pmatrix} \tag{6.20}$$

The transformation procedure is only applicable to the case of one-to-one transformations between the random variables u and x. The cumulative probability P(u) of the dependent variables u can be written as follows:

$$P(u) = \int_{-\infty}^{-\infty} \int_{-\infty}^{-\infty} \cdots \int_{-\infty}^{-\infty} p(u)\, du_1\, du_2 \ldots du_m \tag{6.21}$$

or

$$P(u) = \int_{-\infty}^{-\infty} \int_{-\infty}^{-\infty} \cdots \int_{-\infty}^{-\infty} p(x)\det(J)\, dx_1\, dx_2 \ldots dx_m \tag{6.22}$$

and the probability density function p(u) is as follows:

$$p(u_i) = \frac{\partial P(u_i)}{\partial u_i} \tag{6.23}$$

6.4.2 **The Transform Variable Technique (TVT) Examples**

This study tries to find a method which can effectively find the PDFs of the responses of the mistuned bladed disc. Since blade mistuning introduces a random variable to the dynamic system of a bladed disc, the determination of a PDF for the blade responses may be obtained from transforming the blade parameter distribution. However, the relation or the equation between the blade mistuning parameter and the blade responses is often too difficult to formulate in an explicit way. This creates some difficulties for applying the transform variable technique to a multi-bladed and mistuned system. An approximation to find the explicit equation for the blade parameter and the blade response is thus required. Nevertheless, the transformation of the variate distributions demonstrates the profiles of the PDF shown in Figures 6.1(a).

From the equation of motion of a bladed disc system, the blade parameter distribution seems to be inversely proportional to the blade responses as follows:

$$\{X\} = [\,[\mathbf{K}] - \omega^2[\mathbf{M}] + j(\omega[\mathbf{C}] + [\mathbf{D}])\,]^{-1}\{F\} \tag{6.24}$$

Since the blade mistuning occurs for the elements of the matrices, the relation between the blade responses and the mistuning variable is hence inversely proportional. This condition shows the effect of the logarithm, or the response is only proportional to the logarithm of the stiffness. If the distribution of the stiffness is normal, the distribution of the response will be lognormal. Therefore, the selection of lognormal for the inference fit is sensible. The effect of transformation for an inversely proportional function then shows a skewed distribution after transformation. This can also be demonstrated by a simple function transformation from a normal distribution as follows:

$$y = \frac{a}{x} + b; \qquad p(x) = \frac{1}{\sqrt{2\pi}\,\sigma_x} \exp\left(- \frac{(x - \bar{x})^2}{2\sigma_x^{\,2}} \right) \tag{6.25}$$

Suppose x is the blade natural frequency distribution which has a normal probability density function and has the following properties: $\bar{x}$ = 40 Hz, σ_x = 10 Hz. For convenient, the function y has the following constants: a = $\pm$1000, b = 10. Two values for the constant a are shown here, since these values change the skewness of the curve. Using equation (6.17), the probability density function of y can be found.

Figure 6.5 shows both of these two distributions of y and the normal distribution of x. From the graphs, the probability density function of the variable y seems to be skewed towards the left of the mean value of y. If, however, the function y is negative and inverse to the variable x, the probability density function of y is skewed towards the right of the mean value of y. Therefore, the probability density function studies shown using a simple inverse function look very similar to the probability density function of the blade responses as shown in Figure 6.1a. This might suggest that the profile obtained from simulations may be due to the inverse transformation effect of the random variables. However, further evidence is required and the following sections show the study of obtaining the analytical probability density functions for a single-degree-of-freedom system and a multi-bladed disc system.

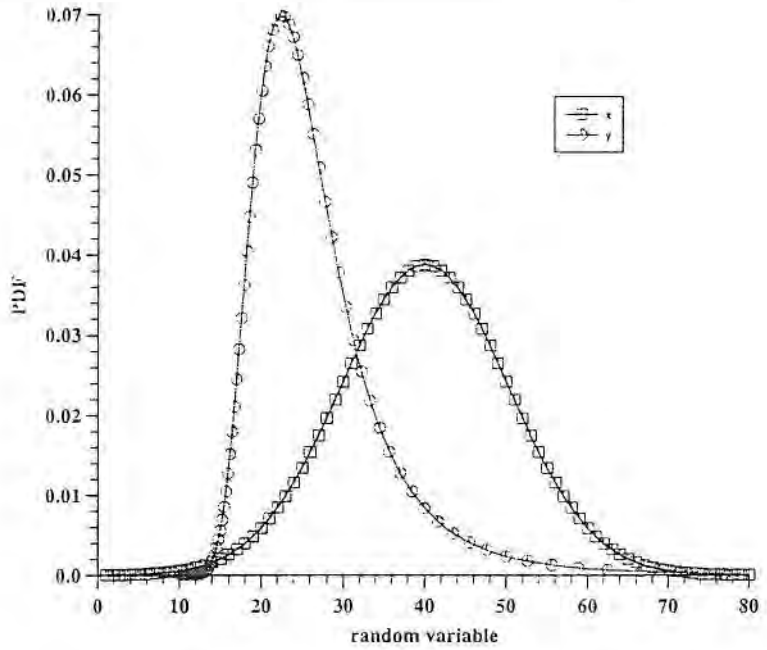

(a)

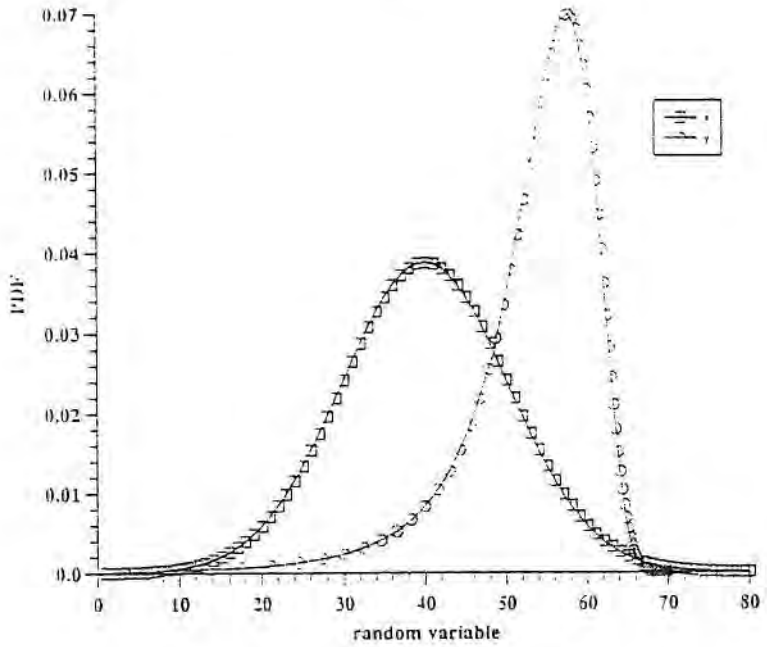

(b)

Figure 6.5 PDFs of a simple inverse function

6.4.2 A Study of Single-Degree-of-Freedom Bladed System

Singh, in 1987, presented a paper showing the probabilistic characteristics of a vibrating cantilever beam due to the effect of random imperfections in the material. Following this, Singh and Ewins tried to apply the technique to a multi-

degree-of-freedom system in 1989. However, they only showed that the process can be very complicated [128]. Recently, Mignolet and Lin [89, 99] showed that a combined closed-form perturbation approach can map the random blade distribution to the blade response distribution.

To show the effect of transformed response distributions, two studies of response distributions demonstrate here the application of the transform variable technique (TVT) on mistuned bladed systems. The first study uses a SDOF lumped-spring system and such a SDOF system is analogous to Singh's study on the vibrating cantilever beam. For the single-degree-of-freedom system, the equation of motion can be written as follows:

$$m\ddot{x} + c\dot{x} + kx = f \tag{6.26}$$

Let $f = F\cos \omega t$ and $x = X\cos(\omega t + \varphi)$, the response function to a unit force or the receptance magnitude is therefore having the form as follows:

$$H = \frac{X}{F} = \frac{1}{\sqrt{(k - \omega^2 m)^2 + c^2\omega^2}} \tag{6.27}$$

From the TVT, the probability density function (PDF) of the blade response can be expressed in terms of the blade stiffness distribution, p(k), as follows:

$$p(H) = p(k) \left|\frac{dk}{dH}\right| \tag{6.28}$$

From equation (6.27), the inverse function of k and the derivative $\frac{dk}{dH}$ can be deduced as follows:

$$k = \omega^2 m \pm \sqrt{\frac{1}{H^2} - c^2\omega^2} \tag{6.29}$$

and

$$\frac{dk}{dH} = \frac{[(k - \omega^2 m)^2 + c^2\omega^2]^{1.5}}{(k - \omega^2 m)} \tag{6.30}$$

Practically, it is reasonable to assume that the PDF for the blade stiffness has a normal or Gaussian distribution as follows:

$$p_k(k) = \frac{1}{\sigma_k\sqrt{2\pi}}\exp\left(-\frac{(k-\bar{k})^2}{2\sigma_k^2}\right) \tag{6.31}$$

where σ_k is the standard deviation for the stiffness distribution and $\bar{k}$ is the mean of the distribution. In this numerical study, the mean blade stiffness, blade mass and damping values were all defined same as in Table 3.1 in Chapter 3. The mean blade stiffness is 65440 Nm^{-1} and the standard deviation for blade stiffness is 3800 Nm^{-1}. The PDF for such a system with the mean excitation frequency at 173.4 Hz is shown in Figure 6.6. In this graph, the profile of the PDF has a similar shape to the one shown in Figure 6.5 with the constant a being positive.

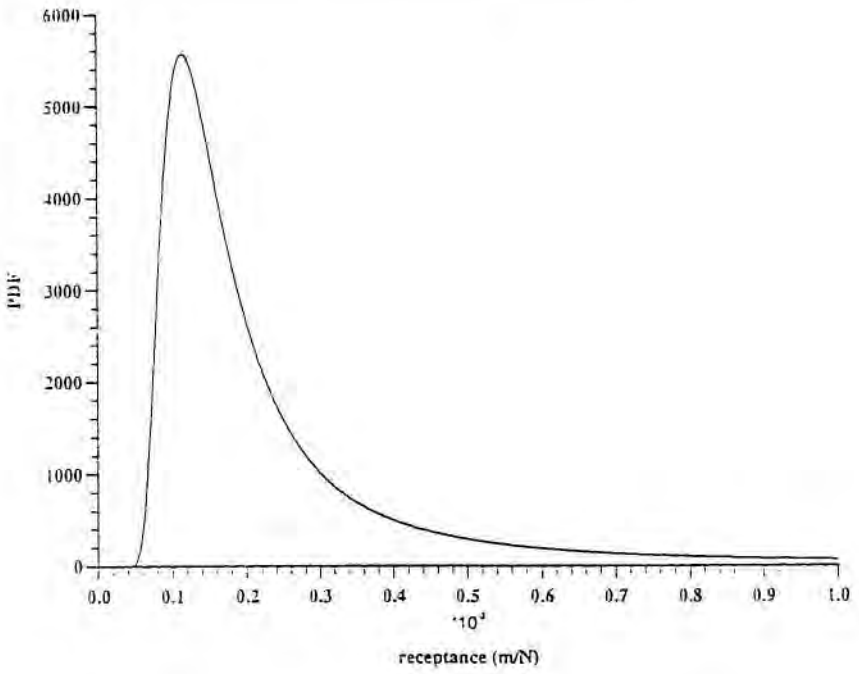

Figure 6.6 PDFs of a single-degree-of-freedom bladed system

6.5 A PROBABILISTIC METHOD FOR MISTUNED BLADED DISCS

For multi-degree-of-freedom systems, the analytical PDF is more difficult to obtain. The transform variable technique is valid only if there exists an analytical expression for mistuned bladed discs. In the past, some researchers have tried several techniques to find such an analytical PDF. Some common ones used to find a PDF are outlined as follows:

6.5.1 The Random Perturbation Technique

Huang, in 1982 [62], was probably the first to show a perturbation technique to find the mean and variance of the responses of mistuned bladed disc. The basic forms of perturbation for both free and forced vibration can be found from Appendix IV. Later, Sinha in 1984 [130], and Sinha and Chen in 1987 and 1989 [20, 131], used the same technique to try to fit a normal distribution of responses with the predicted parameters from the perturbation method. However, their studies assumed that the blade responses had a normal distribution which has been found not to be the case as shown in Figure 6.1a.

6.5.2 The Combined Closed Form-Perturbation Technique

This method was proposed by Mignolet and Lin, in 1989-1990 [89, 99]. The closed-form equation for CPF of the responses can be related to the eigenvalues of the system as follows:

$$P(u) = \int_{-\infty}^{-\infty} \int_{-\infty}^{-\infty} \cdots \int_{-\infty}^{-\infty} p(\lambda)\, \det(J)\, d\lambda_1 d\lambda_2 \ldots d\lambda_m \qquad (6.33)$$

The relationship between the mistuned blade response u and frequency parameter λ may be deduced by the perturbation method.

6.5.3 A Two-step Transformation method

From previous studies, one can find that the dynamic system of a bladed disc consists of too many dependent variables in its equations of motions. This gives rise to difficulties in finding the PDF of a mistuned system. From the equation of motion as follows:

$$[\mathbf{M}]\{\ddot{x}\} + [\mathbf{C}]\{\dot{x}\} + [\mathbf{K}]\{x\} = \{f\} \qquad (6.34)$$

The frequency response function can be related to the applied forces and the responses as follows:

$$\{X\} = [H(\omega)]\,\{F\} \qquad (6.35)$$

where $[H(\omega)]$ is the dynamic flexibility or the frequency response function matrix, $H(\omega)$. However, this matrix is a function of the system natural frequencies ω_r and the blade parameters, such as stiffness (k), damping (c) and mass (m). Furthermore, the blade parameters k, c and m are also dependent variables of the system natural frequency ω_r. This gives rise to a redundant situation for variable

random variable of each blade is the stiffness k_i. The first step required is to find a function relating k_i to the system natural frequencies ω_r. This can be done by using the resonance response equation of a tuned system as follow:

$$x = \frac{C + 2D\cos\psi_r}{-B^2 + A(C + 2D\cos\psi_r)} \tag{6.39}$$

where
$$A = k - m\omega_r^2 + j(\eta k + \omega_r c)$$
$$B = -k(1 + j\eta)$$
$$C = 2K_d + K_g + k - M_d\omega_r^2 + j\eta k$$
$$D = -K_d$$
$$\psi_r = \frac{2\pi r}{N}$$

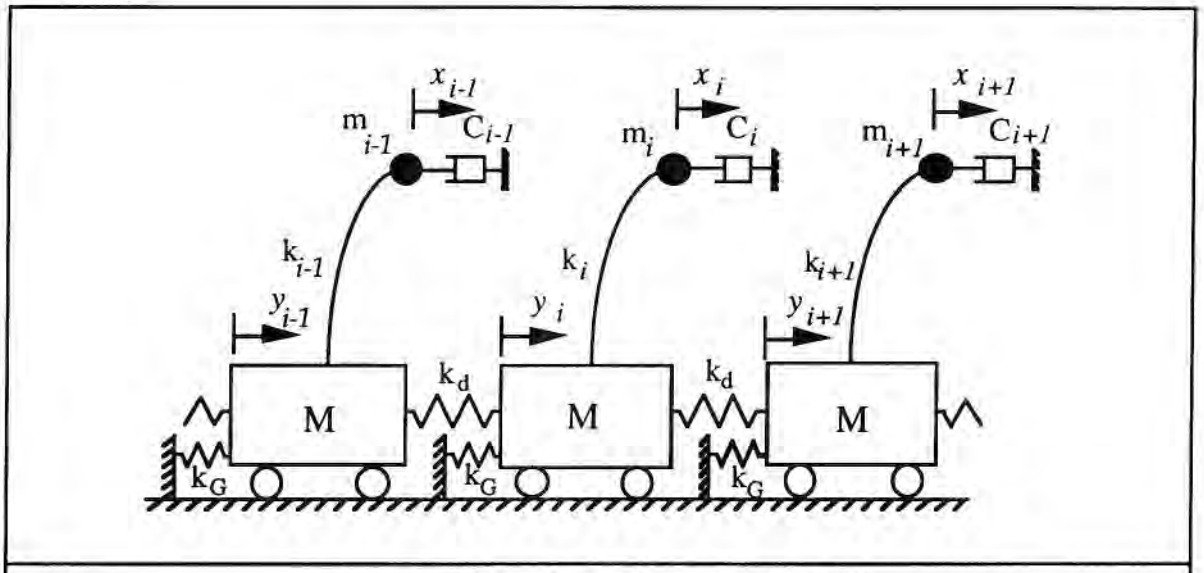

Figure 6.8 Simple mathematical model

For an undamped resonance, the denominator must be zero as follows:

$$-k^2 + (k - m\omega_r^2)(2K_d + K_g + k - M_d\omega_r^2 - 2K_d\cos\psi_r) = 0 \tag{6.40}$$

Therefore, $\frac{\partial k}{\partial \omega_r}$ can be determined by assuming m, K_d, K_g, M_d, and ϕ_r are constants. The second necessary transformation can be obtained from the frequency response function as follows:

$$\{X\} = \sum_{r=1}^{2N} \frac{[\phi]\,[\phi]^T\,\{F\}}{j\omega - s_r} \tag{6.41}$$

where $s_r = \omega_r(\xi + \sqrt{1 + \xi^2})$ is the r th eigenvalue and
ϕ_r is the r th A-normalised eigenvector

The second Jacobian transformation can then be written as follows:

$$\left|\frac{\partial \omega}{\partial X}\right|_i = \sum_{r=1}^{2N} \frac{(j\omega - s_r)^2}{[\phi]\,[\phi]^T\,\{F\}} \frac{\partial s_r}{\partial \omega_r} \tag{6.42}$$

By assuming a Gaussian or normal probability density function of the blade stiffness as follows:

$$p_k(k) = \frac{1}{\sigma_k \sqrt{2\pi}} \exp\left(-\frac{(k-\bar{k})^2}{2\sigma_k^2}\right) \tag{6.43}$$

where $\bar{k}$ is the mean blade stiffness and,
σ_k is the standard deviation of the distribution of the blade stiffness.

The probability density function (PDF) of the blade response can be found as follows:

$$p_X(X_j) = p_k(k_j) \left|\frac{\partial k}{\partial \omega_r}\right| \left|\frac{\partial \omega_r}{\partial X}\right| \tag{6.44}$$

It should be noted that the cyclic symmetric property of the structure can reduce the calculation of finding the PDF of the system by evaluating a single blade PDF of response only [89]. Practically, this will not be the case but for tuned bladed discs, this assumption is valid. Figure 6.9 shows the response PDF obtained from equation (6.44). The bladed disc parameters used in this study are the same as those shown in Table 3.1 so that both the simulation studies and the analytical studies can be compared. The use of the tuned modeshapes in equation (6.41) means that the systems are all tuned but the blade stiffness has a normal distribution. Again, this is not the ideal case yet. Of course, the mistuned system PDF can be obtained if there exists a closed-form equation for the blade responses and the variables, such as the stiffness, the mass or the damping. This expression is indeed very complicated to formulate. Nevertheless, this technique demonstrates the same shape for the PDF as in the SDOF study. This further shows that the profile of the response distribution is a direct result from the property of simulations.

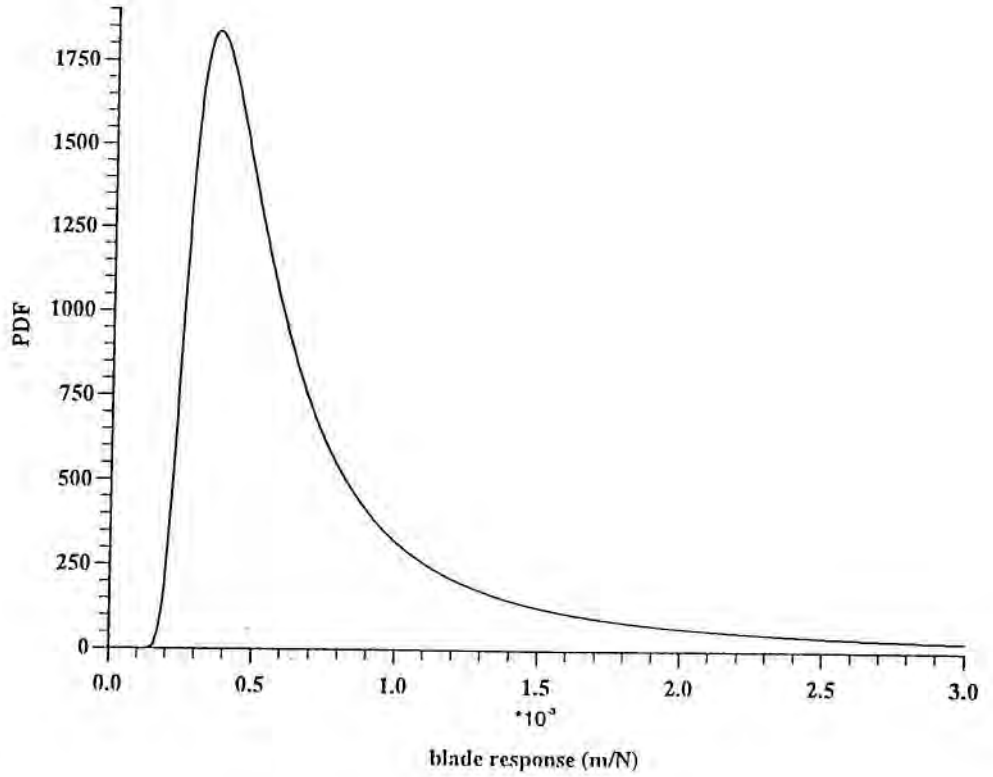

Figure 6.9 PDFs of a 36-bladed disc with 10% blade variations

6.6 CONCLUDING REMARKS

This chapter presents some theoretical methods to find the probabilistic density functions for the blade response scatter plots. From these studies, the following conclusions are made.

In previous chapters, the stochastic or statistical simulations were used to produce the response scatter plots. If the simulations have enough data samples, the solution will converge to the desired results. In statistics, this method is often termed as direct simulation. From the simulation of a 36-bladed disc, it is shown that there is a linear relation between such scatter plots and their probability density functions. It is also possible to fit some known analytical distribution functions onto the numerical data by obtaining the mean and the variance from the data. This method is known as the inference method and numerical results show that the distribution functions for the scatter plots often varied between the lognormal and the normal distributions in the cases of mistuned bladed systems.

Furthermore, a study to find an efficient analytical method to determine the response PDF from blade-alone parameter scatter is also presented. Such an analytical method may reduce the computational effort required by the direct simulation methods. However, an analytical PDF may be found only if a mistuned bladed disc response expression exists. Usually, this is not the case and some approximation techniques must be considered. It is thought that such a method is not very practical since computer hardware is getting faster and cheaper so that the simulation method becomes affordable.

Nevertheless, the most important discovery in this study is using the analytical method to show the reason for the clear-cut profile of the scatter plots from direct simulations. The simulation assumes a normal distribution of stiffness and this distribution is inversely proportional to the blade responses in the dynamic bladed system. This causes the distributions of the blade responses to converge to some lognormal distributions. Since direct simulations mimic the theoretical results, the profile boundaries will be simulated with sufficient data. This also shows that the direct simulation technique can solve complicated physical states where analytical solutions are formidable.

CHAPTER 7

EXPERIMENTAL MEASUREMENT OF MISTUNED BLADED DISC RESPONSES

About this chapter

So far, the effect of mistuning on bladed disc vibrations has been extensively studied using numerical simulations. In Chapters 3, 4 and 5, the parametric studies highlighted some new physical understanding of the behaviour of mistuned bladed disc vibrations. Now, it is appropriate to conduct some experiments to validate the mathematical model and results obtained from the numerical studies.

In this chapter, two experimental tests are presented. The single-shaker test, followed by a conventional modal analysis, is carried out first and the mistuned bladed disc vibration characteristics are identified. The test results are then compared with the numerically simulated ones.

Next, travelling wave responses of a bladed disc rotating past static forces are simulated by two point harmonic forces applied to a stationary disc. Two aspects of the test are reported here. First, some particular bladed disc modes were selected from the numerical simulations which show scattered responses with mistuned bladed discs. Second, the engine-order excitation for these particular bladed disc modes were simulated using two shakers. The target of the experiment was to measure blade responses and to compare them with the numerical predictions.

7.1 INTRODUCTION

The resonant responses of turbomachinery blades are important parameters in the design of new lightweight, high-performance engines. The effect of mistuning on bladed discs can seriously affect the vibration characteristics of the blades. From previous case studies of a mathematical model, the numerical simulations show that under some particular engine-orders (EO) of excitation, the mistuned bladed disc responses display peak variations with the excitation frequency. A practical support for these conclusions will be essential through state-of-the-art experimental techniques. Therefore, the objective for this study is to validate the mathematical model using experimental simulation techniques on an actual bladed disc test-piece.

In Chapter 2, it was shown that a hammer test provided a means to determine the modal characteristic of a bladed disc. This technique is particularly useful to find the experimental natural frequencies and mode shapes. Sometimes, it may even be used to provide the modal parameters to derive a mathematical model, such as the lumped parameter model. Furthermore, it also provides the tool for tuning a bladed disc in practice as shown in Appendix VII.

In this chapter, a single-shaker excitation technique was first used for comparison of the results from tests and numerical studies. A row of the frequency response function matrix was measured at each blade around the rotor. Conventional modal analysis then yielded the mode shapes for the mistuned bladed disc. These modeshapes can be compared with the analytical mode shapes.

However, conventional modal testing techniques can only find the modal properties of a structure. A study of the excitation forces which drive a bladed disc is also essential. Notwithstanding, the tests of forced response on bladed discs are more complicated to conduct than the conventional modal testing. In the past, there were many ways to set up rig-tests to perform forced response testing for bladed disc. Early tests on bladed disc structures were carried out in actual engines [70]. The results from these tests gave good indications of the dynamic behaviour of a bladed disc in practical situations. However, the cost of these tests was very high. Alternatively, multi-air-jets experiments were also used as cheaper test rigs to simulate the engine order excitations as presented by Tobias and

Arnold [142] and Wildheim [159]. The costs of these experiments were less than engine tests but still required a substantial cost to run.

Another technique developed in the past was the dual sine control technique or the two-shaker excitation technique [31]. The cost of this method was cheaper than the other two as shown by Ewins [31] and others. The objective of this technique was to simulate travelling wave excitation on axisymmetric components such as bladed discs, discs or casings and to investigate the mode splitting effect from mistuning. After Ewins demonstrated this technique to show the mistuning effects on a bladed disc [31], Mehdigholi [96], and Stetter and Kellerer [139] showed that the same technique can be applied to a disc. Also, Staples [138] used the same technique to measure the forced responses of an engine fan casing. Nevertheless, in the past, only those of lower diametrical modes of an axisymmetrical structure have been considered, such as the 2nd or the 3rd nodal diametrical (ND) modes. The experiment shown here, however, intends to test at higher engine-orders, such as the 5 EO or the 6 EO excitations.

Furthermore, a key factor to simulate travelling wave excitation by two-point sinusoidal forces is the ability to control the magnitudes of the two forces to be the same while keeping the phase between the two forces by a constant angle. Most of the previous work for the force control was done manually using hardware controllers. A new idea for controlling the two forces by software was developed and tried in this exercise. This software controller gives more flexibility to use than the manual control, and can eliminate human errors. The new control process also aims to give better control around the structural resonances.

7.2 THEORY

7.2.1 Travelling Wave Simulation

The responses around the periphery of a rotating structure, according to Campbell [14], can be written as follows:

$$u = a\sin n\theta \cos\omega t \qquad (7.1)$$

where $a\sin n\theta$ indicates the shape of the vibration. Campbell further showed that this motion can be considered as the superposition of two travelling waves shown as follows:

$$u = \frac{a}{2}\sin n\left(\theta - \frac{\omega}{n}t\right) + \frac{a}{2}\sin n\left(\theta + \frac{\omega}{n}t\right) \tag{7.2}$$

However, the exciting forces acting on the rotating structure are often stationary and they may not change by time, [27]. The generalised forces acting on the rim of a bladed disc according to the principal coordinates can be written as follows:

$$Q = \int_0^{2\pi} f(\theta,t)\sin n\alpha \, d\theta \tag{7.3}$$

This equation represents the convolution of some forcing function with an input signal $f(\theta,t)$ acting on a deflected rotating structure of sine function with a desired nodal diameter pattern, n. The equations of motion in the principal coordinates can be written in the form as follows:

$$\ddot{q} + 2\xi\omega_r\dot{q} + \omega_r^2(1+\eta_r)q = \frac{Q}{m} \tag{7.4}$$

In chapter 3, the modal summation method showed that the response around the rim of the circumferential coordinates can then be written as follows:

$$\{u\} = \sum_{r=1}^{N} \frac{[\phi]\ [\phi]^T\{Q\}}{\omega_r^2 - \omega^2 + j(2\omega_r\omega\xi_r + \eta_r\omega_r^2)} \tag{7.5}$$

Considering a pair of orthogonal n ND modes rotating at speed Ω, the mode shapes on the rim are assumed to be functions as follows:

$$\phi_1 = \cos n\theta, \quad \text{and } \phi_2 = \sin n\theta \tag{7.6}$$

If an exciter is used to excite a disc at a point along the disc rim, the forcing function for the system is in the form as follows:

$$F(\theta,t) = F_0\,\delta(\theta - (\Omega t + \alpha)) \tag{7.7}$$

where $\delta(\theta - (\Omega t + \alpha))$ is a Dirac delta function. For $\theta = \Omega t + \alpha$, this function is equal to unity and for any other values, the function is zero. Using equation (7.3), the generalised force to give the disc with a $\sin(n\phi)$ deflection would have the value as follows:

$$Q = F_0 \sin n(\Omega t + \alpha) \tag{7.8}$$

Similarly, the generalised force to give the disc a cos(nα) deflection would have the value of $F_0 \cos n(\Omega t + \alpha)$. Therefore, a sine wave excitation would excite the sine mode of the structure and similarly, a cosine wave excitation would excite the cosine mode of the structure. This has been explained by Afolabi in 1982 [1]. By substituting equation (7.6) and (7.7) into equation (7.5), the steady-state response solution can be obtained and this has been presented by Mehdigholi [96]. Furthermore, he also proved that a standing wave was obtained by substituting the stationary coordinate into the response equation. This implies that a single shaker test would excite the structure with some cosine or sine modes.

The idea of simulating the travelling wave effects on cyclic symmetrical structures by two point force excitations can be found in References [31] or [138]. This technique is beneficial because the cost of actual engine-order simulation is high. As shown in Figure 7.1, the angles ϕ_1 and ϕ_2 are spatial phases according to a datum, and β is the temporal angle by which F_2 lags to F_1.

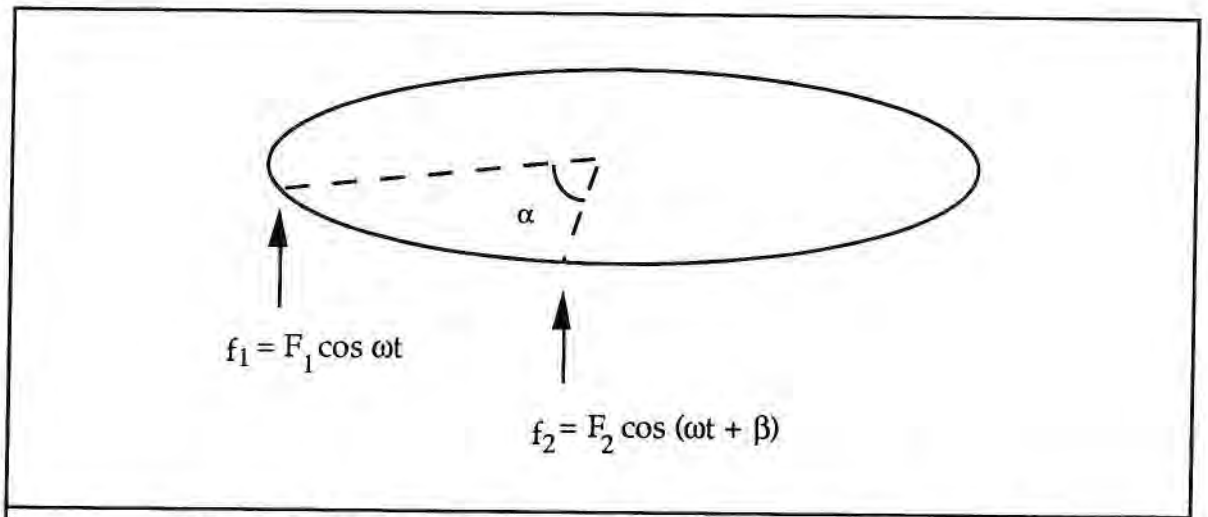

Figure 7.1 Two excitations on a cyclic symmetric structure

The assumed mode of the bladed disc can be simply the cosine and sine shapes around the circumference of the bladed disc. The generalised force can be written as follows:

$$f(\theta,t) = F_1 \delta(\theta + \phi_1) + F_2 \delta(\theta + \phi_2 - \beta) \tag{7.9}$$

and

$$\phi_1 - \phi_2 = \alpha$$

Ewins [31] showed that these two forces can be expressed in terms of their Fourier components as follows:

$$F(\theta,t) = \frac{F_1}{\pi} + \frac{F_2}{\pi} + \frac{F_1}{\pi}\sum_{i=1}^{\infty} \{ \cos n(\theta - \phi_1) \cos \omega t \} + \frac{F_2}{\pi}\sum_{i=1}^{\infty} \cos n(\theta - \phi_2) \cos (\omega t - \beta) \} \quad (7.10)$$

Assuming F_1 equals to F_2 and equals unity, the spatial angle between the two point forces is $(\phi_1 - \phi_2) = \alpha$, the above equation can be further simplified as follows:

$$F(\theta,t) = \frac{2}{\pi} + (A_n \cos n\theta + B_n \sin n\theta) \cos \omega t + (C_n \cos n\theta + D_n \sin n\theta) \sin \omega t \quad (7.11)$$

where

$$A_n = \sum_{i=1}^{\infty} (F_1 + F_2 \cos n\alpha \cos\beta)$$

$$B_n = \sum_{i=1}^{\infty} F_2 \sin n\alpha \cos\beta$$

$$C_n = \sum_{i=1}^{\infty} F_2 \cos n\alpha \sin\beta$$

$$D_n = \sum_{i=1}^{\infty} F_2 \sin n\alpha \sin\beta$$

The first term is a constant which has no effect to the travelling waves, the rest of the terms can be re-arranged into a backward travelling wave plus a stationary wave as follows:

$$F(\theta,t) = \frac{2}{\pi} + [A_n \cos (n\theta - \omega t) + B_n \sin (n\theta - \omega t) - (A_n + D_n) \sin n\theta \sin \omega t - (C_n - B_n) \cos n\theta \sin \omega t] \quad (7.12)$$

By letting $\tan \gamma_1 = \frac{B_n}{A_n}$ and $\tan \gamma_2 = \frac{C_n - B_n}{A_n + D_n}$

one can re-write the above equation as follows:

$$F(\theta,t) = \frac{2}{\pi} + [\sqrt{A_n^2 + B_n^2} \cos(n\theta - \omega t - \gamma_1) - \sqrt{(A_n + D_n)^2 + (C_n - B_n)^2} \sin(n\theta + \gamma_2) \sin \omega t]$$

$$= \frac{2}{\pi} + [A' \cos(n\theta - \omega t - \gamma_1) - B' \sin(n\theta + \gamma_2) \sin \omega t] \qquad (7.13)$$

where

$$A' = \sqrt{A_n^2 + B_n^2}$$

$$B' = \sqrt{(A_n + D_n)^2 + (C_n - B_n)^2}$$

The general force on the structure can then be written as follows:

$$F(\theta,t) = A \sin(n\theta - \omega t + \psi) - B \sin(n\theta + \gamma) \sin \omega t \qquad (7.14)$$

where

$$A = \frac{F_1 + F_2 \cos n\alpha \cos\beta}{\sin \psi}$$

$$B = \frac{F_1 + F_2 \cos n\alpha \cos\beta + F_2 \sin n\alpha \sin\beta}{\cos \gamma}$$

$$\tan \psi = \frac{F_1 + F_2 \cos n\alpha \cos\beta}{F_2 \sin n\alpha \cos\beta}$$

$$\tan \gamma = \frac{F_2 \cos n\alpha \sin\beta - F_2 \sin n\alpha \cos\beta}{F_1 + F_2 \cos n\alpha \cos\beta + F_2 \sin n\alpha \sin\beta}$$

Equation (7.14) consists of a backward travelling wave and a stationary wave. For the condition to excite the backward travelling wave only, the following conditions should be satisfied:

$$\gamma = 0 \quad , F_1 = F_2 \qquad \text{and} \qquad n\alpha - \beta = k\pi \quad (k = 1,3,\ldots) \qquad (7.15)$$

The frequency responses by the dual harmonic forces can be expressed as follows, [31]:

$$x(\theta,t) = \frac{u(\theta,t)}{F} \tag{7.16}$$

The general response from the structure can be written in a similar way as the force as follows:

$$u(\theta,t) = C\sin(n\theta - \omega t + \psi) - D\sin(n\theta + \gamma)\sin\omega t \tag{7.17}$$

where

$$C = \frac{u_1 + u_2\cos n\alpha\cos\beta}{\sin\psi}$$

$$D = \frac{u_1 + u_2\cos n\alpha\cos\beta + u_2\sin n\alpha\sin\beta}{\cos\gamma}$$

$$\tan\psi = \frac{u_1 + u_2\cos n\alpha\cos\beta}{u_2\sin n\alpha\cos\beta}$$

$$\tan\gamma = \frac{u_2\cos n\alpha\sin\beta - u_2\sin n\alpha\cos\beta}{u_1 + u_2\cos n\alpha\cos\beta + u_2\sin n\alpha\sin\beta}$$

Therefore, the normalised frequency response $x(\theta,t)$ is stationary according to the travelling excitation wave.

7.2.2 **Force Control Process**

The two applied forces to the testpiece should, in theory, be equal in magnitude and out of phase if the output signal from the PC has been set in the same manner. However, these two forces will have different magnitudes and phases to their PC output signals when the excitation frequency is close to a resonance frequency of the test piece. This is because the two shakers will affect each other at this stage and compensation is required by adjusting the output signals from the PC. In the past, the force signals were controlled by manually adjusting the two voltage signal generators. Now, the two force signal generation has been done on a digital-to-analogue converter (DAC) card. The advantage of this is to control the two signals by using a transfer matrix created by two more input signals at the same frequency.

Suppose the PC D/A converter card supplies two voltage signals (V), which have same magitudes but different phases, their relationship connect to applied forces (F) can be written into the form as follows:

$$F_1 = H_{11}V_1 + H_{12}V_2$$
$$F_2 = H_{21}V_1 + H_{22}V_2$$

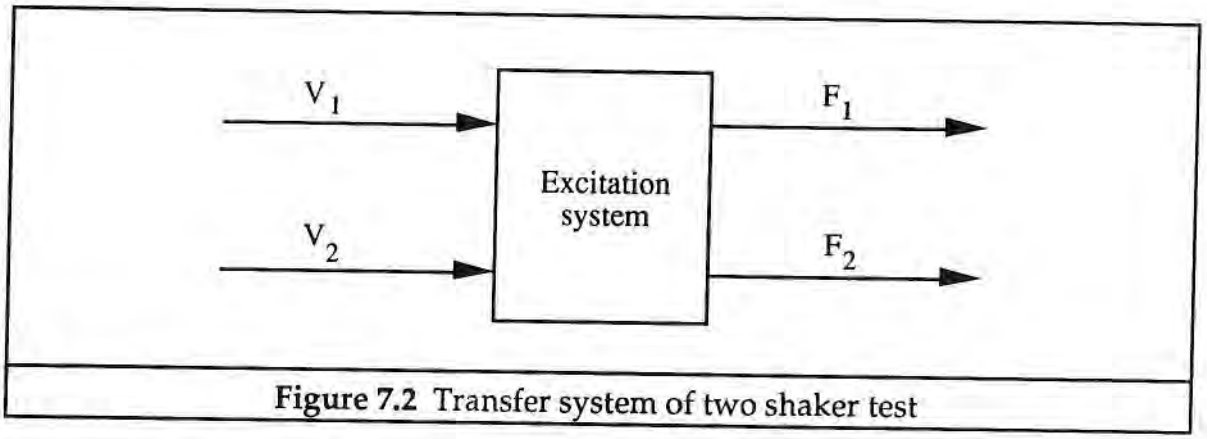

Figure 7.2 Transfer system of two shaker test

where F, V, H are all complex, and H represents the transfer function element of the electrical system. By rewriting the two equations and separating the real and imaginary parts, one can get the sets of system as follows:

$$H_{11}^{r}V_1^{r} + H_{12}^{r}V_2^{r} - H_{11}^{i}V_1^{i} - H_{12}^{i}V_2^{i} = F_1^{r}$$
$$H_{11}^{r}V_1^{i} + H_{12}^{r}V_2^{i} + H_{11}^{i}V_1^{r} + H_{12}^{i}V_2^{r} = F_1^{i}$$
$$H_{21}^{r}V_1^{r} + H_{22}^{r}V_2^{r} - H_{21}^{i}V_1^{i} - H_{22}^{i}V_2^{i} = F_2^{r}$$
$$H_{21}^{r}V_1^{i} + H_{22}^{r}V_2^{r} + H_{21}^{i}V_1^{i} + H_{22}^{i}V_2^{r} = F_2^{i}$$

The superscripts r and i mean real part and imaginary part. Here, there are eight unknowns but only four equations. Therefore, another set of test data are required and these lead to a system as follows.

$$\begin{bmatrix} [V]_{test1} & 0 \\ 0 & [V]_{test2} \end{bmatrix} \{H\} = \{F\} \qquad (7.18)$$

Where the matrix $[V]_{test1}$ and $[V]_{test2}$ both have the form as follows, but element values from two separate tests:

$$[V] = \begin{bmatrix} V_1^r & -V_1^i & V_2^r & -V_2^i \\ V_1^i & V_1^r & V_2^i & V_2^r \\ V_1^r & -V_1^i & V_2^r & -V_2^i \\ V_1^i & V_1^r & V_2^i & V_2^r \end{bmatrix} \tag{7.19}$$

$$\{H\} = \begin{Bmatrix} H_{11}^r \\ H_{11}^i \\ H_{12}^r \\ H_{12}^i \\ H_{21}^r \\ H_{21}^i \\ H_{22}^r \\ H_{22}^i \end{Bmatrix} \quad \text{and} \quad \{F\} = \begin{Bmatrix} F_1^r \\ F_1^i \\ F_2^r \\ F_2^i \\ F_1^r \\ F_1^i \\ F_2^r \\ F_2^i \end{Bmatrix}$$

The transfer matrix can be found as follows:

$$[T] = \begin{bmatrix} H_{11}^r & -H_{11}^i & H_{12}^r & -H_{12}^i \\ H_{11}^i & H_{11}^r & H_{12}^i & H_{12}^r \\ H_{21}^r & -H_{21}^i & H_{22}^r & -H_{22}^i \\ H_{21}^i & H_{21}^r & H_{22}^i & H_{22}^r \end{bmatrix} \tag{7.20}$$

The solution of the above matrix has to be obtained by singular value decomposition (SVD) since some of the elements of the linear matrix may be zero, depending on the phase selected. The inverse of the matrix can be used to check the transfer matrix and the results should be such that the transfer matrix times any of the voltage vector will result the force vector as measured. Furthermore, the control and the accuracy may be done by iterating the process several times until the forces converge to the desired conditions.

7.3 SINGLE-SHAKER TEST

This experiment uses a 30-bladed disc. This bladed disc consists of simple uniform beams and a uniform flat disc. The physical dimensions of the structure and numerical predictions of natural frequencies are shown in Chapter 2. The single-shaker or the *sine-sweep* test, measures the FRFs for all the blades for to one excitation point. Therefore, a complete measurement around the bladed disc was performed and modal analysis can be applied. The purpose of the single-shaker

test is to determine the mistuned mode shapes of the blade disc. The hammer tests used in Chapter 2 were not good results to show the mistuning effects of a bladed disc because it was necessary to apply exponential windows to the measured signals in order to obtain the transient state. These put artificial damping effects and hence they smear the slightly mistuned effects on the bladed disc.

7.3.1 Experimental Procedure

The single-shaker test used the Solartron 1254 Frequency Response Analyser to set the input force signal to the structure, and to measure the response signals. Figure 7.3 shows the set-up of the single-shaker test. The calibration of the system and the types of equipment used are shown in Appendix VIII.

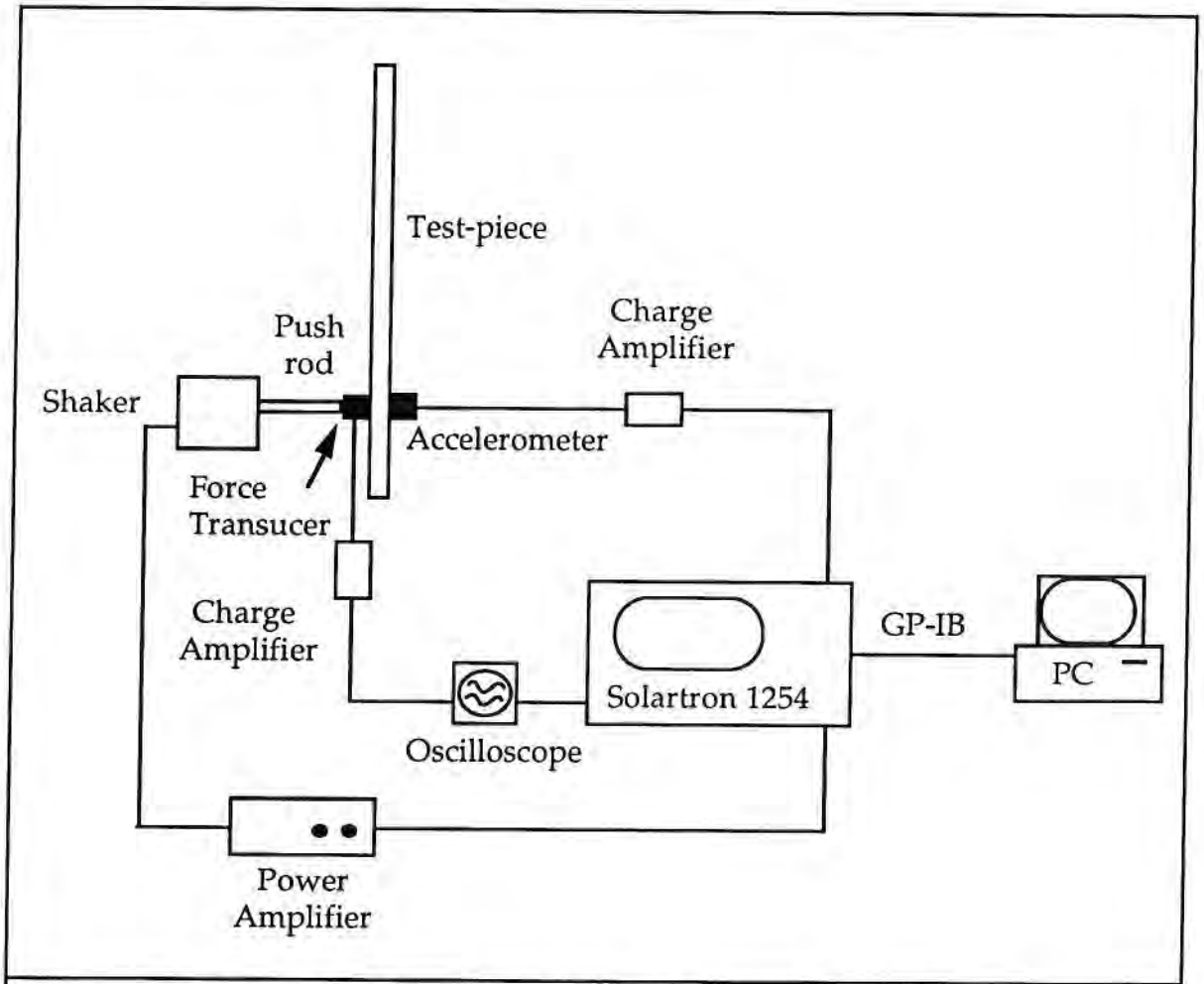

Figure 7.3 Experimental set-up for single shaker test

The control of the sequence of a sine-sweep test was achieved by connecting the 1254 with a PC and using the data acquisition program MODACQ [60] to transfer the data from the 1254 to the PC at each frequency step. Usually, MODACQ used a broad sweep before the fine sweep and it has been found that very fine

frequency steps were required around the resonances since the structure is lightly damped. Therefore, several separate measurements were made. Their frequency ranges were set as 160-166 Hz, 190-200 Hz, 210-220 Hz, and 220-230 Hz. These ranges actually covered the 3ND, the 4ND, the 5ND, and the 6ND modes of the bladed disc.

7.3.2 Measurement Results

The single-shaker test performs test results as the hammer test for each blade position FRF but with a harmonic excitation instead of the impulse force. A row of the frequency response function matrix $[H_{ij}]$, was obtained for modal analysis. The frequency range of the single shaker test covers the 3ND, 4ND, 5ND and 6ND modes. The modal analyses were applied to obtain the mistuned modeshapes for these modes. Furthermore, the amount of mistuning was also measured and the technique to measured the bladed cantilever frequencies was shown in Appendix VII. The analytical modeshapes of the mistuned bladed disc from can then be found. The correlation technique, first presented in Chapter 3, can be used to compare the modeshapes from test and theory, and known as the modal assurance criterion chart (MAC), see for example the book by Ewins [38]. Figure 7.4 shows the MAC tables as the comparisons of these modes.

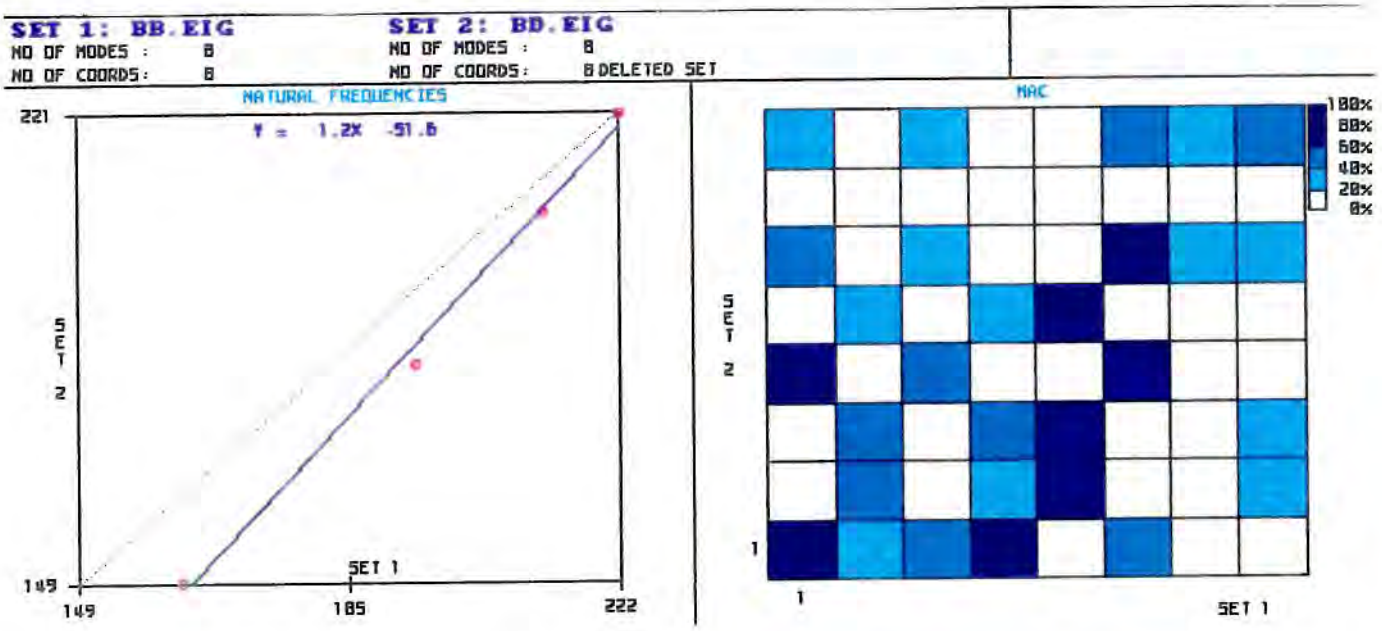

Figure 7.4 MAC plots and correlation diagrams

Figures 7.5a and 7.5b show the 3ND and 4ND modes with their discrete Fourier transform (DFT) coefficients showing the nodal diameter components.

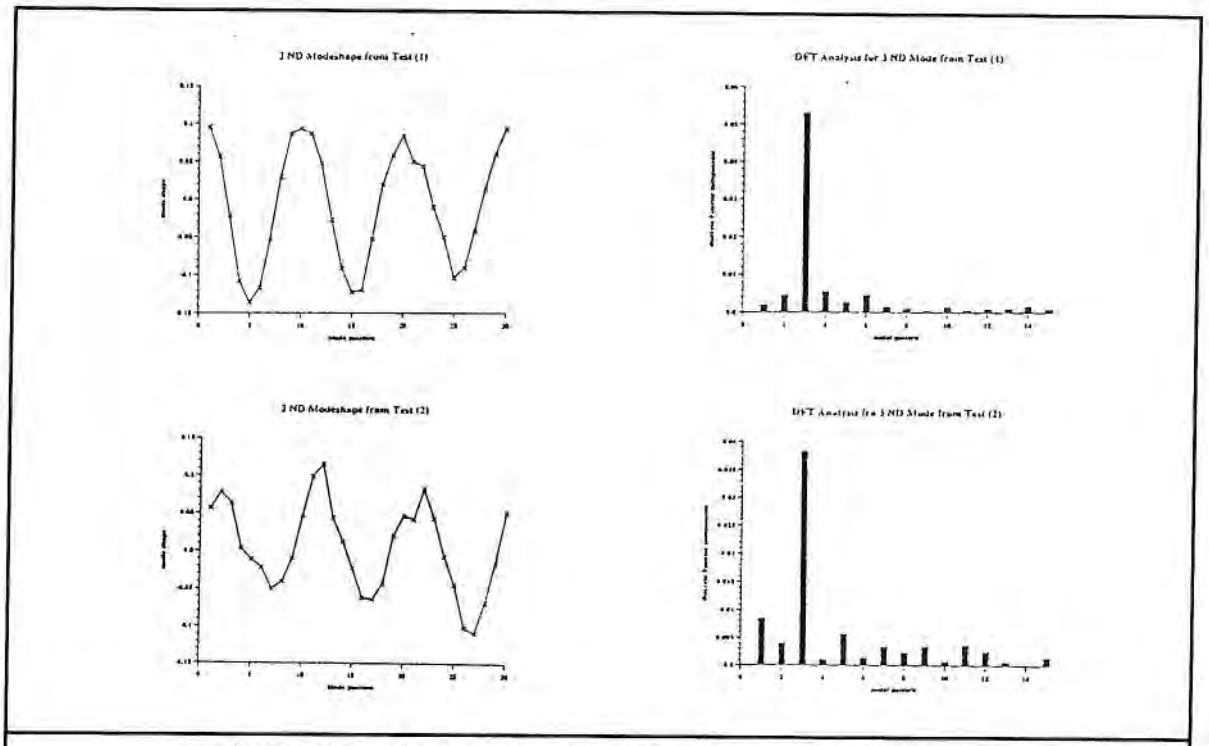

Figure 7.5a 3ND modeshapes from experimental tests

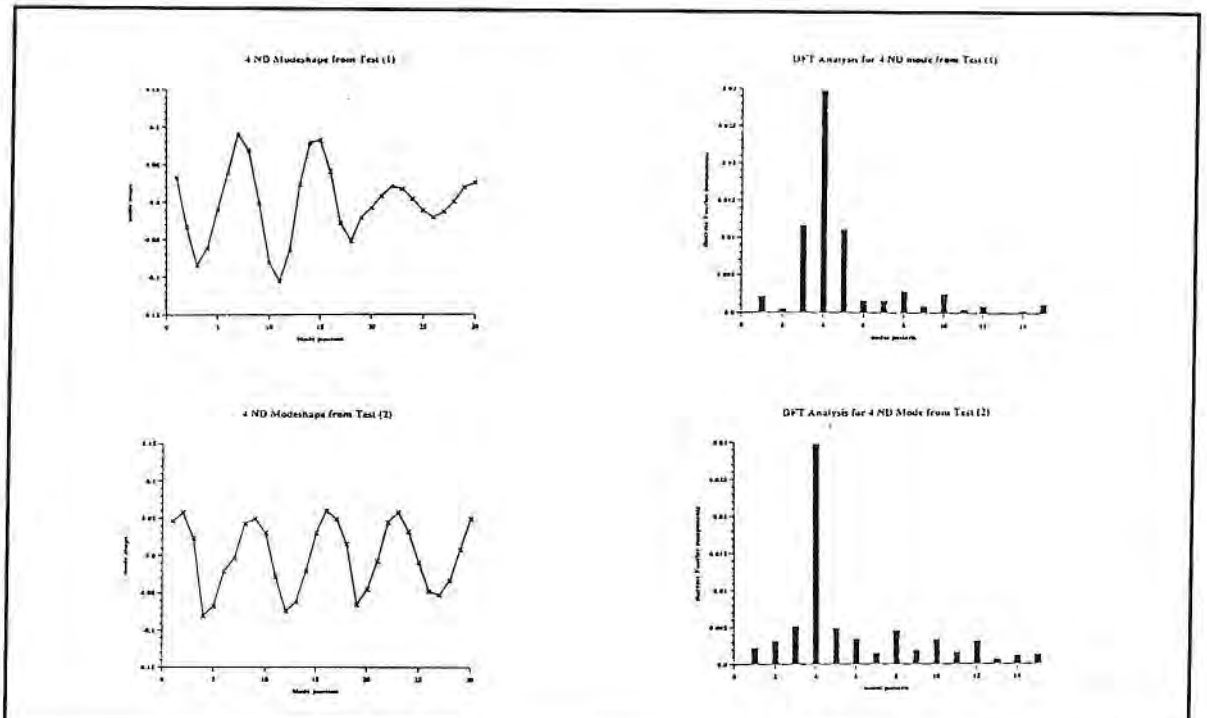

Figure 7.5a 4ND modeshapes from experimental tests

Figures 7.6a and 7.6b are the numerically-calculated modeshapes with their DFT coefficients.

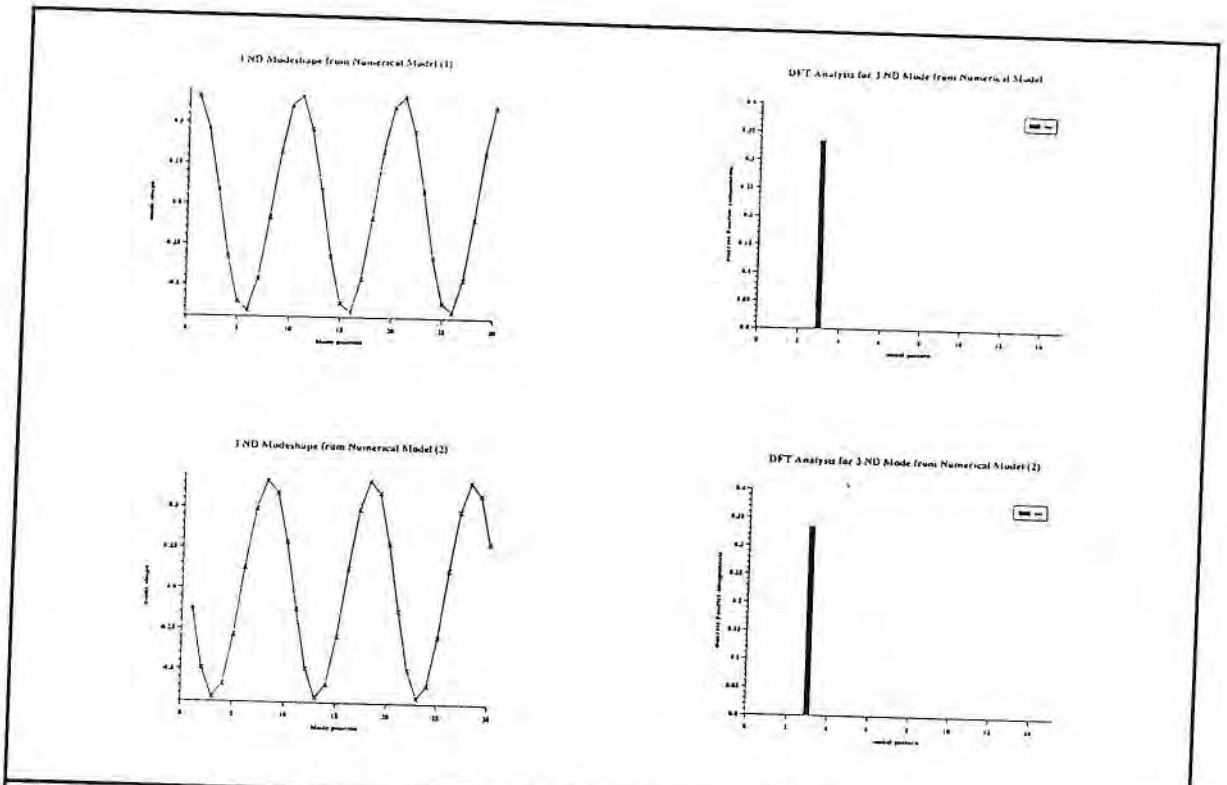

Figure 7.6a 3ND modeshapes from mathematical model

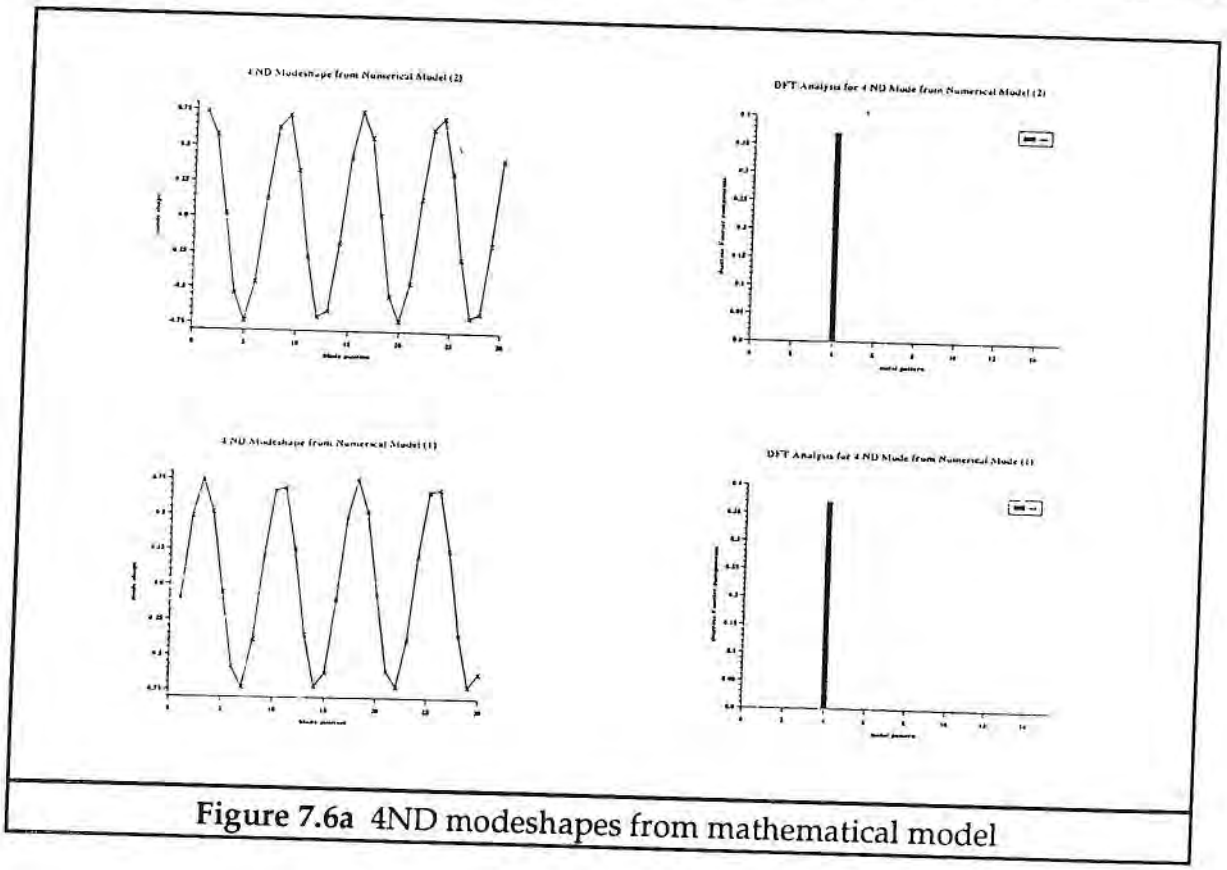

Figure 7.6a 4ND modeshapes from mathematical model

From the above studies, although the MAC table did not show good correlation, the mode shapes for the lower modes still can be identified. The mode shapes obtained from the test may appear differently than the numerically-calculated ones.

7.4 THE DUAL-SHAKER TEST

The second test uses two shakers arranged in a manner to simulate travelling wave excitations. Since the dual shaker or dual-shaker test takes more time to run than conducting the single-shaker test, only two measurements were made from two blades and the measured blade responses were the accelerations of the blades.

7.4.1 Numerical Simulations

In Chapters 2 and 3, the physical dimensions and the vibration characteristics of the 30-bladed disc have been described. A lumped mass-spring model has also been made to simulate the blade responses under engine-order excitations and on some numerical studies based on this model has also shown in previous chapters. Nevertheless, this numerical model needs to be validated. Thus, the objective of the experimental work is to validate this model by simulating some engine-order or travelling wave excitations using the dual-shaker test. Figure 7.7 shows the lumped parameter model with two point force excitations.

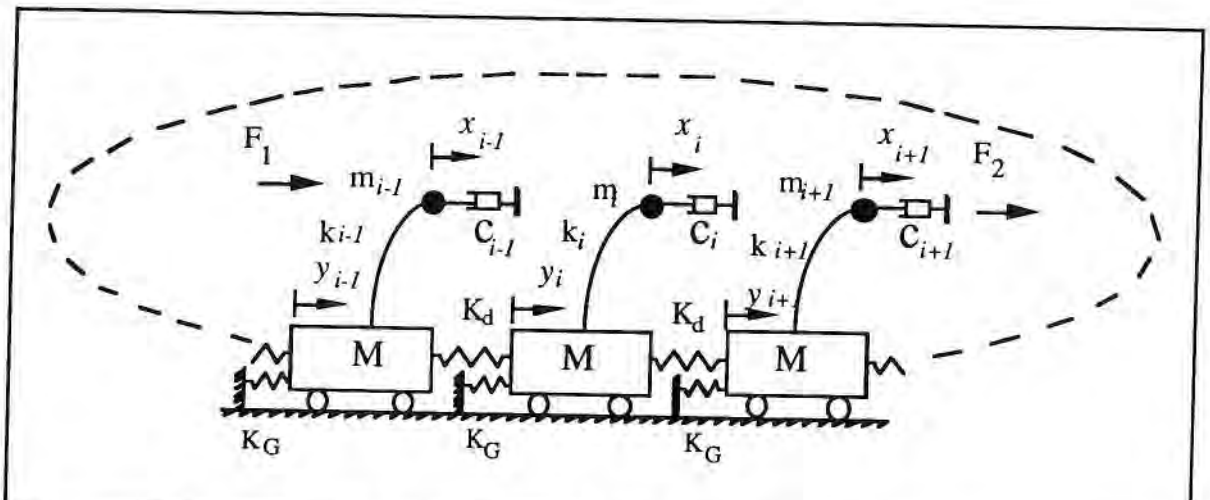

Figure 7.7 Numerical model of 30-bladed disc under two point harmonic force

First, some studies show the numerical simulations using the dual force excitation for the above model. Three different tests representing three different forcing

functions were carried out. These forcing functions, in theory, would excite the 3ND, 5ND and 6ND modes of the bladed disc assembly. The blade responses under engine order excitations can be simulated using the forcing functions as indicated in equation (7.15). Figure 7.8 shows responses under dual forces on the mistuned bladed disc set up to excite the 3ND, 5ND and 6ND modes. The conditions, according to equation (7.15), for exciting these modes are shown as follows:

Nodal diameter	α	β
3 ND	30°	90°
5 ND	36°	0°
6 ND	60°	90°

Table 7.1

In the second case, the 5ND mode is suppressed in the tuned case. The other two forcing functions would excite the 3ND and the 6ND modes as the dominated modes in tuned case.

7.4.2 Experimental Set-Ups

The experimental apparatus consists of a 386 PC with a multi-channel D/A converter card fitted in it to generate two signals to the test system. Two power amplifiers are used to connect from the PC card and then to two shakers respectively. The signals from the vibrating bladed disc are picked by four transducers: two force signals are measured by B&K force gauges and two response signals are measured by Endevco 2222C. All signals are amplified though charger amplifiers, type Endevco 3735, before sending to the Solartron 1254, a four-channel frequency response analyser. Further details of the experimental set-up can be found from the drawings in Figure 7.8. A synchroniser link is also required by the 1254 to measure the values at the frequency generated by the PC.

The General Propose Interface Bus (GPIB) was used to communicate between the PC and the 1254 analyser. A computer program has been written to set the IEEE card fitted in the PC and then to send the commands to the 1254 analyser by line feed mode. All the GPIB commands for the 1254 have been given in the Solartron 1250 series user manual [14]. Data capture from the 1254 analyser can be done by a slightly different way of carriage return plus line feed mode.

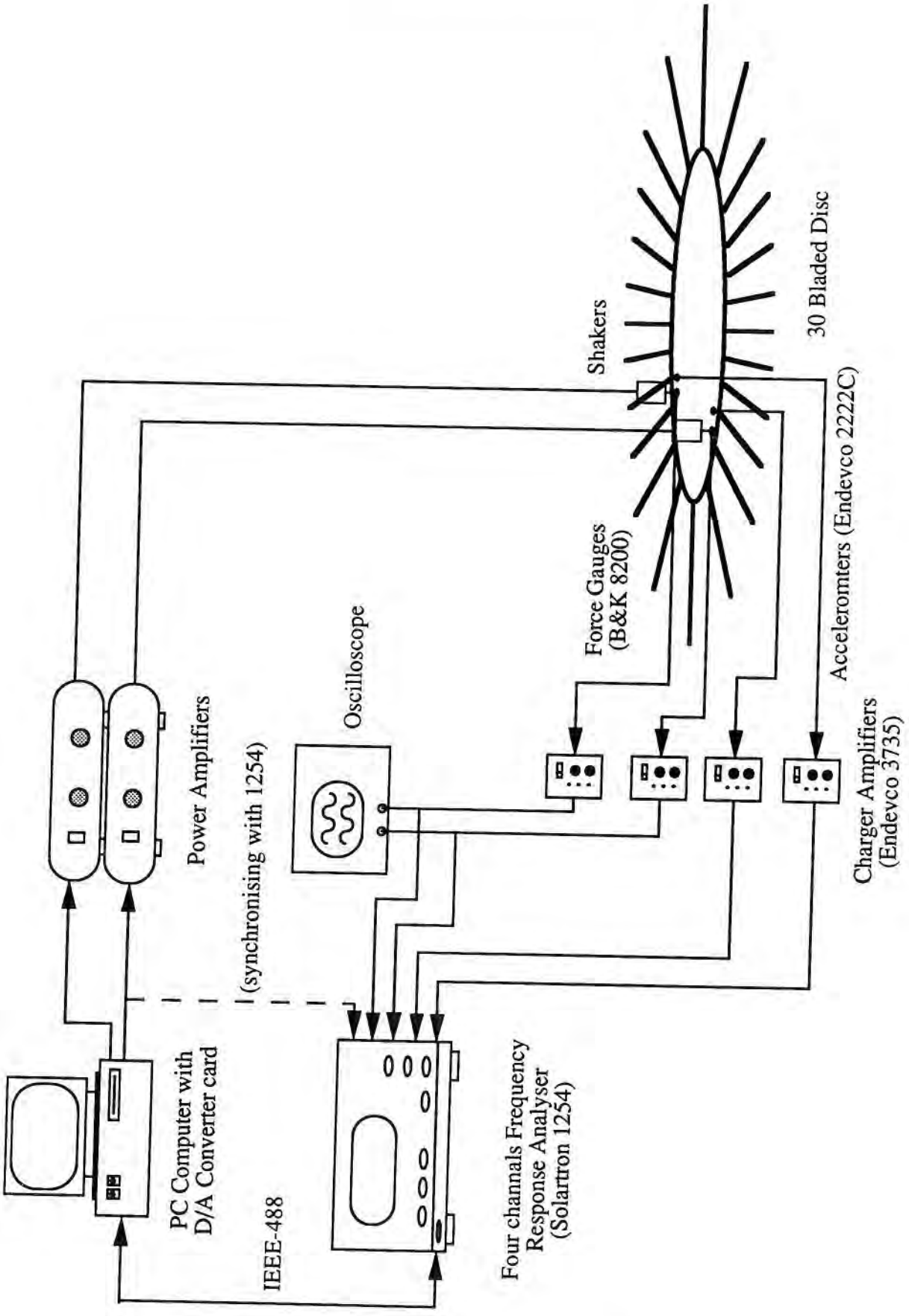

Figure 7.8 Experimental apparatus for due-shaker test

Calibrations of the electronic measuring system is necessary, since it is practical to ensure that all the equipment used are functioning properly. The procedure for calibration of the system is shown in Appendix VIII.

7.4.3 **Measurement Results**

From the numerical studies of two force excitations on a cyclically symmetrical structure, it shows that for mistuned cases, the mode splittingsets the two double modes to be separated to two resonances. Ewins, in 1969, defined a quantity to compare the mode splitting effect due to mistuning [31]. He defined the frequency split factor as follows:

$$S = \frac{(\omega_1 - \omega_2)}{0.5\,(\omega_1 + \omega_2)} \tag{7.21}$$

Here, ω_1 and ω_2 are the two resonant frequencies because of the mistuning effect. Nevertheless, the dual shaker excitation test must be controlled under conditions of the same force amplitudes with the phase specified as shown in Table 7.1. Figure 7.9 shows the ratio of the two forces and the phase difference between them in an attempt to simulate the 3 EO excitation.

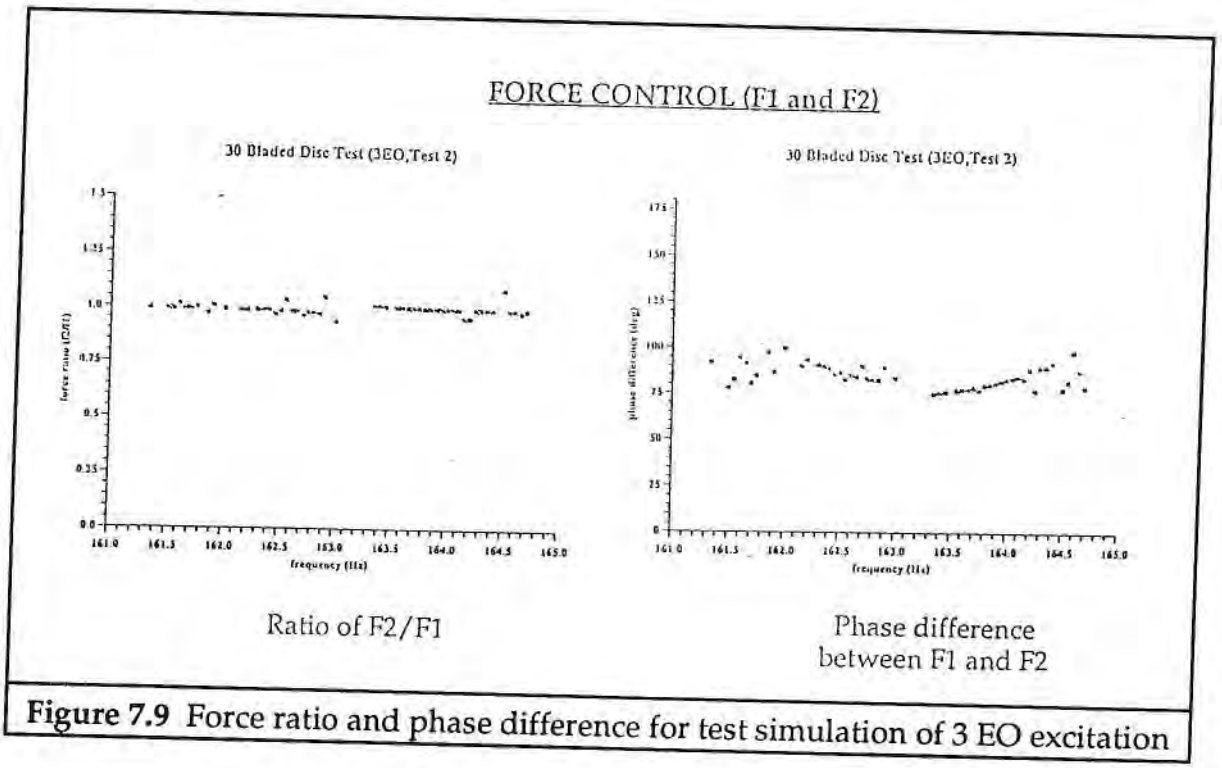

Figure 7.9 Force ratio and phase difference for test simulation of 3 EO excitation

Figure 7.10 shows the frequency responses of the 3 EO excitation from 162 Hz to 164 Hz with the two shakers having a spatial angle separated at 30° and the

temporal angle between the two shakers is 90°. Two forces applied to two of the blades, numbers 18 and 15, and the responses from these two blades were measured by two accelerometers. The responses were then divided by the mean force of the inputs to get response per unit force. The force and phase controls show exactly the expected conditions are achieved by the control algorithms. However, during the test, it was found that the control often became unstable. In many instants, large voltages were causing shocks on the shakers. Therefore, a limit of 5 volts was set as a top limit to prevent any damage to the shakers. Furthermore, the structure itself was lightly damped and this gives rise to some difficulties for conducting the test. Ewins used electromagnets to add uniform damping to the structure [31]. For the tests shown here, pads were used to add damping and longer delay time to improve the stability of the control algorithm.

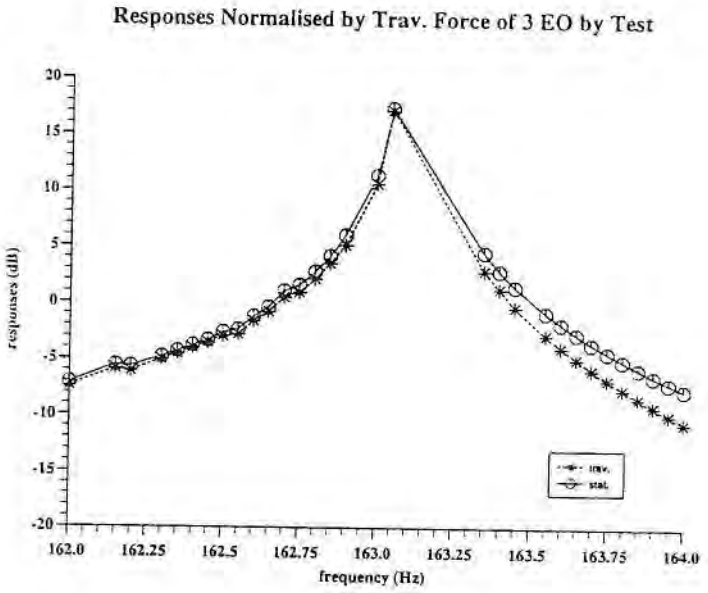

Figure 7.10 Responses under dual forces simulating 3 EO excitation from test

Furthermore, Figure 7.11 shows the numerically-calculated 3 EO response. The mistuning pattern used in this study took the experimentally-measured individual blade cantilever natural frequencies shown in Appendix VII. Here, these two graphs show some agreements with each other. The response curves for both experimental ones and the numerical ones are similar.

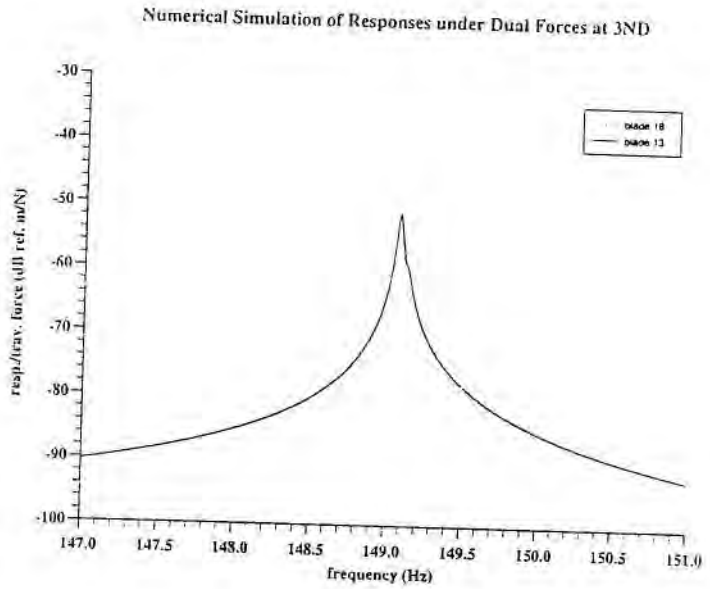

Figure 7.11 Responses under dual forces simulating 3 EO excitation numerically

A second test was performed in an attempt to simulate 5 EO excitation. A spatial angle of 36° between the two shakers and a temporal angle of 0° was set. The exciting frequency range was selected around 210 to 213 Hz, in the vicinity of the 5ND mode. Theoretically, these conditions will isolate the 5ND modes in tuned bladed disc. However, the presence of mistuning causes the travelling wave excitation part to be dominated. Figure 7.12 shows the ratio of the two forces and the phase difference between these two forces from the test.

Figure 7.13 shows blade responses of the test measurements from the experiment. Figure 7.14 shows the numerically simulated blade responses under the excitation using two forces separated at an angle of 36° and in phase with each other. The damping loss factor (η = 0.023%) used in this study is also obtained from the report [18] by Yiu in the earlier studies. Basically, the modal analysis will give the loss factor values. The damping loss factor used here is measured using single shaker modal testing method. In these cases, the frequency split factor from numerically calculated response is about 0.14%, while the frequency split factor from experimentally measured response is about 0.095%.

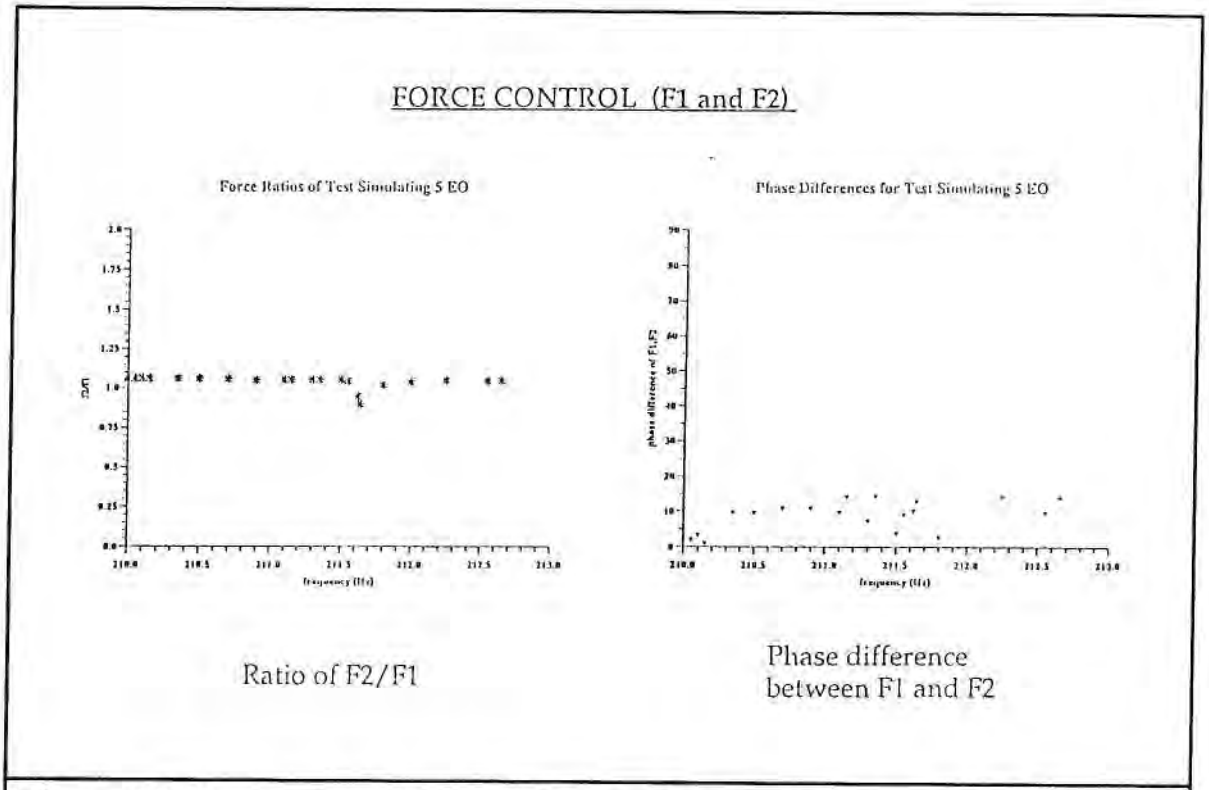

Figure 7.12 Force ratio and phase difference for test simulation of 5 EO excitation

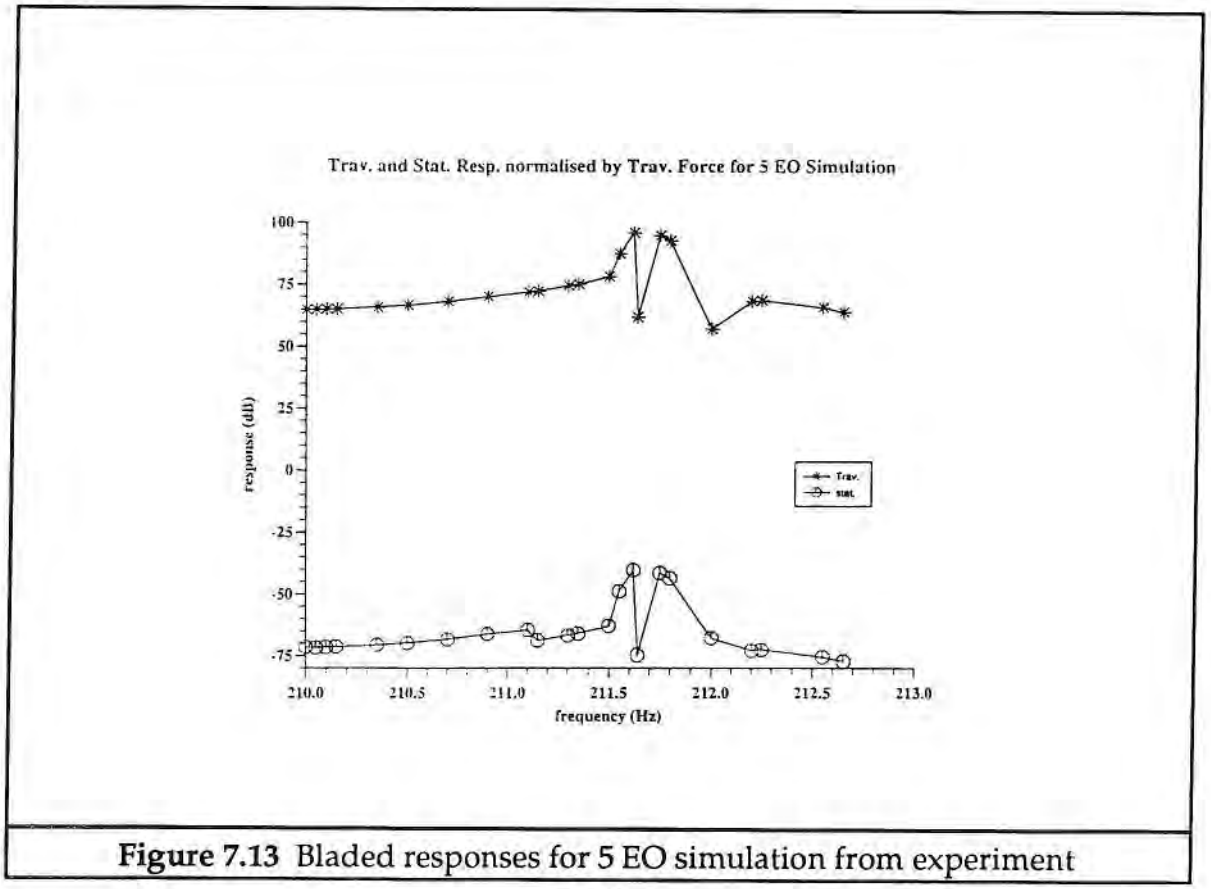

Figure 7.13 Bladed responses for 5 EO simulation from experiment

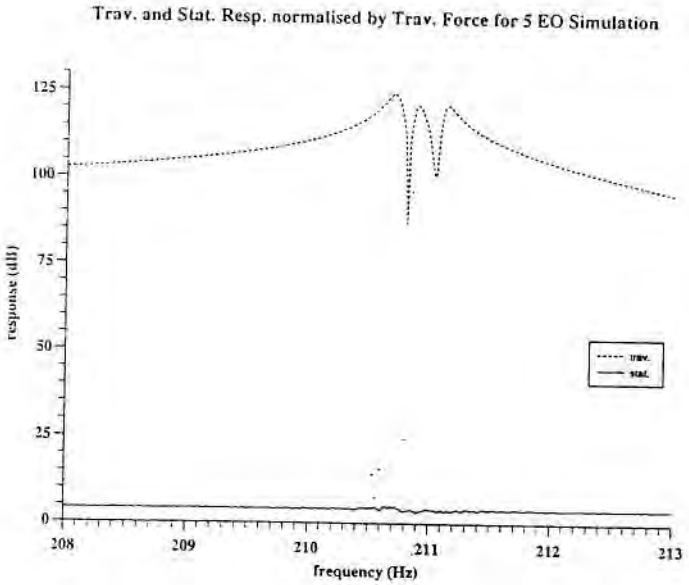

Figure 7.14 Numerical calculated bladed responses using dual forces simulating 5 EO excitation

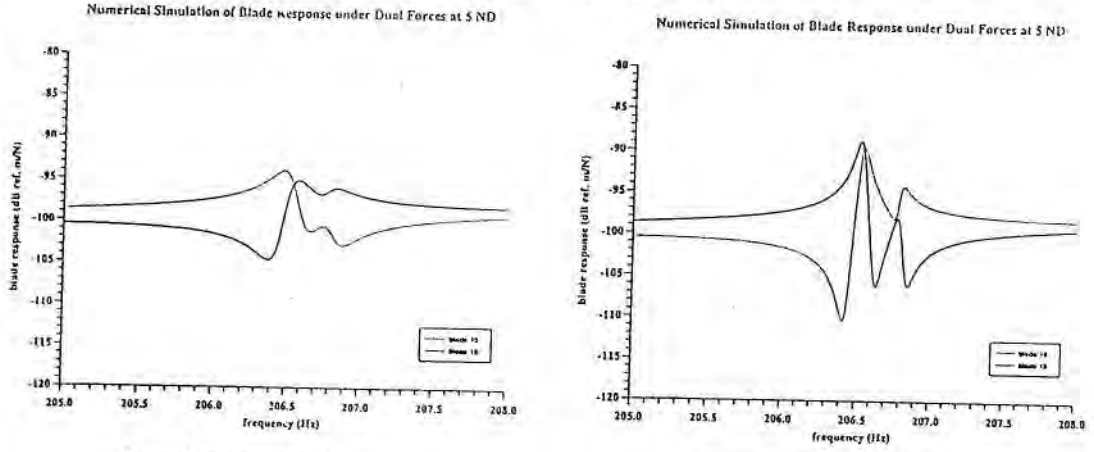

Figure 7.15 Numerically simulating two cases of damping loss factor different for the 5 EO excitation

Nevertheless, the factor of damping is also an important factor in this simulation test. The study of the relation between the split factor and the damping factor has been clearly presented by Ewins in 1969 [2]. Figure 7.15 shows two different damping levels from numerical simulations. From this graph, it can be seen that the level of damping used may affect the mistuning effect, especially at the resonances. Therefore, it is important to use the correct damping value for the numerical simulations to obtain reliable results.

Finally, the last test was used the dual-shakers to simulate a 6 EO excitation. In this test, a frequency range of 220-225 Hz was selected to cover the 6 ND mode. Figure 7.17 shows the travelling wave excitation for 6 EO excitation simulation from test while Figure 7.18 shows the travelling wave excitation for 6 EO excitation simulation from numerical prediction. In these two graphs, the frequency split factor from numerically-calculated response is about 0.14%, while the frequency split factor from experimentally measured response is about 0.3%. Furthermore, the response curves from this test show slight differences with the numerically-calculated ones. These discrepancies may be a result that this nodal diametral mode is within the cluster of the close modes.

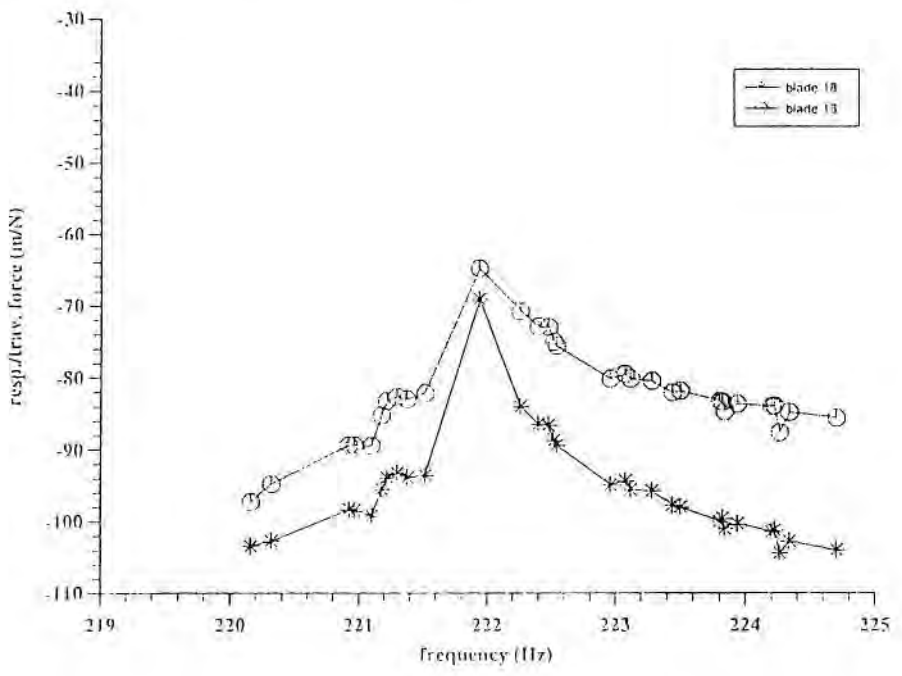

Figure 7.16 Travelling and stationary waves of responses normalised by travelling wave excitation for 6 EO excitation simulation from test

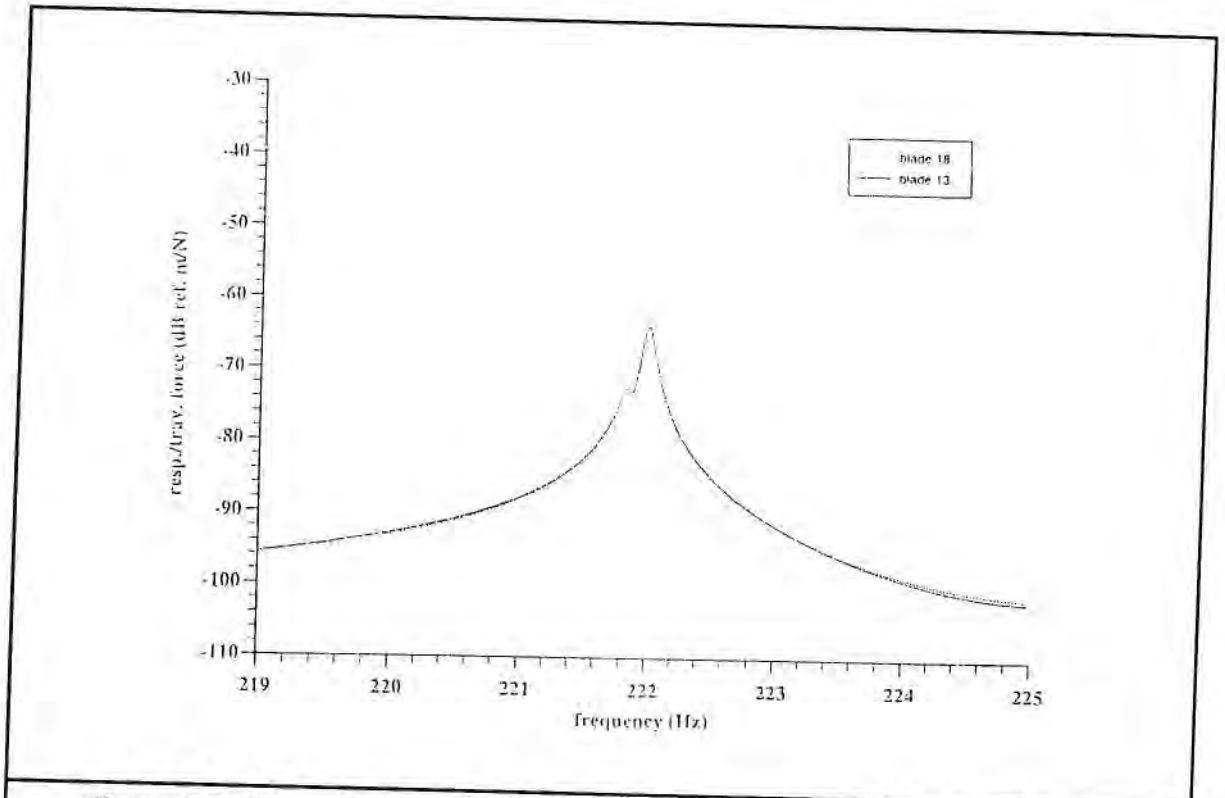

Figure 7.17 Travelling and stationary waves of responses normalised by travelling wave excitation for 6 EO excitation simulation from numerical model

7.5 CONCLUDING REMARKS

A study of the experimental methods for mistuned bladed disc has been presented. The objectives of these studies are to validate the numerical model used in the previous chapters and to investigate whether there is any mode splitting from the experimental modal analysis. The followings are some conclusions obtained from this study.

The single-shaker tests showed the slight splitting effect from the two natural frequencies presented as double modes. However, the sine sweep test required very fine frequency steps in order to get the results. In these tests, the frequency steps were selected in the range of 0.01 Hz which was the finest step could take from the 1254 analyser. The modeshapes are compared between the test ones and numerical ones. The MAC table did not show good correlation because the modeshape obtained from the tests may be different than the one from calculated.

The experiments of dual-shaker tests were set and the results of attempts to simulate travelling wave excitation were presented. A control algorithm for dual

force balancing was also developed and applied in the test. The dual shaker test can only isolate a particular mode. However, it remains a valid test for simulation of the travelling wave responses if the spatial angle and the temporal angle for the shakers are carefully chosen. The 3ND, 5ND and 6ND modes were simulated from both numerical technique and experiments. The comparison between the calculations and the tests show some agreement.

However, the primary object of this study is to show that the lumped-mass-spring model is valid to use for the numerical studies of bladed disc response behaviour. This comparison can be observed from some of the blade responses between the simulated and the calculated ones. However, the response results are extremely sensitive to external conditions since the close modes of a bladed disc. Some damping and long delay time are necessary for the tests. The results of the numerical simulation and the experimental tests shown in this study show some agreements. Therefore, the lumped-parameter model can be used for simulating bladed disc vibration problems.

Furthermore, the control algorithm is only a linear control. Most structures may behave with a degree of nonlinearity around the resonance, it is extremely difficult to control around these regions. At some particular frequencies, the control algorithm may even fail and diverge. Therefore, many measurements were taken and once the algorithm failed the data can be scared. This inevitably may cause error in the experimental results. From these, one can find that mistuning disturbs all the harmonic components as shown. This result agrees with other researchers' finding, such as Ewins [8]. Finally, damping may give stability to the control algorithm and this is also a fact agree with other researchers.

CHAPTER 8

CONCLUSIONS AND FURTHER WORK

About this chapter

The primary purpose in these studies of mistuned bladed discs is to gain more understanding of the subject, and hence to establish some guidelines which may be useful for design or for enabling the designer to control the unexpectedly high stresses due to blade mistuning. This last chapter mainly discusses the results obtained from the whole study and summarises the contributions from the work to add to the understanding to the subject. However, it is very often that the solutions of newly-solved problems start an era of other new problems, if they are not too confusing. Further recommendations for work on mistuned bladed discs draw the whole project to an end.

8.1 DISCUSSION

At the beginning of this thesis, there was a survey made of different groups of research in mistuned bladed discs. From this survey, one could see that it was a trend in the past to find some best practice for mistuned bladed discs once mistuning had been identified to be significant for a bladed disc configuration. However, this could not be done without an understanding of the physical behaviour of mistuned bladed discs. After the early work by Whitehead and Ewins, who showed the importance of mistuning on bladed discs [138,27], many researchers were looking for the worst and the best arrangements of mistuned blades for a given set of blades on a disc. Furthermore, the effects of mistuned blades on both flutter and forced response levels are both among the interests of researchers. Among them, Kielb's work on mistuning effects on flutter [70], and Griffin's work on statistical analysis of forced responses of blades [46], were perhaps significant papers in the subject. They showed quite a detailed understanding of the mechanism of mistuning in bladed discs. However, there are still outstanding questions about the subject, as presented in Chapter 1. This project has therefore aimed to answer some of these unsolved questions by further studies. Chapter 2 showed various mathematical models used in the past. The aim here was to compare different mathematical models used to simulate bladed disc vibrations. Although the results based on a tuned bladed disc study, the advantages and disadvantage for the various mathematical methods were gained.

Since numerical studies provide a cheap alternative for analysis, they have become a major tool for many research areas. After the effort of extensive numerical studies shown in Chapters 3 and 4, a more basic understanding to frequency-mistuned bladed discs was gained. The most significant results shown in this study are the introduction of coupling effects to mistuning and the discovery of the re-arrangement influence on peak blade response levels. It has been recognised that there are many factors affecting the mistuning effects on bladed discs. This argument has also been raised by Cargill who tried to generalise some factors in the effects of mistuning from some simple models using a perturbation approach, [18]. However, the dependence of different factors made the analysis very complicated to solve. In the present studies, the mistuning effects have been classified into frequency and damping mistuning types. For a uniformly damped system with frequency mistuned bladed discs, which constitutes of quite a range of bladed discs, the effects of mistuning seem to depend on the coupling elements between the blades, such as the disc or shroud,

and the amount of mistuning among the blades. These factors of coupling and the amount of mistuning can be considered as the global or the maximum possible effects for a particular bladed disc configuration. In other words, a bladed disc model with a specified coupling value and amount of mistuning limited by manufacturing tolerances may have its highest blade response at a particular combination of these two parameters for a particular bladed disc. This effect also depends upon the arrangements of the blades around the row. It has been shown that the critical blade response varied in a range of multiplication factor to the tuned bladed disc response of 1.3 to 2.1. Furthermore, the arrangement depends on the blade-alone natural frequency patterns as well. A numerical study of the critical blade arrangement pattern has been shown in Chapter 3. This study may be used as an understanding to different mistuning patterns.

The study of the effect of damping mistuning has been shown in Chapter 5. During this study, it has been found that damping mistuning also depends on the coupling influence. This effect is particularly obvious for the 'rainbow test' simulation which has been used in practice but with little understanding. During this study, it was shown that a strongly coupled disc can smear the damping mistuning effect and so that the disc vibration may be dominant. Furthermore, the influence of the damping elements in the system is localised, as shown in the study, and this is why by selecting higher engine-orders of excitation, the 'rainbow test' shows it functions.

Chapter 6 presents a theoretical study of probability density functions of the response scatter plots. The most significant contribution in this chapter was the demonstration of the clear-cut profile of the response scatter plots. It has been found that the inverse relation between the distribution parameter and the response results in a lognormal-shaped distribution of the response. This shape agrees with the results obtained from direct numerical simulations. This further shows that the direct simulation approach is a very effective tool to show complicated physical phenomena where an analytical approach is formidable.

Finally, experimental data are required for validating theoretical predictions and sometimes may even provide the modal parameters to derive a mathematical model, such as the lumped mass model [1]. Both single-shaker and dual-shaker tests were conducted on an experimental 30-bladed rotor. The experimental results show some agreement with the numerical results using a mathematical model. This mathematical model was previously used for all the parametric studies.

8.2 PRACTICAL GUIDES FOR MISTUNED BLADED DISCS

From the above discussion, some summaries can be drawn from this research work that would be useful for the design of bladed discs and for testing of blades. Also, from Chapter 1, some questions have been put up as targets for this research after a careful and detailed study on all previous knowledge towards mistuning. These questions are therefore re-quoted as follows:

Q.1 What is the effect of blade mistuning on forced vibration response?
- (i) What is the worst effect by a certain mistuned blade pattern?
- (ii) What is the nature of "rogue blades"?

Q.2 If blade mistuning causes significant changes than an otherwise tuned bladed disc, are there any factors which may directly affect the mistuning effects? Can these factors be used to avoid some blades may suffering higher than tuned responses if mistuning problem happened in practice?
- (i) Any disc coupling effect on blade mistuning?
- (ii) What is the change of peak responses with different amount of mistuning levels?

Q.3 How much worse will a mistuned bladed disc vibration response be than for a tuned system?
How can this higher than tuned blade response level controlled in design?

Q.4 Which blade will be mostly affected by mistuning?
In practice, where should strain gauges be sited so as to get the most useful experimental results?

Q.5 What is the optimum arrangement of a set of blades?
- (i) How much mistuning can be allowed for a fixed range of responses?
- (ii) What should be the maximum stability? (For example: can the mistuning effects be used as a passive control towards flutter?)

Since mistuning is an inevitable phenomenon in blade manufacturing, blade designers must be aware the effects of mistuning and of the factors influencing the mistuning effects. Questions 1, 2 and 3 are exactly focusing on the outcomes of mistuning effect as well as the factors influencing the response levels of mistuned bladed discs. This thesis provides a guide for such purposes so that one can

predict the severity of blade mistuning from known factors such as disc coupling, amount of mistuning and damping mistuning.

As shown in Chapter 3, the worst effect from blade mistuning on a bladed disc has been shown using a stochastic approach. The critical blade responses may well over twice the factor than the tuned response level. Therefore, the classical 'rogue blade' phenomenon has been defined as a particular blade response being much higher than the rest of blade responses. This research work exactly shows this fact. Furthermore, from this research, the author notices that these rogue blades are not necessarily meaning some particular blade or a group of blades as defined by previous researchers. These rogue blades depend upon factors such as blade and disc coupling, amount of mistuning and the excitation. This discovery is perhaps firstly reported according to the author's knowledge. Also, in Chapter 4, a theoretical coupling ratio was derived and numerical studies showed that the coupling ratio lies in the range between zero and unity. Hence, the bladed disc coupling effect can be classified into three categories: namely, (i) strongly coupled, (ii) moderately coupled and (iii) weakly coupled blades. From these three categories, the designer may predict the worst possible effect of the critical blades. He could also specify the amount of mistuning as the tolerance required by blade manufacturers.

In practice, if blade mistuning plays a role in the final testing stage, it is often too late to redesign the whole assembly. In this case, one may try to determine the re-arrangement of blades to keep the blade responses to a minimum level. In Chapter 3, a study of the arrangements has been presented and some conditions for best practice were also shown. Alternatively, friction dampers could be used to lower the resonant response levels as well. Nevertheless, the damping effect is also closely related to the coupling factors, as shown in this study. Therefore, a careful selection to use dampers is essential as well.

Finally, the selection of blades for strain gauges has also been studied. The results show that unless sufficient numbers of strain gauges are used for a test, it would not be reliable to interpolate the results for the locations of the highest possible blade responses. It is, however, found that the mean of blade responses from some limited numbers of strain-gauge measurements gives quite reasonable and close value to the mean of the whole assemble and even the mean value of the whole blade distribution. It is therefore recommended to the test engineers to use the mean values of the strain-gauge results and then to estimate the highest possible blade response from some numerical evaluations.

8.3 RECOMMENDATIONS FOR FURTHER WORK

From Chapter 2, several different numerical methods for solving bladed disc vibration problems have been presented and discussed. The discrete lumped parameter model was used extensively in this exercise because it is a more suitable model at the moment, particularly for large simulation purposes. However, the development of a continuous model is also desired so that other effects such as centrifugal stiffening and rotatory inertia can be included to make the simulation closer to real life. Secondly, the coupled effect from bending and torsion will result in combined loadings on the blades. These will cause the principle stresses to be greater than that of simple cases of bending or torsion. This is a significant fact for fan blade rotors and most steam turbine wheels when the blades are long and twisted. Nevertheless, the continuous model shown in Chapter 2 can include this problem for the analysis. The trial case shown in the thesis only demonstrates the methodology.

One main contribution of this work was to show some conditions for a set of blades with optimal responses on a disc. These conditions could be used as inputs to some optimisation routines and hence to specify the best arrangement of a given set of blades. Another similar procedure for blade selection is to create a database so that all the practical hints and numerical experiences can be compared and combined in future design.

Finally, in practice, there are always nonlinear factors existing, such as root friction damping devices. These effects ought to be included into the model in future. In the present studies, damping mistuning of a special case, the rainbow test configuration, has been studied and numerical results show strong disc coupling influence with its damping. However, the mechanism of damping mistuning is more complicated than the simplified and linear models used for this study.

8.4 CONCLUSIONS

To close, when the author first picked up mistuning for studying, there were many different views about the effects of mistuning. However, in the author's view, mistuning is a random parameter effect and if a linear system is used for modelling, the mistuning effect should also be linear. The combination of the forward and backward travelling responses may give rise to a factor greater than

expected as if the bladed disc is tuned. However, it can be judged by some system parameters or factors as shown during the studies. Some basic rules to predict the effects from mistuning are drawn and hopefully these results can help for the design of more reliable engines. Of course, the author cannot claim that this is the final work. In fact, more studies and more experimental data are required to make yet more detailed and precise conclusions in future. This work here is therefore hoping to provide some suggestions for the final goals.

REFERENCES

[1] **Afolabi, D.H.**
Vibration of Mistuned Bladed Disc Assemblies
Ph.D. Thesis, University of London, 1982.

[2] **Afolabi, D.H.**
A Note on the Rogue Failure of Turbine Blades
Journal of Sound and Vibration, Vol. 122, No. 3, 1988, pp 535-545.

[3] **Afolabi, D.H.**
Vibration Amplitudes of Mistuned Blades
Trans. ASME, Journal of Turbomachinery, Vol. 110, Apr. 1988, pp 251-257.

[4] **Armstrong, E.K.** and **Stevenson, M.A.**
Some Practical Aspects of Compressor Blade Vibration
Journal of the Royal Aeronautical Society, Vol. 64, No. 591, 1960, pp 117- 130.

[5] **Armstrong, E.K., Christie, P.I.** and **Hague, W.M.**
Natural Frequencies of Bladed Disks
Applied Mechanics Convention, IMechE, London, 1966.

[6] **Armstrong, E.K.**
Recent Blade Vibration Techniques
Trans. ASME, Journal of Engineering for Power, Vol. 1, 1967, pp 437-444.

[7] **Ang, A.H.S.** and **Tang, W.H.**
Probability Concepts in Engineering Planning and Design Vol. I and II
John Wiley & Sons, Inc., 1984.

[8] **Basu, P.** and **Griffin, J.H.**
The Effect of Limiting Aerodynamics and Structural Coupling in Models of Mistuned Bladed Disk Vibration
Trans. ASME, Journal of Vibration, Acoustics, Stress and Reliability in Design, April 1986, Vol. 108, pp 132-139.

[9] **Bendiksen, O.O.**
Flutter of Mistuned Turbomachinery Rotors
Trans. ASME, Journal of Engineering for Gas Turbines and Power, Vol. 106, Jan. 1984, pp 25-33.

[10] **Bishop, R.E.D.**
The Treatment of Damping Forces in Vibration Theory
Journal of the Royal Aeronautical Society, Vol. 59, Nov. 1955, pp 738-742.

[11] **Bishop, R.E.D.**
On Damped Free Vibration with Particular Reference to Systems having Nearly-Equal Natural frequencies
The Aeronautical Quarterly, Vol. 9, Feb. 1958, pp 71-95.

[12] **Bishop, R.E.D.** and **Johnson, D.C.**
Mechanics of Vibrations
Cambridge University Press, UK, 1960.

[13] **Bliven, D.O.** and **Soong, T.T.**
On Frequencies of Elastic Beams with Random Imperfections
Journal of the Franklin Institute, Vol. 287, No. 4, April 1969, pp .

[14] **Campbell, W.**
The Protection of Steam-Turbine Disk Wheels from Axial Vibration
Trans. ASME, vol. 46, 1924, pp 31-160.

[15] **Carnegie, W.**
Static Bending of Pre-twisted Cantilever Blading
Proceedings of IMechE, London, Vol. 171, 1957, pp 873-894.

[16] **Carnegie, W.**
Vibration Characteristics of Cantilever Blading
Applied Mechanics Convention, IMechE, London, 1966.

[17] **Cargill, A.M.**
Mistuning Analysis for a Pair of Coupled Oscillators
Rolls Royce Report No: TSG0672, Rolls Royce plc, March 1993.

[18] **Cargill, A.M.**
A Note on the Response of Mistuned Blade Discs
Rolls Royce internal report No. TSG0669, Rolls Royce plc, March 1993.

[19] **Carta, F.O.**
Coupled Blade-Disk-Shroud Flutter Instabilities in Turbojet Engine Rotors
Trans. ASME, Journal of Engineering for Power, Vol. 1, 1967, pp 419-426.

[20] **Chen, S.** and **Sinha, A.**
Probabilistic Method to Compute the Optimal Slip Load for a Mistuned Bladed Disk Assembly with Friction Dampers
Trans. ASME, Journal of Vibration and Acoustics, Vol. 112, Apr. 1990, pp 214-221.

[21] **Cottney, D. J.**
The Receptance Analysis of Disc, Blade and Shroud Vibration
Ph.D. Thesis, University of London, 1975.

[22] **Cottney, D. J.** and **Ewins, D.J.**
On Predicting the Natural Frequencies of Shrouded Bladed Disks
ASME paper: 75-DET-113, 1975.

[23] **Craig, R.R. Jr.** and **Chang, C.J.**
A Review of Substructure Coupling Methods for Dynamic Analysis
NASA Report No: CP-2001, Washington D.C., USA, 1976.

[24] **Crawley, E.F.**
In-Plane Inertial Coupling in Tuned and Severely Mistuned Bladed Disks
Trans. ASME, Journal of Engineering for Power, Vol. 105, July 1983, pp 585-590.

[25] **Crawley, E.F.** and **Hall, K.C.**
Optimization and Mechanism of Mistuning in Cascades
Trans. ASME, Journal of Engineering for Power, Vol. 107, Apr. 1985, pp 418-426.

[26] **Crawley, E.F.**
Aeroelastic Formulation for Tuned and Mistuned Rotors
AGARDograph No.298, 1988, pp 19 (1-24).

[27] **Dugundji, J.** and **Bundas, D.J.**
Flutter and Forced Response of Mistuned Rotors Using Standing Wave Analysis
AIAA Journal, Vol. 22, No. 11, 1984, pp 1652-1661.

[28] **Dye, R. C. F.** and **Henry, T.A.**
Vibration Amplitudes of Compressor Blades Resulting from Scatter in Blade Natural Frequencies
Trans. ASME, Journal of Engineering for Power, July 1969, pp 182-188.

[29] **Ehrich, F.**
A Matrix Solution for the Vibration Modes of Nonuniform Disks
Trans. ASME, Journal of Applied Mechanics, March 1956, pp 109-115.

[30] **EL-Bayoumy, L. E.** and **Srinivasan, A. V.**
Influence of Mistuning on Rotor-Blade Vibration
AIAA Journal, Vol. 13, No. 4, Apr. 1975, pp 460-464.

[31] **Ewins, D. J.**
The Effect of Detuning Upon the Forced Vibration of Bladed Disks
Journal of Sound and Vibration, Vol. 9, No. 1, 1969, pp 65-79.

[32] **Ewins, D. J.**
A Study of Resonance Coincidence in Bladed Discs
Journal of Mechanical Engineering Science, Vol. 12, No. 5, 1970, pp 305-312.

[33] **Ewins, D. J.**
A Study of the Vibration Modes of a Bladed Turbine Wheel
Proceedings of Inst. Mech. Engrs., Conference on Vibrations in Rotating Systems, London, 1972, pp 1-14.

[34] **Ewins, D. J.**
Vibration Characteristics of Bladed Disc Assemblies
Journal of Mechanical Engineering Science, Vol. 12, No. 5, 1973, pp 165-186.

[35] **Ewins, D. J.**
Vibration Modes of Mistuned Bladed Disks
Trans. ASME, Journal of Engineering for Power, July 1976, pp 349-355.

[36] **Ewins, D. J.**
An Experimental Investigation of the Forced Vibration of Bladed Discs due to Aerodynamic Excitation
Proceedings of ASME on Structural Dynamics Aspects of Bladed Disk Assemblies, Dec. 1976, pp 15-27.

[37] **Ewins, D.J.** and **Rao, Y.V.K.S.**
A Theoretical Study of the Damped Forced Vibration Response of Bladed Discs
Proceedings of ASME on Structural Dynamics Aspects of Bladed Disk Assemblies, Dec. 1976, pp 57-71.

[38] **Ewins, D. J.**
Further Studies of Bladed Disc Vibration: Effects of Packeting
Proceedings of Inst. Mech. Engrs., 1980, pp 97-102.

[39] **Ewins, D.J.**
Bladed Disc Vibration: A Review of Techniques and Characteristics
Int. Conf. of Recent Adv. Struct. Dynamics, Southampton, UK, 1980, pp 187-210.

[40] **Ewins, D.J. and Han, Z.S.**
Resonant Vibration Levels of a Mistuned Bladed Disk
Trans. ASME, Journal of Vibration, Acoustics, Stress and Reliability in Design, Vol. 106, 1984, pp 211-217.

[41] **Ewins, D.J. and Imregun, M.**
Aeroelastic Vibration Analysis of Tuned and Mistuned Bladed Systems
Proceedings of the Second Symposium on Unsteady Aerodynamics of Turbomachines and Propellers, Cambridge, Oct. 1984.

[42] **Ewins, D.J.**
Modal Testing - Theory and Practice
Research Studies Press (1984)

[43] **Ewins, D.J. and Henry, R.**
Structural Dynamic Characteristics of Individual Blades
AGARDograph No. 298, 1988, pp 14 (1-27).

[44] **Ewins, D.J.**
The Effects of Blade Mistuning on Vibration Response – A Survey
IFToMM Conference, Prague, Czechoslovakia, August 1991.

[45] **Fabunmi, J.A.**
Forced Vibrations of a Single Stage Axial Compressor Rotor
Trans. ASME, Journal of Engineering for Power, Vol. 102, Apr. 1980, pp 322-328.

[46] **Ford, R.A.J. and Srinivasan, A.V.**
Twin Mode Analysis of Aeroengine Fan Vibration and Flutter for Use in Design Studies
Proceedings of ASME on Vibrations of Bladed Disk Assemblies, Deaborn, Michigan, Sept. 1983, pp 97-104.

[47] **Ford, R.A.J.**
Analysis of the Vibration of Mistuned Bladed Disk Assemblies Using Twin Modes and Including Harmonic Components
Proceedings of ASME on Bladed Disk Assemblies, Boston, Massachusetts, Sept. 1987, pp 43-48.

[48] **Frazer, R.A.A.; Duncan W.J. and Collar, A.R.**
Elementary Matrices and Some Applications to Dynamics and Differential Equations
Cambridge University Press, Cambridge, UK, 1932.

[49] **Griffin, J.H. and Sinha, A.**
The Interaction Between Mistuning and Friction in the Forced Response of Bladed Disk Assemblies
Trans. ASME, Journal of Engineering for Gas Turbines and Power, Vol. 107, 1984, pp 205-211.

[50] **Griffin, J.H. and Hoosac, T.M.**
Model Development and Statistical Investigation of Turbine Blade Mistuning
Trans. ASME, Journal of Vibration, Acoustics, Stress and Reliability in Design, Vol. 106, 1984, pp 204-210.

[51] **Griffin, J.H.**
On Predicting the Resonant Response of Bladed Disk Assemblies
Trans. ASME, Journal of Engineering for Gas Turbines and Power, Vol. 110, Jan. 1988, pp 45-50.

[52] **Griffin, J.H.**
Optimizing Instrumentation when Measuring Jet Engine Blade Vibration
ASME paper No. 91-GT-71, 1991.

[53] **Gu, J.** and **Gao, H.**
Vibration Characteristics of a Well-Modelled Mistuned Bladed Disk
Proceedings of ASME on Bladed Disk Assemblies, Boston, Massachusetts, Sept. 1987, pp 55-59.

[54] **Hoel, P.G.**
Introduction to Mathematical Statistics
John Wiley & Sons, Inc. New York, USA, 1962.

[55] **Hodges, C.H.**
Confinement of Vibration by Structural Irregularity
Journal of Sound and Vibration, 1982, Vol. 82, No. 3, pp 411-424.

[56] **Hodges, C.H.** and **Woodhouse, J.**
Vibration Isolation from Irregularity in a Nearly Periodic Structure: Theory and Measurements
Journal of the Acoustical Society of America, 1983, Vol. 74, No. 3, pp 894-905.

[57] **Hoyniak, D.** and **Fleeter, S.**
Aerodynamic Detuning Analysis of an Unstalled Supersonic Turbofan Cascade
Trans. ASME, Journal of Engineering for Gas Turbines and Power, Vol. 108, Jan. 1986, pp 60-67.

[58] **Hoyniak, D.** and **Fleeter, S.**
Aerodynamic and Structural Detuning of Supersonic Turbomachine Rotors
AIAA Journal of Propulsion and Power, Vol. 2, No. 2, Mar-Apr. 1986, pp 161-167.

[59] **Hoyniak, D.** and **Fleeter, S.**
Forced Response Analysis of an Aerodynamically Detuned Supersonic Turbomachine Rotor
Trans. ASME, Journal of Vibration, Acoustics, Stress and Reliability in Design, Vol. 108, Apr. 1986, pp 117-124.

[60] **Hoyniak, D.** and **Fleeter, S.**
The Effect of Circumferential Aerodynamic Detuning on Coupled Bending-Torsion Unstalled Supersonic Flutter
Trans. ASME, Journal of Turbomachinery, Vol. 108, Oct. 1986, pp 253-260.

[61] **Huang, W.H.**
Free and Forced Vibration of Closely Coupled Turbomachinery Blades
AIAA Journal, Vol. 19, No. 7, 1981, pp 918-924.

[62] **Huang, W.H.**
Vibration of Some Structures with Periodic Random Parameters
AIAA Journal, Vol. 20, No. 7, 1982, pp 1001-1008.

[63] **Hurty, W. C.** and **Rubinstein, M.F.**
Dynamics of Structures
Prentice-Hall, Inc. 1964.

[64] **ICATS - Imperial College, Analysis, Testing and Software**
Reference Manual: MODACQ/MODENT/MODESH/COUPLE
Dynamics Section, Mechanical Engineering Department, Imperial College of Science, Technology and Medicine (1992)

[65] **Imregun, M.** and **Ewins, D.J.**
Aeroelastic Vibration Analysis of Tuned and Mistuned Bladed Systems
Symposium Proceedings on Unsteady Aerodynamics of Turbomachines and Propellers, Cambridge England, Sept. 1988, pp 149-161.

[66] **Imregun, M.**
User's Guide to BLIPA
Dynamic Section Report No. 8801, Imperial College, 1988.

[67] **Imregun, M.** and **Ewins, D.J.**
Complex Modes - Origins and Limits
Proceedings of the 13th IMAC, Nashville, Tennessee, USA, 1995, pp496-506.

[68] **Irretier, H.** and **Schmidt, K.J.**
Mistuned Bladed Disk – Dynamical Behaviour and Computation
IFToMM Rotordynamic Problems in Power Plant, Rome, Italy, Sept. 1982, pp 215-226.

[69] **Irretier, H.**
Coupled Vibrations of Blades in Bending-Bending-Torsion and disk in Out-of-Plane and In-Plane Motion
ASME paper No. 79-DET-90, Design Engineering Technical Conference, St. Louis, USA, Sept. 1979.

[70] **Jay, R.L.; MacBain, J.C.** and **Burns, D.W.**
Structural Response Due to Blade Vane Interaction
Trans. ASME, Journal of Engineering for Gas Turbines and Power, Vol. 106, Jan. 1984, pp 50-56.

[71] **Johnson, D.C.** and **Bishop, R.E.D.**
The Modes of Vibration of a Certain System having a Number of Equal Frequencies
Trans. ASME, Journal of Applied Mechanics, 1956, pp 379-384.

[72] **Jones, D.I.G.** and **Muszynska, A.**
Bladed Disk Dynamics Investigated by A Discrete Model: Effects of Travelling Wave Excitation, Friction and Mistuning
Proceedings of Machinery Vibration Monitoring and Analysis Meeting, Oak Brook, Illinois, 1982.

[73] **Jones, D.I.G.** and **Muszynska, A.**
A Discrete Model of A Multiple Bladed System with Interblade Slip
Proceedings of ASME on Vibrations of Bladed Disk Assemblies, Deaborn, Michigan, Sept. 1983, pp 137-146.

[74] **Kaiser, T.** and **Hansen, R.S.**
Experimental/Analytical Approach to Understanding Mistuning in a Transonic Wind Tunnel Compressor
Proceedings of 5th Conference in Advances in Structural Dynamics, Southampton, UK, 1994, pp 515-526.

[75] **Kaneko, Y.; Mase, M.; Fujita, K.** and **Nagashima, T.**
Vibrational Response Analysis of Mistuned Bladed Disk
JSME International Journal, Series C, Vol. 37, No. 1, 1994, pp 33-40.

[76] **Kaza, K.R.V.** and **Kielb, R.E.**
Flutter and Response of a Mistuned Cascade in Incompressible Flow
AIAA Journal, Vol. 20, No. 8, Aug. 1982, pp 1120-1127.

[77] **Kaza, K.R.V.** and **Kielb, R.E.**
Coupled Bending-Bending-Torsion Flutter of a Mistuned cascade with Nonuniform Blades
NASA Technical Memorandum 82813, Lewis Research Center, Cleveland, Ohio, USA, 1982.

[78] **Kaza, K.R.V.** and **Kielb, R.E.**
Flutter of Turbofan Rotors with Mistuned Blades
AIAA Journal, Vol. 22, No. 11, Nov. 1984, pp 1618-1625.

[79] **Kaza, K.R.V.** and **Kielb, R.E.**
Vibration and Flutter of Mistuned Bladed-Disk Assemblies
Journal of Propulsion and Power, Vol. 1, No. 5, Sept.-Oct. 1985, pp 336-344.

[80] **Kempthorne, O.** and **Folks, L.**
Probability, Statistics, and Data Analysis
The Iowa State University Press, Ames, Iowa, USA, 1971.

[81] **Kielb, R.E.** and **Kaza, K.R.V.**
Aeroelastic Characteristics of a Cascade of Mistuned Blades in Subsonic and Supersonic Flows
Trans. ASME, Journal of Vibration, Acoustics, Stress and Reliability in Design, Vol. 105, Oct. 1983, pp 425-433.

[82] **Kielb, R.E.** and **Kaza, K.R.V.**
Effects of Structural Coupling on Mistuned Cascade Flutter and Response
Trans. ASME, Journal of Engineering for Gas Turbines and Power, Vol. 106, Jan. 1984, pp 17-24.

[83] **Kielb, R.E.** and **Ramsey, J.K.**
Flutter of a Fan Blade in Supersonic Axial Flow
Trans. ASME, Journal of Turbomachinery, Vol. 111, Oct. 1989, pp 462-467.

[84] **Kaza, K.R.V.; Mehmed, O.; Williams, M.** and **Moss, L.**
Analytical and Experimental Investigation of Mistuning in Propfan Flutter
NASA Report NO. TM-88959, Apr. 1987.

[85] **Khader, N.** and **Masoud, S.**
Vibration of Mistuned Bladed Disks Supported by Flexible Continuous Shafts
Journal of Sound and Vibration, Vol. 149, No. 3, pp 471-488.

[86] **Lane, F.**
System Mode Shapes in the Flutter of Compressor Blade Row
Journal of the Aeronautical Science, Jan. 1956, pp 54-66.

[87] **Leissa, A.**
Vibrational Aspects of Rotating Turbomachinery Blades
Applied Mechanics Reviews, Vol. 34, No. 5, 1981, pp 629-635.

[88] **Lee, J,K.; Leissa, A.W.** and **Wang, A.J.**
Vibrations of Blades with Variable Thickness and Curvature by Shell Theory
ASME, Journal of Engineering for Gas Turbines and Power, Vol. 106, Jan. 1984, pp 11-16.

[89] **Lin, C.C.** and **Mignolet, M.P.**
Effects of Damping and Damping Mistuning on the Forced Vibration Response of Bladed Disks
ASME paper No. 93-GT-194, 1993.

[90] **Lin, R.M.**
Identification of the Dynamic Characteristics of Nonlinear Structures
PhD thesis, Imperial College, University of London, May 1991.

[91] **Liang, Z.; Tong, M.** and **Lee, G.C.**
Damping Modelling in Dynamics
Proceedings of the 10th IMAC, Kissimme, Florida, 1993, pp 1535-1542.

[92] **MacBain, J.C.** and **Whaley, P.W.**
Maximum Resonant Response of Mistuned Bladed Disk
Trans. ASME, Journal of Vibration, Acoustics, Stress and Reliability in Design, Vol. 106, pp 218-223.

[93] **Malkin, I.**
On A Generalization of Kirchhoffs Theory of Transversal Plate Vibration Problem of Steam Turbine Disk
Journal of the Franklin Institute, Vol. 234, 1942, pp 355-370 and pp 431-452.

[94] **Martin, A.I.**
Some Integrals Relating to the Vibration of a Cantilever Beam and Approximation for the Effect of Taper on Overtone Frequencies
The Aeronautical Quarterly, May 1956, pp 109-124.

[95] **Mcleod A.J.** and **Bishop, R.E.D.**
The Forced Vibration of Circular Flat Plates
Mechanical Engineering Science, Monograph No. 1, Mar. 1965, IMechE, London, pp 1-33.

[96] **Mehdigholi, H.**
Forced Vibration of Rotating Discs and Interaction with Non-rotating Structures
PhD thesis, Imperial College, University of London, May 1991.

[97] **Mehmed, O.** and **Murthy, D.V.**
Experimental Investigation of Propfan Aeroelastic Response in Off-Axis Flow with Mistuning
AIAA Journal of Propulsion and Power, Vol. 7, No. 1, Jan-Feb. 1991, pp 90-98.

[98] **Meirovitch, L.**
Elements of vibration engineering
McGraw-Hill Book Company, 1989.

[99] **Mignolet, M.P.** and **Lin, C.C.**
The Combined Closed Form-Perturbation Approach to the Analysis of Mistuned bladed Disks
ASME paper No. 92-G-125, 1992.

[100] **Millwater, H.R.; Smalley, A.J.; Wu, T.Y.** and **Evans, B.F.**
Computational Techniques for Probabilistic Analysis of Turbomachinery
ASME paper No. 92-G-167, 1992.

[101] **Mitchell, L.D.**
Complex Modes: A Review
Proceedings of the 8th IMAC, Kissimme, Florida, 1991, pp 891-899.

[102] **Muszynska, A.** and **Jones, D.I.G.**
A Parametric Study of Dynamic Response of a Discrete Model of Turbomachinery Bladed Disk
Trans. ASME, Journal of Vibration, Acoustics, Stress and Reliability in Design, Vol. 105, Oct. 1983, pp 434-443.

[103] **Muszynska, A.** and **Jones, D.I.G.**
On Tuned Bladed Disk Dynamics: Some Aspects of Friction Related Mistuning
Journal of Sound and Vibration, Vol. 86, No. 1, 1983, pp 107-128.

[104] **Muszynska, A.; Jones, D.I.G.; Lagnese, T.** and **Whitford, L.**
On Nonlinear Response of Multiple Blade System
Shock and Vibration Bulletin, Vol. 51, Part 3, 1981, pp 89-110.

[105] **Myklestad, N.I.**
A New Method of Calculating Natural Modes of Uncoupled Bending Vibrations of Airplane Wings and Other Types of Beams
Journal of the Aeronautical Sciences, April 1944, pp 153-162.

[106] **Myklestad, N.I.**
New Method of Calculating Natural Modes of Coupled Bending-Torsion Vibration of Beams
Transactions of ASME, January 1945, pp 61-647.

[107] **Myklestad, N.I.**
The Concept of Complex Damping
Trans. ASME, Journal of Applied Mechanics, Sept. 1952, pp 284-286.

[108] **Newland, D.E.**
Mechanical Vibration Analysis and Computation
Longman Group UK Ltd., 1989.

[109] **Nissim,E.**
Optimization of Cascade Blade Mistuning, Part I: Equations of Motion and Basic Inherent Properties
AIAA Journal, Vol. 23, No. 8, August 1985, pp 1213-1221.

[110] **Nissim, E.** and **Haftka, R.T.**
Optimization of Cascade Blade Mistuning, Part II: Global Optimum and Numerical Optimization
AIAA Journal, Vol. 23, No. 9, September 1985, pp 1402-1410.

[111] **Omprakash, V.** and **Ramamurti, V.**
Analysis of Bladed Disk – A Review
Shock and Vibration Digest, Vol. 20, No. 11, 1988, pp 14-21.

[112] **Ortolano, R.J.; La Rosa, J.A.** and **Welch, W.P.**
Long Arc Shrouding – A Reliability Improvement for Untuned Steam Turbine Blading
Trans. ASME, Journal of Engineering for Power, Vol. 103, 1981, pp 522-531.

[113] **Panwalker, A.S.; Rajamani, A.** and **Ramamurti, V.**
Turbomachinery Blade Dynamics – A Review
Shock and Vibration Digest, Vol. 22, No. 12, 1990, pp 3-9.

[114] **Phrol, M.A.**
A General Method for Calculating Critical Speeds of Flexible Rotors
Trans. ASME, Journal of Applied Mechanics, Sept. 1945, pp (A)142-(A)148.

[115] **Pierre, C.**
Weak and Strong Vibration Localization in Disordered Structures: A Statistical Investigation
Journal of Sound and Vibration, 1990, Vol. 139, No. 1, pp 111-132.

[116] **Pierre, C.**
Mode Localization and Eigenvalue Loci Veering Phenomena in Disordered Structures
Journal of Sound and Vibration, 1988, Vol. 126, No. 3, pp 485-502.

[117] **Prescott, J.**
Applied Elasticity
Dover Publications Inc. New York, 1946.

[118] **Press, W.H.; Flannery, B.P.; Teukolsky, S.A.** and **Vetterling, W.T.**
Numerical Recipes
Cambridge University Press, 1989.

[119] **Rao, J.S.**
The Fundamental Flexural Vibration of a Cantilever Beam of Rectangular Cross Section with Uniform Taper
The Aeronautical Quarterly, May 1965, pp 139-144.

[120] **Rao, J.S.**
Turbine Blading Excitation and Vibration
Shock and Vibration Digest, Vol. 9, No. 3, Mar. 1977, pp 15-22.

[121] **Rao, J.S.**
Turbine Blading Excitation and Vibration
Shock and Vibration Digest, Vol. 19, No. 5, Mar. 1987, pp 3-10.

[122] **Rzadkowski, R.**
Free Vibration of the Mistuned Bladed Disc
Proceedings of Inst. Mech. Engrs. International Conference on Vibrations in Rotating Machinery, Heriot-Watt University, Edinburgh, Sept. 1988, pp 151-161.

[123] **Rzadkowski, R.**
The Optimal Distribution of the Detuned Blades Around the Disk from the Stress Point of View
IFToMM 3rd International Conference on Rotordynamics, Lyon, France, Sept. 1990, pp 147-152.

[124] **Rzadkowski, R.**
The General Model of Free Vibrations of Mistuned Bladed Disc, Part I: Theory
Journal of Sound and Vibration, Vol. 173(3), 1994, pp 377-393.

[125] **Sanliturk, K.Y.**
Vibration Analysis of Mistuned Bladed System
PhD Thesis, University of London, 1992.

[126] **Schlumberger Technologies**
SI 1250 Frequency Response Analyser Operating Manual
Issue 8, Nov. 1992.

[127] **Singh, M.P.**
Turbine Blade Dynamics: A Probabilistic Approach
Proceeding of ASME on Vibration of Blades and Bladed Disk Assemblies, 1985.

[128] **Singh, M.P.** and **Ewins, D.J.**
A Probabilistic Analysis of Mistuned Bladed Turbine Disc
Proceedings of Inst. Mech. Engrs. International Conference on Vibrations in Rotating Machinery, Heriot-Watt University, Edinburgh, Sept. 1988, pp 143-150.

[129] **Sinha, A.** and **Griffin, J.H.**
Effects of Friction Dampers on Aerodynamically Unstable Rotor Stages
AIAA Journal, Feb. 1985, Vol. 23, No. 2, pp 262-270.

[130] **Sinha, A.**
Calculating the Statistics of Forced Response of a Mistuned Bladed Disk Assembly
AIAA Journal, Vol. 24, No. 11, Nov. 1986, pp 1797-1801.

[131] **Sinha, A.** and **Chen, S.**
A Higher Order Technique to Compute the Statistics of Forced Response of a Mistuned Bladed Disk Assembly
Journal of Sound and Vibration, Vol. 130, No. 2, 1989, pp 207-221.

[132] **Sogliero, G.** and **Srinivasan, A. V.**
Fatigue Life Estimates of Mistuned Blades Via A Stochastic Approach
AIAA Journal, Vol. 18, No. 3, Mar. 1980, pp 318-323.

[133] **Srinivasan, A. V.** and **Frye, H.M.**
Effects of Mistuning on Resonant Stresses of Turbine Blades
Proceedings of ASME on Structural Dynamics Aspects of Bladed Disk Assemblies, Dec. 1976, pp 57-71.

[134] **Srinivasan, A. V.**
Influence of Mistuning on Blade Torsional Flutter
NASA Report, No. CR-165137, 1980.

[135] **Srinivasan, A.V.**
Vibrations of Bladed-Disk Assemblies – A Selected Survey
Trans. ASME, Journal of Vibration, Acoustics, Stress and Reliability in Design, Vol. 106, 1984, pp 165-168.

[136] **Srinivasan, A.V.** and **Tavares, G.G.**
Direct Use of Unsteady Aerodynamic Pressure in the Flutter Analysis of Mistuned Blades
ASME paper No. 94-GT-347, June 1994.

[137] **Stange, W.A.** and **MacBain, J.C.**
An Investigation of Dual Mode Phenomena in a Mistuned Bladed Disk
Trans. ASME, Journal of Vibration, Acoustics, Stress and Reliability in Design, Vol. 105, July 1983, pp 402-407.

[138] **Staples, B.C.**
Excitation of Travelling Wave Response in Axi-symmetric Structures
Proceedings of the 15th Int. Seminar on Modal Analysis, Leuven, Belgium, Sept. 1990, pp 1339-1354.

[139] **Stetter, H.** and **Kellerer, R.**
Double Mode Behaviour of Bladed Disk Assemblies in the Resonance Frequency Range, Visualized by Means of Holographic Interferometry
ASME, The International Gas Turbine and Aeroengine Congress and Exposition, Cologne, Germany, 1992.

[140] **Swanson Analysis Systems, Inc.**
ANSYS User's Manual, Revision 5.0
Swanson Analysis Systems, Inc. 1992.

[141] **Thomson, W.T.**
Matrix Solution for the Vibration of Nonuniform Beams
ASME, Journal of Applied Mechanics, Sept. 1950, pp 337-339.

[142] **Tobias, S.A.** and **Arnold, R.N.**
The Influence of Dynamical Imperfection on the Vibration of Rotating Disks
Proceedings of the Inst. Mech. Engrs., Vol. 171, No. 2, 1957, pp 669-690.

[143] **Topp, D.A.** and **Fleeter, S.**
Splitter Blades as an Aeroelastic Detuning Mechanism for Unstalled Supersonic Flutter of Turbomachine Rotors
Trans. ASME, Journal of Turbomachinery, Vol. 108, Oct. 1986, pp 244-252.

[144] **Tong, M., Liang, Z.** and **Lee, G.C.**
Physical Space Solutions of Non-Proportionally Damped System
Technical Report NCEER-91-0002, National Center for Earthquake Engineering Research, State University of New York at Buffalo, USA.

[145] **Trumpler, W.E. Jr.** and **Owen, H.M.**
Turbine-Blade Vibration and Strength
Trans. ASME, 1955, pp 337-341.

[146] **Valero, N.A.** and **Bendiksen, O.O.**
Vibration Characteristics of Mistuned Shrouded Blade Assemblies
Trans. ASME, Journal of Engineering for Gas Turbines and Power, Vol. 108, Jan. 1986, pp 293-299.

[147] **Vorobiev, Yu.S., Korsunsky, M.L.** and **Shepel, A.I.**
Vibrations of Bladed Disk and Their Elements Including Interblading Bonds and Mistuning
IFToMM 3rd International Conference on Rotordynamics, Lyon, France, Sept. 1990, pp 143-146.

[148] **Wagner, J. T.**
Coupling of Turbomachine Blade Vibrations Through the Rotor
Trans. ASME, Journal of Engineering for Power, Vol. 89, No. 4, Oct. 1967, pp 502-513.

[149] **Wang, J.H.** and **Yau, H.L.**
Design of Blade-Shroud to Minimize the Sensitivity of Response to Preload Mistuning
IFToMM 3rd International Conference on Rotordynamics, Lyon, France, Sept. 1990, pp 535-540.

[150] **Ward, P.F.**
The Transverse Vibration of a Rod of Varying Cross Section
Phil. Mag. (6), Vol. 25, pp 85, 1913.

[151] **Weaver, W. Jr., Timoshenko, S.P.** and **Young, D.H.**
Vibration Problems in Engineering
Fifth Edition, John Wiley & sons, Inc., 1990.

[152] **Wei, S.T.** and **Pierre, C.**
Localization Phenomena in Mistuned Assemblies with Cyclic Symmetry Part I: Free Vibrations
Trans. ASME, Journal of Vibration, Acoustics, Stress and Reliability in Design, Vol. 110, Oct. 1988, pp 429-438.

[153] **Wei, S.T.** and **Pierre, C.**
Localization Phenomena in Mistuned Assemblies with Cyclic Symmetry Part II: Forced Vibrations
Trans. ASME, Journal of Vibration, Acoustics, Stress and Reliability in Design, Vol. 110, Oct. 1988, pp 439-449.

[154] **Wei, S.T.** and **Pierre, C.**
Effects of Dry Friction Damping on the Occurrence of Localized Forced Vibrations in Nearly Cyclic Structures
Journal of Sound and Vibration, Vol. 129, No. 3, 1989, pp 397-416.

[155] **Wei, S.T.** and **Pierre, C.**
Statistical Analysis of the Forced Response of Mistuned Cyclic Assemblies
AIAA Journal, Vol. 28, No. 5, May 1990, pp 861-868.

[156] **Visser, W.J.**
Dynamic Modelling of Turbomachinery Blading
Msc Dissertation, Department of Mech. Eng., Imperial College, University of London, 1988.

[157] **Whitehaed, D. S.**
Effect of Mistuning on the Vibration of Turbomachine Blades Induced by Wakes
Journal of Mechanical Engineering Science, Vol. 8, No. 1, 1966, pp 15-21.

[158] **Whitehead, D.S.**
Research Note: Effect of Mistuning on Forced Vibration of Blades with Mechanical Coupling
Journal of Mechanical Science, Vol. 18, No. 6, 1976, pp 306-307.

[159] **Wildheim, S.J.**
Excitation of Rotationally Periodic Structures
Trans. of the ASME, Journal of Applied Mechanics, Vol. 46, Dec. 1979, pp 878-882.

[160] **Wrinch, D.M.**
The Lateral Vibrations of Bars of Conical Type
Proc. Roy. Soc. A, Vol. 101, pp 493, 1922.

[161] **Yiu, H.**
A Review of the Literature on Mistuning Effects in Bladed Disc Vibration
Report No. VUTC/E/92001, Centre of Vibration Engineering, Imperial College, Dec. 1992.

[162] **Yiu, H.**
Vibration Characteristics of Mistuned Bladed Discs - Part I: Some Numerical Studies
Report No. VUTC/E/92009, Centre of Vibration Engineering, Imperial College, 1992.

[163] **Yiu, H.**
Vibration Characteristics of Mistuned Bladed Discs - Part II: Coupling Effects
Report No. VUTC/E/93004, Centre of Vibration Engineering, Imperial College, 1993.

[164] **Yiu, H.**
Vibration Characteristics of Mistuned Bladed Discs - Part III: Damping Effects
Report No. VUTC/E/93009, Centre of Vibration Engineering, Imperial College, 1993.

[165] **Yiu, H.**
Vibration Characteristics of Mistuned Bladed Discs - Part IV: Maximum Peak Response Studies
Report No. VUTC/E/93016, Centre of Vibration Engineering, Imperial College, 1993.

[166] **Young, W.C.**
Roark's Formulas for Stress and Strain
Sixth edition, MacGraw Hill Books Company, 1989.

[167] **Zienkiewicz, O.C.** and **Taylor, R.L.**
The Finite Element Method Vol.1,2
Fourth Edition, McGraw-Hill Book Company, 1989.

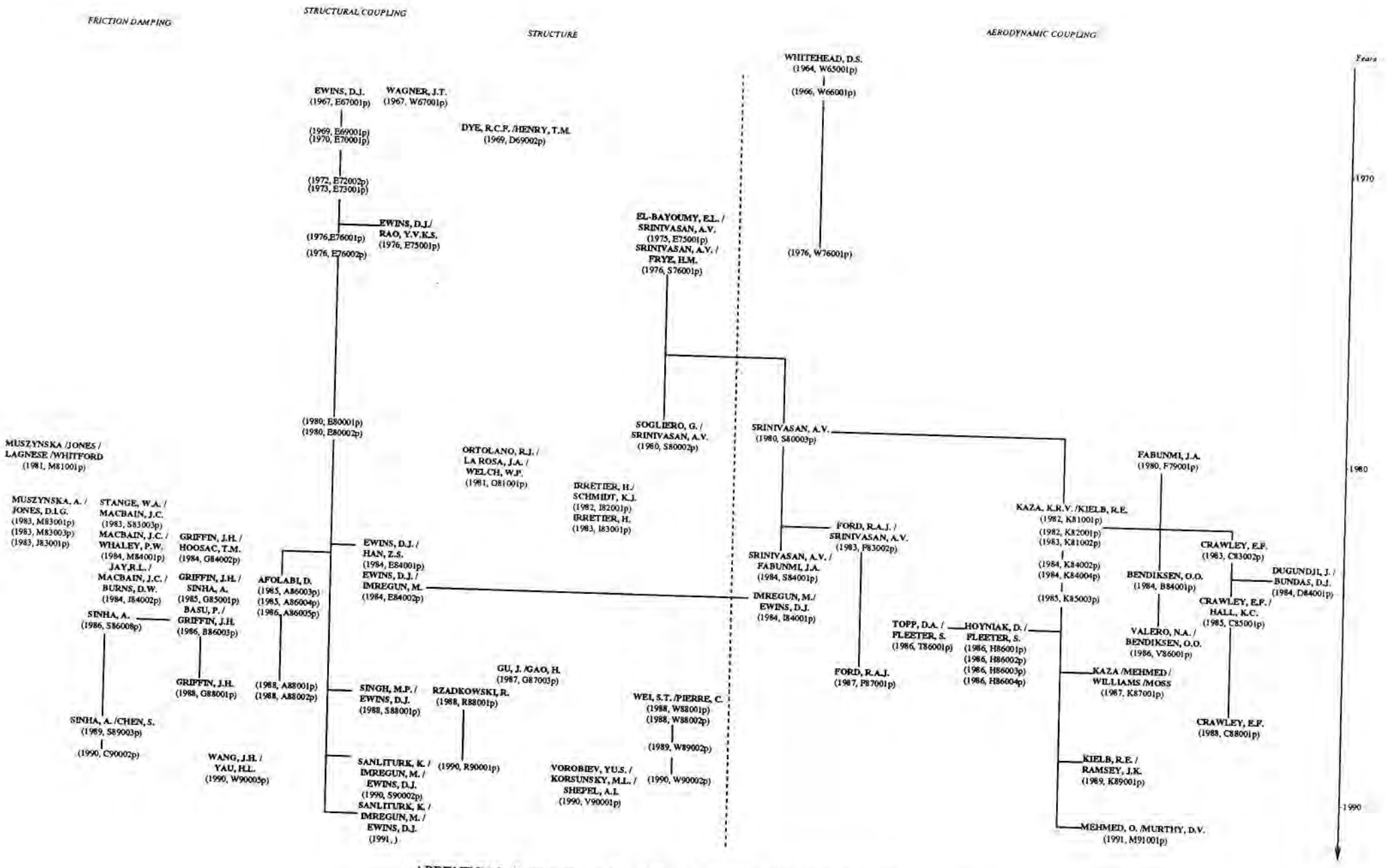

APPENDIX 1 Family tree of the studies in mistuning effects on bladed disc assemblies

APPENDIX II

Boundary Value Formulation

The equations of motions for a continuous beam (also known as Bernoulli-Euler Beam) are classical formulations beam vibration problems and they have the forms as follows:

Transverse bending mode:
$$E_b I_{yy} \frac{\partial^4 u}{\partial^4 x} + \rho_b A \frac{\partial^2 u}{\partial^2 t} = p_b(x,t) \qquad \text{(A2.1a)}$$

Twisting or torsion mode:
$$GJ \frac{\partial^2 u}{\partial^2 x} + \rho_b I_p \frac{\partial^2 u}{\partial^2 t} = T_b(x,t) \qquad \text{(A2.1b)}$$

where u is the deflection of the beam. Similarly, a thin vibrating plate has its the governing equation as follows:

$$D\nabla^4 u + \rho_d h\ddot{u} = p_d(x,y,t) \qquad \text{(A2.2)}$$

where u is the deflection of the plate. All these differential equations belong to the class of Strum-Lionville equation which has a general form as follows:

$$L\,u = F \qquad \text{(A2.3)}$$

where L is a linear operator which include all the differentials of $\frac{\partial^n}{\partial^n x}$ for n being any nth order of the differential. In free vibration analysis, the external forces are zero and hence the term F is zero. For the Rayleigh-Ritz method, it states that if there exists a *functional* R such that R is a function of u and differentiable within the boundary enclosed by Ω. It is often can be approximated by an approximation function of u^* which may contain simple functions, namely shape functions $S_i(x)$, with weighting coefficients of a_i. The function of u^* can then be expressed as follows:

$$u^* = \sum_{i=1}^{m} a_i S_i(x) \qquad \text{(A2.4)}$$

where m is the number of functions required for convergence to the real solutions, u. The procedure of minimisation of the functional R with respect to the weighting coefficients is known as *variational formulation* and can be defined as follows:

$$\frac{\partial}{\partial a_i}\int_{\Omega} R(x,a)\,dx = 0 \qquad \text{(A2.5)}$$

In structure mechanics, this functional R(x,a) are simply the energy terms and equation A2.5 is also known as the energy minimisation principle. Theoretically, it can be proved that equation (A2.5) is equivalent to equation A(2.3). Nowadays, many Finite Element textbooks provide this fundamental proof, such as the one by Zienkiewicz and Taylor [167]. Therefore, readers should refer to Chapter 9 of the reference [167] for detailed proofs.

APPENDIX III

Tests of Randomness of Random Numbers

Generating uniform random numbers is a fundamental step in stochastic simulations. There are quite a few random number generators coded in FORTRAN language, for example, see the "Numerical recipes in FORTRAN" by Press et. al. [118]. Most of these routines base on the algorithm of linear congruential generator. This method sets a set of recursion formulae as follows:

$$X_{n+1} = aX_n + b \qquad \text{mod}(m) \quad \text{for } n \geq 0 \qquad \text{(A3.1)}$$

where a is called the multiplier and b is the shift or increment. If m, a, and b are properly chosen, then the period of repeating will be of maximal length. However, a test for the random number generator is required to check whether the values generated are 'random'. A very simple way to test a random number generator is the π-test. This test also checks the number of samples required for convergence.

Test of RAND01:

# samples	PI	(4/3)*PI
2	2.000000	4.000000
4	1.000000	2.000000
8	1.500000	2.000000
16	2.500000	3.500000
32	2.750000	3.500000
64	2.687500	3.625000
128	3.000000	3.562500
256	3.062500	3.906250
512	3.164062	4.156250
1024	3.136719	4.179688
2048	3.121094	4.125000
4096	3.137695	4.138672
8192	3.134277	4.133789
16384	3.145508	4.175781
32768	3.138428	4.172852
actual values	3.141593	4.188790

Table A3.1 π-test results for the random number generator used

Theoretically, the value of π is equal to the area of a circle with unit radius and the locus of a point on a circle may be found if two numbers, x and y, satisfy the condition of $x^2 + y^2 = 1$, for x and y values between (0,1). Since the random numbers are generated in the range (0,1), two random numbers can be drawn at the same time and if the following condition is satisfied:

$$x^2 + y^2 \leq 1 \qquad \text{(A3.2)}$$

Then, we can say that a particular point (x,y) is within the quarter of a circle. A simple simulation can be done by generating many pairs random numbers so that the area of the circle can be filled. The number of occurrence of the points within the quarter of the circle is equal to the area of the quarter of the circle. The value of π is therefore four times the number of occurrence of the points within the quarter of the circle. Furthermore, the Box-Muller method is probably the most ingenious way to generator Guassian or normal deviates. Details of the algorithm can also be found in reference [118] by Press et al.

APPENDIX IV

A Linear Perturbation Analysis for Vibration Systems

There is much literature on the subject of perturbation methods. The following formulation is a very popular method which is used for mistuning studies. It first appeared from a paper by Huang [62] in 1980 and later, Sinha [130], Sinha and Chen [131], Wei and Pierre [152, 153] and Lin and Mignolet [89] were also using a similar technique for their studies of the forced response analysis of mistuned bladed discs. In the present work, the author also found that the free vibration perturbation equations on linear dynamic systems are actually the same equations as those for sensitivity of eigenvalues and eigenvectors.

Suppose the eigenvalue equation of a tuned system has the following form:

$$\lambda_o [M_o] \{\phi\} = [K_o] \{\phi\} \qquad \text{(A4-1)}$$

which can be transformed to the generalised eigenvalue equation form as follows:

$$\lambda_o [I] \{\phi\} = [A_o] \{\phi\} \qquad \text{(A4-2)}$$

If there are changes to the elements of matrix [A], these changes are naturally the perturbations to the matrix $[A_o]$ and the new status [A] matrix can be expand as a function of a small perturbation parameter, ε. This small perturbation parameter is also known as the *disorder factor* or *mistuning parameter*.

$$[A] = [A_o] + [A_1]\varepsilon + [A_2]\varepsilon^2 + ... + \text{H.O.T.}$$

In perturbation theory, the eigenvalues and eigenvectors can be expanded in a power series form in terms of ε as follows:

$$\lambda = \lambda_o + \lambda_1\varepsilon + \lambda_2\varepsilon^2 + ... + \text{H.O.T.}$$
$$\{\phi\} = \{\phi_o\} + \{\phi_1\}\varepsilon + \{\phi_2\}\varepsilon^2 + ... + \text{H.O.T.}$$

By considering the first-order terms only, one can re-formulate the eigensolution problem as follows:

$$([A_o] + [A_1]\varepsilon)(\{\phi_o\} + \{\phi_1\}\varepsilon) = (\lambda_o + \lambda_1\varepsilon)[I](\{\phi_o\} + \{\phi_1\}\varepsilon) \qquad \text{(A4-3)}$$

By expanding equation (A4-3) and equating the coefficients of ε for first-order only, one can arrive at the sets of equations as follows:

$$\lambda_o [I] \{\phi_o\} = [A_o] \{\phi_o\} \qquad \text{(A4-4a)}$$

$$\lambda_1 [I]\{\phi_o\} + \lambda_o [I]\{\phi_1\} = [A_o] \{\phi_1\} + [A_1] \{\phi_o\} \qquad \text{(A4-4b)}$$

From equation (A4-4b), the first-order perturbed eigenvalues are expressed as follows:

$$\lambda_1 = \frac{\{\phi_o\}^T [A_1] \{\phi_o\}}{\{\phi_o\}^T \{\phi_o\}}$$

Therefore, the new status of the eigenvalues can be written as follows:

$$\lambda = \lambda_o + \lambda_1\varepsilon = \lambda_o + \frac{\{\phi_o\}^T [A_1] \{\phi_o\}}{\{\phi_o\}^T \{\phi_o\}}\varepsilon \qquad \text{(A4-5)}$$

Furthermore, the new status of the eigenvectors can be obtained from the principle of orthogonalisation on Equation (A4-4b) as follows:

$$\{\phi\} = \{\phi_o\} + \{\phi_1\}\varepsilon = \{\phi_o\} + \sum_{j=1\ i\neq j}^{N} \frac{\{\phi_o\}^T [A_1] \{\phi_o\}}{(\lambda_i - \lambda_j) \{\phi_o\}^T \{\phi_o\}} \{\phi_o\}\varepsilon \qquad \text{(A4-6)}$$

Equations (A4-5) and (A4-6) look similar to the first-order eigen-sensitivity equations. In fact, it can be shown that these two equations are identical to the eigen-sensitivity equations by expanding the derivatives of the eigenvalues in a Taylor series form as follows:

$$\delta\lambda = \frac{\partial\lambda}{\partial a}\delta a + \frac{1}{2}\frac{\partial^2\lambda}{\partial a^2}\delta a^2 + ... + \text{H.O.T.}$$

where δa is the small modification or change due to the matrix [A]. By considering $\varepsilon = \delta a$, $\lambda_1 = \frac{\partial\lambda}{\partial a}$, and $[A_1] = [\frac{\partial A_{ij}}{\partial a}]$, one can easily deduce the eigen-sensitivity equations from equations (A4-5) and (A4-6).

For forced response analysis, an unperturbed or tuned system can have its equation of motion written in the form as follows:

$$[\mathbf{Z}(\omega)]\{x\}_o = \{f\} \qquad \text{(A4-7)}$$

A small perturbation $[\delta Z]$ can be added to the impedance matrix $[Z(\omega)]$ as a result of slight changes in elemental properties in the receptance matrix. Then, the new state of the equation of motions of the system have the form as follows:

$$[[\mathbf{Z}(\omega)] + [\delta Z]]\{x\} = \{f\} \qquad \text{(A4-8)}$$

Pre-multiplying both sides of equation (A4-2) by $[\mathbf{Z}(\omega)]^{-1}$, we obtain the equation as follows:

$$[[\mathbf{I}] + [\mathbf{Z}(\omega)]^{-1}[\delta Z]]\{x\} = [\mathbf{Z}(\omega)]^{-1}\{f\} \qquad \text{(A4-9)}$$

Suppose that the systems are under the same excitation forces (such as in a mistuned bladed disc and a tuned bladed disc system), equation (A4-3) and equation (A4-1) can be combined, leading to the following equation:

$$[[\mathbf{I}] + [\mathbf{Z}(\omega)]^{-1}[\delta Z]]\{x\} = \{x\}_o$$

or

$$\{x\} = [[\mathbf{I}] + [\mathbf{Z}(w)]^{-1}[\delta Z]]^{-1}\{x\}_o \qquad \text{(A4-10)}$$

The last equation can have the series expansion form as follows:

$$\{x\} = [[\mathbf{I}] - [\mathbf{Z}(w)]^{-1}[\delta Z] + ([\mathbf{Z}(w)]^{-1}[\delta Z])^2 + \ .... + \text{H.O.T.}\ ]\{x\}_o \qquad \text{(A4-11)}$$

By neglecting the higher-order terms and taking only the first order term, the mistuned response can be hence written as a relation to the tuned responses.

$$\{x\} = [[\mathbf{I}] - [\mathbf{Z}(w)]^{-1}[\delta Z]\ ]\{x\}_o \qquad \text{(A4-12)}$$

APPENDIX V

A NOTE ON TERMINOLOGIES FOR DISORDERED PERIODIC STRUCTURES

Periodic structures are structures made up of repeated substructures or components, each with identical structural parameters. If the first substructure and the last substructure of the assembly are joined together, it is known as a closed or cyclically periodic structure. A bladed disc assembly is one such structure and there are numerous examples for the open system as well.

If all the substructures of a system have the same material properties, engineers call such a structure a ***tuned*** system while physicists name it a ***perfect*** system. One significant feature of all periodic structures is that there exist many closely spaced natural frequencies. If a small change is made to the parameters of one of the substructures, the natural modes of each substructure changes regardless some of the substructures still have the tuned properties. This phenomenon is known as the ***mistuning*** effect or structural ***imperfection***. If the properties are distributed randomly among all the substructures, the term ***disordered*** is used which means randomness of the parameter values. The term ***nearly periodic structure*** is used for such a kind of structure and ***quasi-axisymmetric structures*** is used for bladed disc assemblies or space reflectors. Another interesting feature which exists in cyclically symmetric structures only is the ***double mode*** situation or ***degenerate modes***. This happens only in the perfectly tuned cases and, in practice, exact eigenvalue degeneracy does not exist. Mistuning on the blades always causes the vibration of the bladed disc to have mode ***splitting*** or ***bifurcation*** [2].

The main reason for the dynamic behaviour changes in an imperfect structure is attributed to the ***coupling*** effect between the substructures. Each substructure is coupled with the adjacent substructures and subjected to some coupled elasticity from the adjacent sections. This is known as ***structural coupling***. There is also some coupling between the plane of axes, since there are 6 degree-of-freedom in space. A structural member with a flapwise, bending mode may be coupled with a torsion motion, and with an axial or a edgewise bending, depending on how the motion acts along the principal axes. Valero and Bendiksen [146], in 1986, considered the flap-lag coupling effect with different blade interface angles.

The consequences of disorder on coupled periodic structures will lead to ***mode localisation*** or ***normal mode localisation***. of the structures. Pierre [116] defined the localisation phenomena as follows; "localisation is similar to damping as it manifests itself by a spatial decay of the vibration amplitude along the structure, even though for localised vibrations the energy is ***confined*** near the source of excitation, while for damping it is dissipated as it propagates". The direct outcome of localisation will be some local regional vibration leading to larger amplitudes and there may be prone to damage. This is the reason that localisation is also known as ***vibration confinement***. According to the different ratios of disorder to coupling, localisation can be classified as weak or strong. Ewins in 1969 [31] first use the ratio between detuning strength to the damping value to observe the peak responses for a detuned bladed disc. Since then, much work has been concentrated on studies of the effects of disordered structures [30, 40]. In 1984, Bendiksen defined a mistuning parameter [4] and this value is in fact the scaling factor of the perturbation. Pierre et al. [152, 153] defined the coupling ratio as the ratio between the coupling stiffness and the substructure stiffness. Moreover, they defined a ***weakly coupled*** system by considering the mistuning parameter to the coupling ratio being very small. In other words, the dominated substructure parameter is much larger than the coupling terms. In a bladed disc, this is the case when the disc is flexible. On the other hand, a ***strongly coupled*** system means that the coupling stiffness is much dominated. In this case, the disc is either rigid or nearly rigid (These definitions made by the workers in the applied mechanics field may be different from the engineers). Pierre, in 1988, defined the coupling ratio as the coupling stiffness divided by the substructure stiffness. After this, many research workers have followed this same rule [116].

Perhaps, Pierre and others [115, 116, 152, 153] were using the perturbation technique, which has been found to be applicable only in strongly coupled system. This is because the perturbation method can only give a linear output. However, in mistuned or disordered systems, the result is ***catastrophic***which means that a small change of order in the structural parameter may result in a much larger change in the natural modes [3]. In 1987, Pierre, et al. [152], reported a modified perturbation method (MPM). They showed that this method can be used for the weakly coupled system. However, they did not consider the intermediate coupled system.

Finally, Pierre also demonstrated, in 1988 [116], that the eigenvalues depend upon the system parameters. As first discovered by Leissa, the loci of the eigenvalues

could be plotted versus the disorder parameter or the mistuning parameter. The result shows that when two eigenvalue loci approach each other, they either cross or do not cross. Very often, the latter case happens even though the loci nearly intersect each other. The interesting point is that they veer away from each other after getting very close together. This phenomenon is named *Curve veering*.

APPENDIX VI

Damping Theory

A6.1 Single-degree-of-freedom System

For a tuned bladed disc, all blade parameters are the same and hence the single-degree-of-freedom system can be applied in such a case. Figure A5.1 shows the frequency response curve and the equivalent system.

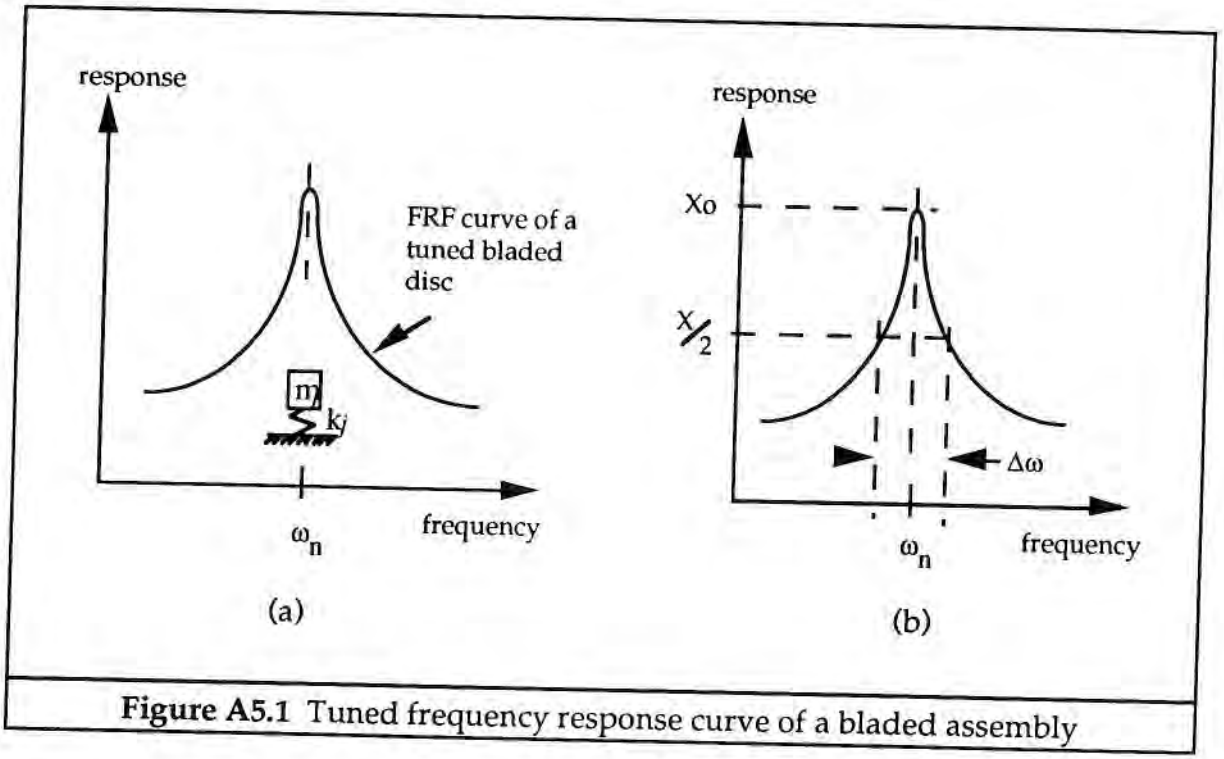

Figure A5.1 Tuned frequency response curve of a bladed assembly

This condition for the ith blade of a tuned system can be evaluated by the Heaviside D-operator theory as summarised by Mitchell [101] as follows:

$$D = \frac{c_i}{2m_i} \pm \sqrt{\frac{c_i^2}{4m_i} - k_i} \qquad \text{(A4.1)}$$

where m_i, k_i are the apparent mass and stiffness of the equivalent single-degree-of-freedom system.

The damping of a particular blade can be described in terms of the critically damped condition and the critical condition are found as follows:

$$c_0 i^2 - 4 m_i k_i = 0 \qquad \text{or} \qquad c_0 i = 2\sqrt{m_i k_i} \tag{A4.2}$$

The viscous damping ratio ζ_i can be defined as follows:

$$\zeta_i = \frac{c_i}{c_0 i} \tag{A4.3}$$

By putting the conditions of (6) and (7) into equation (5), one can get the damped eigenvalue in the form as follows:

$$s_r = \omega_n (-\zeta_i \pm j\sqrt{1 - \zeta_i^2}) \tag{A4.4}$$

where ω_n is the assembly undamped natural frequency of the system.

A6.2 **Damping Estimations**

Although damping exists in all mechanical systems, it is not a easy task to quantify the amount of damping added to a system. If a complicated system can be simplified to a single-degree-of freedom system, there are some technique to estimate the amount of damping in a system. A very simple method to estimate the level of damping is to use the logarithmic decrement which is the logarithmic of the ratio between two consecutive oscillating cycles [108]. In mathematical form, the logarithmic decrement, δ, is defined as follows:

$$\delta_i = \frac{2\pi\zeta_i}{\sqrt{1 - \zeta_i^2}} \tag{A4.5}$$

If ζ_i is small, the logarithmic decrement can also be approximated as follows:

$$\delta_i \approx 2\pi\zeta_i \tag{A4.6}$$

Another check for the level of damping is measuring the sharpness of the steady-state harmonic response curve, $H(\omega)$, as shown in Figure 5.1(b). A quantity Q (also known as the quality factor), usually used in electrical engineering, defines as the ratio between the resonant frequency to the bandwidth (or half-power $\Delta\omega$) frequency at the root-mean-squared (r.m.s) amplitude. The peak frequency for a lightly-damped system would occur at the value as follows:

$$\omega_r = \omega_n (-\zeta_i \pm j\sqrt{1 - \zeta_i^2}) \tag{A4.7}$$

When the damping ratio ζ is very small, the module can be expressed as follows:

$$|\omega| = \omega_n \sqrt{1 + \zeta_i^2} \approx \omega_n (1 + 2\zeta_i) \tag{A4.8}$$

Hence, by assuming small ζ_r, the Q factor is defined as follows:

$$Q = \frac{\omega_r}{\Delta\omega} = \frac{1}{2\zeta_j} \tag{A4.9}$$

A6.3 **Theory of State-space Equation**

One can write the state-space equation (5.4) in the following form for steady-state harmonic excitation

$$(s[A] + [B])\{Y\}e^{st} = \{p\}e^{st} \tag{A4.10}$$

The general eigenvalue problem can be solved for $\{p\} = \{0\}$ as follows:

$$s_r [A] \{\psi_r\} = [B] \{\psi_r\} \tag{A4.11}$$

and the transform between the physical coordinates and the principal coordinates are related as follows:

$$\{Y\} = \sum_{i=1}^{N} \psi_{ir} \{q_i\} \tag{A4.12}$$

where $\{\psi_r\}$ is the rth mode of the eigenvector matrix and by pre-multiplying all the terms in equation (A4.11) by $[\psi_r]^T$, the following

$$(j\omega [\psi_r]^T [A] [\psi_r] + [\psi_r]^T [B] [\psi_r]) \{q\} = [\psi_r]^T \{p\} \tag{A4.13}$$

If the eigenvector is "A-matrix normalised", such that the following conditions can be obtained.

$$[\psi_r]^T [A] [\psi_r] = [a_r], \qquad [\psi_r]^T [B] [\psi_r] = [b_r], \qquad \text{and} \quad \lambda_r = \frac{a_r}{b_r}$$

Then, the "A-matrix normalised" eigenvector can be defined as follows:

$$\{\theta_r\} = \frac{\{\psi_r\}}{\sqrt{a_r}}$$

so that $[\theta_r]^T[A]\,[\theta_r] = [\,I\,]$ and $[\theta_r]^T\,[B]\,[\theta_r] = [\,s_r\,]$.

Therefore, equation (A4) now becomes the form as follows:

$$[\,j\omega - s_r\,]\,\{q\} = [\theta_r]^T\,\{p\} \quad \text{or} \quad \{q\} = [\,j\omega - s_r\,]^{-1}\,[\theta_r]^T\,\{p\}$$

From equation (A3), the physical coordinates are therefore can be expressed as follows:

$$\{Y\} = \sum_{i=1}^{N} \frac{[\theta_{ir}]\,[\theta_r]^T\,\{p\}}{j\omega - s_r} \qquad \text{(A4-14)}$$

A6.4 **Numerical examples**

Examples 1 and 2 are for non-proportional structural damping of a 3-DOF system from reference 10 (page 50-51) solved by using the complex modal summation technique (equation 12).

Example 1. (case 1c of reference 10, page 50)

$$[\,s_r\,] = \begin{bmatrix} 30.94\text{-}1.03j & 0.0000 & 0.0000 \\ 0.0000 & 57.91\text{-}0.12j & 0.0000 \\ 0.0000 & 0.0000 & 81.85\text{-}3.19j \end{bmatrix}$$

$$[\,\phi\,] = \begin{bmatrix} 0.462(-5.5^o) & 0.217(-7^o) & 1.321(1^o) \\ 0.537(0^o) & 0.784(1^o) & 0.316(173^o) \\ 0.637(1^o) & 0.492(179^o) & 0.142(176^o) \end{bmatrix}$$

$$[\,\phi\,]^* = \begin{bmatrix} 0.463(-5.5^o) & 0.217(173^o) & 1.321(181^o) \\ 0.537(0^o) & 0.784(181^o) & 0.316(-6.7^o) \\ 0.636(1^o) & 0.492(-1.3^o) & 0.142(-3.1^o) \end{bmatrix}$$

Comparison of natural frequencies

mode	reference [42] (Hz)	state-space solver (Hz)
1	4.9290	4.9276
2	9.2173	9.2168
3	13.0374	13.0374

Example 2. (case 2c of reference 10, page 51)

$$[\,s_r\,] = \begin{bmatrix} 31.76\text{-}1.58j & 0.0000 & 0.0000 \\ 0.0000 & 62.79\text{-}0.62j & 0.0000 \\ 0.0000 & 0.0000 & 63.78\text{-}0.97j \end{bmatrix}$$

$$[\,\phi\,] = \begin{bmatrix} 0.578(-4^{o}) & 0.851(-18^{o}) & 0.685(-140^{o}) \\ 0.569(2^{o}) & 0.570(79^{o}) & 1.020(-4^{o}) \\ 0.589(2^{o}) & 0.848(-168^{o}) & 0.560(130^{o}) \end{bmatrix}$$

$$[\,\phi\,]^{*} = \begin{bmatrix} 0.578(-4^{o}) & 0.851(162^{o}) & 0.685(40^{o}) \\ 0.569(2^{o}) & 0.570(101^{o}) & 1.019(176^{o}) \\ 0.588(2^{o}) & 0.848(12^{o}) & 0.560(-50^{o}) \end{bmatrix}$$

Comparison of natural frequencies

mode	reference [42] (Hz)	state-space solver (Hz)
1	5.0606	5.0606
2	9.9950	9.9945
3	10.1507	10.1511

Note: $[\,\phi\,]$ are the mass normalised mode-shapes and $[\,\phi\,]^{*}$ are the reference mode shapes taken from reference [42].

APPENDIX VII

INDIVIDUAL BLADE CANTILEVER FREQUENCY MEASUREMENTS

The 30-bladed disc testpiece has mistuning on the blades due to slight manufacturing tolerances and also there are threaded screw holes on the tip of each blade. Therefore, it is necessary to measure the individual cantilever blade natural frequency. To do this, the disc ideally has to be rigidly clamped. However, this is very difficult to achieve in practice. Here, two thick lead plates were used to clamped the disc. The B&K FFT Analyser 2032 was used to get a blade tip response signal by hammering the blade. A microphone was used instead of accelerometer to ensure that no extra mass added to the blade. Figure 11 shows the experimental setup.

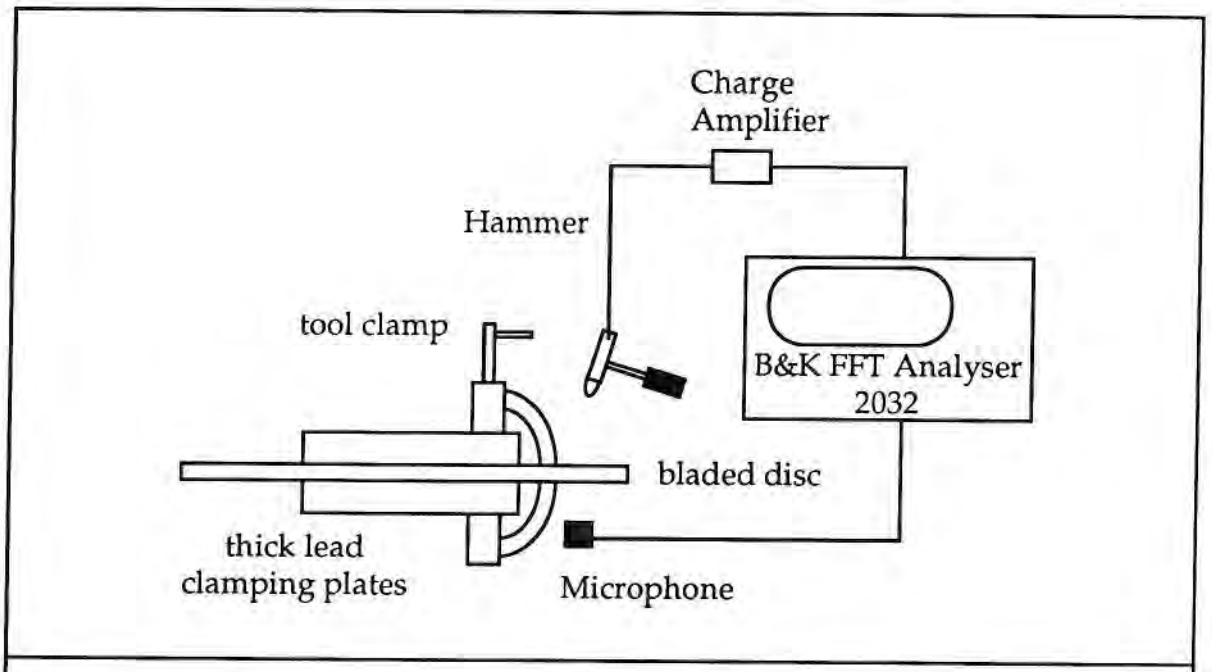

Figure A7.1 Blade cantilever natural frequency measurement

It has been found that the two clamping plates cannot isolate the blades from being coupled with the disc. In fact, the whole structure behaves rather like blades weakly coupled on a big disc. Therefore, an extra tool clamp was introduced at the rim of the disc with the clamping plates, as shown in Figure A7.1. By doing this, the measurements were improved slightly and the results seem to be repeatable from time to time. The blade cantilever natural frequencies from measurements were shown below. A better recommendation in future is to put the experiment setup into a hydraulic press and then clamping the rim of the disc

with a uniform pressure. Furthermore, the two clamping plates were slightly smaller than the disc. This gave rise to some difficulties to adjust the clamping plates exactly at the position that a blade was isolated form its root.
Individual blade cantilever natural frequency of the 30 bladed disc

Blade No.	Nat. Freq. (Hz)	Blade No.	Nat. Freq. (Hz)
1	250.0	16	247.5
2	248.0	17	249.0
3	248.0	18	247.5
4	249.0	19	246.5
5	250.5	20	251.0
6	249.5	21	246.5
7	249.5	22	251.5
8	250.0	23	251.0
9	249.5	24	250.5
10	249.0	25	250.5
11	248.5	26	250.0
12	249.0	27	250.5
13	249.0	28	248.5
14	249.5	29	250.0
15	247.5	30	248.0

min.	246.5 Hz
max.	251.5 Hz
mean	249.17 Hz
st. dev. (n-1)	1.315 Hz

APPENDIX VIII

SYSTEM CALIBRATIONS FOR DUAL-FORCE EXCITATION TEST

The Solartron 1254 analyser has four channels and each channel could be connected to a different transducer, e.g. an accelerometer or a force gauge. All transducers had their own calibrated sensitivities according to their manufacturers. However, the overall sensitivities including the cables, and charge amplifiers are still required. This calibration process has been done from both taking the manufacturer quoted sensitivities, and by measuring each set of transducers. The latter method was done by using a mass of 1 kilogram steel rod hanged freely as shown below in Figure A8.1.

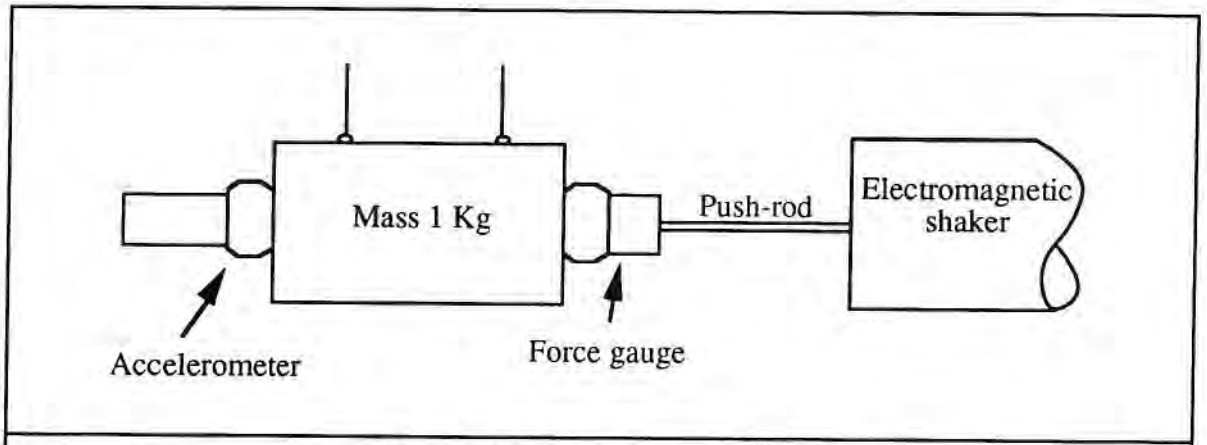

Figure A8.1 Calibration set-up

The relationship between the force gauge and the accelerometer is defined as follows:

$$\frac{F}{\ddot{x}} = \text{mass}$$

or

$$\text{mass} = \frac{\text{channel 1 (Ch1)}}{\text{channel 2 (Ch2)}}$$

All the signals from the accelerometer and the force gauge were measured by the Solartron 1254 analyser through charge amplifiers. The accelerometers and force gauges were marked and connected to the corresponding charge amplifiers because the sensitivity of each transducers is different from others.

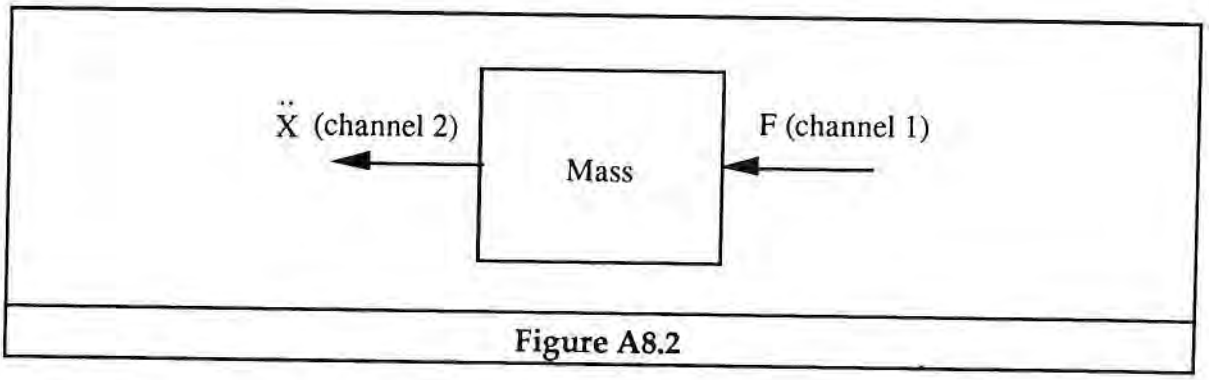

Figure A8.2

Table A8.1 shows the sensitivities of the transducers from their manufacturers.

Ref. No.	manufacturer	model	serial No.	sensitivity	type
No. 1	B&K	8200	995823	3.98 pC/N	force gauge
No. 2	B&K	8200	1049736	3.92 pC/N	force gauge
No. 1	Endevco	2222C	AB9Y3	1.369 pC/g	acc.
No. 2	Endevco	2222C	ACAA4	1.519 pC/g	acc.

Table A8.1 Sensitivity table of transducers used

The calibration carried out by three tests. These tests paired the transducers in the order of force gauge No. 1 to accelerometer No. 1, force gauge No 1 to accelerometer No. 2 and force gauge No 2 to accelerometer No. 2. All signals generated were sine signals at 100 Hz. Channel 1 of the 1254 analyser was used to measure the signal from force gauges and channel 2 was used for accelerometers. Table A8.2 shows the values of Ch1/Ch2 for all the tests.

Transducers		Ch1/Ch2	
Force gauge	accelerometer	real	imaginary
1	1	+1.080	-3.60E-2
1	2	+1.074	-4.24E-3
2	2	+1.035	-5.62E-2

Table A8.2 Analyser readings of channel 1/channel 2

From these tests, it can be confirmed that all the measuring instruments are function properly. The errors from the calibration tests are generally below 10%. Since the Endevco 2222C accelerometers are small and light, it easily give some error to the measurements. Furthermore, they were attached on the structure by using wax only. Great care has to be taken to make sure that they do not fall off.